A thesis entitled

INVESTIGATION OF LOW DENSITY LAYERS USED AS STORAGE TARGETS FOR TELEVISION PICK-UP TUBES

by

GEOFFREY OWEN TOWLER, B.Sc., Grad. Inst. P.

Presented for the degree of
Doctor of Philosophy
in the
University of London

Department of Physics
Imperial College of Science and Technology
London SW7

ABSTRACT

After discussing the problems of writing and reading a charge image in general terms, the specific case of using an S.E.C. tube as a detector of faint optical images is considered. An expression is formed for the equivalent quantum efficiency, and the resolving power is expressed as a function of the illumination. The need for a high photocathode quantum efficiency, high target gain, and low amplifier noise is brought out in the analysis. Amplifier noise is then considered separately for both the valve and transistor case.

The remainder of the work details mainly with the properties of the S.E.C. target. A demountable vacuum system is described in which the targets can be easily tested. The problems of target stability are considered, and a method of improving stability has been tried by forming a composite two layer target. The structural and electrical assessment of these targets is given in detail, together with properties of the normal KCl target.

A phenomenon whereby an enhanced gain can be produced in S.E.C. targets is discussed, and how such a property

can be used to create negative images.

Lastly, the sealed-off tubes, which were constructed in parallel with the target assessment, are described. A tube is also described which combines high sensitivity with stability, and contains an intensifier cascade screen together with a composite target.

CONTENTS

			Page
CHAPTER 1	THE PROBLEMS OF WRITING AND READING A CHARGE IMAGE		
	1.1	Light to Charge Conversion	8
	1.2	Mechanisms of Charge Image Production and Storage	10
	1.3	Stabilising the Potential of a Storage Surface by Electron Beams	23
	1.4	The Methods of Read-out	30
	1.5	The Resolution Obtainable by Charge Storage Methods	34
	1.6	The Speed of Response of the Charge Imaging Process	42
	1.7	The Capacity of the Target	47
	1.8	Non-Linear Effects in the Storage Process (Gamma)	49
	1.9	The Charge Storage Time	51
CHAPTER 2	THE USE OF TELEVISION TECHNIQUES IN THE DETECTION OF FAINT OPTICAL IMAGES		
	2.1	The Ideal Detector and Quantum Limitations of Resolving Power	53
	2.2	The Intensifier and Ordinary S.E.C. Tubes as Detectors of Faint Optical Images	57
	2.3	The Effect of Background on Resolving Power at Maximum Exposure	68
	2.4	The Detection of Faint Low Contrast Images	71
	2.5	The Effect of the Modulation Transfer Function (M.T.F.) of the S.E.C. Tube on the Resolving Power	73

CHAPTER 3 THE READ-OUT SYSTEM FOR THE S.E.C. TUBES

3.1 The Head Amplifier Tube Combination 78

3.2 The Best Performance of a Valve Head Amplifier 78

3.3 The Best Performance of a Field Effect Transistor Head Amplifier 86

3.4 The Advantages of Slow Speed Scanning 94

CHAPTER 4 A DEMOUNTABLE VACUUM SYSTEM FOR THE ASSESSMENT OF S.E.C. TARGETS

4.1 The Need for such a System 97

4.2 Methods of Writing an Image 98

4.3 The Making of the Test Pattern Mask and the Ultra-Violet Photocathode 102

4.4 The Reading Section 105

4.5 Installing and Testing Targets in the System 105

CHAPTER 5 IMPROVING THE STABILITY OF S.E.C. TARGETS

5.1 How the Targets can become Unstable 111

5.2 Methods of Improving Stability 112
(a) Mesh Trip Circuit
(b) Stabiliser Mesh
(c) Flood Gun
(d) Modifying the Target Surface Properties

5.3 Increasing the Gain of Stabilised S.E.C. Targets 124

CHAPTER 6 THE PREPARATION OF COMPOSITE TARGETS AND THE STUDY OF THEIR STRUCTURE

6.1 The Preparation and Mounting of the Thin Supporting Film 127

6.2 The Triple Evaporation 128

6.3 Mass Determination of the KCl in the Layers 133

6.4 Mass Determination of the ZnS in the Layers 135

6.5 Total Layer Thickness Determination 139

6.6 Estimation of the Density of the KCl and ZnS Deposits 140

6.7 Calculation of the Thickness of the Two Low Density Layers in a Composite Target 142

CHAPTER 7 PROPERTIES OF THE COMPOSITE TARGET

7.1 The T.S.E. Gain (Measured Under Video Signal Generating Conditions) 145

7.2 The S.E.C. Gain 150

7.3 The Inference of B.E.C. Gain 154

7.4 Transfer Characteristic 160

7.5 Modulation Transfer Function (M.T.F.) 162

7.6 Target Capacity 165

7.7 Lag 167

7.8 Cross-Over Potential V_1 173

7.9 Equilibrium Potential V_E 174

7.10 Integration and Charge Storage 175

CHAPTER 8 GAIN ENHANCEMENT FROM LOW DENSITY LAYERS

8.1 Method of Creating an Enhanced Gain 117

8.2 A Qualitative Explanation of the Enhancement Process 179

8.3 Negative Images 185

8.4 Correlation of Optical Images 187

CHAPTER 9 TUBES AND ANCILLARY EQUIPMENT

9.1 Various Types of Tube 191

9.2 Camera Equipment 201

9.3 Television Camera Channel 206

CHAPTER 10 CONCLUSIONS 222

APPENDICES

A.1 Derivation of the Amplifier Term in Equation (1.25) for F 232

A.2 The Threshold Exposures Required for Detectors to Obtain a Given Resolving Power 233

A.3 The Signal-to-Noise Ratio Obtainable from a Valve Head Amplifier 235

A.4 The Signal-to-Noise Ratio Obtainable from an F.E.T. Head Amplifier 238

A.5 Relationships between Scanning Frequencies, Bandwidth, and Equivalent Spatial Frequency cut-off 240

REFERENCES 242

LIST OF SYMBOLS 248

ACKNOWLEDGEMENTS 255

CHAPTER 1

THE PROBLEMS OF WRITING AND READING A CHARGE IMAGE

A feature common to all television pick-up tubes is the production on some storage surface of a charge image, which resembles the original optical image. This charge image can be read by a method of multiplexing using a scanning electron beam to sample each picture element sequentially.

1.1 Light to Charge Conversion

A charge image can be formed from a light image, by either of the following three physical phenomena.

1. The Photoemissive Effect

   Here, electrons are emitted from such a surface by the action of light. The maximum energy of emission E_m for a given wavelength λ of the incident light is given by the well known Einstein photo-electric equation

$$E_m = h\nu - \phi \qquad (1.1)$$

   where ϕ is the work function of the surface in electron volts. h is Plancks constant and ν is the frequency of the radiation = $\frac{c}{\lambda}$.

A charge image can be formed by suitably collecting the emitted electrons or by utilizing the positive charge left behind on the photoemissive surface, providing it is non-conducting.

2. The Photoconductive Effect

Certain forms of some semiconducting elements and compounds dramatically change their resistivity when exposed to light. This is because of the creation of electron-hole pairs enabling band conduction in the solid. If a suitable electric field is developed across such a layer, charge transport can take place in the light areas and a charge image can be formed.

3. The Photovoltaic Effect

A suitable metal-semiconductor interface when illuminated with light, will produce a current which is proportional to the intensity of illumination. This has the advantage that no external voltage is required, but the barrier layer capacitance is so high[1] that the frequency response would not be suitable for television techniques.

1.2 Mechanisms of Charge Image Production and Storage

Any television system that only collects image information during the picture element sampling time is very wasteful, and although it is possible to produce high definition images by the Farnsworth image dissector[2] methods, the loss in sensistivity is so large that it normally outways any advantages these methods may have. It can easily be seen that for a system that can store the information for the frame sampling time, that this will have a gain in sensitivity over that of any image dissector system, which will be given by the ratio of the total image area to the picture element sampling area. For a high definition systems this ratio is necessarily large, which shows the need for a storage in such systems.

Fig. 1.1 shows the four possible arrangements which can be used in a television storage pick-up tube. In (a) and (b) the surface 1 can be either a photoemissive or a photoconductive surface, and serves both as the image transducer and the storage medium. For (c) and (d) however, the surface 1 must be a photoemissive surface, but this is no longer used for storage as this is done on the surface 2.

An arrangement as in Fig. 1(a) was used in the very

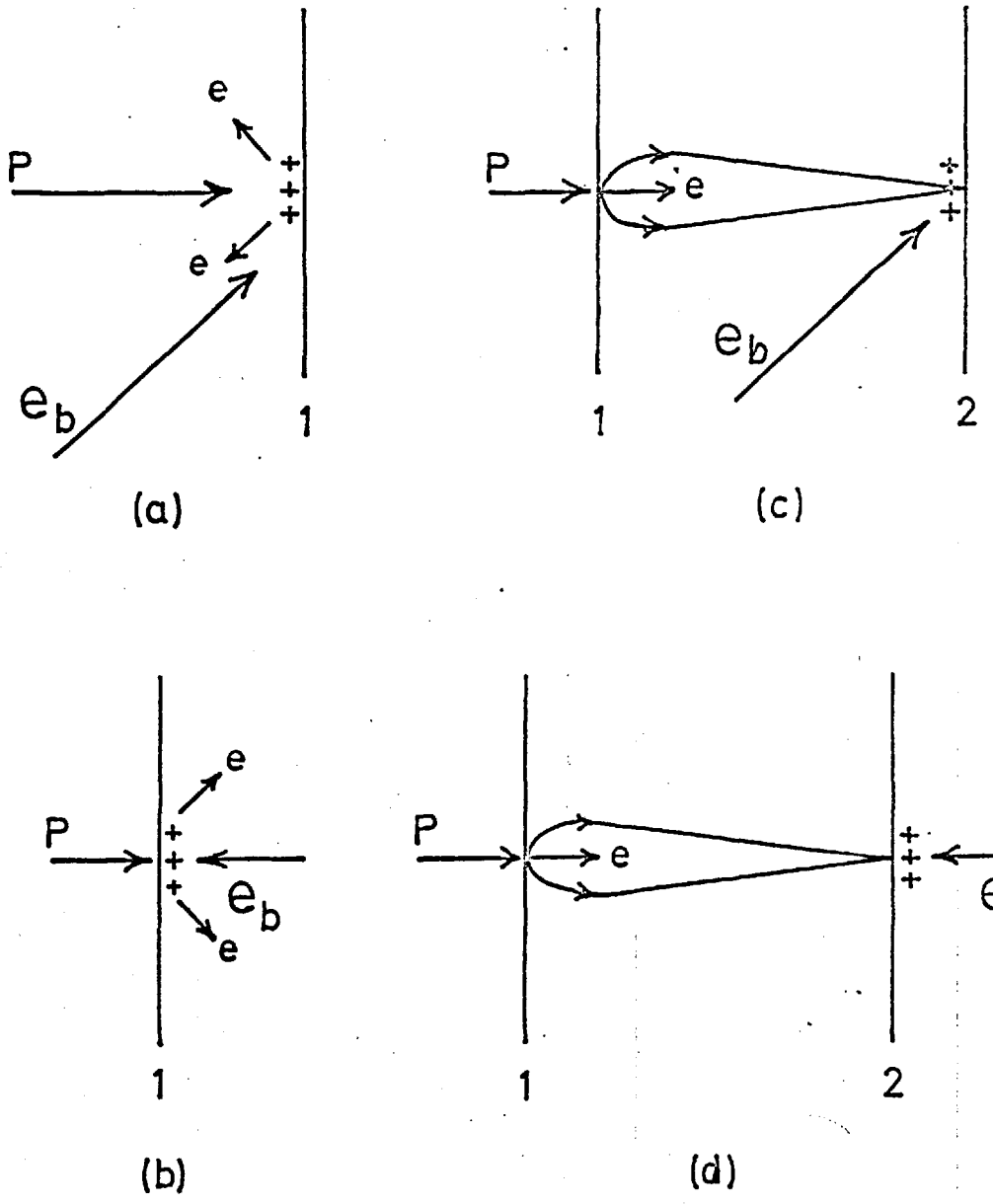

P light image (photons)

e_b scanning beam of electrons

e electrons

Fig. 1.1

early pick-up tubes such as the Emitron[4] and Iconoscope[5]. Here a positive charge image was formed on the surface 1 by photoemission, and stored by virtue of the fact that the photoemissive surface was made up of a very large number of small isolated islands on an insulating substrate. This was necessary as photocathode structures are of a semiconductor nature, and would have too low a surface resistivity to retain a charge image. Such an arrangement required the writing of the optical image by the light beam P, and the reading of the charge image by the electron beam eb to be carried out on the same side of the surface 1. A more convenient arrangement is as in Fig. 1.1(b), where the optical image is written from one side of the surface 1, and the charge image is read from the opposite surface. This requires a transmission type photocathode also to be made in islands on the scanning side of 1, and a transparent conducting film to be formed on the opposite side for the signal plate electrode (see section 1.4). The C.P.S.[6] Emitron and the Orthicon[7] are examples of the arrangement in Fig. 1.1(b) using the photoemissive effect. An example of the arrangement of Fig. 1.1(b) where the surface 1 is a photoconductor, and the signal plate is held at a suitable positive potential with respect to the scanned surface, to

build up a suitable positive charge image on this surface, is the vidicon[8].†

Such tubes can be made small and compact with a simple construction. In the early tubes rather high dark currents, and the existence of lag in the charge transport process set a limit to the usefulness of the device. These defects have been largely overcome by using lead monoxide[9] for the photoconductive material in the form of a P.I.N. diode.

In principle a photoconductor could be used in the arrangement of Fig. 1.1(a) but to the authors' knowledge such a system was never developed at the time when photoemissive surfaces were used in this arrangement. Today the arrangement of Fig. 1.1(b) is much to be preferred.

The advantage of the arrangements of Fig. 1.1(c) and (d) is that a charge gain mechanism can be used in the process of storage. A disadvantage of using photoemissive surfaces for storage as in Fig. 1.1(a) and (b) is that the necessity for isolated islands of the photoemitter causes a reduction of approximately 50% in the overall quantum efficiency of the surface, which cannot be regained whatever the method of read-out.

† For earlier work on photoconductors see:
MILLER, H., and STRANGE, J.W., Proc.Phys.Soc., 50, 374 - 384 (1938)

Methods of Producing a Charge Gain During Image Storage

1. Secondary Emission

All solid materials, if bombarded with energetic electrons, will produce further electrons, which are emitted back from the surface characteristically having a few electron volts energy. These are called secondary electrons. Fig. 1.2 shows a plot of the number of secondary electrons per incident primary δ (secondary emission coefficient) as a function of the primary electron accelerating potential V. It can be seen that there is an accelerating potential V_M which gives a maximum secondary electron yield δ_m, high values of which are fortunately obtained for insulators[3] where values of δ_m from 5 to 10 are not uncommon. The positive charge left stored on the insulating surface, is the difference between the incident charge and the secondary emission charge, and is stored with a charge gain of δ-1. An arrangement as in Fig. 1.1(c) has been used where the surface 2 was a mica sheet; this was known as the Super Emitron[10] or the Image Iconoscope[11]. The problems of having to scan with the electron beam at an oblique angle did not, however, enable the full charge gain to be realised. Khan[12] and Mende[13] at Imperial College made a storage tube

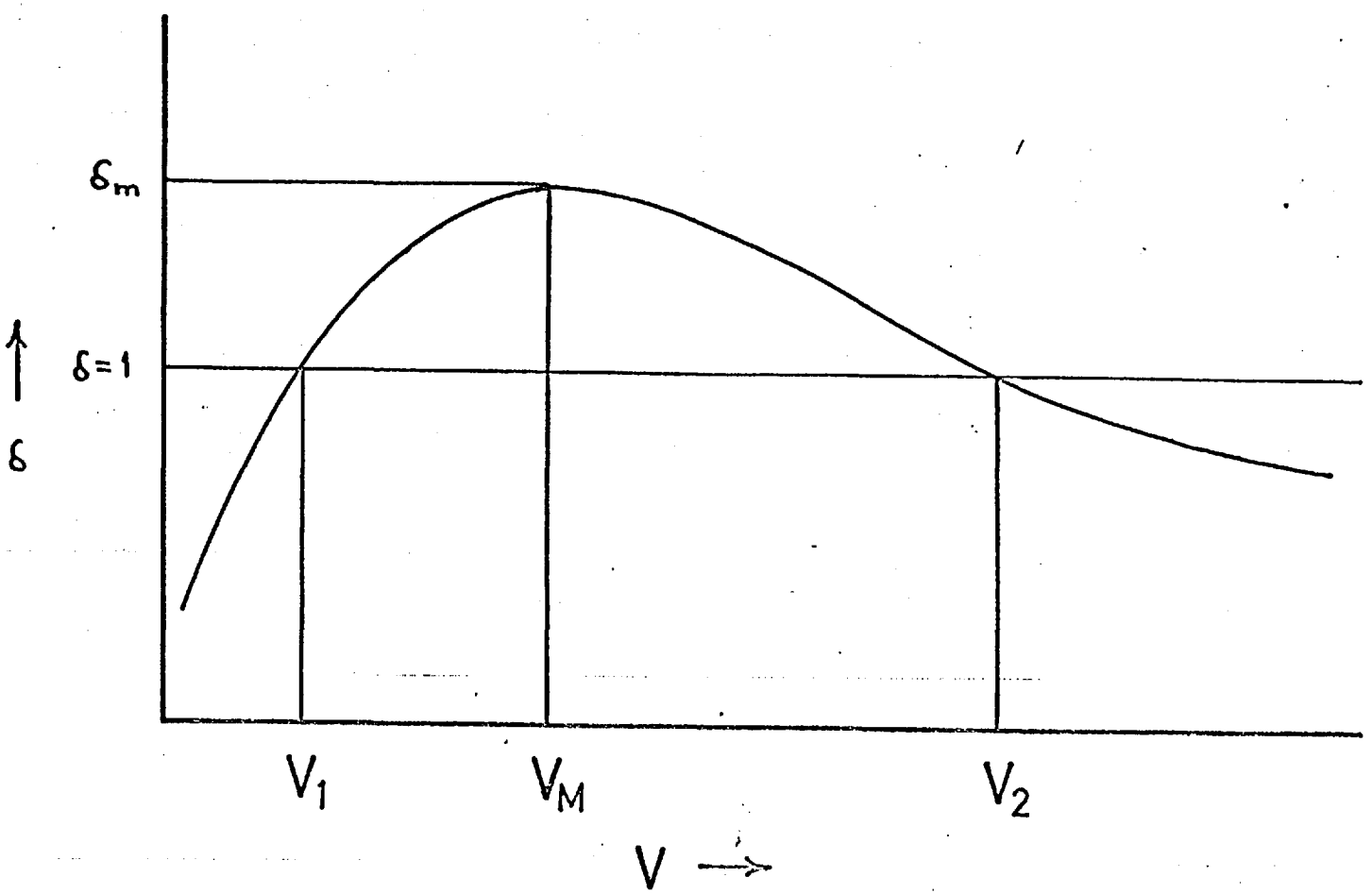

Fig. 1.2

with an arrangement similar to Fig. 1.1(c), the charge image was written from a photocathode 1 onto a secondary emitting insulating surface 2 of magnesium fluoride. The electron scanning beam was also generated from the photocathode by using flying spot scanning techniques. A similar method of storage was used by Beurle[14] and Slark[14,15], the method of writing being as in Fig. 1.1(c), but for the reading process the storage surface 2 was rotated through 180°, and scanned as in Fig. 1.1(d). The last two devices have the disadvantage that writing and reading can only be done sequentially.

The image orthicon[16] is an example of Fig. 1.1(d). Here a positive charge image is formed by secondary emission on the photocathode side of the storage layer. A negative charge of similar magnitude is deposited on the scanning side of the layer during read-out by the electron beam, and neutralisation then occurs by conduction through the layer. The material normally used for the layer 2 is a glass film. This must have the correct value of resistivity, so that lateral spreading of charge is negligible, to retain a high resolution image, The product of the dielectric constant and the resistivity of the layer should be such as to give a time constant comparable to the frame time. The early

glasses that were used were ionically conducting; this caused a deficiency of sodium ions on the photocathode side of the layer after a few hundred hours use, and gave rise to image retention, caused by the highly insulating layer that was formed. This has been overcome by the development of electronically conducting glasses.

The collector electrode plays an important role in any system where charge is stored by secondary emission. In the image orthicon this consists of a mesh mounted close to the storage layer, 2, (the target) on the photocathode side, and held at a potential of about 2v positive with respect to it. The secondaries will be collected by this mesh, unless the light level is such that the target potential rises to that of the mesh potential. Then secondaries will begin to be returned to the target surface; this causes edge contrast enhancement at first to the image but for higher light levels it causes an objectional black halo effect, where the returned secondaries have depressed the surface potential around the highlight. The onset of this effect causes the charge gain to decrease, and the storage to become non-linear, a "knee" is formed in the transfer characteristic at this point.

2. Electron Bombardment Induced Conductivity (E.B.I.C.)

It is found that[14(6)(6)17] if certain solid materials are bombarded with energetic electrons, usually with several KeV energy, that their resistivity will decrease. This is due to the presence of band conduction of the electron-hole pairs created, and is very similar to the process of photoconduction. Unlike the photon, however, the energetic bombarding electron is able to produce hundreds of electron-hole pairs along its track in the material, which can be made to flow by means of a polarising field to give a target gain of several hundred or even thousands. Such a material could be used as the storage surface, 2, in Fig. 1.1(d). Schneeberger et al[18] have made such tubes where the target 2 consisted of a thin aluminium oxide support membrane coated with a thin aluminium signal plate onto which the EBIC material was deposited. The energetic primaries from the photocathode 1 were imaged onto the target where they were able to penetrate through the thin support membrane and signal plate, losing most of their energy in the EBIC material. The charge carriers produced were made to flow by means of the polarising field between the signal plate and the scanned surface to leave a charge image stored on this surface.

An EBIC target could be used in Fig. 1.1(c), and this was tried by Slark in the reversible target tube, and investigated by Khan in the photocathode scanned tube; here no thin support membrane is required and the signal plate can be a metal disc.

The high intrinsic gain of the storage process indicates a favourable method of storage; however, the existence of solid state lag, and the difficulties encountered in producing blemish free targets of the right capacitance have prevented the widespread use of this device.

3. Secondary Electron Conduction(S.E.C.)[21,22]

Here the basic principle by which the charge image is created is secondary emission, but because of the physical nature of the secondary emitting storage material, it behaves very differently to normal secondary emission by reflection from solids.

The arrangement used is as in Fig. 1.1(d) and the storage target 2 is very similar to that used by Schneeberger for the EBIC process. The only difference being that the dielectric is no longer a solid layer, but is evaporated as a very porous deposit. This is done[19] by

evaporating the material in an atmosphere of argon at a pressure of ~ 1 torr. A cross section of the target structure is shown in Fig. 1.3. The imaging photoelectrons are accelerated to a few KeV energy; this enables them to penetrate through the aluminium oxide support layer and the signal plate into the relatively thick layer of the very porous storage material. The material is chosen to have a very high secondary emission coefficient: and potassium chloride has been found to be very suitable and has been used by several workers[19,20].

As a photoelectron penetrates through the KCl it loses progressively more and more of its energy; this is used in the production of secondary electrons along its track, which escape into the vacuum pores in the material. Under normal circumstances such secondaries would be of no consequence, as they would not normally contribute to the charge build up on the layer, as their probability of escape would be very small, so they would just recombine with the positive charge sites they had just formed. If, however, an internal electric field is established through the layer by making the signal plate electrode more positive than the scanned surface, then these secondaries produced in the pores inside the layer can be collected

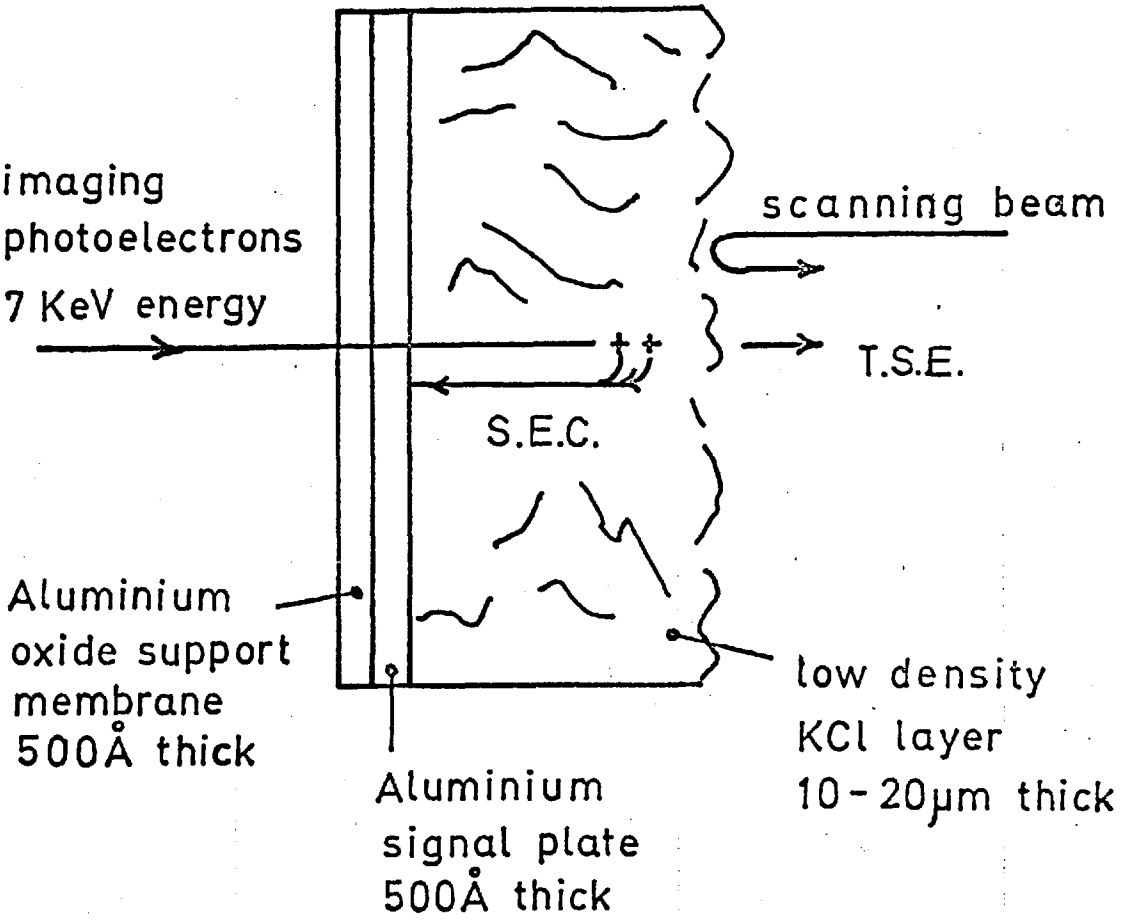
imaging
photoelectrons
7 KeV energy
scanning beam
T.S.E.
S.E.C.
Aluminium
oxide support
membrane
500Å thick
low density
KCl layer
10 - 20μm thick
Aluminium
signal plate
500Å thick

Fig. 1.3

by the signal plate, leaving a positive charge image stored in the layer. This process is termed Secondary Electron Conduction[21] (S.E.C.) and is different from E.B.I.C. in as much as the electrons are truly free from the solid, and will not therefore exhibit any solid state lag.

It is possible for secondaries to be produced near to the scanned side of the target and to leave this surface for the nearest positive electrode. This is termed Transmission Secondary Emission (T.S.E.) since the secondaries leave the opposite side of the target to which the primary photo-electrons were incident. The stored positive charge is therefore stored with a total gain G_t made up of the two components, $G_{S.E.C.}$ the S.E.C. gain and $G_{T.S.E.}$, the T.S.E. gain.

i.e. $$G_t = G_{S.E.C.} + G_{T.S.E.} \quad (1.2)$$

With the signal plate positive with respect to the scanned surface, the electric field is such as to hinder the escape of the T.S.E. electrons, and thus under normal conditions $G_{T.S.E.}$ is much smaller than $G_{S.E.C.}$.

If, however, the signal plate is at a more negative potential than the scanned surface, then the internal electric field in the target will enhance the T.S.E. gain. This

is not a suitable mode for operation, however, as the S.E.C. electrons will have reversed their direction of motion with the reversal of the electric field, they will now be moving in a direction so as to cancel the charge created by the T.S.E. electrons. This can be seen from equation (1.2); when the $G_{S.E.C.}$ is negative Gt is small; this is further discussed in Chapter 7.

S.E.C. tubes have been reported by Goetze et al[20,21] and Filby[19,22,23] et al which have had target gains Gt of over a hundred for a few tens of volts between the positive signal plate and the scanned surface.

1.3 Stabilising the Potential of a Storage Surface by Electron Beams

In the early tubes it was necessary to read the image on the target from the same side as it was written, as in Fig. 1.1(a) and (c). This required the scanning beam to be at an angle to the storage surface, and so "keystone correction" was required of the scan to obtain a rectangular raster.

With the introduction of transmission photocathodes and the optically transparent signal plate, reading the charge image from the opposite side of the target to which it was written became possible. The main advantage of

using this configuration, apart from the better geometrical design, was to be found in the possible potentials at which the scanned surface could be stabilized by the electron beam.

1. Anode Potential Stabilisation

If the storage surface is scanned with an electron beam of energy eV and V lies between V_1 and V_2 of Fig. 1.2 then each primary electron in the beam will produce on average δ secondaries, which is a mean value greater than unity.

This means that more electrons leave the surface than land on it from the beam, so the potential of the surface will rise. This will continue until its potential has risen to that of the nearest accelerating electrode, when the secondaries will no longer be extracted by a positive field and collected by this electrode. The majority will now return to the storage surface; only the most energetic secondaries will reach this electrode (e.g. wall-anode). Eventually an equilibrium will be reached where only one secondary will manage to get to this electrode for each primary electron incident in the scanning beam. The storage surface is then said to be Anode Potential Stabilized.

This method of target stabilisation was used in the Emitron(Iconoscope) and the Super Emitron (Image Iconoscope) camera tubes, but it has the disadvantage that the returning secondaries produce charge redistribution, which cause spurious signals of a rather complex nature often known as "tilt and bend". This charge redistribution also causes a reduction of the integration time for the charge image, to much less than the frame time, and destroys the possibility of providing a black level reference to the video signal.

To a certain extent the redistribution effect can be reduced by mounting a fine-mesh barrier grid[24] very close to the target. If the potential of this mesh is less than that of the wall-anode electrode, any secondaries passing through the mesh will not be able to get back to the target. If, however, the potential of the target does rise above that of the mesh, the secondaries will be returned to the target by the mesh, but at a point very close to where they were emitted.

A better method of preventing the effects of redistribution is by pulse biasing[25,26]. Here the reading and writing processes are carried out sequentially by making use of the frame blanking period. During the first

half of this period the target is prepared by flooding the photocathode with light, at the same time the collector electrode is pulsed to a lower positive potential; this causes the target surface to anode potential stabilise at the new lower collector potential. During the second half of the blanking period the image is displayed, with the collector electrode returned to its normal working potential, which is now more positive than the target so that the secondaries can be efficiently collected without any redistribution effects. The target is then scanned during the frame period with the high velocity electron beam.

If instead of framing at the normal rate the camera tube is used to make a long exposure with a single frame read-out, no pulsing of the collector electrode is required during the blanking period, as this electrode can now be switched for the preparation, write, and read operations.

2. Cathode Potential Stabilisation

If the scanning electron beam is incident on the target surface with an energy eV, such that V is less than V_1 of Fig. 1.2, then on average less secondaries will leave the surface than primaries are arriving. The net result is

that the target surface will acquire more and more negative charge, reducing its potential to that of the gun cathode, but as the beam tries to drive the surface more negative than this, it will be prevented from landing by reflection in the negative potential gradient. The target is then said to be cathode potential stabilised.[28a]

The main advantage of this method of target stabilisation is that there are no troublesome effects due to secondary electron redistribution, and the whole of the frame period is utilized for charge image integration.

In order that the whole target surface will stabilize at cathode potential, in an electromagnetic system using magnetic deflection; it is necessary for the scanning beam to be incident normal[28b] to the scanning surface over its entire area.

If this is not so, and the scanning beam is incident at an angle θ to the normal of the target surface, then this point on the surface will stabilise at a potential $V \sin^2 \theta$ more positive than at a point where the scanning beam is incident normally, (V is the potential through which the beam has been accelerated at its magnetic deflection centre).

This landing error which has been described by

Lubszynski[27], can cause a "porthole effect". This will also be the case for a beam that has been deflected electrostatically. For if a beam is at an angle θ to the axis of the tube whilst at a potential V, then its axial energy will be $V\sin^2\theta$ less than for an on axis beam. This is the direct consequence of a scalar field, where there can be no change in total energy, and hence some of the axial energy is converted into tangential energy.

In both cases at large angles of incidence it is possible for the target to become unstable because the tangential energy increases with the angle of deflection θ, and the energy of the electrons as they graze the surface soon becomes large enough for the secondary emission coefficient to become larger than unity; once this has happened the surface will rapidly assume anode potential. This means that the arrangements of Fig. 1.1(a) and (c) cannot be used for this method of target stabilisation.

Although this method of stabilising has much to be preferred in comparison with anode potential stabilisation, it does introduce some undesireable features. These are mostly associated with the fact that the electron beam has very little energy when it is incident on the target. When trying to bring the scanning beam to a focus, under

these conditions, the mutual repulsion of the electrons will set a limit to the spot size. Also chromatic abberation effects become important factors of beam imaging. An oxide cathode giving a good emission at a low temperature is essential to obtain a low energy spread.* The storage of a charge image on a target creates a voltage pattern across the target surface which sets up transverse electric fields that can deflect the low velocity scanning beam to the high voltage areas of the image, when it should be landing on the neighbouring low voltage areas. This is known as beam bending, and can be recognised by the apparent growth of the "white" areas of an image. The onset of this condition sets a limit to the useful storage capacity of the tube for a given target capacitance (the maximum voltage excursion found possible on the S.E.C. target, before such effects could be observed was ≈ 5v).

Unlike anode potential stabilization this mode of operation is not inherently stable. It can be seen from Fig. 1.2 that if the voltage excursion on the target surface exceeds V_1, then δ will exceed unity, and the target surface will then restabilise at anode potential. Methods of providing protection against such overload signals will be discussed in Chapter 5.

*Note however, that a larger axial energy spread is produced by the divergence of the beam through the limiting aperture.

3. Second Cross-Over Potential Stabilisation

Again referring to Fig. 1.2, it will be seen that if a target is bombarded with an electron beam whose energy eV is such that V is greater than V_2, then δ is once again less than unity. This will cause a net negative charge to be deposited until the target potential has fallen to V_2, then exactly one secondary will leave for each primary electron incident in the scanning beam and so the target will stabilise at this potential. As the scanning beam has been accelerated through a higher potential than V_2, there will exist a positive potential gradient from the target surface which will prevent redistribution effects. Although this mode has been investigated[28] it has been rejected because of the inability to find materials which have a sufficiently large slope to the curve of Fig. 1.2 at V_2, to provide enough beam acceptance to give an efficient discharge of the target.

1.4 The Methods of Read-Out

1. Signal Plate Read-Out

Here a resistor is connected to a conducting backing electrode which is capacitively coupled to the storage layer. As each point of the charge image is neutralised by the scanning beam, the inductively held charge flows

to earth through the resistor to develop a video voltage waveform. For photoemissive, and secondary emitting surfaces a charging current flows through the resistor during the writing process, which produces a signal of opposite polarity. This is not normally a nuisance as the mean signal level is usually constant, so this just provides a D.C. signal. It can prove troublesome in telecine apparatus, as the advancement of the film will create an A.C. signal from this charging component. This method of read-out has been used in the majority of camera tubes because of its simplicity, Its main disadvantage as will be seen in Chapter 3 is the additional noise which is introduced by the head amplifier particularly for large bandwidths.

2. Return Beam Read-Out

If m_b is the fraction of the beam current that neutralises the charge in one point of the image, then $1-m_b$ is not required and is reflected by the target surface. This travels back towards the gun cathode along a similar path by which it came because of the nature of the electron optics. This return component of the scanning beam can be deflected onto the first dynode of an electron multiplier,

where at the output it will provide a high level output signal, which has very little degradation in the signal-to-noise ratio to that at its input.

This method has been used to advantage in the image orthicon, and some special purpose vidicons, where a high signal-to-noise ratio is required at large bandwidths. The beam current shot noise sets a limit to the smallest possible working signal level. The beam current is kept as small as possible, but it must be large enough to cope with a peak whitesignal; one of the difficulties is that it is not possible to modulate the beam 100% (m_b = 0.3 is a realistic figure for a peak "white" signal) and this requires more beam current producing a higher beam shot noise component. Another undesirable feature is that the maximum beam is reflected in the black areas of the image, so the beam current shot noise will be a maximum in these areas.

3. Isocon Read-Out

In a normal return beam there are electrons of two different components; there are those which have been specularly reflected near the target surface, and these are

those which have been scattered. The number of scattered electrons are proportional to the voltage excursion on the target surface, so if they could be separated out they would provide a signal of reversed polarity to 2, which would contribute negligible noise in the black areas of an image. This has been done by using a scanning beam, whose transverse energy has been deliberately increased so that the electrons describe large helical paths. The specularly reflected electrons will describe similar paths in the return beam, and will be collected on a separator electrode. The scattered electrons return without any excessive helical motion and pass through the aperture in the centre of the separator electrode and strike the first dynode of the electron multiplier.

Early investigations of this method of read-out were made by Weimer[29] for the image isocon which had a glass target similar to the image orthicon. Cope[30] et al[30] have also investigated isocon scan, including the use of photo-conductors. In recent years Mouser, Ruggles, and Slark[31] have developed both 3" and 4½" image isocons with electronically conducting glass targets. It appears that almost any form of television storage tube would benefit by the isocon method of read-out if

maximum signal-to-noise ratio is required, providing enough scattering can be produced by the material at the target surface.

1.5 The Resolution Obtainable by Charge Storage Methods

In general each transfer stage in a camera tube is an imaging process which has a spatial frequency response associated with it. The image formed on the photocathode (or photoconductive layer) is usually of high resolution, but there will still be a finite limit to the spatial frequency components. The normalised sine wave response at different spatial frequencies is a good measure of its resolving capabilities, and is quoted as the Modulation Transfer Function (M.T.F.). The sine wave response has the advantage that the M.T.F. of the entire system is just the product of the M.T.F.'s of the individual transfer stages.

$$\text{i.e.} \quad R_{syst} = R_L R_I R_T R_b R_A \qquad (1.3)$$

where R_L = sine wave response of the lens,

R_I = sine wave response of the image section,

R_T = sine wave response of the target,

R_b = sine wave response of the scanning beam,

R_A = sine wave response of the video amplifier.

If a separate charge storage surface is used as in Figs 1.1(c) and (d), then the imaging of the photoelectrons onto this surface has to be considered. The M.T.F. of the electron image focused onto the target will depend upon the electron optical design. For a system using uniform parallel electrostatic and magnetic fields to provide a single loop focus, Filby[32] has computed the spread function for a point image using experimental data for the angular and energy distributions of the photoelectrons. These results have indicated that such a system should be capable of imaging very high spatial frequencies, and confirming experimental results were obtained using a phosphor in the target plane.

The next stage in the system is the charge storage on the target. An obvious cause of poor spatial frequency response here is due to lateral conduction, especially in target materials relying on conduction to transfer charge from the image surface to the scanning surface of the target. This aspect has been dealt with by Frysman[33], and it sets a limit for the normal image orthicon and vidicon targets, when they are used to store images for long periods.

If the image is written by energetic electrons penetrating right through the target as in the S.E.C. tube, there is the possibility of a loss of resolution due to electron scattering. The scattering angular distribution as observed by Butkevich and Butslov[34] was more directional in the forward direction than a cosine distribution, which would not cause much loss of resolution for the target thicknesses normally used.

It has been shown by Krittman[35] that another limitation of the target resolution is set by the thickness of the storage layer. This is because the transformation of a charge pattern into a potential pattern, suffers a degradation in its sine wave response depending on the target thickness, and it is this which is sensed by the reading beam.

By means of Fourier transforms, Knittman has shown that the normalised sine wave response $R(f_s)$ for a storage surface at a distance z_t from the conducting signal plate is

$$R(f_s) = \frac{1 - e^{-4\pi f_s z_t}}{4\pi f_s z_t} \qquad (1.4)$$

where f_s is the spatial frequency.

It is possible under certain conditions to obtain better resolution than one would expect, from the limitations imposed by the potential pattern.

This can occur if there is any form of charge redistribution on the target surface. Such improvements have been observed for image orthicons[35]; after a few scans of a continuously displayed image, the sine wave response was much improved in comparison to that of the first scan (which was a close approximation to the theoretical relationship as given by equation (1.4)).

The sine wave response of an S.E.C. target has been reported by Beyer and Goetze[36]. An optically scanned tube designed for high resolution was used, where the read-out beam was of very small diameter, and beam bending effects were minimised by using a strong magnetic field for focusing. The sine wave response of the target was estimated by these authors from the response of the entire system by correcting for the known responses of the optical lens, the imaging section, the read-out beam, and the amplifier. In Fig. 1.4. the points have been taken from their estimated response curve, and the line is a plot of equation (1.4) with z_t = 12μm, which gives the best fit to the experimental points at low spatial frequencies

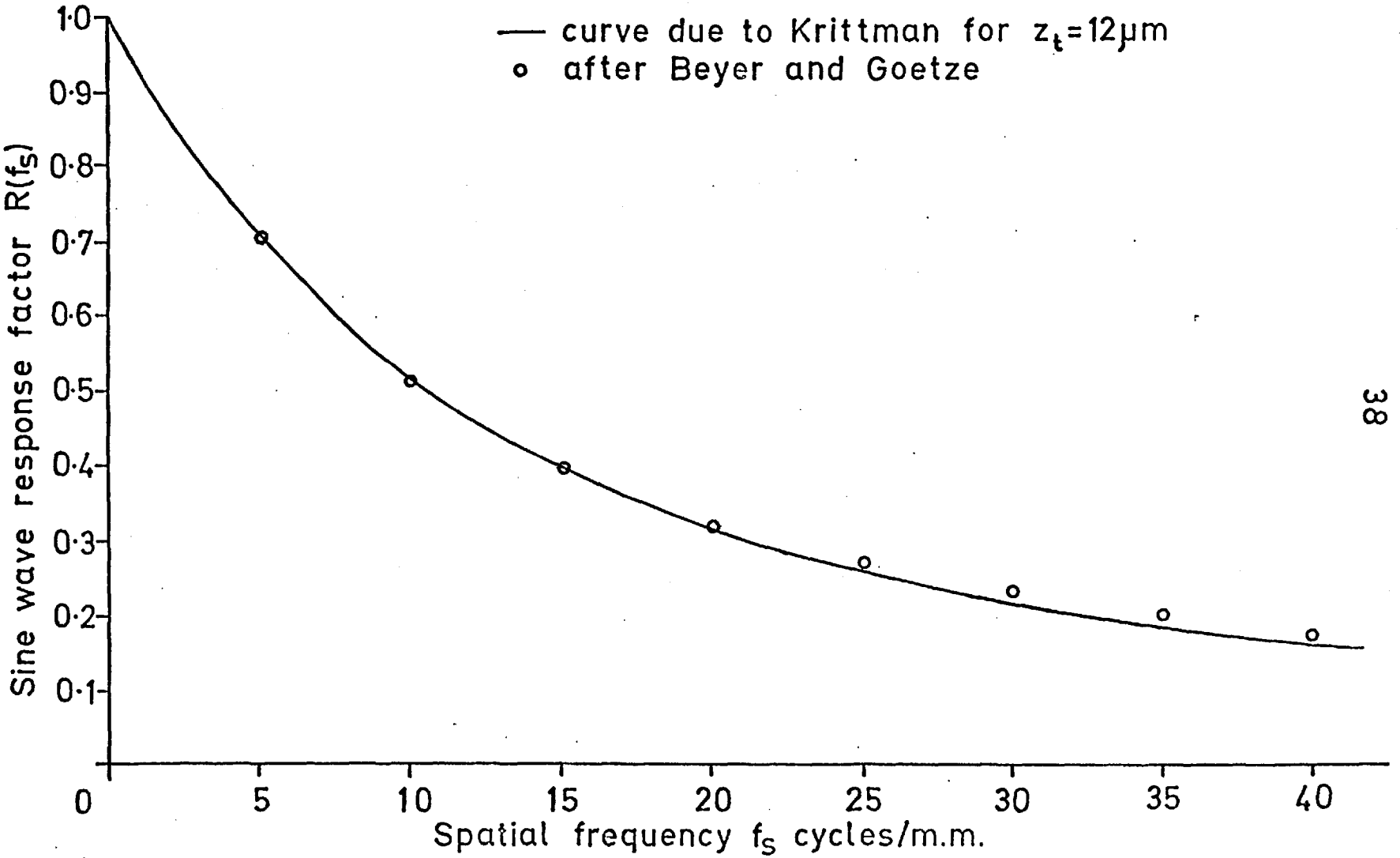

Fig. 1.4 Sine wave response factor for an S.E.C. target

where the results are expected to be most accurate. It can be seen that the fit is extremely good, and 12μm would seem to be a reasonable figure, although the thickness was not stated by Beyer and Goetze. These results were always for the first scan, as in their tube a flood beam was used to discharge completely the target between successive scans.

The effect of the scanning beam having a finite cross section is to degrade the sine wave response of the system. High velocity beams can have fine cross sections but are not usually used, because of the redistribution effects. Low velocity beams are widely used for read-out in pick-up tubes. The cross section of the beam is more difficult to control because axial energy spread of the beam electrons can cause large chromatic aberration effects in the electron optical focus of the beam, transverse electric fields can cause beam bending, and a slow moving beam near the target surface can easily be defocused.

In Fig. 1.5(a) there is shown[37] ~~that~~ the current distribution $i_b(x)$ that would be measured through an infinitely thin slit dx for a $\cos^2$ beam as it scans across the slit (curve 1). This is known as the line spread function of the beam, and can be written as $i_b(X) = i_6 \cos^2 \frac{\pi X}{\delta}$

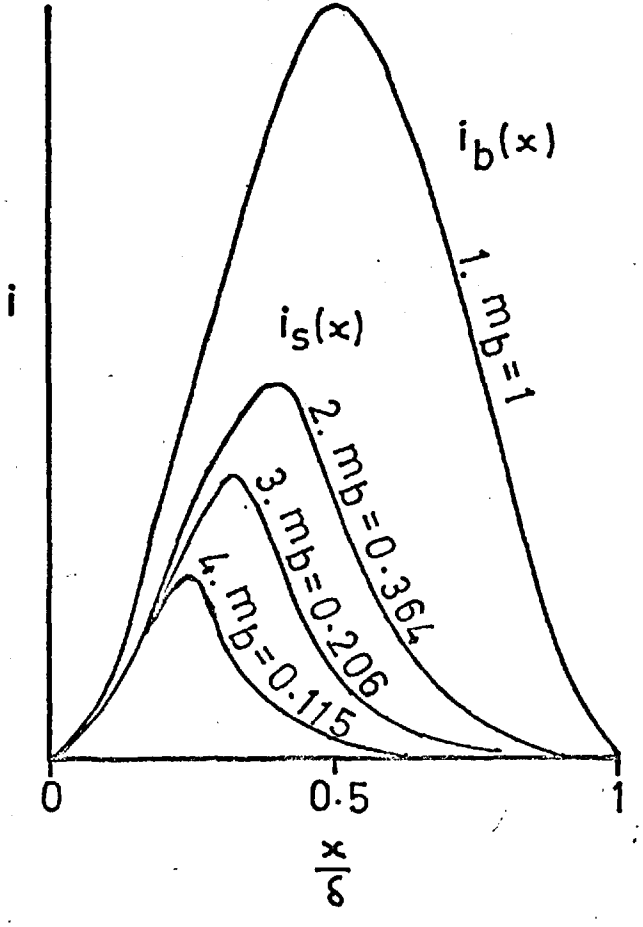

Fig.1.5(a)

Normalised response curves for $\cos^2$ beam of diameter δ.

defining $f_\delta = \frac{1}{\delta}$ then for $\delta = 30\mu m$

$f_\delta = 33$ cycles/m.m.

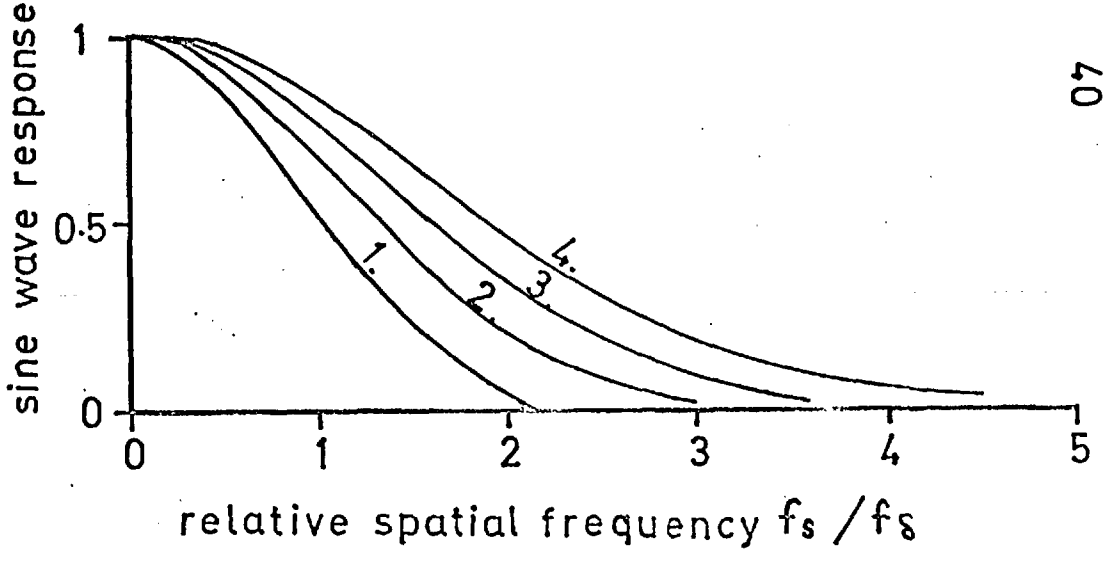

Fig.1.5(b)

where δ is the beam diameter, and $X = x - \frac{\delta}{2}$. The sine wave response of such an aperture is given in curve 1 of Fig. 2.5(b).

Now for such a beam scanning an insulating surface under cathode potential stabilising conditions, if the signal is not too high the fraction of the beam current m_b required to effect a discharge will be small. The leading edge of the beam profile will begin to discharge the insulator, but as soon as its surface potential has returned to cathode potential the rest of the beam current will be reflected $(1-m_b)$. Clearly for a low modulation factor the surface is discharged by a fraction of the total beam cross section, as can be seen in curves 2,3 and 4. The current distribution $i_s(x)$ for the effective beam profile is integrated to obtain the signal current is which is given by

$$i_s = \int_{-\infty}^{\infty} i_s(x)dx = m_b \int_{-\infty}^{\infty} i_b(x)dx \qquad (1.5)$$

$$= m_b I_b = m_b \frac{i_b \delta}{2} \quad \text{for a } \cos^2 \text{ beam.}$$

The sine wave response increases inversely to the width of the effective aperture, and the beam is said to be "self-

sharpening". The worst response is obtained for target potentials near the saturation value of the beam acceptance curve where m_b is close to unity and no beam sharpening can occur, this can be seen in Fig. 1.5(a) curve 1. Better responses are shown in curves 2, 3 and 4 of Fig. 1.5(b) which correspond to the same number curves in Fig. 1.5(a).

The overall response will depend on how the video signal is processed by the amplifier. For tube assessment it is normal to have a flat frequency response, although for most applications it is possible to apply a certain amount of aperture correction to the response (i.e. the falling frequency response of the tube is compensated by a rising response in the video amplifier up to its cut-off frequency).

1.6 The Speed of Response of the Charge Imaging Process

For any form of dynamic imaging it is necessary that the charge image build up is rapid, and the discharge by the scanning beam has no lag in its response.

If the charge image is written by photoemission or secondary emission processes the response is extremely rapid, and the charge build up time can be less than a nanosecond. This time is mainly determined by the potential

and structure of the collecting electrode.

When solid state band conduction is responsible for the charge image build up as in photoconduction and E.B.I.C. processes, there is a lag to the response due to charge carriers falling into "traps" (i.e. energy levels caused by impurities in the solid). Band conduction can take place some time after the initial charge writing process due to the thermal release of the carriers from these traps. This prevents all of the charge image being read at the end of the first frame, some of it being carried over into the successive frames where it can cause objectionable trailing effects to any moving object. These effects have been much reduced in the lead monoxide targets where th bulk of the material is an intrinsic semiconductor. It will be seen that for S.E.C. targets, where the charge image is essentially formed by secondary emission processes, that under normal conditions the lag is very low.

The ability of a low velocity beam to discharge the target depends on the axial velocity distribution of the electrons in the beam, and on the reflection coefficient of the target surface for low energy electrons. A typical beam acceptance curve for the current deposited on a target for voltage excursions below the first cross-over is given

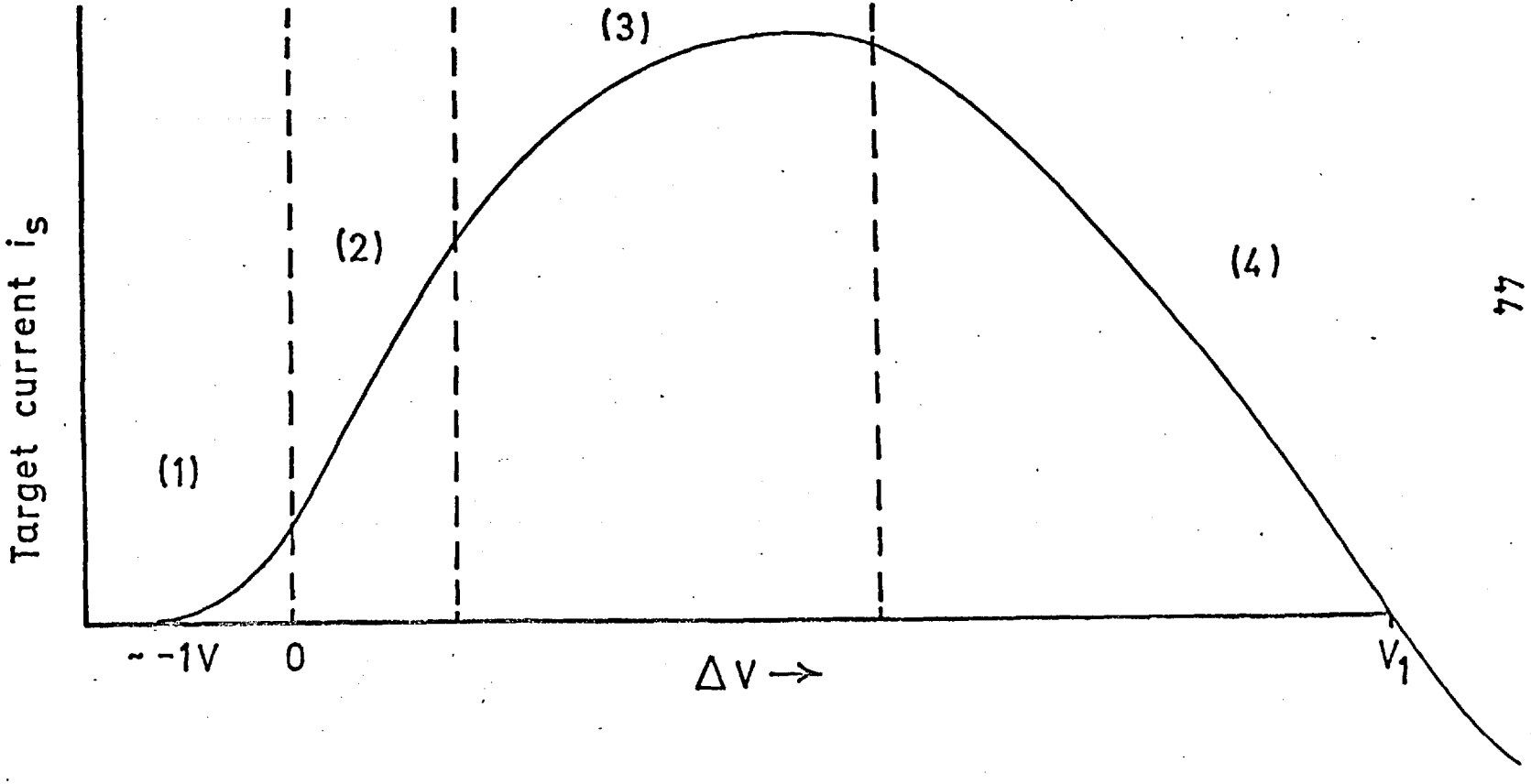

Fig.1.6 Beam acceptance curve at low voltage excursions

In Fig. 1.6. There are four main regions of interest. Region (1) is for $\Delta V<0$; here the shape of the curve is determined by the Maxwellian distribution, and the target current is is given by

$$i_s = i_\theta \exp\left(\frac{e\Delta V}{kT}\right) \quad \text{for } \Delta V<0, \tag{1.6}$$

where T is the temperature of the gun cathode and i_θ is a constant.

The more energetic electrons in the beam will eventually drive the potential of the target surface slightly more negative than the gun cathode. The second region (2) for $\Delta V>0$ is approximately linear and it has been shown by Meltzer[38] that the theoretical relationship is

$$i_s = i_\theta \left(1 + \frac{e\Delta V}{kT}\right) \quad \text{for } \Delta V>0. \tag{1.7}$$

In the region (3) the relationship is no longer linear owing to the effects of saturation of the beam current and the increase of the reflection coefficient of the target surface with voltage. The region (4) is where the effects of secondary emission by reflection from the target surface by the scanning beam becomes predominant,

the beam acceptance becoming zero at the first cross-over potential.

It is the region (1) which is responsible for the effects of discharge lag, because as the target surface goes progressively more negative, the velocity spread in the electron beam prevents an efficient discharge. The first scan of the charge image will not bring the target surface to its stabilising potential, and each successive scan will reduce the target potential in successively smaller steps until the lag signal obtained is comparable with the noise level.

In the region (2) the reciprocal of slope of the curve gives an effective beam resistance R_B such that

$$R_B = \frac{kT}{ei_6} \quad . \qquad (1.8)$$

It can be seen that for a low beam resistance a low gun cathode emission temperature is required, It is found in practice that a beam temperature of 1000°C is about the lowest that can be achieved whatever the source of emission. For discharge lag not to be objectionable the time constant $R_B C_t$ should be much less than T_f, where C_t is the target capacitance and T_f is the frame period. Discharge lag

can be reduced for a high capacitance target requiring a fast read-out time by applying a bias light so that the average operating potential is in the linear region of the discharge curve.

1.7 The Capacity of the Target

The effects of target capacity on discharge lag and resolution have already been discussed. It has also been pointed out that beam bending can limit the maximum allowable target surface potential, which for a given target capacitance sets a limit to the maximum storable charge. The choice of target capacitance is thus a compromise between the efficient discharge that can be obtained with a low capacitance target, and the high resolution and high charge storage that can be obtained with a high capacitance target.

The target capacitance used in practical devices is normally set by broadcasting requirements, and the physical size of the target has to be tailored to meet these requirements. The target capacitance of the image orthicon is set by how close the suppressor mesh can be mounted to the target, without causing such effects as microphony or the mesh and target touching. A spacing of $\sim$ .002" is possible, but this gives rather a low value for the target

capacitance of a standard 3" diameter tube (i.e. a target diagonal of 1.8"). To improve the signal to noise ratio of the stored image, the amount of stored charge had to be increased; this could only be done by making the target area larger to increase C_t, and for this reason the $4\frac{1}{2}$" diameter tube was developed.

The opposite problem has been experienced in tubes where a thin film of storage material is deposited on a signal plate. The early vidicons had very high target capacities and suffered severely from discharge lag. The target capacitance has been gradually reduced, by reducing the target area as in the 1" and $\frac{1}{2}$" vidicons[39], which required improvements in electron gun design, and by reducing the permitivity of the storage layer by depositing it in a porous form.

A thin layer, high capacitance target, could be of some use however for observing faint low contrast objects. It would have a higher resolution, and because of the large amount of charge that could be integrated in a long exposure, lower signal to noise ratio images could be detected. The single frame read-out could be done at slow speed so as to reduce the effects of discharge lag and amplifier noise.

1.8 Non-Linear Effects in the Storage Process (Gamma)

For a linear device the stored charge is directly proportional to the integrated light flux. This is a desired characteristic if photometric measurements are to be made on the video waveform. The gamma is said to be unity, as that is the index of the power law for the transfer characteristic. For cathode ray tube displays however the gamma is approximately two with the normal triode type gun structure, and so it is necessary to provide a signal from the camera which has a gamma of less than unity to compensate. Some storage processes have the required value of gamma, but for processes which have a unity gamma, gamma correction can be applied to the video amplifier.

Unity gamma is observed for photoemissive storage surfaces, provided the photocurrent is saturated, and no redistribution effects are allowed, such is the case with the C.P.S. Emitron. Secondary emission gives a similar result for the image orthicon at small signal levels, until the target surface is charged to the potential of the suppressor mesh, and the secondaries will no longer be efficiently collected, This causes an abrupt reduction in the gamma, at this point which is known as the "knee" of the characteristic. This effect provides a crude form of gamma correction.

The gamma of photoconductors[40] used in vidicon targets is typically ≈ 0.4 - 0.85 depending upon light level and signal plate potential, the gamma reducing at high light levels. The lead monoxide target has a gamma approaching unity[9]. This has been achieved by forming an intrinsic layer containing large single crystals between blocking contacts (P.I.N. diode). Such a layer will be relatively free from traps, and will have a high uniform internal electric field so that recombination of the carriers is less likely, even at high signal levels when the field is reduced.

The E.B.I.C. targets typically have gammas less than unity[18], with values similar to that of the normal vidicon targets (o.6 → 0.8) and a similar dependence on signal plate potential.

For an S.E.C. target the gamma is unity at small signal levels, but this gradually reduces at higher signal levels. This is because the target gain is not only dependent on the creation of the secondaries, but also on their efficient collection. This is done by the high internal electric field, and if this is reduced by a high voltage excursion on the scanned surface, causing its potential to approach that of the signal plate, then the collecting efficiency will drop, and the gamma of the signal will decrease.

1.9 The Charge Storage Time

For any storage medium it is necessary that there should be no lateral leakage of the charge image during the storage time. This is usually set by the requirements of a broadcasting system, and is usually very short $\simeq \frac{1}{25}$ sec., but if the target is used for a long exposure, in a similar manner to that of a photographic plate, then the storage time can run into hours, and extremely high resistivities are required for the storage material.

A leakage time constant $R_1 Ct$ can be defined for a given target, where R_1 is the leakage resistance and Ct is the target capacitance. This will produce a similar effect to the low intensity reciprocity failure observed in photographic emulsion, because, if the exposure time Te is too long (i.e. $Te > R_1 Ct$) then the charge will leak away at a rate comparable to that at which it is being stored, preventing an image integrating up on the surface.

Photocathodes can only be used for storage if they are formed as a mosaic with each picture element insulated from the rest; this can be done, but reduces the responsive quantum efficiency of the surface. Photoconductors do not make good storage targets as they are formed from semiconductors, and therefore do not have a high enough resistivity.

Insulating materials are the ideal storage materials, and either secondary emission or E.B.I.C. can be used as the method of charge creation. The S.E.C. process is of special interest, as the target material here is not only an insulator, but is of a physical form (porous) which lends itself to extremely high resistivities.

In the following chapters only the S.E.C. characteristics will be considered.

CHAPTER 2

THE USE OF TELEVISION TECHNIQUES IN THE DETECTION OF FAINT OPTICAL IMAGES

2.1 The ideal detector and quantum limitations of resolving power

It is a well known fact that, because of the discrete nature of light, very faint objects cannot be resolved in any detail with a limited exposure time, however efficient the apparatus of detection. These light quanta or photons, as they are called, are emitted randomly and have a Poissonian statistical distribution. For a mean number of photons $\bar{P}$ emitted from a source in a given time, there will be a root mean square deviation from this number, or a noise, of $\sqrt{\bar{P}}$ in the individual readings. Hence a signal to noise ratio can be defined for detecting this mean number of photons $\bar{P}$ as $S/N = \bar{P}/\sqrt{\bar{P}} = \sqrt{\bar{P}}$.

Now let us consider a surface onto which a mean number of photons per mm^2 $\bar{n}_{sl}$ are incident in a given time, and that we sample mean areas $\bar{a}$ of this surface. If between two adjacent areas the mean difference signal is $2C_o\bar{n}_{sl}\bar{a}$ as shown in Fig 2.1(i) where C_o is some fraction of the mean signal $\bar{n}_{sl}\bar{a}$, then the noise will be $(\bar{n}_{sl}\bar{a})^{\frac{1}{2}}$ and the difference signal-to-noise ratio K can be written ,

$$K = \frac{2C_o\bar{n}_{sl}\bar{a}}{(\bar{n}_{sl}\bar{a})^{\frac{1}{2}}} = 2C_o(\bar{n}_{sl}\bar{a})^{\frac{1}{2}} \qquad (2.1)$$

$$= 2C_o\left(\frac{s}{\bar{n}}\right)\bar{a}^{\frac{1}{2}}$$

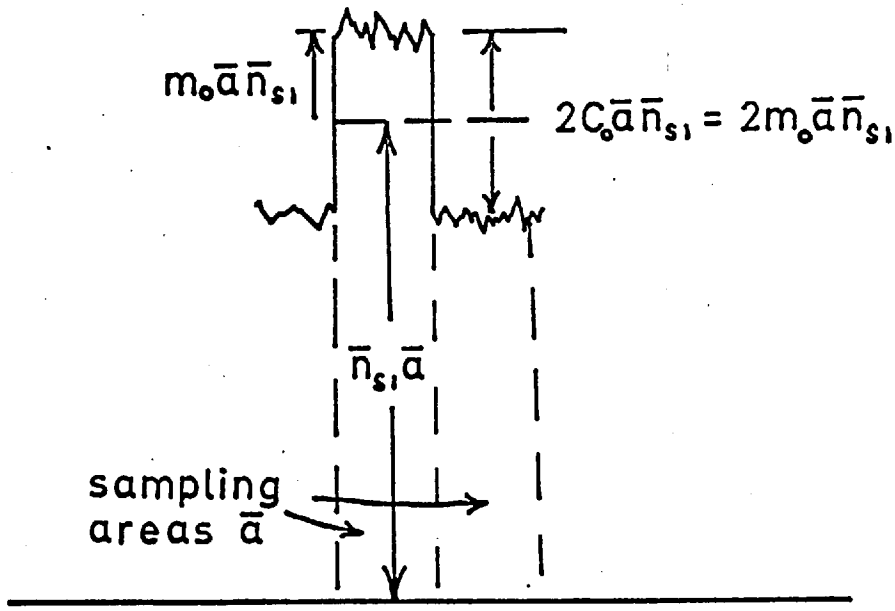

Fig. 2.1. (i)

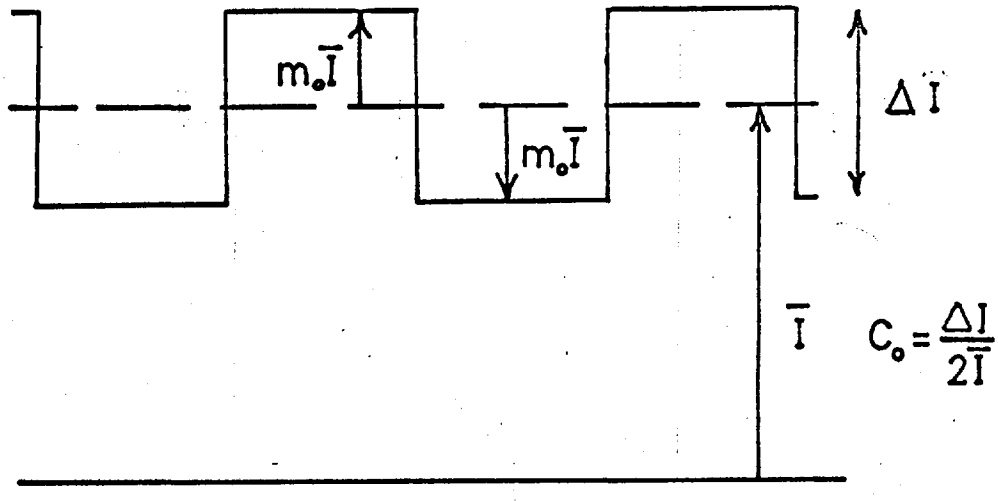

Fig. 2.1. (ii)

where C_o by definition is the contrast of the difference signal against the mean signal, and $(\frac{s}{n})$ is the absolute signal to noise ratio for unit area of the mean signal. A similar expression was first obtained by Rose[41,42,43] who obtained a threshold value for $K = K_c$ by a series of subjective measurements. K_c is known as the coefficient of certainty, and the value usually taken for it is 5, which means that when the difference signal is five times the r.m.s. noise, the probability of detecting this signal is already tending to unity. Fig 2.1(ii) shows a high light mean intensity $\bar{I}$ for a bar image of less than unity contrast C_o. The peak to peak variation in intensity is ΔI. Here we can also define the optical image modulation depth m_o as used by Schade[44], and it can be seen that,

$$C_o = \frac{\Delta I}{2\bar{I}} = \frac{2\bar{m}_o\bar{I}}{2\bar{I}} = m_o \qquad (2.2)$$

Let us consider using a Baum[45] pattern as a test image, the resolution wedge is so designed that the ratio of the length l to width w of the bars in the wedge is a constant over the range of spatial frequencies in the wedge,

$$\text{i.e. } l = 10w \text{ and } w = \frac{1}{2f_s}$$

where f_s is the spatial frequency of the bars of width w. This is so designed to keep the coefficient of certainty a constant. Therefore the sampling area $\bar{a}$ as seen by the

eye is,

$$\bar{a} = wl = 10w^2 = \frac{10}{4f_s^2} \quad (2.3)$$

For a nominal white light source the conversion equation between the mean number of photons per mm^2 $\bar{n}_{sl}$ and the mean exposure $\bar{E}$ in metre candles seconds is,

$$\bar{E} = \bar{n}_{sl}/7.5 \times 10^9 \text{ m.c.s.} \quad (2.4)$$

For fs in the pattern to be visible, from equations (2.1) (2.2) and (2.3) and substituting in (2.4)

$$\bar{E} = \frac{K_c^2 fs^2}{m_o^2} \times 1.33 \times 10^{-11} \text{ m.c.s.} \quad (2.5)$$

Taking the coefficient of certainty $K_c = 5$ as used by Rose and for an image of 100% contrast i.e. $m_o = 1$, then the minimum exposure $\bar{E}_o$ is,

$$\bar{E}_o = f_s^2 \times 3.3 \times 10^{-10} \text{ m.c.s.} \quad (2.6)$$

or expressing the resolving power as a function of the mean exposure $\bar{E}$ and the optical image modulation m_o,

$$f_s = m_o \bar{E}^{\frac{1}{2}} \times 5.5 \times 10^4 \text{ line pairs/mm} \quad (2.7)$$

A plot of this function can be seen in Fig 2.3 for $m_o = 1$. This shows that even for an ideal detector in order to resolve high spatial frequencies, a large exposure must be made. If the intensity of the source is low, and a high resolution is required, then a long exposure time must be used. Even if such a relation could be realised

in practice to such high resolutions, the total storage capacity would have to become unrealistically large for such resolving powers to be achieved.

2.2 The intensifier and the ordinary S.E.C. tubes as detectors of faint optical images

A schematic diagram of an Intensifier S.E.C. tube is shown in Fig 2.2. The optical image is focused onto the primary photocathode, which is of the transmission type having a quantum efficiency σ_1; this can be of any type, and should be chosen to have the highest quantum efficiency in keeping with the required spectral sensitivity. Thus for an optical image consisting of a mean number $\bar{n}_{s1}$ photons per unit area (mm^2) incident on the photocathode, there will be a mean number of photoelectrons $\bar{n}_{s2}$ per unit area leaving the photocathode, together with a mean background count of $\bar{n}_{b2}$ electrons per unit area which are of various origins. These can be due to thermal emission from the photocathode, field emission, stray light causing extraneous photoemission, or perhaps produced by secondary emission processes during the electron imaging from the photocathode to the next stage. Thus $\bar{n}_2$ is the total mean number of electrons imaged onto the next stage, which is an intensifier stage with a mean electron gain $\bar{G}_p$. This consists of a phosphor-photocathode sandwich[46], where the two are closely optically coupled by means of a thin mica support membrane. The phosphor efficiency should be as

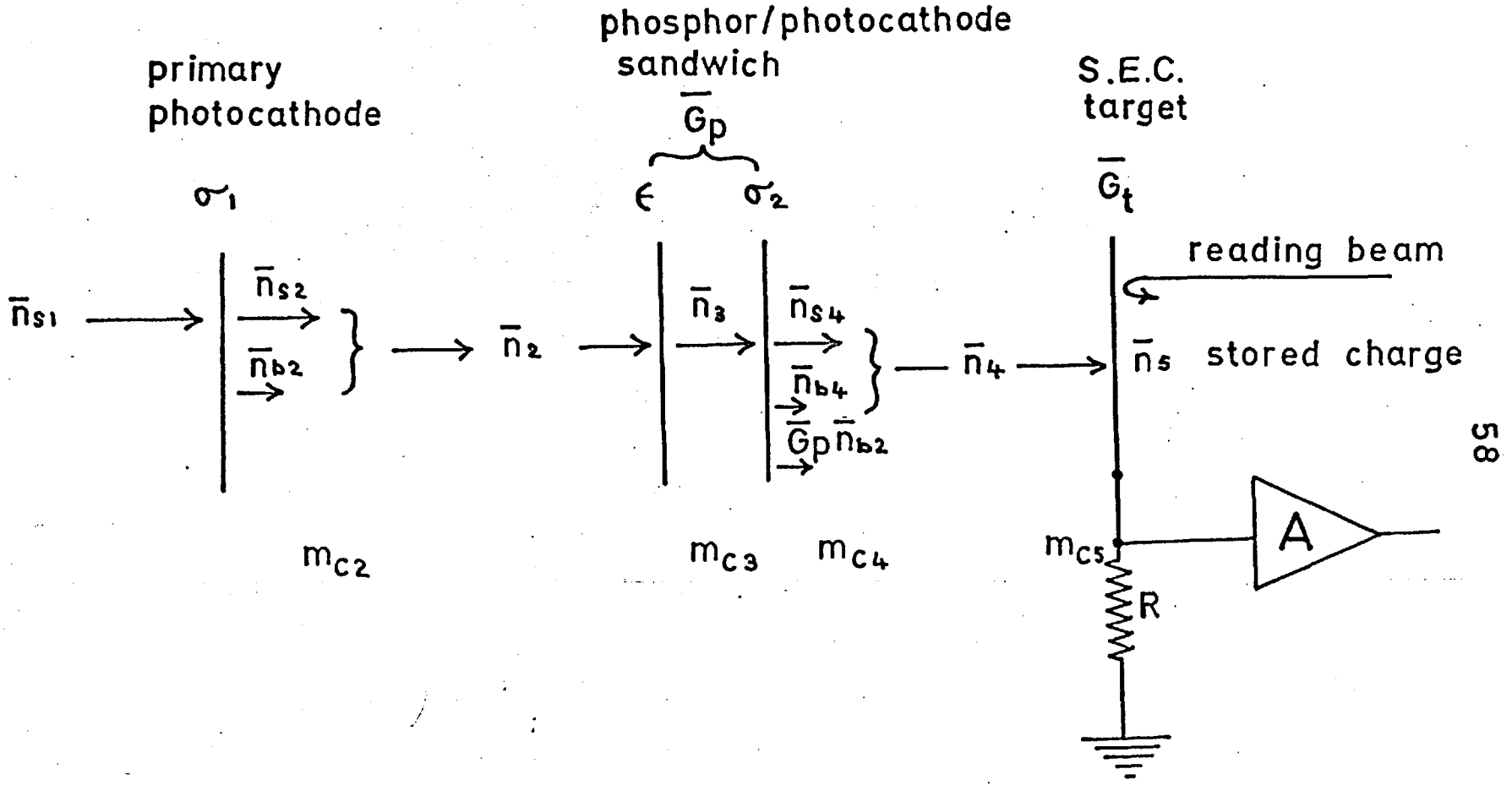

Fig. 2.2 Schematic Diagram of an Intensifier S.E.C. tube.

high as possible, as should the quantum efficiency σ_2 of the photocathode, which should be matched as closely as possible to the spectral response of the emission from the phosphor.

Hence, $\bar{G}_p = \varepsilon\sigma_2$. (2.8)

That is the $\bar{n}_2$ electrons per unit area incident on the phosphor give rise to $\bar{n}_3$ photons per unit area which are incident on the photocathode to produce $\bar{n}_{s4}$ photoelectrons per unit area, to which must be added another background count of $\bar{n}_{b4}$ electrons per unit area. Thus the mean signal imaged onto the S.E.C. target consists of $\bar{n}_4$ electrons per unit area, and because of the S.E.C. process the target has a high mean electron gain $\bar{G}_t$, and so the target will store $\bar{n}_5$ mean number of electron charges per unit area.

The charge image is read out by a low velocity electron beam scanning the target surface, the generated signal current, develops a video voltage across R which is processed by the amplifier A. From Fig 2.2 it is now possible to write down some relationships between the various particle densities. For the photoelectrons from the photocathode

$$\bar{n}_{s2} = \bar{n}_{s1}\sigma_1 \qquad (2.9)$$

For the signal photons from the phosphor,

$$\bar{n}_{s3} = \bar{n}_{s1}\sigma_1\varepsilon \qquad (2.10)$$

and for the signal photoelectrons from the photocathode of the sandwich,

$$\bar{n}_{s4} = \bar{n}_{s1}\sigma_1\varepsilon\sigma_2$$
$$= \bar{n}_{s1}\sigma_1\bar{G}_p \text{ (from 2.8)} \qquad (2.11)$$

and finally, for the stored signal electrons on the target,

$$\bar{n}_{s5} = \bar{n}_{s1}\sigma_1\varepsilon\sigma_2\bar{G}_t = \bar{n}_{s1}\sigma_1\bar{G}_p\bar{G}_t \qquad (2.12)$$

Schade[44] has called the ratio of the signal to the total particle density in a transfer stage i, the carrier modulation factor m_{ci}.

$$\text{i.e. } m_{ci} = \frac{\bar{n}_{si}}{\bar{n}_{si} + \bar{n}_{bi}} = \frac{\bar{n}_{si}}{\bar{n}_i} \qquad (2.13)$$

In general, every independent carrier or particle stream in a system is a source of noise and has a modulation factor m_{ci}. Therefore, for Fig 2.2 we can write,

1. For the particle stream from the photocathode to the sandwich,

$$m_{c2} = \frac{\bar{n}_{s2}}{\bar{n}_{s.2} + \bar{n}_{b2}} \qquad (2.14)$$

2. For the photons in the sandwich,

$$m_{c3} = \frac{\bar{n}_{s2}\varepsilon}{(\bar{n}_{s2} + \bar{n}_{b2})\varepsilon} = m_{c2} = \frac{\bar{n}_{s2}}{\bar{n}_3}\varepsilon \qquad (2.15)$$

i.e. no excess particle noise introduced from the phosphor

3. For the particle stream from the sandwich to the target

$$m_{c4} = \frac{\bar{n}_{s2}\bar{G}_p}{\bar{G}_p(\bar{n}_{s2} + \bar{n}_{b2}) + \overline{n_{b4}}} = \frac{\bar{n}_{s4}}{\bar{n}_4 + \overline{n_{b4}}} \qquad (2.16)$$

It can be seen that $\overline{\bar{n}_{b4}}$ has a negligible effect on m_{c4} since $\overline{\bar{n}_{b2}} \approx \overline{\bar{n}_{b4}}$ and therefore $\bar{G}_p\ \bar{n}_{b2} \gg \bar{n}_{b4}$.

4. m_{c5} for the target will be equal to m_{c4} unless there is an excess particle density left over from an incomplete discharge during the previous read out due to lag.

Now let us consider evaluating the signal-to-noise ratio for a unit area at the output of the system $(\frac{S}{n})_{syst}$. As the signal is common to all stages i in the system, and different values of noise are introduced at each stage, it is more convenient to consider the noise to signal ratio in each stage.

$$\text{i.e. } \left(\frac{S}{n}\right)^2_{syst} = \left[\left(\frac{n}{s}\right)^2_{I.1.} + \frac{\left(\frac{n}{s}\right)^2_P}{\gamma^2_P} + \frac{\left(\frac{n}{s}\right)^2_T}{\gamma^2_T} + \frac{\left(\frac{n}{s}\right)^2_A}{\gamma^2_A} \right]^{-1} \qquad (2.17)$$

where, $\left(\frac{n}{s}\right)_{I.1.}$ is the noise to signal ratio in the first image section.

$\left(\frac{n}{s}\right)_P$ is the noise to signal ratio of the phosphor

$\left(\frac{h}{s}\right)_T$ is the noise to signal ratio at the S.E.C. target

and $\left(\frac{n}{s}\right)_A$ is the noise to signal ratio at the output of the head amplifier

and where,

γ_P is the gamma of any non-linear effects of the phosphor stage transferred to the output (γ_P= 1 for the intensities used)

γ_T is a similar quantity for the S.E.C. target, and γ_A is the gamma correction applied to the amplifier.

Now using equations (2.13) to (2.16) and assuming all the noise sources obey Poissonian statistics then,

$$\left(\frac{n}{s}\right)^2_{I.1} = \frac{\bar{n}_{s2} + \bar{n}_{b2}}{\bar{n}^2_{s2}} = \frac{1}{m_{c2}\bar{n}_{s2}} = \frac{1}{m_{c2}\bar{n}_{s1}\sigma_1} \qquad (2.18)$$

No excess particle density is introduced by the phosphor, (as seen by equation (2.15) $m_{c3} = m_{c2}$ as $\bar{n}_{b3} = 0$), to add to the noise, but because the phosphor is made up of grains, this introduces a fixed pattern noise. The noise to signal ratio can be measured by uniformly flooding it with an electron beam, and scanning it with a microphotometer aperture.

If a_m is the area of the aperture, and $\left(\frac{N}{S}\right)_P$ the measured noise to signal then,

$$\left(\frac{n}{s}\right)^2_P = \left(\frac{N}{S}\right)^2_P . a_m \qquad (2.19)$$

The Background in the second image section gives,

$$\left(\frac{n}{s}\right)^2_{I2} = \frac{1}{m_{c4}\bar{n}_{s4}} = \frac{1}{m_{c4}\bar{n}_{s1}\sigma_1\bar{G}_p} \qquad (2.20)$$

and for the target any residual stored charges ~~lowers~~ increases the (n/s) to,

$$\left(\frac{n}{s}\right)^2_{T_{shot}} = \frac{1}{m_{c5}\bar{n}_{s5}} = \frac{1}{m_{c5}\bar{n}_{s1}\sigma_1\bar{G}_p\bar{G}_t} \qquad (2.21)$$

The target, being made up of aggregates of a low density insulator, also has a fixed pattern noise associated with it. This could be measured by flooding the target with a uniform electron beam, and then scanning the target with a reading beam of cross sectional area a_e, using a low noise method of read out to measure the fixed pattern noise to signal ratio (N/S)T.

$$\left(\frac{n}{s}\right)^2_{T_{\substack{\text{fixed}\\ \text{pattern}}}} = \left(\frac{N}{S}\right)^2_T . a_e \qquad (2.22)$$

Substituting equations (2.18) to 2.22) in (2.17) and putting $\gamma_p = \gamma_T = \gamma_A = 1$ we get,

$$\left(\frac{s}{s}\right)^2_{syst} = \bar{n}_{s1}\left[\frac{1}{m_{c2}\sigma_1} + \bar{n}_{s1}\left(\frac{N}{S}\right)^2_p . a_m + \frac{1}{m_{c4}\sigma_1 \bar{G}_p} + \frac{1}{m_{c5}\sigma_1 \bar{G}_p \bar{G}_t} + \bar{n}_{s1}\left(\frac{N}{S}\right)^2_T . a_e + \bar{n}_{s1}\left(\frac{n}{s}\right)^2_A\right] - 1 \qquad (2.23)$$

If the tube had behaved as an ideal detector then,

$$\left(\frac{s}{n}\right)^2_i = \bar{n}^2_{s1} / \bar{n}_{s1} = \bar{n}_{s1} \qquad (2.24)$$

It can be seen from equations (2.23) and (2.24) that in order to make $(s/n)^2_{syst}$ equal to $(s/n)^2_i$ the exposure must be increased by a factor F, (i.e. $\bar{n}_{s1}$ increasedby a factor F) which is the term in square brackets

$$\text{i.e.}\quad F = \frac{1}{m_{c2}\sigma_1} + \bar{n}_{s1}\left(\frac{N}{S}\right)^2_p . a_m + \frac{1}{m_{c4}\sigma_1 \bar{G}_p} + \frac{1}{m_{c5}\sigma_1 \bar{G}_p \bar{G}_t}$$

$$+ \bar{n}_{s1}\left(\frac{N}{S}\right)^2_T . a_e + \bar{n}_{s1}\left(\frac{n}{s}\right)^2_A \qquad (2.25)$$

The fact that this detector requires more quanta to obtain the same signal-to-noise ratio and hence resolving power, than the ideal detector, means that it is not making the most efficient use of the quanta available. This has led to the concept of equivalent quantum efficiency ξ, developed from the original ideas of Rose[41,42,43] by Fellgett[47]. The same concept is referred to by Clark Jones[48,49] as the detective quantum efficiency and is defined as

$$\xi = \frac{(S/N)^2_o}{(S/N)^2_i} \qquad (2.26)$$

where $(S/N)_o$ is the signal to noise ratio at the output and $(S/N)_i$ is the signal to noise ratio at the input. For an ideal device it is quite easy to show that equation (2.26) gives $\xi = \sigma$, the responsive quantum efficiency of the photocathode. From equations (2.23)(2.24) and (2.25) and using the definition of equation (2.26) we obtain that

$$\xi = \frac{1}{F} \quad . \qquad (2.27)$$

F is usually called the noise factor for the device, and can be used as a measure of the degradation of the signal to noise ratio, rather than using the equivalent quantum efficiency.

In Fig 2.3 we see a plot of equation (2.7) of the absolute photon limit for $m_o = 1$ (curve 1) for the threshold resolving power of the Baum pattern wedge. Curve 2 is for a good S·20 photocathode of 5% mean quantum efficiency (i.e. $\sigma_1 = 0{\cdot}05$) and it can be seen that the noise factor F is twenty The noise factor for the intensifier S.E.C. tube (I.S.E.C.) given by equation (2.25) can be simplified under special conditions. The amplifier noise term has been evaluated in the appendix A.1 for a valve head amplifier. Using this and assuming negligible fixed pattern noise in the phosphor and the target, and for carrier modulation factors of unity (i.e. no excess particle noise), then from equation (A.1.5), equation (2.25) becomes

$$F = \frac{1}{\sigma_1} + \frac{1}{\sigma_1 \bar{G}_p} + \frac{1}{\sigma_1 \bar{G}_p \bar{G}_t} + \frac{4 f_A^2 \left[(\alpha+\beta) \frac{1}{f_b} + \eta f_b \right]}{\sigma_1^2 \bar{G}_p^2 \bar{G}_t^2 \bar{n}_{sl}} \quad (2.28)$$

This will increase the threshold exposure for a given resolving power in accordance with the equations in Appendix A.2. This is shown in curves 3 and 4 for ISEC tubes with $\sigma_1 = 0.05$ $\bar{G}_p = 50$; curve 3 is for $\bar{G}_t = 100$ and curve 4 for $\bar{G}_t = 10$. The amplifier noise component is taken for the optimum bandwidth for the tube type M as in Fig. 3.1 i.e. $f_b = 200$ KH$_2$, and for $f_A = 30$ line pairs/mm. It can be seen that for both curves at low exposures where the amplifier noise predominates, the resolving power is proportional to the exposure, but at high exposures it approximates to the

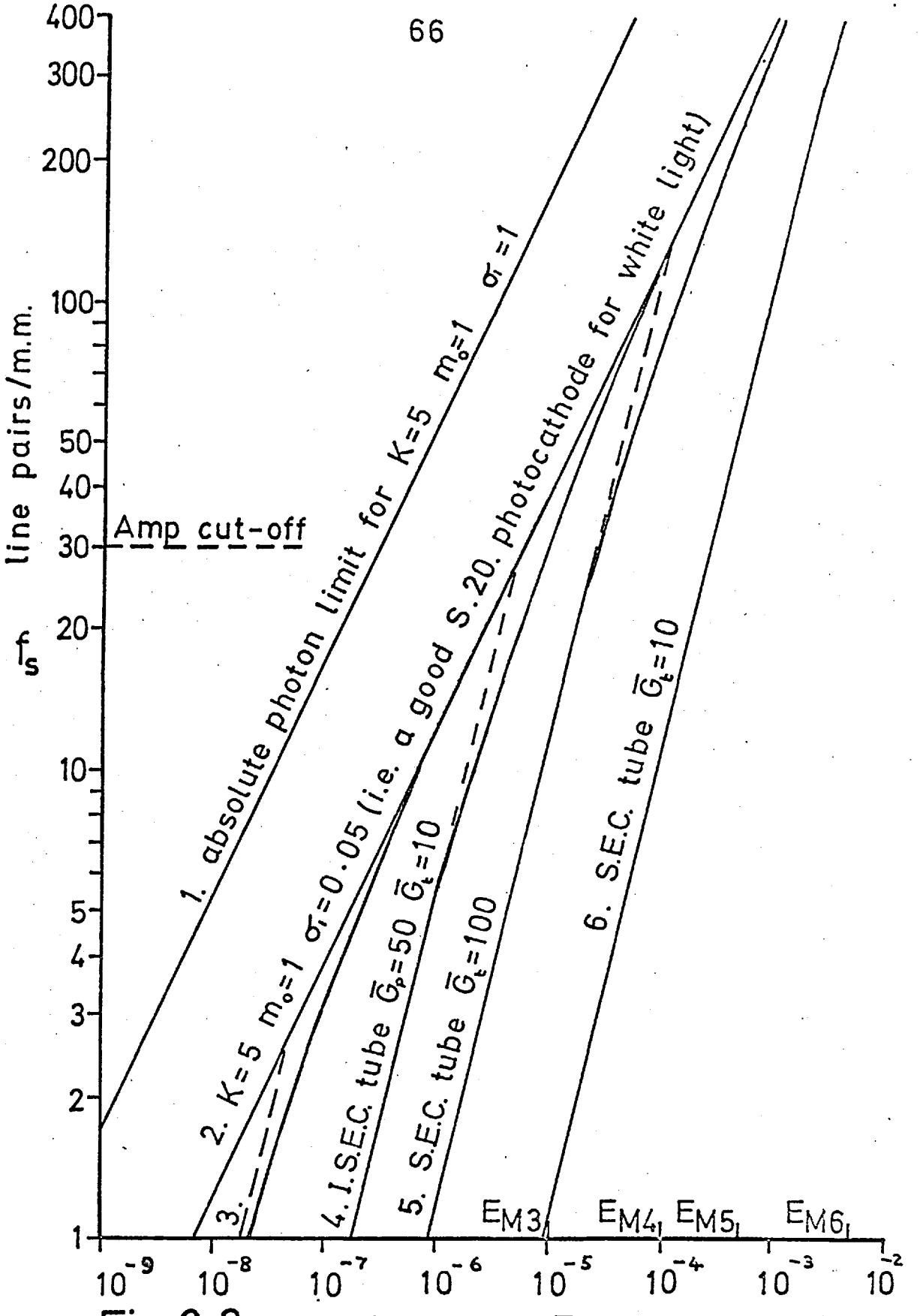

Fig. 2.3 Mean Exposure ($\bar{E}$) m.c.s.

resolving power obtained just from the photocathode noise. The tube with the higher target gain has the lower exposure threshold.

For an ordinary SEC tube without any pre-target gain an equation similar to equation (2.28) can be written,

$$F = \frac{1}{\sigma_1} + \frac{1}{\sigma_1 \bar{G}_t} + \frac{4 f_A^2 \left[(\alpha + \beta) \frac{1}{f_b} + \eta f_b \right]}{\sigma_1^2 \bar{G}_t^2 \bar{n}_{sl}} \qquad (2.29)$$

The resolving power functions are given in curves 5 and 6 for two SEC tubes using the same data as for the ISEC tubes, curve 5 being for $\bar{G}_t = 100$ and curve 6 for $\bar{G}_t = 10$. It can be seen from these two curves that one does not approach the photoelectron noise limit of resolving power until such large values of exposure that they could never be realised in practice.

Also shown in Fig. 2.3 is the maximum exposure $E_{M3} \ldots\ldots E_{M6}$ of which each tube is capable, taking for each case a target capacitance/unit area C_1 of 0.6 pf/mm^2 and a maximum target voltage excursion of 5V. This shows that all four tubes approach the photoelectron limit near their maximum exposures, but only those tubes with high gain remain photoelectron noise limited at small exposures.

2.3 The effect of background on resolving power at maximum exposure

One of the applications of such a tube as the S.E.C. tube is in the integration of faint images. From 2.3 it is obvious that to obtain maximum detail the exposure should be the maximum set up by the beam bending limit for the given target capacitance, that is E_{M5} and E_{M6} in the case of the ordinary S.E.C. tubes, and E_{M3} and E_{M4} in the case of the intensifier S.E.C. tubes. The amount of background present in these exposures will depend upon the length of the exposures. The dark current measured for a typical tube at a rather high ambient temperature of 45°C was 1.36×10^{-15} A/cm^2, this is in keeping with results by Charman and Hewitt[50] at this temperature, but should be taken only as an upper limit, as the tube is not normally working at such a high temperature. This represents an electron count $d\bar{n}_b/dt$ of 85 electrons/mm^2/sec. Hence, the carrier modulation factor for the first image section m_{c2} can be written down as a function of the exposure time Te. Using

equations (2.14), (2.9) and (2.4),

$$m_{c2} = \frac{\sigma_1 E_{M\ eq.} \times 7.5 \times 10^9 - \frac{d\bar{n}_b}{dt} \cdot Te}{\sigma_1 E_{M\ eq.} \times 7.5 \times 10^9} \qquad (2.30)$$

where $E_{M\ eq.}$ is the equivalent maximum exposure, that is the maximum exposure that could have been made in the absence of dark current as in Fig 2.3. A plot of m_{c2} for these four tubes is given in Fig 2.4 as a function of exposure time Te. As to be expected, the higher the overall tube gain, the lower the maximum exposure time.

As can be seen from equation (2.16) $m_{c2} \simeq m_{c4}$ for an ISEC tube provided $\bar{G}_p$ is large, also if the tube has little lag then $m_{c4} \simeq m_{c5}$. The noise factor for a tube with negligible fixed pattern noise can then be written from equation (2.25)

$$F = \frac{1}{m_{c2}}\left\{\frac{1}{\sigma_1} + \frac{1}{\sigma_1 \bar{G}_p} + \frac{1}{\sigma_1 \bar{G}_p \bar{G}_t} + \frac{4 f_A^2 \left[(\alpha+\beta)\frac{1}{f_b} + nF_b\right]}{\sigma_1^2 \bar{G}_p^2 \bar{G}_t^2 \bar{n}_1}\right\}$$

$$= \frac{1}{m_{c2}} F_1 \qquad (2.31)$$

where $\bar{n}_1$ is the photon equivalent density for the signal with the background and F_1 is the noise factor for carrier modulation factors of unity.

Equation (2.31) also holds true for the ordinary SEC tubes, F_1 in this case being obtained from equation (2.29) It can be seen from equation (2.31) that the noise factor for such tubes increases inversely with the carrier

Fig.2.4 THE REDUCTION IN THE MODULATION CARRIER FACTOR WITH THE INCREASE IN INTEGRATION TIME

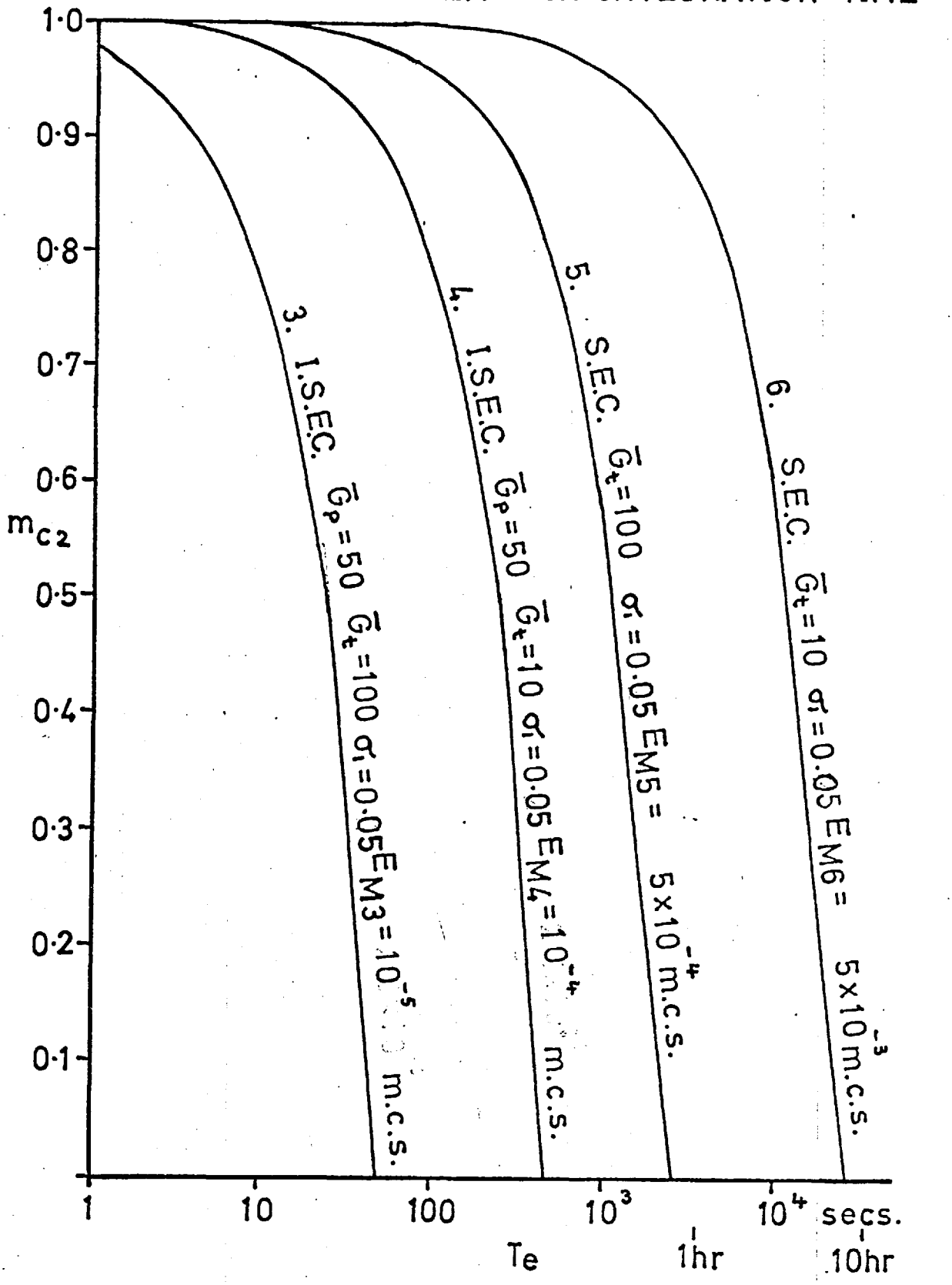

modulation factor m_{c2}, so it is advisable when carrying out an exposure with a long integration time to be aware of the value of m_{c2} in case it sets a limit to the detectability of the image.

2.4 The detection of faint low contrast images

Just as the carrier modulation factor m_{c2}, being less than unity due to the background in the first image section, causes the exposure factor F to be larger than unity, so that a longer threshold exposure is required to resolve the same detail, so will be the effect, if the image contrast is less than unity. This is expressed in Appendix A.2, where $\bar{E}_1$ is the threshold exposure in the photoelectron noise limited case as given by equation (A 2.2), and for the case where the photoelectron noise is small in comparison with the amplifier noise, then the system can be considered to have a constant noise source, and for this condition the threshold exposure E_1' is given by equation (A.2.5). In Fig 2.5 we see the effects of image contrast on resolving power of an ordinary SEC tube with a target gain of 100 (i.e. curve 5 of Fig 2.3). The other two curves show the resolving power as a function of the mean exposure for contrasts m_o of 0.1 and 0.01. It will be seen that for the tube to resolve 2 l.p./mm the minimum exposure at 100% contrast is 2 x 10^{-5} m.c.s. but if m_o is only 0.1 the $\bar{E}$ has to be increased to 2 x 10^{-5} m.c.s.

Fig.2.5. The effect of image Contrast on Resolving Power

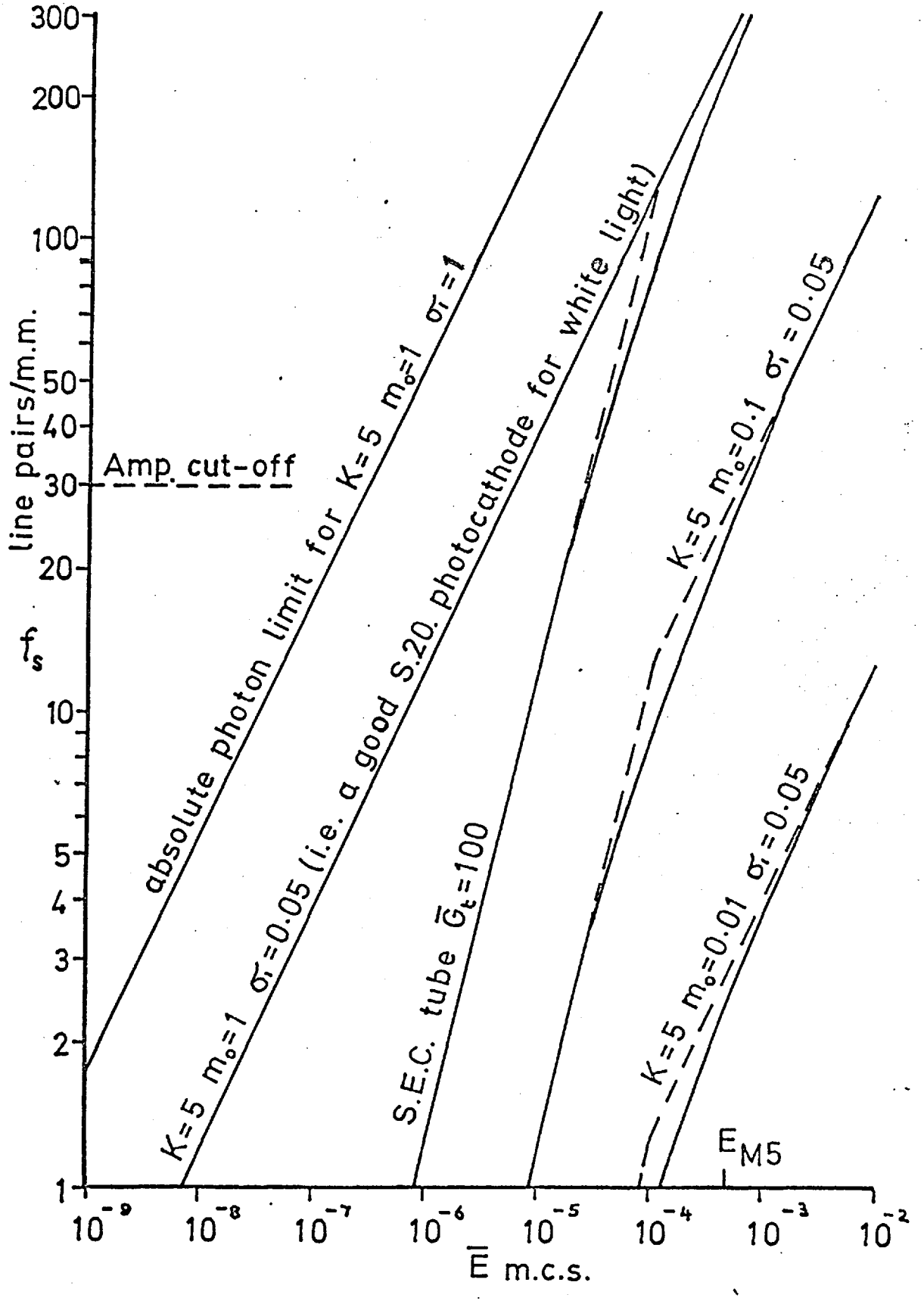

before the 2 l.p./mm pattern can be resolved, and if m_o is 0.01 then a minimum exposure of 4×10^{-4} m.c.s. is required.

It can also be seen that the exposure at which the photoelectron noise becomes important in the determination of the resolving power is a constant for any image contrast and occurs at a mean exposure of 8×10^{-4} m.c.s. The limited target capacity sets the maximum exposure at $E_{M5} = 1.25 \times 10^{-4}$ m.c. and thus it can be seen from Fig 2.5 that the resolving power at $m_o = 0.01$ is only ≈ 2 l.p./mm., where at $m_o = 0.1$ it is ≈ 20 l.p./mm and for $m_o = 1$ the photoelectron noise limited resolving power is ≈ 200 l.p./m.m. The last result cannot be realised in practice because of the Modulation Transfer Function of the device which will be discussed in 2.5. The limit to the detection of low contrast images is, therefore, set by the limited storage capacity of the device, which would have to be enormous if very low contrast images were to be resolved in any detail.

2.5 The effect of the Modulation Transfer Function (MTF) of the S.E.C. tube on the resolving power

Even for a 100% contrast optical image (i.e. $m_o = 1$) and a zero background signal (i.e. $m_{ci} = 1$), at high spatial frequencies, the modulation of the output signal of the system will not be 100%. This is because of the inability of the detector to image a scene through its various transfer stages with a point to point correspondence. A measure of this image smearing which sets a limit to the resolving power of

the system is the Modulation Transfer Function (M.T.F.). This determines the modulation depth of the signal at various spatial frequencies. This has already been discussed in Chapter 1, and in Fig 7.6 of Chapter 7 there is shown a plot of the sine wave response $R(f_s)_{syst}$ and the square wave respnse $r(f_s)_{syst}$ of a typical SEC tube.

In Fig 2.6 we can see a re-plot of curve 5 from Fig 2.3 for the SEC tube with $\bar{G}_t = 100$. Curve 1 of Fig 2.6 is the amplifier noise component of the resolving power, curve 2 being the resolving power for the complete noise factor, including photoelectron shot noise. It will be seen that over this exposure range the device is amplifier noise limited as curve 2 closely follows curve 1 especially at low exposures. Curve 3 shows the resolving power as a function of exposure when the square wave response M.T.F. of Fig 7.6 is included, the noise factor being modified for the case as in equation (A.2.7.). It can be seen that the M.T.F. coupled with the limited storage capacity of the target sets a limit to the maximum resolution obtained from the device.

For the case of an overall high gain device such as curve 3 in Fig 2.3 which is for an ISEC tube with $\bar{G}_p = 50$, and $\bar{G}_t = 100$, it is possible to approach the photoelectron noise limit at relatively low exposures as shown by curve 4 in Fig 2.7. Curve 3 shows the amplifier noise component and curve 2 the photoelectron noise component. It

Fig. 2.6. The effect of the M.T.F. on the theshold resolving power for an S.E.C. tube
($\sigma_i = 0.05$ $\bar{G}_t = 100$ $f_A = 30$ l.p./m.m.)

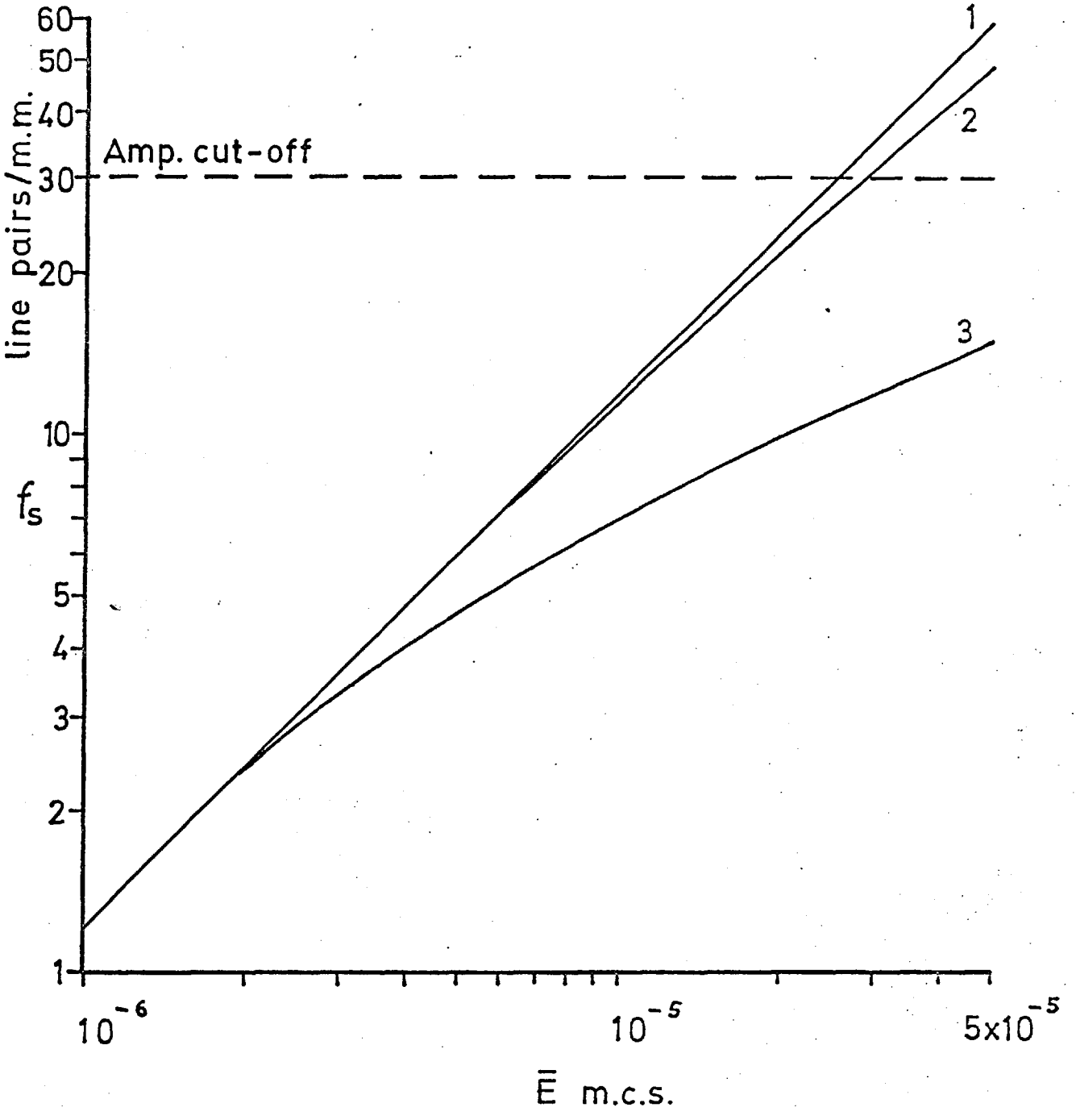

Fig.2.7 The effect of the Modulation Transfer Function upon the Resolving Power of an Intensifier S.E.C. tube with a high target gain

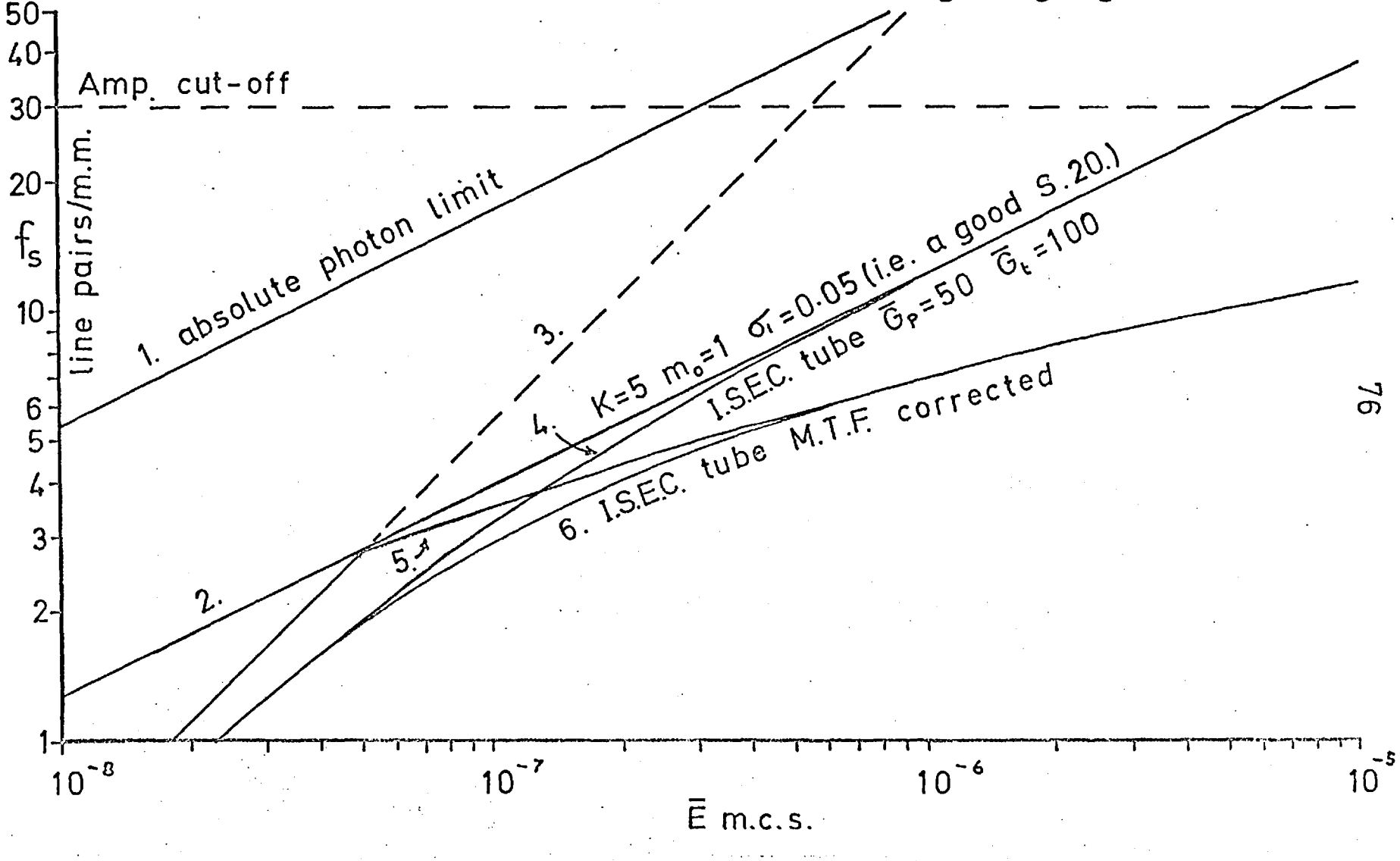

can be seen from curve 4 that at exposures greater than 10^{-5} m.c.s. the resolving power approaches that of curve 2 whilst below exposures of 10^{-8} it approaches that of curve 3. Curve 5 shows the MTF corrected resolving power of curve 2 given by equation (A.2.4) and curve 6 is the MTF corrected resolving power for the I.S.E.C. tube. This curve shows the maximum resolving power for the photoelectron noise limited case; it can be seen that the nearest one can get to the absolute resolving power as set by the photocathode noise in curve 2 is at an exposure of $1{\cdot}5 \times 10^{-7}$ m.c.s., any lower than this the amplifier noise becomes prohibitive, and any higher exposures are limited by the M.T.F.

CHAPTER 3

THE READ-OUT SYSTEM FOR THE S.E.C. TUBES

3.1 The head amplifier tube combination

All of the S.E.C. tubes made at Imperial College[51] and the majority reported by Westinghouse[52] have been of the signal plate read-out type. Unlike return beam read-out tubes, which have electron multiplication built into the tubes to provide a high signal level at the output, the signal plate read-out tubesmust be considered in conjunction with their head amplifiers. It can be seen from Chapter 2 that the head amplifier noise component can be a considerable proportion of the total system noise. To a large extent the signal-to-noise ratio that will be required in the head amplifier will depend upon the target gain $\bar{G}_t$. It would be advisable in most cases to work with the highest signal-to-noise ratio that is obtainable in head amplifier design, so that $\bar{G}_t$ can be kept as small as possible to prevent the limited storage capacity all being used to store too few events. Conversely, the highest signal-to-noise ratio that is obtainable with a given head amplifier design will depend upon the design features of the tube, as we shall see.

3.2 The best performance of a valve head amplifier

It has been shown by Beurle[53] that for the signal plate method of read-out, any noise that might be

introduced by the action of the electrons in the low velocity scanning beam causing fluctuations in the target surface potential, nominally at gun cathode potential, will be negligible in comparison to the noise in the amplifier. Beurle has also shown that the main contributions to noise in the amplifier are, the anode shot noise of the first valve, the grid shot noise of this valve, and thermal noise of the signal resistor often known as the Johnson noise. It is common practice to define an equivalent noise resistance R_n for this first valve, which is a means of dealing with the anode shot noise component in a similar manner to the Johnson noise of the signal resistor.

In Appendix A.3 an expression is derived for the noise to signal power ratio for a valve head amplifier similar to that obtained by Mende et al[54]. This is given by equation (A.3.14).

$$\left(\frac{N}{S}\right)^2_{App} = \frac{1}{\bar{n}^2_{s5pp}}\left[(\alpha+\beta)\frac{1}{f_b}+\eta f_b\right]$$

$$= \left(\frac{N_R}{S}\right)^2 + \left(\frac{N_G}{S}\right)^2 + \left(\frac{N_A}{S}\right)^2 \qquad (3.1)$$

where α is the Johnson noise coefficient of the signal resistor, and $(N_R/_S)^2$ its noise to signal power ratio.
β is the grid shot noise coefficient and $(N_G/_S)^2$ its noise to signal power ratio.
η is the anode shot noise coefficient and $(N_A/_S)^2$ its noise to signal power ratio.

From equation (A.3.17) it can be seen that to keep η as small as possible it is necessary to choose the lowest value of R_n for a given input capacitance. A triode is preferred as R_n of a pentode is approximately three times that of a triode. A triode having a high mutual conductance is necessary as,

$$R_n = \frac{2.5}{g_m} . \qquad (3.2)$$

Another advantage of having a high g_m is that it makes the noise contribution from the second and proceeding stages negligible, and hence only the first valve has to be a low noise triode. As can also be seen from equation (A.3.17) the value of C, the shunting capacitance is very important in determining the value of η since it appears squared in the expression. Unfortunately, the Miller capacitance in a triode tends to produce a large effective shunting capacitance and to achieve the necessary equalization a considerable amount of frequency dependent feedback has to be applied in the head amplifier. White[55] et al[55] have described such methods of feedback and James[56] has described a head amplifier which uses a cascode circuit at the input to reduce the effects of Miller capacitance.

For the amplifier tube combination the total shunting capacitance C will be,

$$C = C_S + C_L + C_A \qquad (3.3)$$

where C_S is the tube stray capacitance
C_L is the input lead capicatance
C_A is the input capacitance of the amplifier

It is of interest to draw up a table for the shunting capacitance of the tube-amplifier combination for two different tube constructional types, M is a tube with a target to mesh spacing of 2 m.m.s and K is a tube with a target to mesh spacing of .5 mm.

	M	K
C_S	11 pf	60 pf
C_L	20 pf	20 pf
C_A	6.4pf	6.4pf
C	37.4pf	86.4pf

It can be seen that although there is 6:1 ratio in C_S for the two tube types, there is only a 2:1 ratio in C. This is largely the result of the capacitance of the co-axial cable required to couple the tube to the valve head amplifier.

The head amplifier used had an R5559 high gm triode as the input valve in a cascode stage, for which the following data was applicable,

$R_n = 100\ \Omega$
$i_g = 4 \times 10^{-9}$ amps
$C_A = 6.4$ pf
$R = 2.7 \times 10^6 \Omega$ (value of signal resister used)

The coefficients α, β and η can be evaluated from equations

(A.3.15), (A.3.16) and (A.3.17). The anode shot noise coefficient will have one of two values depending upon which tube type the amplifier is operated with. Taking a rather upper limit value for $\bar{n}_{s5pp}$ of 10^5 electrons per picture point, (which corresponds to a target excursion voltage of 5V for a target capacitance of 600pf and with a 405 line system), then from equation (3.1) $(N_R/S)^2$, $(N_G/S)^2$ and $(N_A/S)^2$ can be evaluated for a bandwidth f_b. Fig 3.1 shows these components plotted as a function of the bandwidth f_b. Asβ is a constant for the valve, it can be seen that there is no point in making $\alpha << \beta$ which can be re-written using equations (A.3.15) and (A.3.16) to state that there is no point in making

$$R \gg \frac{2kT}{e\, i_g} .$$

Using the above data it can be shown that there is not much advantage to be gained in making R much greater than $1.3 \times 10^7 \Omega \approx 10\ M\Omega$.

This is a different conclusion to that arrived at by Theile[57] who did a similar calculation but ignored the grid shot noise component and hence concluded that at small bandwidths the higher the value of the signal resistor, the better the signal to noise ratio. As can be seen from Fig 3.1 for the head amplifier used, the Johnson noise is greater than the grid current shot noise, and this component becomes predominant at small bandwidths. The resultant

Fig.3.1 BEST PERFORMANCE OF R5559 AS THE HEAD AMPLIFIER TO TUBES STORING 10^5 ELECTRONS/PICTURE POINT

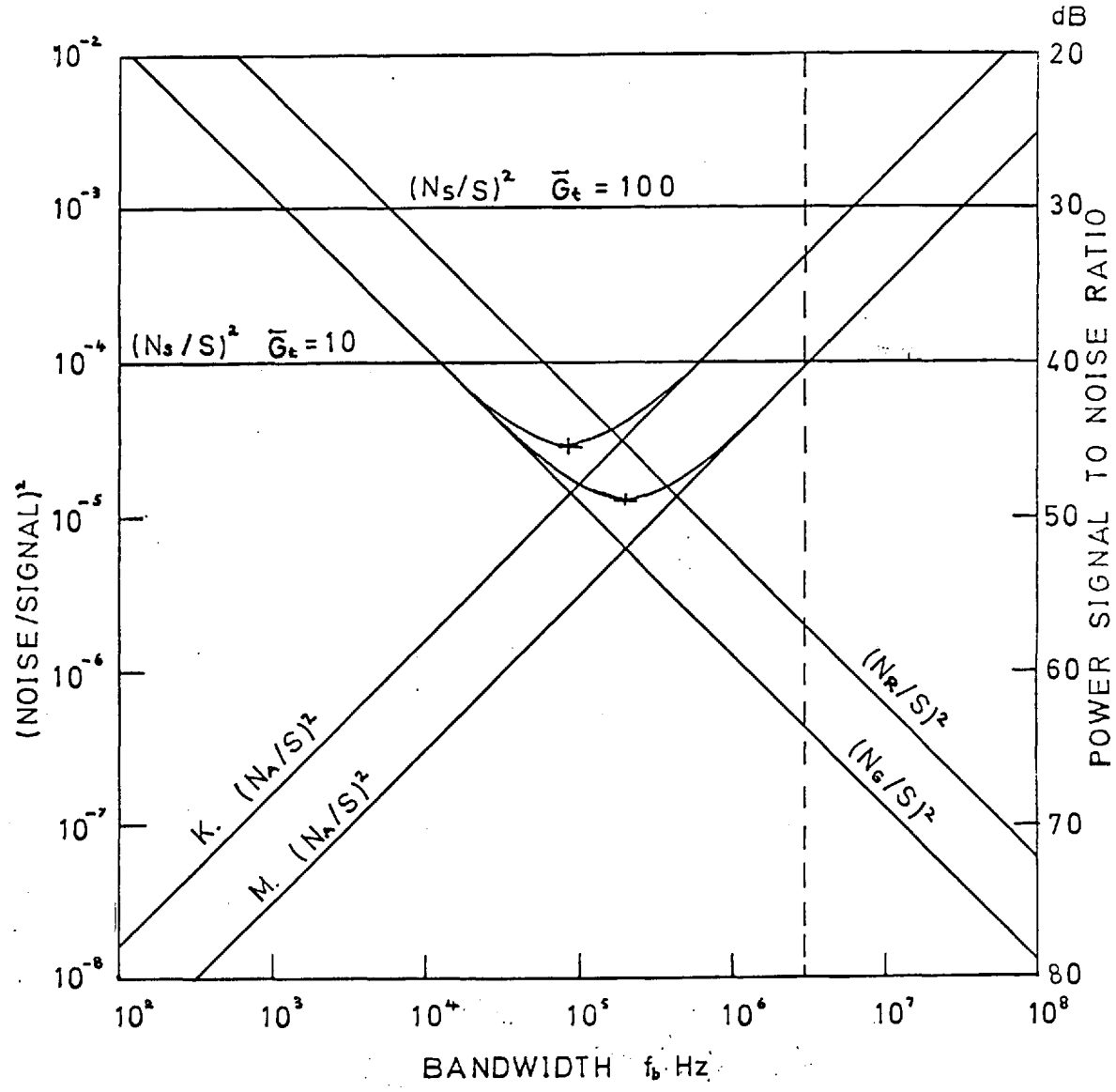

amplifier noise to signal power curves $(N/S)^2_{App}$ are shown for the best performance theoretical case assuming $R \geq 10M\Omega$.† It can be seen that there is an optimum bandwidth f_{bo} depending upon the tube type, at which the noise to signal ratio is a minimum. This value can easily be obtained by differentiating the expression of equation (3.1) with respect to f_b and equating to zero, and solving for f_{bo}.

This gives,

$$f_{bo} = \sqrt{\frac{\alpha}{\eta} + \beta} \qquad (3.4)$$

which for the best performance of the amplifier (i.e. when $\alpha << \beta$) becomes,

$$f_{bo} = \sqrt{\frac{\beta}{\eta}} = \sqrt{\frac{3ei_g}{8\pi^2 kTC^2 R_n}} \qquad (3.5)$$

(i.e. substituting equations (A.3.16) and (a.3.17) into equation (3.4))

The optimum bandwidth for the amplifier with a tube type M is 200 KHz, whilst the optimum for a tube type K is 90 KHz; the tube type M having the lower optimum noise to signal ratio.

It is of interest to consider the noise to signal ratio (N_s/S) for the stored charge, assuming it to be photoelectron shot noise stored by a noiseless target gain $\bar{G}_t$. This 'white' noise contribution from the signal is shown for

† See the note on page 241

target gains of 10 and 100. It can be seen in Fig. 3.1 that for a target gain of 10 at a bandwidth of 3 MHz (i.e. f_b required for a 405 line 50 field system) the amplifier noise for the tube type K is much greater than the photoelectron shot noise, whilst that for the tube type M. is comparable in value.

At their optimum bandwidths the photoelectron shot noise is greater than the amplifier noise in both cases; under such conditions there would be no advantage in using a return beam electron multiplier as has been pointed out by Theile.[57] For the case of $\bar{G}_t = 100$ it can be seen that both tubes should still be photoelectron noise limited at 3 MHz. In the light of what has been said of the effects of background, image contrast, and the MTF on the signal to noise ratios in Chapter 2. these results can only be taken to represent the best possible case. It also becomes impossible to store 10^5 electrons per picture point if higher definitions are required, because the capacitance of the picture element decreases, but the maximum voltage excursion permissible on the target surface is a constant.

In the above discussion no account has been taken of flicker noise caused by the random variations in cathode activity. It has a $\frac{1}{f}$ characteristic, and predominates in the sub audio frequency region. The last few years have seen the introduction of a range of small compact valves

/called

nuvistors. A triode form has an equivalent noise resistance of the order of 200 to 500 ohms[58], this seems large compared with the R5559, but because of their compact form stray capacitances are small, and the signal lead capacitance C_L can be very much reduced by mounting such a compact valve on the tube.

3.3 The best performance of a Field Effect Transistor head amplifier

In these days of solid state technology, it would appear that the obvious component to use in a head amplifier is the transistor. Its freedom from heater requirements, and its compactness, would make it the ideal component to mount directly onto the camera tube target pin, so that any lead eapacitance could be eliminated.

Unfortunately, normal bipolar transistors are essentially current operated devices, and they cannot be made to work with high enough input impedances to produce high signal to noise ratios. The last few years, however, have seen the introduction of a wide range of field effect transistors. Unlike normal bipolar transistors, the output current consists of majority carriers flowing in a continuous medium of semiconductor which can be made either n-type or p-type. This continuous medium is called the channel, and the end from which the majority carriers start is called the source, and the end to which they flow is called the drain.

The current in the channel can be controlled by forming a depletion region within the channel, by having a reverse-biased diode junction, fabricated from the channel and a transverse region of complementary doped semiconductor. The electrode to this region is called the gate, and is similar in its function to the grid in a thermionic valve; as it and the channel form a reverse biased diode, the input impedance will be very high, and very little gate current will flow. Any variation in bias potential will cause a variation in depletion width which will vary the channel current. Such a device is often referred to as a J.F.E.T. (i.e. a junction field effect transistor). A similar device, but which has a thin insulating membrane inserted between the gate electrode and the channel is referred to as an I.G.F.E.T. (insulated gate field effect transistor), and has the added advantage that the leakage current is extremely small so that extremely large input impedances can be used.

It has been shown by van der Ziel[59] that the total noise in a F.E.T. pre amplifier can be expressed by four components.

1. The thermal noise of the conducting channel modified by the effect of the channel width modulation.

2. A noise current which flows in the gate and is caused by noise modulation of the depletion layer width.

3. A noise current due to thermally generated reverse current in the gate channel junction.

4. The Johnson noise of the gate resistor

The noise due to 1. and 2. were represented by van der Ziel as an equivalent noise resistance, the theoretical lower limit for which is given by,

$$R_n = \frac{0.7}{gm} . \qquad (3.6)$$

It may appear at first sight, that if one is prepared to work with small bandwidths so the channel shot noise component can be made small, an insulated gate F.E.T. would be preferable to a junction F.E.T. This would reduce the gate shot noise component and enable a high value of signal resistor to be used to keep the Johnson noise small. Unfortunately, the mutual conductance, gm, of the IGFET's is typically much less than that for the JFET's, a value of 2mA/V is a good figure for the former, whilst a value of 7mA/V is not uncommon for the latter. Equation (3.6) gives an indication of the equivalent

noise resistances to be expected in both cases, but this must only be taken as a lower limit as it is found in practice that R_n is not a constant for these devices but increases as the frequency f decreases. This means that the channel shot noise does not decrease as rapidly with decrease in bandwidth as does the anode shot noise component of a valve. Hence, even if the device has an extremely high input impedance so that Johnson noise and gate current shot noise components are very small, then even at small bandwidths the channel current shot noise can be the limiting component of the system. Although a JFET does not have such a low leakage current as a IGFET, the current is still small and of the order of picoamperes. Both Blalock,[60] and Smith and Cline[61] have used JFET's in preamplifiers with signal resistors of the order of 10^9 ohms.

The noise characteristics of FET's cannot be given by a simple number or equation, and even transistors of the same type differ widely in their characteristics. At low frequencies a $\frac{1}{f}$ noise component exists due to surface recombination and prevents a simple figure being quoted for an equivalent noise resistance.

Manufacturers have quoted the noise of these devices in many ways, such as spot noise figures at some frequency and input impedance, but perhaps the most informative now being given by some manufacturers is a curve of the equivalent input current and voltage generators as a function of frequency. Such curves are given in Fig 3.2 for a JFET type 2N3684, where e_n is the input noise voltage in microvolts per root cycle, and i_n is the input noise current in picoamperes per root cycle. Hence a noise equivalent resistance can be defined as a function of frequency by,

$$e_n = \sqrt{4kTR_n} \qquad (3.7)$$

such that,

$$R_n = \frac{e_n^2}{4kT} .$$

By means of a log-log plot it can be shown that R_n can be represented by,

$$R_n = 10^6 f^{-0.75} \Omega \qquad (3.8)$$

for the range

$$10^2 < f < 10^5 \text{ Hz}$$

and for $f > 100\text{KHz}$ R_n is approximately constant at 100Ω.

By a similar log-log plot for the noise current per root cycle it is possible to obtain the following empirical expression for i_n,

i.e. $$i_n = .0017 + 3.8 \times 10^{-5} f^{0.55} \text{ pico amps/root cycle} \qquad (3.9)$$

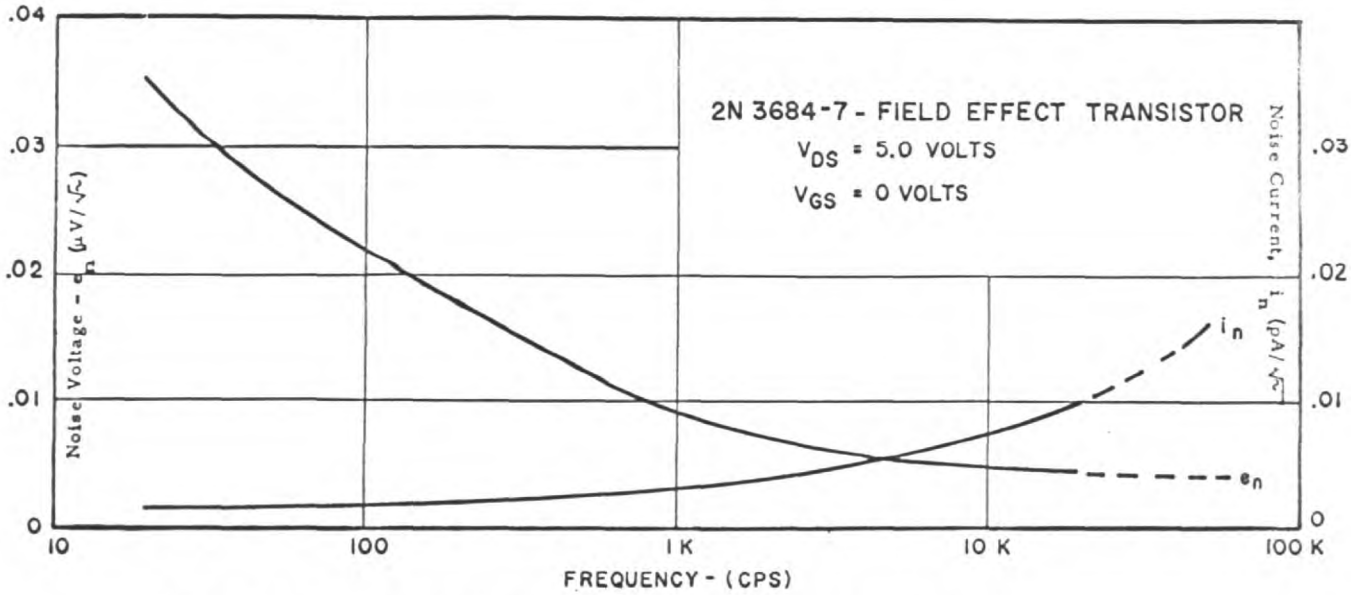

Fig. 3.2 EQUIVALENT INPUT NOISE VOLTAGE AND CURRENT VERSUS FREQUENCY

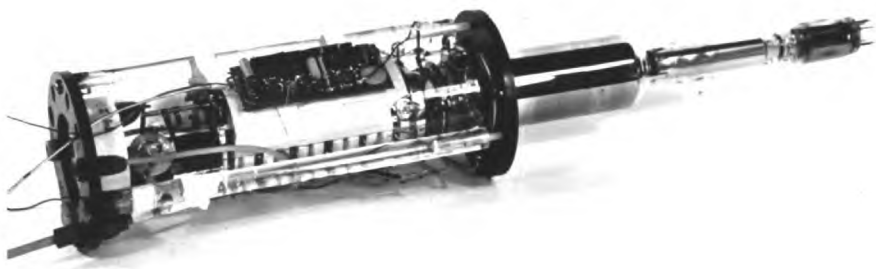

Fig. 3.3 Photograph of an S.E.C. tube with a F.E.T. amplifier mounted near to the target pin

In Appendix A.4 an expression is obtained for the noise to signal in a head amplifier using equations (3.8) and (3.9) for the JFET type 2N3684.

The shunt capacitance C in equation (A.4.2) will be given as in equation (3.3), but the lead shunt capacitance can be made negligible by mounting such a small amplifier on the camera tube so that the target pin is connected directly to the input as shown in Fig 3.3. The total shunt capacitance for the same tube types as in the valve amplifier case† is given in the following table.† (see p.81.)

	M	K
C_S	11 pf	60 pf
C_L	~0 pf	~0 pf
C_A	8.2pf	8.2pf
C	19.2pf	68.2pf

It can be seen that for the tube type M, the absence of the lead capacitance has reduced C to about half of the value for the valve case. The improvement in the case of the higher capacitance is not so dramatic however.

A plot is given in Fig 3.4 for the signal to

Fig. 3·4. BEST PERFORMANCE OF A F.E.T. 2N3684 AS THE HEAD AMPLIFIER TO TUBES STORING 10^5 ELECTRONS/PICTURE POINT

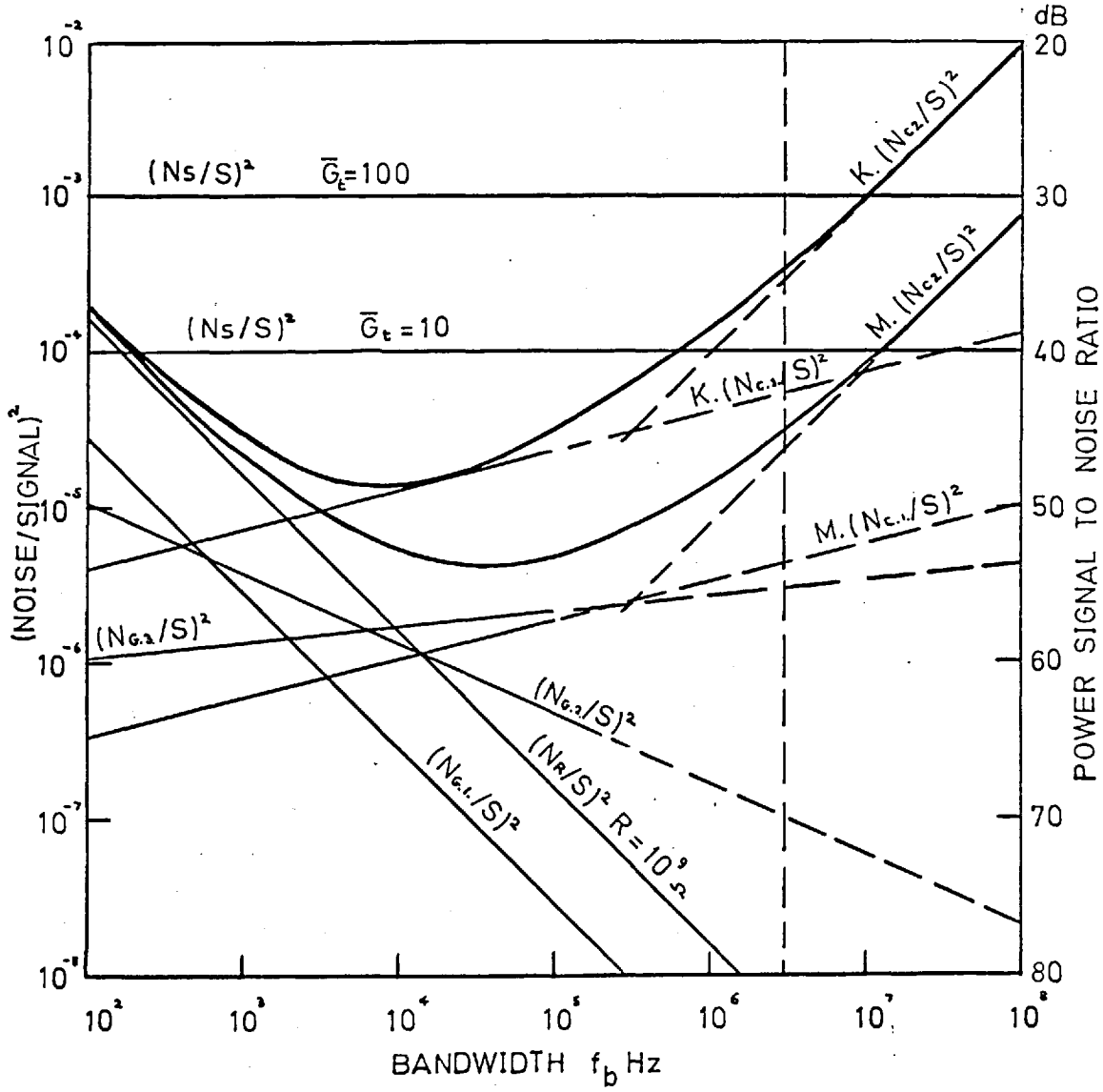

noise power ratio of such an amplifier using the above values of capacitance, and for a signal resistance of 10^9 ohms. These values being used in the equations of Appendix A.4. As R_n is approximately constant at 100 Ω for f ≥ 100KHz then equation (3.8) is no longer valid, so the channel shot noise component $(N_{c2}/S)^2$ for the high frequency components as given by equation(3.1) has been used. It can be seen from Fig 3.4 that the optimum bandwidths for the tube types M and K are 25 KHz and 10 KHz respectively; these correspond to optimum signal to noise power ratios of 53dB and 49dB respectively. Comparing these results with those of the valve amplifier of Fig 3.1 it can be seen that the F.E.T. amplifier has the higher signal to noise ratio at the corresponding optimum bandwidths, although it is correspondingly slightly worse at a bandwidth of 3MHz (optimum signal to noise ratios of the valve amplifier are 49dB and 45dB with tubes M and K respectively).

3.4 The advantages of slow speed scanning

It has been shown in sections 3.2 and 3.3 that there is an optimum bandwidth for operating the head amplifier tube combination which gives a maximum signal to noise ratio. In order to operate at these smaller bandwidths, it is necessary to scan at slower

rates than for conventional systems.

Once the bandwidth f_b to be used is decided upon, the line frequency f_L will be set by the definition required in the picture. If the picture height on the target is h, and for a raster with a 4 x 3 aspect ratio, then the equivalent spatial frequency cut-off is given by equation (A.55) of Appendix A.5:

$$\text{i.e. } f_A = \frac{3f_b}{4f_L h} . \qquad (A.55)$$

There is no point in making f_A very much greater than the limiting resolution (as set by the M.T.F. and the limited storage capacity of the tube) which is ~20 l.p./m.m. for the average S.E.C. camera. Now that the line frequency is fixed by equation (A.55), the frame frequency will be automatically determined by equation (A.5.4) such that,

$$f_f = \frac{\frac{2}{3}f_L^2}{f_b} \qquad (3.10)$$

Depending on the head amplifier tube combination used, and the definition required, typical frame times T_f range from 1 sec. to 10 sec. This would obviously be a serious disadvantage for broadcasting use, where high frame sampling rates are necessary, but for special applications such as in astronomy or low contrast spectroscopy a single image is built up by a long exposure, and so the rather long read-out time after the long exposure creates no problems.

One of the advantages of slow speed scanning is that the amount of charge that can be stored on the target will not tend to be current limited by the scanning beam; this will enable the target to be more efficiently discharged. As beam bending will still set a limit to the maximum voltage excursion that can be tolerated on the target surface, another advantage can be gained by making the target capacitance higher. More charge can now be stored, and as T_f is large the ratio $\frac{T_f}{C_t}$ can still be kept sufficiently large to effect an efficient discharge.

CHAPTER 4

A DEMOUNTABLE VACUUM SYSTEM FOR THE ASSESSMENT OF S.E.C. TARGETS

4.1 The need for such a system

The early work done at Imperial College by Filby[62] et al[62] on S.E.C. targets demonstrated the feasibility of making a sensitive camera tube, by incorporating either S.9 or S.20 photocathodes, and using a low velocity electron scanning beam for a signal plate method of read-out.

It soon became clear that the bulk of the work being done was investigating target behaviour, and that this could be done more efficiently by building a continuously pumped demountable target tester, which simulated the camera tube by having a writing section and a scanning reading section. The target could be installed through an O-ring seal, and this would eliminate the continuous need for glassblowing and the making of stainless steel electrode structures. Also, the need for photocathode processing would be eliminated by using a thermionic emitter or an inert ultra violet sensitive photoemitter in the writing section. The scanning gun structure could be made to push fit into a ceramic gun base, that could be mounted inside the vacuum space, so that it could be easily replaced without any glassblowing if the cathode became poisoned by water vapour getting into the system.

Such a system was built at the beginning of the author's

research period with the assistance of Dr. R.S. Filby[63].

4.2 Methods of writing an image

The early arrangement used a flood beam of electrons for writing the image; this was derived from a tungsten hairpin which was held at a potential of -7 kV with respect to the target signal plate potential. The flood current could be set by adjusting the voltage across the hairpin. A Modulator electrode in front of the hairpin was used to control the flood current, this could be made up to 100 v negative with respect to the hairpin. An equipotential drift space between this writing gun and the target was provided by a stainless steel cylinder held at the signal plate potential. The target was thus flooded by a cone of 7KeV electrons. Immediately in front of the target a metal foil was mounted into which a test pattern had been etched, this cast a shadow on the target, which was a replica of the test pattern etched in the foil.

This method yielded good results, (see Fig. 4.1) but there was a limit to the resolution that could be obtained in etching the test pattern into the .00075 in. copper foil. The etch factor obtained was such that undercutting of 10μm occurred on a straight edge, and the photoresist used for the etching process was of the printed circuit type which had a quoted line resolving width of .001 in; these two factors made it difficult to etch bar patterns with greater

Fig. 4.1.

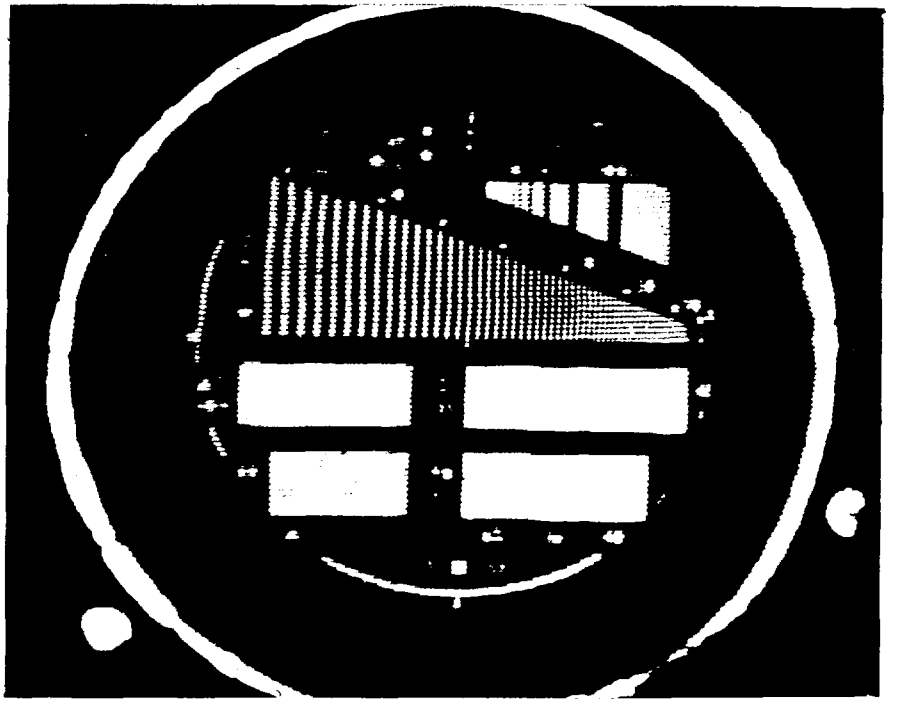

Copper foil Baum pattern, diameter 20mm.
(lines successfully etched down to ~ 13 lp./mm.)
KCl S.E.C. target Vsp = +30V. E.H.T. = 7KV.

than 10-15 line-pairs/mm.

Recently a higher resolution image section has been made by using an ultra-violet photocathode, which can be demounted to the atmosphere, on a silica end plate. To eliminate the need for quartz optics, and the need for imaging in the ultra-violet, high resolution test patterns have been made on the photocathode, so that only flooding with U.V. light is necessary.

A diagram of the system is shown in Fig 4.2. The ultra-violet emission is obtained from a mercury discharge lamp 1. from which the outer glass envelope has been removed. The intensity of illumination of the silica plate 5 can be adjusted either by placing the lamp at different distances from it, or by placing suitable absorption filters in the holder 2. (these can be meshes with different window ratios). The test pattern mask and the photocathode 6 are formed on the opposite side of the plate to that of the lamp. The test pattern being confined to the central region of the plate, so that paraxial ray imaging is valid to a good approximation. The photocathode is held at a potential of $\sim$-7kV, This is supplied by a polythene insulated cable 3 which is connected to a copper washer, which presses against a platinised ring that has been painted round the edge of the plate 5, and makes contact to the conducting mask of the photocathode 6. A perspex cylinder and collar 4 is

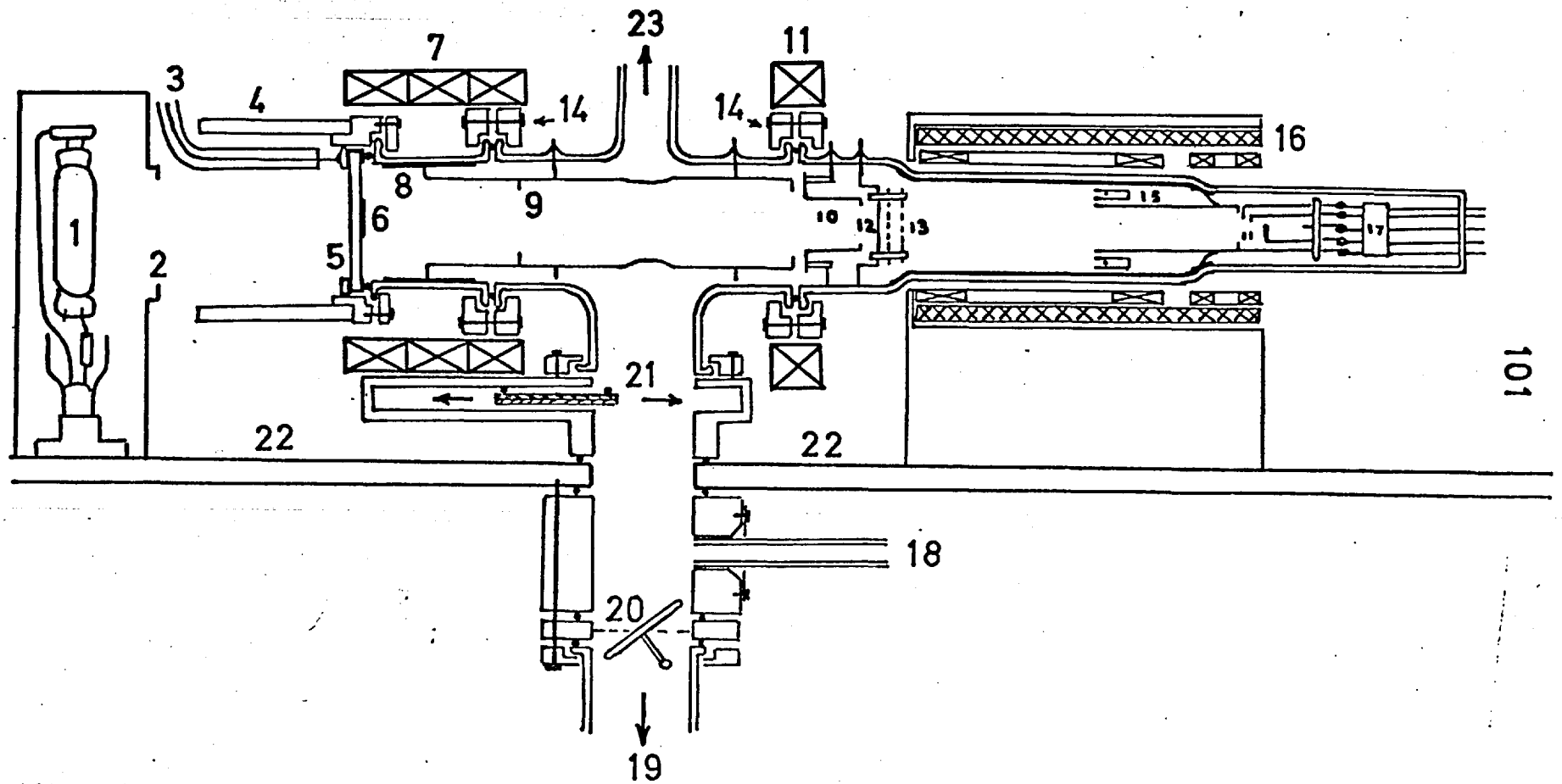

Fig. 4.2

fitted around the photocathode. It serves three purposes; firstly it aligns the silica plate and the O-ring seal to the pyrex glass flange, secondly it prevents electrical discharge, and thirdly it provides a safety guard for the high voltage region. A high electric field is established at the photocathode because the wall of the pyrex cylinder is platinised 8 to within a millimetre of the ground glass flange and is maintained at earth potential, which is also the case for the two stainless steel cylinders 9 and 10. An equipotential drift region is provided by sections 8, 9 and 10 to the target 12. Two thin magnetic lenses 7 and 11 are provided to image the test pattern from 6 onto 12. By adjusting the magnitude and ratios of the currents in the two coils it is possible to adjust the focus and magnification of the image on the target (magnifications of $\sim$ 1 and 0.5 were found to be the two most useful values). The duralumin clamps 14 were made to align and hold together (during pump down) the various sections of the apparatus at the O-ring seals, and were used as the supports for the magnetic lenses.

4.3 The making of the test pattern mask and the ultra-violet photocathode

A spectrosil silica plate was used for the photocathode end plate, because of its high transmission in the ultra violet down to wavelengths $\approx$2000 Å. A .25 in. platinum ring was

painted round the two faces and the edge of the plate, so that electrical contact could be made to the vacuum side of the plate from the atmospheric side. The plate was then placed in a demountable evaporating system, where aluminium was evaporated onto one face to such a thickness that the film became opaque. The plate was then brought out of the system and the aluminium film was coated with Kodak K.T.F.R. micro-circuit photoresist. An 8 mm diameter Baum Pattern was copied onto a maximum resolution photographic plate; this was used in a vacuum printing frame to expose the resist to an ultra-violet source. The resist became polymerised in the transparent areas of the photographic plate, and in the opaque areas it remained unpolymerised. By means of a development technique it was possible to dissolve away the unpolymerised resist leaving the aluminium film in these areas uncovered.

After a bake at 80^{o}C to harden the tender resist left on the plate, an etching solution of ammonium persulphate (2 gms/100 cc of H_2O) plus a drop of ammonia was used to remove the uncovered aluminium. After cleaning and vacuum stoving the silica plate, now containing a Baum test pattern etched into the aluminium film, was placed in a demountable evaporating plant to process the ultra violet photocathode. It was arranged so that the silica plate formed part of the wall of the vacuum chamber by means

of an O-ring seal. This was done so that an ultra violet lamp could be used to monitor the sensitivity of the photocathode during its evaporation. Palladium was found to be a suitable material, that gave good photoemission in the U.V. and was sufficiently inert so that it could be demounted to the atmosphere without severe losses in sensitivity. This was evaporated from a small bead on a tungsten wire.

There are four advantages of this method over that of the flood gun and foil method. Firstly, higher resolution test patterns can be etched if a high resolution resist is used, providing the film is thin enough. This is necessary because it is not possible to etch line widths much less than the thickness of the film because of the effects of undercutting. To etch a high resolution pattern into a foil, it has to be so thin that it becomes very delicate and no longer self supporting. For this reason it is much easier to deposit on a silica substrate a thin film which can be very thin and very robust.

Secondly, the size of the test pattern imaged onto the target can be varied with the electron optical design, this is not the case when the image is produced by the foil in the flood beam casting a shadow on the target.

Thirdly, it is possible to deflect the image onto different areas of the target, whereas in the case of the foil the image is fixed, since for the highest edge definition of the shadow,

the foil must be close to the target; this fixes the position of the image to that of the position of pattern in the foil. Fourthly, there is no need to provide a thermionic heater supply, thus eliminating any difficulties that can arise when such a supply has to be maintained at such a high potential as 7 kV.

4.4 The reading section

This was made to the dimensions of the miniature C.P.S. Emitron scanning section, as used for the sealed off S.E.C. tubes, so as to fit the focusing and scanning yoke 16 (Fig.4.2). The guns that were used were the ordinary 1-in.vidicon guns ; these were pushed into an internal ceramic base 17, so that they could easily be changed if their cathodes became poisoned by water vapour entering the system. The wall-anode was extended for the C.P.S. Emitron section by platinizing the inside of the glass tube from the shoulder where the 1 in. vidicon wall anode was clipped on by three 120° mounted spring clips, to the region of the meshes 13.

4.5 Installing and testing targets in the system

Whenever it was necessary to demount the system for the removal or installation of a target, the butterfly valve 20 was closed to isolate the diffusion pump from the system and a tap was closed on the backing line. Then dry argon was admitted through the roughing line 18 via a

constriction to reduce the line conductance so that the entering gas would not rupture the target. When the argon has reached atmospheric pressure in the system the gate valve 21 was closed, and the sealed system was removed from the table 22, and placed in a dry-box. Here the scanning section clamp 14 was undone, and the small cylinder electrode 10, and the target assembly (containing the target 12 and the meshes 13) were unclipped from their tungsten pins. The old target 12 was removed from the target assembly by unscrewing three clips, which held the titanium target ring in the aperture of the stainless steel plate of the target assembly, onto which the meshes 13 were mounted by three ceramic rods, the first mesh being separated by mica washers, and the second mesh by glass spacers. The new target was screwed into the assembly and if necessary the vidicon gun was changed, then the structure was reassembled in the dry-box. The system was brought back to the pump table 22 and placed over the pumping port, the roughing line was flushed with dry argon, the gate valve was opened and the system was evacuated. An ion gauge was connected to the stem 23, and once the pressure was below 2×10^{-6} torr the gun cathode was processed and the system was ready for use.

A photograph of the system is shown in Fig. 4.3, most

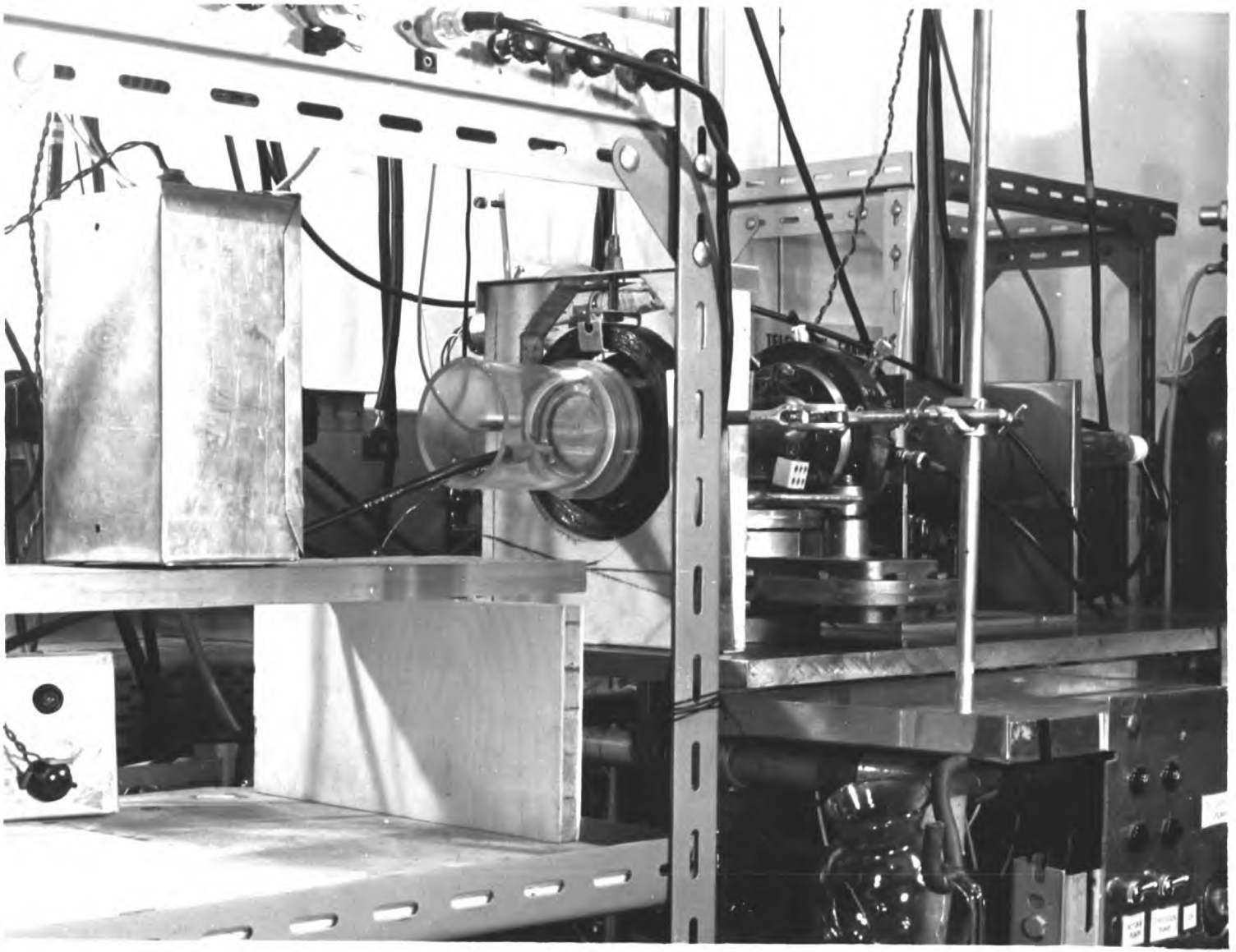

Fig. 4.3.

of the features of Fig. 4.2 can be clearly seen. Apart from the connections to the base of the scanning section, the signal plate lead to the target, and the leads to the two mesh pins were the only leads required. These were supplied through co-axial leads to a collar attached to the scanning section clamp 14; decoupling capacitors and resistors for the mesh supplies were mounted under this collar. The cylinders 8, 9 and 10 were connected to earth, and the signal plate was directly coupled to the head amplifier which was terminated to earth. The polarising field across the layer was achieved by altering the potential of the gun cathode with respect to earth.

A few results achieved with the system can be seen in Fig. 4.4. A photographic copy of the test pattern mask that was formed on the silica plate onto which the U.V. photocathode was deposited can be seen in Fig.4.4(a). The end of the resolution wedge represents $\sim$50 lp/mm. on the photocathode. Fig. 4.4(b) and (c) are photographic copies of images obtained on a phosphor screen which was substituted for the target. Observing the screen through a microscope, the end of the resolution wedge could be resolved for an 8 mm. diameter Baum pattern image, and for a 4 mm. diameter image $\sim$60 lp/mm. could be resolved. Unfortunately, it has been difficult to get good accurate photographic copies of these observations. Fig. 4.4(d)

Fig. 4.4. Results from the demountable vacuum system

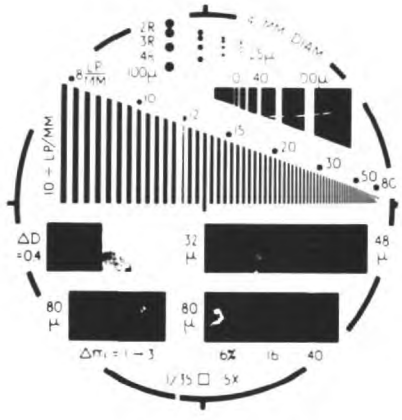

(a) Photographic copy of the test pattern mask (Baum pattern 8mm. diameter)

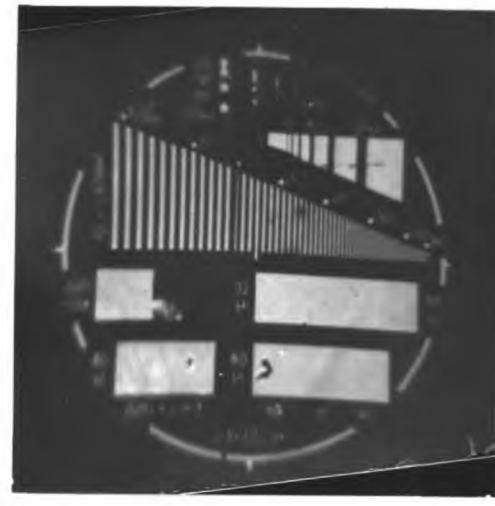

(b) Image on a phosphor in the target plane (Baum pattern ~ 4mm. diameter M ~ 0.5)

(c) Image on a phosphor in the target plane (Baum pattern ~ 8mm. diameter M ~ 1)
EHT = 7.5KV.

(d) Monitor display from a S.E.C. target (Baum pattern ~ 8mm. diameter)

shows a monitor display from an S.E.C. target. The image section magnification M is ~1 (i.e. the Baum Pattern is ~8 mm in diameter), and it can be seen that the resolution (~14 lp/mm) is considerably less than in the phosphor images of Figs. 4.4(b) and (c). This shows that the image section is not the resolution limiting element, which it tended to be in the flood beam and foil test pattern system.

CHAPTER 5

IMPROVING THE STABILITY OF THE S.E.C. TARGETS

5.1 How the targets can become unstable

As already mentioned in Chapter 1, an S.E.C. target has some promising characteristics: it has an inherent charge gain built into its storage process, which makes it very sensitive, the storage layer has an extremely high resistivity enabling very long storage times to be used, and there is no appreciable lag. But in spite of these good features it has the disadvantage that it can become unstable, under large signal conditions. This is because whenever cathode potential stabilisation is used there is always the danger that the scanned surface will restabilise at the nearest positive electrode potential, if the secondary emission coefficient of the scanned surface is allowed to become greater than unity. (see 2.3). For a material to produce a high S.E.C. gain it must be a good secondary emitter, and the consequence of this is to produce a scanned surface of the target whose secondary emission coefficient becomes greater than unity for relatively low incident energies of the beam electrons (i.e. the first cross-over potential V_1 in Fig 1.2 is relatively low).

The fact that cathode potential stabilisation is not an inherently stable mode of operation for such targets is a nuisance in itself, but to a certain extent it could be accepted as such, and the electrode potentials could be

adjusted to restabilise at cathode potential whenever an overload occurred, if it were not for the fact that permanent damage can occur to the S.E.C. target whenever anode potential stabilisation occurs. This is because, when this happens an extremely high internal field is created in the storage layer, owing to the fact that the signal plate potential is within a few tens of volts of the gun cathode potential, but the scanned surface has assumed the nearest positive electrode potential, which will be several hundred volts above that of the gun cathode, leaving a large potential difference across a layer whose thickness is only a few tens of microns. Such high internal electric fields cause dielectric breakdown to occur; this can cause the film to puncture in the region of the breakdown, which causes a blemish that resembles a "pin-hole"[64].

5.2 Methods of improving stability

(a) Mesh trip circuit

As already mentioned, if the voltage excursion ΔV on the target surface is greater than V_1, the surface will no longer cathode potential stabilise. The beam acceptance will take on a negative value since more electrons will leave the surface by secondary emission, than are given to it by the beam. Such a signal is known as a "blacker than black" signal, and can be used as a sign of instability, that occurs during the C.P.S. to A.P.S. transition.

This blacker than black signal can be used to trigger an electronic trip circuit, which can lower the potential of the field mesh (or wall-anode) momentarily to a potential.below V_1, then when the target surface has re-cathode potential stabilised, it will return it to its normal working potential.

Although such a circuit can be built and made to operate reasonably effectively, it has the undesirable feature that its operation depends upon detecting that instability has occurred. It is possible that damage may still be done to the target, there will be a temporary loss of vision in a continuously scanned system, and for a single frame integration, all the stored information will be lost.

(b) Stabiliser mesh

The scanned surface of the target can be prevented from becoming unstable, and restabilising at anode potential, by including a mesh close to the scanned surface that is at a potential below V_1. Such a mesh can be seen at 13 in Fig 4.2 along with the field or ion trap mesh. The action of the mesh is such that if the target surface is at a potential above that of the mesh, and is scanned by the reading beam, any secondaries produced will be returned to the target surface by the negative electric field until the target potential has been decreased to that of the mesh,

Then as the mesh potential is below that of V_1, fewer secondaries will leave the surface than beam electrons arriving, and the surface will continue to charge more negatively until it stabilises at cathode potential. The mesh is called a stabiliser mesh, and it will prevent the target surface charging more positive by electron emission once its potential has reached that of the mesh. Such a mesh was originally used in the stabilised C.P.S. Emitron[65] to render it completely stable to excessive illumination.

A similar mesh has been used in the demountable system and in some sealed-off S.E.C. tubes, and although it makes the target completely stable to overload signals it has its disadvantages. For the normal potassium chloride S.E.C. target, V_1 is only 15V, thus the mesh must be mounted very close to the target surface if a high electric field is to be maintained at the target surface so that the reading beam focus is not degraded. If, however, this spacing is small, there is a danger that the target may be damaged by touching the mesh, particularly during assembly, as in the dry assembly atmosphere it is possible for the target to charge up, and to be pulled to the mesh by electrostatic forces, unless a shorting link is always applied between the target and this mesh. During use the mesh may be in focus, and the increased capacitance can give rise to microphony and the shunting of the signal current which has already been discussed in Chapter 3. A

spacing of 0.3 mm has been found to be not an entirely satisfactory compromise.

(c) Flood gun

It was suggested by Dr. McMullan[66], that a flood gun could be used to prevent the target surface from becoming unstable. This would have to be arranged so that it covered the whole of the target, and the filament would have to be biased to a potential below V_1 but above the 'peak white' voltage excursion of the target surface, so that it would not affect the normal operation of the tube. For an overload condition, the flood gun electrons would land and prevent the target excursion potential rising above that of the filament bias. This being below the first cross-over potential V_1, would then enable the reading beam to return the target surface to the potential of the reading gun cathode.

Such an arrangement was installed in the demountable system, and can be seen at 15 in Fig 4.2. It consisted of a 0.001" tungsten filament mounted as an anulus round the outside of the vidicon wall-anode and surrounded by a suitable shield; this being insulated from the wall-anode by a mica strip. The bias potential and the filament current were both introduced via spare pins on the vidicon gun base. The gun was made to perform as expected, but there were some

undesirable side effects. Spurious signals were generated in the video circuits; these were attributed to the deflection of the flood beam by the scanning coils. This produced a variable beam acceptance current in the target mounting ring, which being at signal plate potential would be more positive than the flood gun. Also the flood beam current that was collected by the field mesh varied with the deflection of the flood beam; this varying current could cause the field mesh potential to vary since its supply was fed via a resistor. Such variations in potential would be capacitively coupled to the target where they would introduce a spurious signal into the video.

Although it may have been possible to make improvements to the design to eliminate these spurious signals, the greatest objection to the use of a flood gun is that the flood current would be unable to cope with very intensive illumination levels such as those created by flash bulbs. However brief, these very intense photocurrents are, once the voltage excursion has exceeded V_1, the target surface will restabilise at the field mesh potential from then on, and severe target damage will result.

(d) Modifying the target surface properties

If the target surface were made of a material such that δm in Fig 1.2, as obtained in reflection

by the reading beam, was less than unity, then V_1 would not exist, and it would not be possible to restabilise at the nearest positive electrode potential.

It is unlikely that such a material would make a good S.E.C. target, as for δ_m to be less than unity it would probably have to be a metal which could not be used for a charge storage layer, and also since S.E.C. is basically a secondary emission process if δ_m is small then it is to be expected that the S.E.C. gain will be small also. Things are not quite so bad as they seem, since stability can normally be obtained by imposing a less severe restriction, as will be shown, but quite a big improvement can be made if V_1 is increased for the surface. This is because if V_1 is higher, the stabiliser mesh can be held at a higher potential, and the same electric field can be maintained at the target surface with a larger mesh to target spacing.

From a table of the secondary emitting properties of materials given by Hachenberg and Brauer[67], it looked as if ZnS might be a promising material to use for S.E.C. targets to increase the first cross-over potential. Zinc sulphide was also chosen as it was readily available in a pure form, and it was a material that was known to be relatively easily evaporated under vacuum in thin films for anti-reflectant coatings.

It was found that it could be deposited in a low density porous form by evaporating in a few torrs pressure of argon.

Low density layers of ZnS 20μm thick were made, and found to have a first cross-over potential V_1 of 100V, but the target gain was only 10, which prevented it from being a very attractive target material.

It was suggested by the author that it may be possible to prepare a high-gain target, that also had a high crossover potential, by preparing a composite target of two low density materials. The first layer, that nearest the signal plate, being of a high secondary emitting material such as KCl, and the second layer that facing the scanning beam, being of the poorer secondary emitter such as ZnS. The former layer should make up the bulk of the target thickness to give it sufficient gain, whilst the latter layer should be as thin as possible, providing V_1 is increased to a suitable value. A cross section of a typical target is shown in Fig 5.1. It was found experimentally that the gain of the target decreased with an increasing thickness of ZnS, but V_1 was raised. The reduction in overall gain was quite small for a thickness of ZnS which gave $V_1 \simeq 50V$ (mean thickness of the order of a few tenths of a micron). The

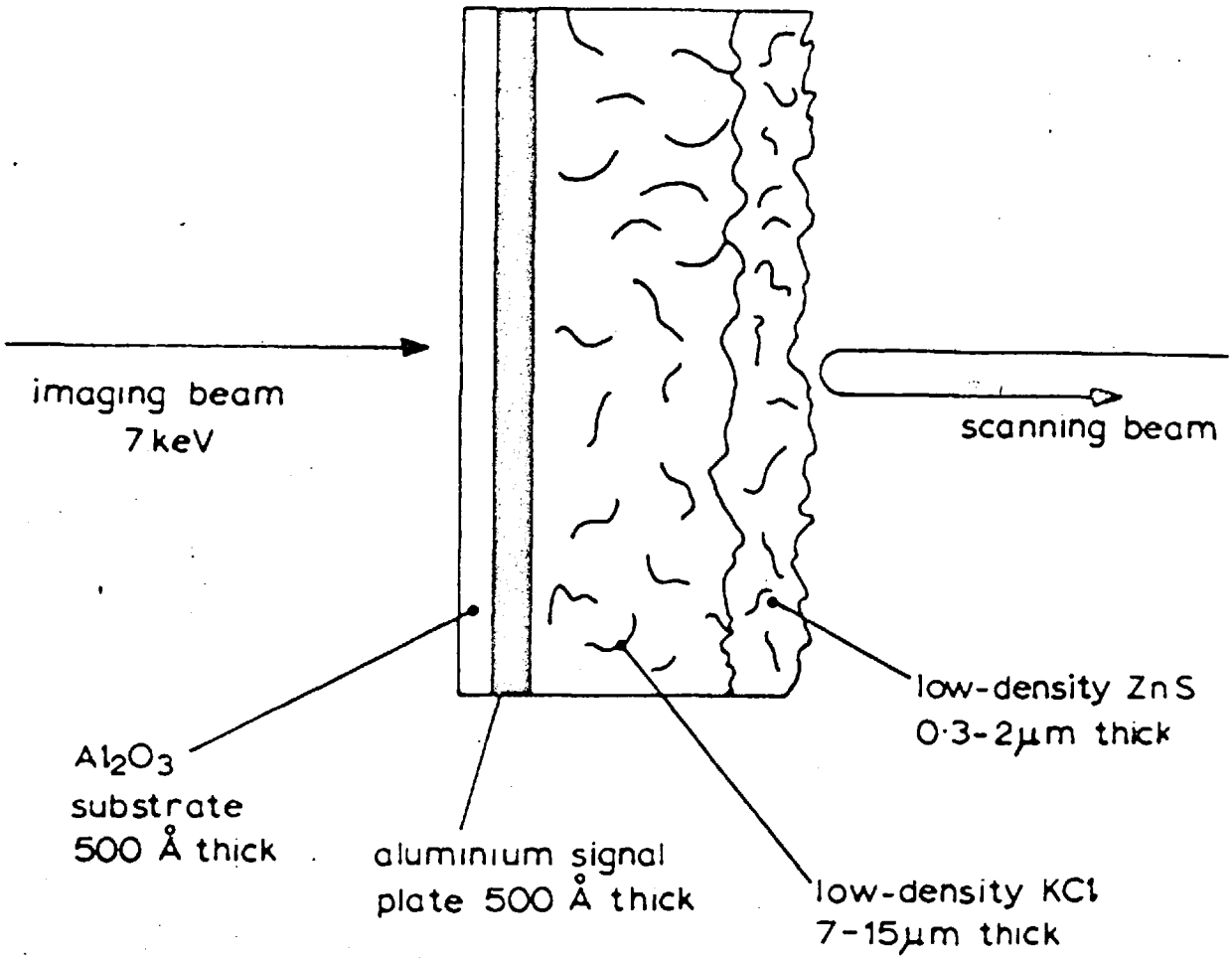

Fig. 5.1 *Cross-section of a composite target*

increase in V_1 enabled the stabiliser mesh to be held at a higher potential, and therefore to be placed further away from the target.

By using a slightly thicker covering of ZnS it was found that the target could be made inherently stable. The surface potential (of the scanned side of the target) could not be raised by the imaging electrons above the cross-over potential V_1, and thus the stabiliser mesh was no longer required.

To investigate the condition for stability the target gain G_t will be considered. It was stated in Chapter.1.that G_t had two components: the S.E.C. gain G_{SEC} due to the collection of secondary electrons by the signal plate, and the T.S.E. gain $G_{T.S.E.}$ due to those secondary electrons which leave the scanned surface of the target and are collected by the nearest positive electrode.

This was stated by equation (1.2) as,

$$G_t = G_{S.E.C.} + G_{T.S.E.} \qquad (5.1)$$

For normal small signal conditions with the signal plate at a positive potential of V_{sp} with respect to the reading gun cathode, then $G_{S.E.C.} \gg G_{T.S.E.}$ because the comparatively high internal electric field causes the secondaries to go to the signal plate except for those produced very near the scanned surface.

Now if the imaging beam is very large so that an overload condition exists, the storage surface potential will rise to a high positive value, causing the internal electric field to decrease, and then to reverse. This is assuming that a low potential stabiliser mesh is not mounted close to the storage surface. As the internal field falls $G_{S.E.C.}$ will fall, and will also reverse, but $G_{T.S.E.}$ will continue to increase as the reduction and the eventual reversal of the internal field enables more secondaries to leave the surface. The potential across the layer will eventually reach an equilibrium when $G_{S.E.C.}$ is equal and opposite to $G_{T.S.E.}$ so that G_t is zero. If the equilibrium potential[68] is V_E, then the maximum value of the potential excursion ΔV of the surface from its cathode potential stabilised value is,

$$\Delta V_{max} = V_E + V_{SP} \qquad (5.2)$$

Now two conditions can exist:

(1) $\Delta V_{max} \geq V_1$

This is the unstable condition, because as the potential excursion is greater than the first cross over potential, the reading beam will charge the surface even more positively, unless a stabiliser mesh is fitted at a potential below V_1.

(2) $\Delta V_{max} < V_1$

This is the stable condition, since the reading beam will always be able to discharge the target following an overload.

For a 7.5μm KCl target, $V_1 \simeq 15V$ and $V_E \simeq 80V$, with normal mesh spacings and potentials, so the stability condition (2) cannot be satisfied for any positive signal plate potential (which is the normal high-gain mode of operation). If the KCl layer is covered with a 1.5μm layer of ZnS, not only is V_1 increased to 90V but V_E is only 25V. This is because $G_{T.S.E.}$, which depends on the number of secondary electrons produced near the surface is decreased. With this thickness of ZnS $G_{S.E.C.}$ is also less, but to a certain extent V_{sp} can be increased to offset this. It can be seen from equation (5.2) and the condition (2) when using the above values of V_1 and V_E, that for the target to be stable V_{sp} must be less than 65V. This is not found to be the real limitation in practice as for V_{sp} higher than 55V spurious white signals are developed owing to the reading beam beginning to penetrate right through to the signal plate. In Fig 5.2, $G_{S.E.C.}$, $G_{T.S.E.}$ and G_t can be seen plotted as functions of the target surface excursion potential ΔV, for $V_{sp} = 50$ V. As can be seen, the typical small signal gain of a composite target with $V_{sp} = 50V$ is about 100, ΔV_{max}

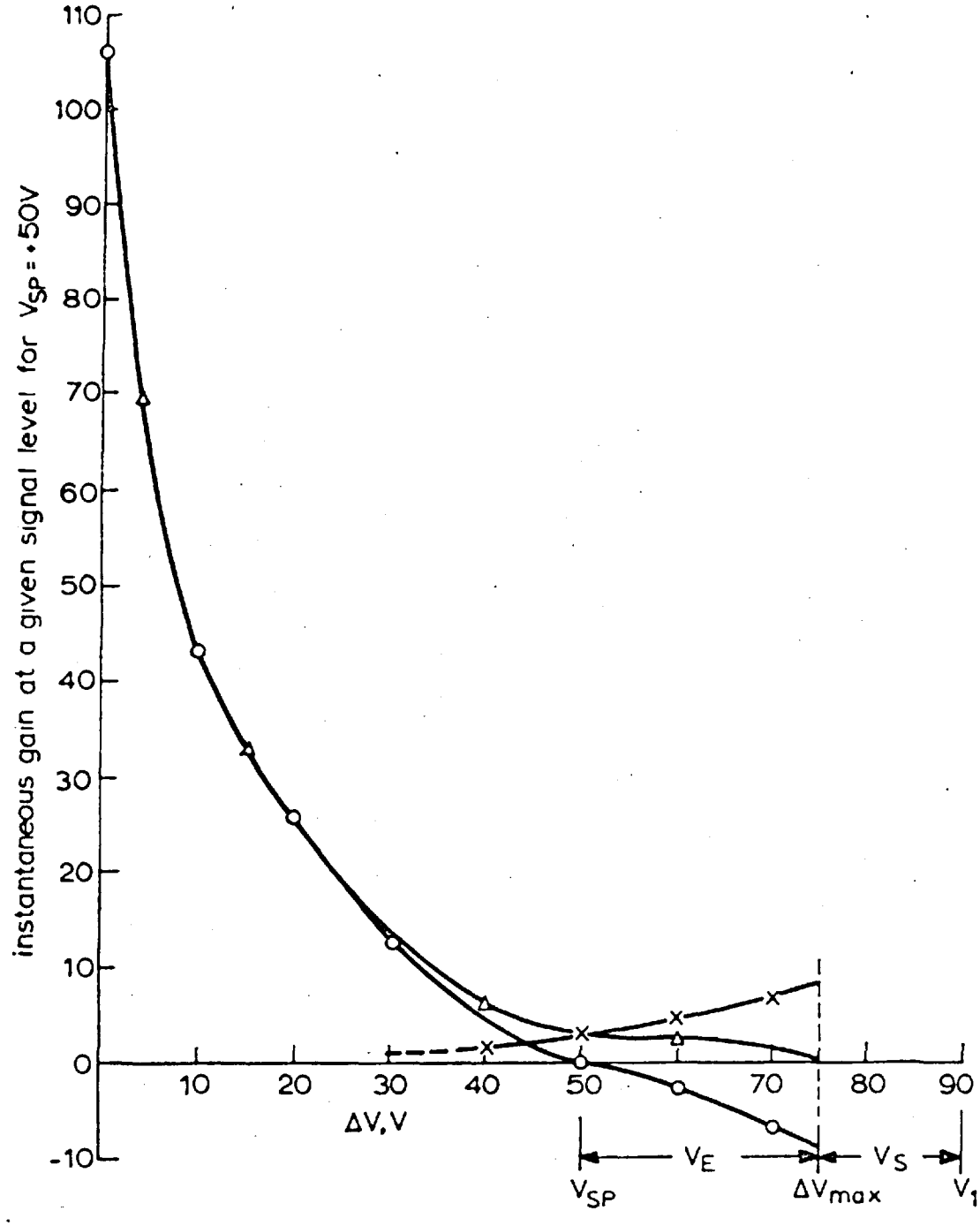

Fig. 5.2 *Instantaneous gain of KCl–ZnS target as a function of voltage excursion on target surface*

$V_{SP} = +50$V
○ s.e.c. gain
× t.s.e. gain
△ total gain
KCl thickness = 7·5 μm
ZnS thickness = 1·5 μm

is shown at the potential where $-G_{S.E.C.} = G_{T.S.E.}$ A stability margin V_s can be defined as the difference between V_1 and ΔV_{max}, this is 15V, and is sufficient to allow for the transient condition when the tube is switched on, and potentials can rise above their normal values because of inter-electrode charging currents. It is also enough to ensure good beam acceptance, and hence a rapid discharge of the target if ΔV_{max} is reached.

5.3 Increasing the gain of stabilised S.E.C. targets

Since there is a certain amount of reduction in target gain between normal and coated layers, when operated at the same signal plate potential, it is worth considering whether a more suitable material could be used in place of potassium chloride. A suitable material would enable not only high gain normal targets to be made, but for the case of the composite target one would also expect good stability, since in the event of an overload condition arising, the high S.E.C. gain in this material would readily compensate the T.S.E. gain from the ZnS. Potassium chloride, which has been exclusively used as the S.E.C. target material in commercially available tubes[69] to date, is an insulator, which as either an amorphous or crystalline solid exhibits good secondary emission properties. Tables of experimental values of the secondary emission coefficient of solids do not show materials with

strikingly better values than KCl. This may be because of the lack of experimental measurements, or even poor experimental technique on the measured materials or it may be that there is no material with an appreciably higher value. From the considerations of the energy loss per unit length of a primary electron in a material by Bethe processes[70], caesium iodide seemed a good choice. This material had already been reported by Edgecumbe and Garwin[71] for use as low density secondary emitting dynodes in linear accelerators at primary energies of the order of several MeV. This material was tried by the author for fabricating S.E.C. targets and although relatively high target gains were obtained, the material was not pursued, because better results than with potassium chloride were not obtained, and difficulty was found in making the evaporated low density CsI stick to the aluminium-aluminium oxide substrate. It was concluded that KCl still appeared to be the best material to use, although CsI was capable of producing comparable gains to that of KCl; it was more difficult to deposit in a low density form, but it did show signs of being less prone to attack by water vapour. This last property might enable less stringent

dry box procedures to be adopted during tube assembly. This could possibly make the assembly work easier with less danger of reduction in target gain from water vapour poisoning. The advantages are of a marginal nature, however, and so no composite targets or sealed-off tubes have been constructed incorporating CsI.

CHAPTER 6

THE PREPARATION OF COMPOSITE TARGETS AND THE STUDY OF THEIR STRUCTURE

6.1 The Preparation and Mounting of the Thin Supporting Film

The thin aluminium oxide support films were made by a method described by Harris[72] and originally adopted by Emberson[73] to produce support membranes in the T.S.E. image intensifier. Only a brief account will now be given of the methods used for preparing the films for the S.E.C. targets, as a very good account has been given by Filby[74].

The process consists of mounting household aluminium foil on tufnol rings, and anodising one surface in an electrolyte that is a buffer solution (pH 5.5) of tartaric acid and ammonia. The required thickness of oxide is formed on the foil by controlling the voltage between the foil anode, and the sheet aluminium cathode (500 Å requires 40v). The excess aluminium left in the foil is then etched away with hydrochloric acid, and the thin aluminium oxide film is left self supporting on the tufnol ring.

After washing and drying, the film is mounted onto the titanium target ring. This is done by coating the ringwith a 0.1% potassium silicate solution, and slowly

bringing the ring near the surface of the film until it is pulled into contact by the forces of surface tension. When the solution has dried, the film is trimmed around the edge of the ring, by using the tip of a moistened paint brush.

The films that were made by this method were given a bake in air at 280°C to slightly slacken the films, and to prevent stresses being set up during the evaporation which would make the layers prone to rupture. The slackening occurred because the expansion coefficient of the supporting ring (titanium) was chosen to be slightly greater than that of the aluminium oxide so that plastic flow occurred in the film during the bake which left a slight wrinkle on cooling.

6.2 The Triple Evaporation

The low density layers were fabricated by the evaporation techniques developed by Rosenbloom[75]. The only difference being that to produce a composite layer three evaporation sources were required. A diagram of the demountable system is shown in Fig. 6.1. Before the support films were introduced into the system the evaporators were prepared, a triple stranded tungsten wire 1. was loaded with small aluminium wire "hairpins", themolybdenum

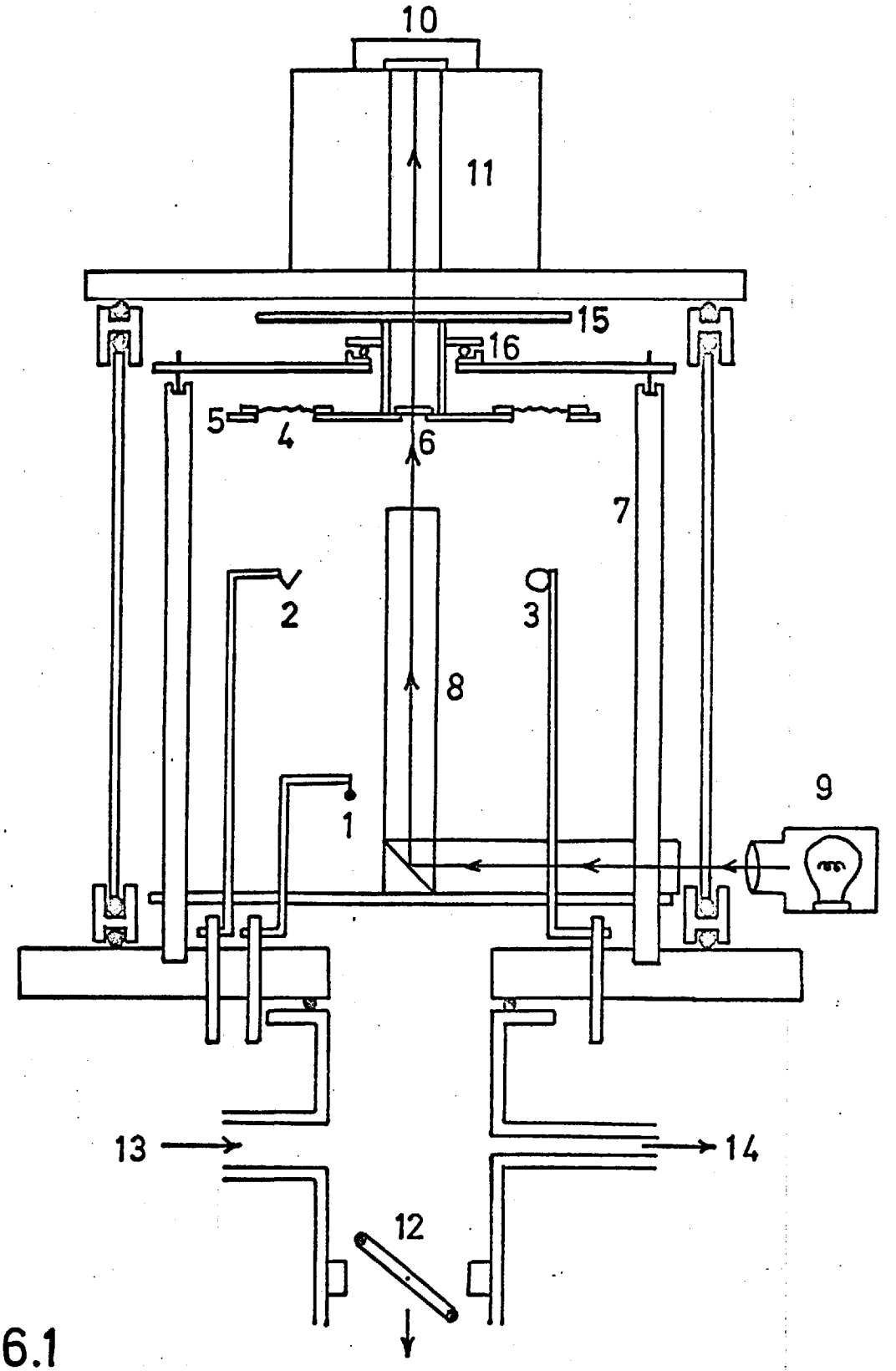

Fig. 6.1

boat 2. was packed with a stiff paste made from finely ground potassium chloride in a little distilled water, and the tungsten spiral 3. was filled with a "cake" of zinc sulphide, also made by forming a paste from the powder with distilled water. When the pastes were dry the system was evacuated, and the evaporators were resistively heated in turn.

The tungsten wire 1. was heated until the aluminium melted and formed a bead which wetted the wire, then the boat 2. was degassed and then heated sufficiently to melt the KCl so that on cooling it formed a crystalline solid, the tungesten spiral 3. was finally heated to degas the ZnS and form a sintered "cake". The spiral had to be heated up very slowly to prevent particles of ZnS jumping off; it was maintained at a temperature of about 900°C for an hour[76]. This was necessary as ZnS can readily decompose into ZnO and hydrogen sulphide if suddenly raised to a high temperature in the presence of water vapour. The temperature was then raised to ≈ 1400°C until degassing stopped. A sintered "cake" was formed as ZnS evaporates by sublimation, and even when the utmost care was taken during the degassing procedure the system always smelt slightly of H_2S on demounting.

Four thin support films 4. were mounted in a rotating film holder 5. along with a glass monitoring plate 6. The holder was placed in the vacuum system on three pillars 7. which located it two inches above the evaporators 2. and 3. The metal chimney 8. was used to protect a 45° prism from deposition from the evaporating sources. This prism was used to project a light beam from the lamp 9. through the monitoring plate 6. onto the photovoltaic cell 10. All three evaporations were monitored by the optical transmission of the plate 6. which was displayed on a gavanometer that measured the photocurrent of the cell 10.

After the system was evacuated the aluminium was evaporated from the tungsten filament 1. until the transmission dropped to 1%. This corresponded to a thickness of $\sim$ 500 Å, sufficiently thick to be conducting. The following two low density evaporations were carried out in an argon atmosphere at a pressure of the order of two torr. This was achieved by isolating the pump from the system by the butterfly valve 12. and admitting dry argon through a needle valve 13. until a low vapour pressure oil manometer at 14. indicated the correct chamber pressure. It was necessary to rotate the film holder during these

two evaporations, because turbulence set up in the gas would otherwise cause an uneven deposit. The rotation was achieved by means of an induction motor 11. placed outside the vacuum space, but situated above a copper disc 15. that was connected by a brass tube to the film holder. The turning torque was provided by the eddy currents set up in the disc, which was free to rotate on the thrust bearing 16. The field current of 11. was adjusted so that the disc rotated at 1 revolution per second. The potassium chloride was evaporated from 2. over a period of appoximately ten minutes, so that the optical transmission fell by 40%. This was followed by the zinc sulphide evaporation from 3. which produced a further 20% drop in transmission, the evaporation rate being such that it took some two to five minutes to deposit.

The layers could be removed from the system on completion of this last evaporation, but because of their susceptibility to water vapour, (which has the effect of greatly reducing their gain) this was done in a dry box, which was lowered around the demountable system. The box was flushed out with dry nitrogen, and then the system was let down to dry argon. By means of the rubber glove ports the film holder was transferred from the system to a large desiccator

which was situated in the box. This was then taken to another dry box that was used for the assembly of the tubes or the target tester.

6.3 Mass Determination of the KCl in the Layers

A conductimetric method was used similar to that described by Rosenbloom[75]. The low density deposit was washed off a layer by a fixed amount of double distilled water, the volume of which was accurately measured by a pipette (2, 5 or 10 cc used depending on thickness of the deposit). The conductivity of the solution was measured in a standard cell, under A.C. conditions to avoid polarisation of the electrolyte. The ZnS did not contribute to this reading as it is insoluble in water. A calibration curve was obtained (see Fig. 6.2) by making up some accurate standard solutions from analar potassium chloride for a suitable range of concentrations. The conductivity of each of these solutions was measured in the cell, and a linear relationship between the conductivity and the concentration was found.

It was simple to determine the mass of KCl in the layer once the conductivity of the layer solution had been measured, particularly if a 10 cc solution was used as the abscissa of Fig. 6.2 then gave the mass directly in milligrams.

Fig. 6.2

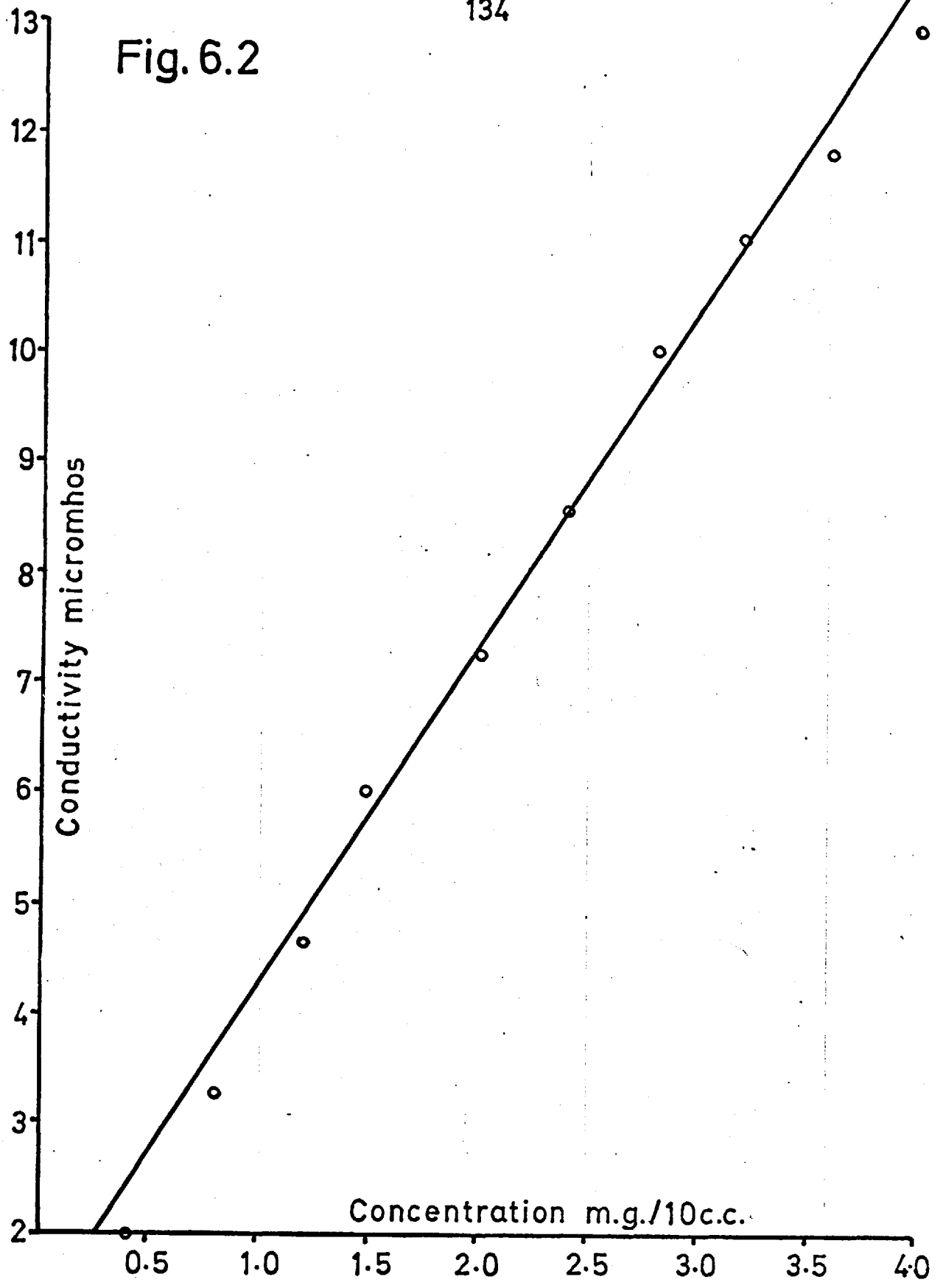
Conductivity micromhos
13
12
11
10
9
8
7
6
5
4
3
2
Concentration m.g./10c.c.
0·5
1·0
1·5
2·0
2·5
3·0
3·5
4·0

6.4 Mass determination of the ZnS in the layers

The mass of ZnS in the layers was determined by a method that was developed by the author, which made use of a colorimetric technique[77] to find the mass of zinc that had been taken up into solution. From this the mass of zinc sulphide was calculated assuming its chemical formula.

The layer solution was retained from the conductivity measurement together with any residue that was present. To all these layer products 5 ccs of 3N hydrochloric acid was added to take the zinc into solution. An indication that this had been achieved was when hydrogen sulphide was no longer evolved. The excess acid was then neutralised with 3N sodium hydroxide solution, and the neutral solution was made up to 50 ccs in a standard flask.

A known proportion of the solution was taken, to which 10 ccs of a pH9 buffer was added, plus 3 ccs of a zinc complexing reagent, Zincon. The total volume was made up to 50 ccs in a standard flask. (The reagent was prepared by dissolving 0.13 gm of Zincon in 2 ccs of 4% sodium hydroxide solution and diluting to 100 ccs with distilled water).

A standard solution of a soluble salt of zinc was

prepared, and this was used to prepare eight calibration solutions containing from 0.03-0.1 mg of zinc in 0.01 mg steps, each solution containing 10 cc of pH9 buffer and 3 cc of the complexing reagent and being made up to a total volume of 50 ccs. A reagent blank was also prepared without the zinc salt. The zinc complex formed in these solutions produces maximum light absorption, at a wavelength of 6200 Å, and for a pH of 9. The light absorption for the different solutions was measured as in Fig. 6.3, by placing each solution in turn, into the cell and measuring the light transmitted I. through the filter by the photocell, and comparing this with the light transmitted I_o, when the reagent blank was used. The filter was made from a combination of two Schott glasses OG3 (3 mm) and BG 38 (2 mm), and had a transmittance peak at 6440 Å with a pass band of ≈ 500 Å, just wide enough to include the absorption peak of the zinc complex.

As can be seen by Fig. 6.4 a linear relation exists between the measured optical density ($\log_{10} I_o/I$) and the zinc concentration. So once the optical density has been measured for the layer solution, the mass of zinc in the layer can be obtained and hence the amount of ZnS. It has been established by Rush and Yoe[78] that Beer's law (i.e.

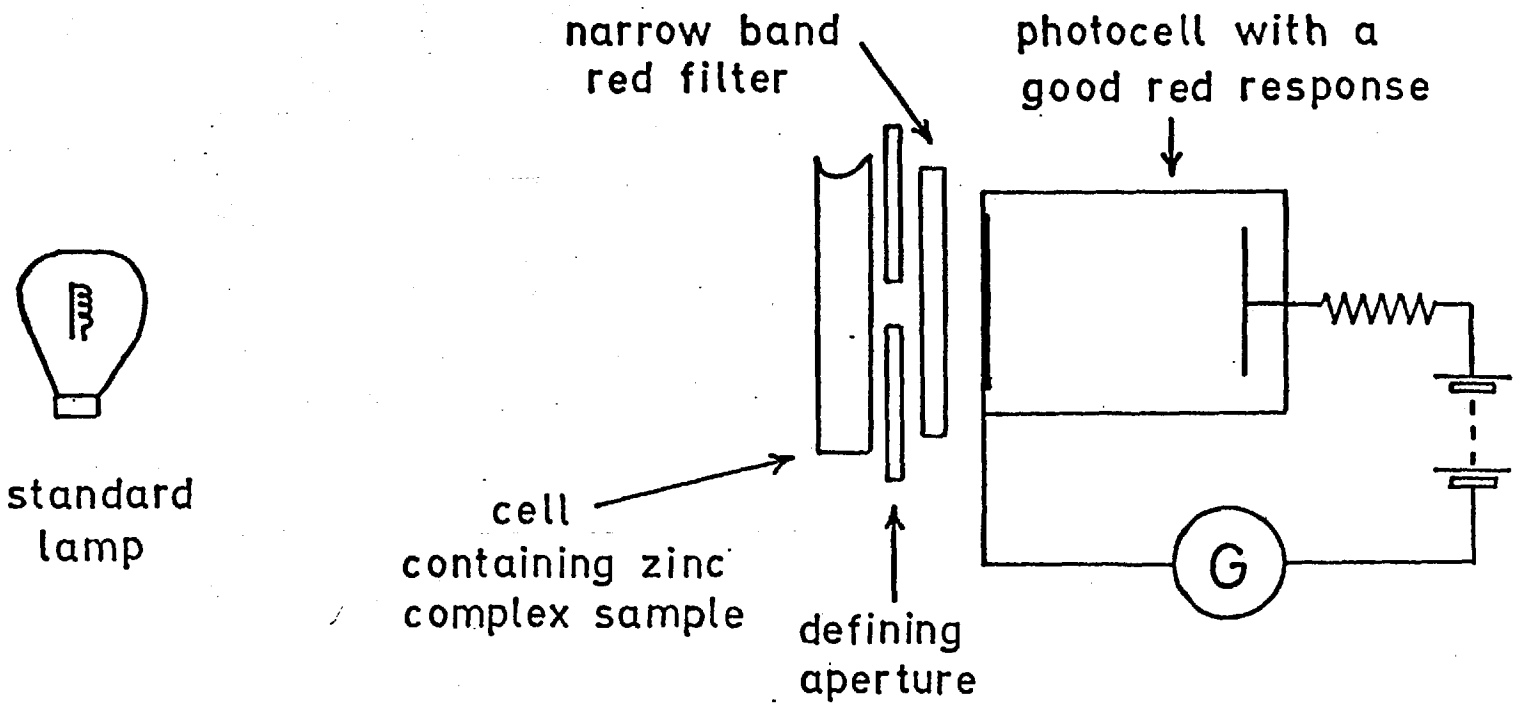
narrow band
red filter
photocell with a
good red response
standard
lamp
cell
containing zinc
complex sample
defining
aperture
G

Fig.6.3

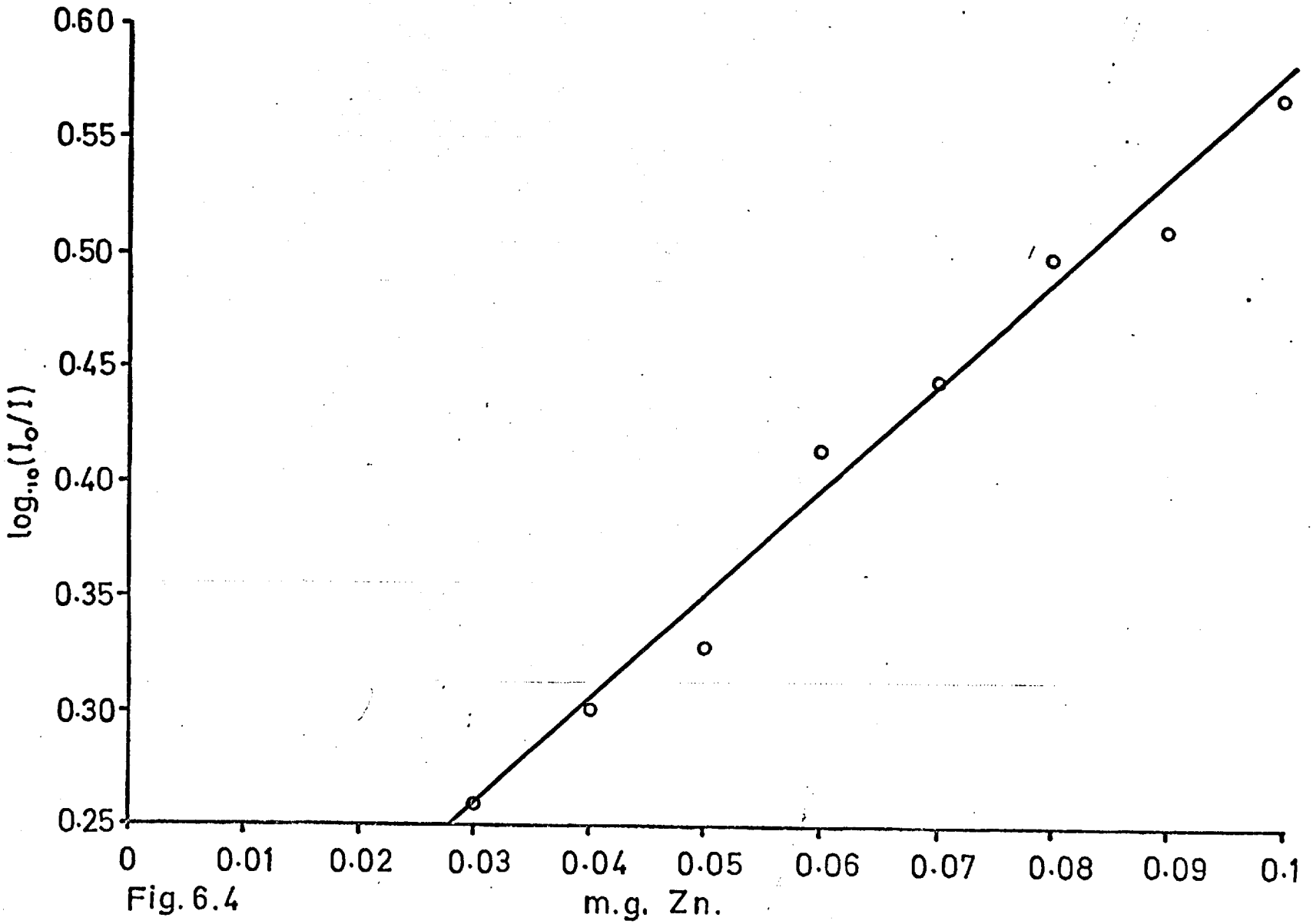
0.60
0.55
0.50
0.45
0.40
0.35
0.30
0.25
log10(I0/I)
0
0.01
0.02
0.03
0.04
0.05
0.06
0.07
0.08
0.09
0.1
m.g. Zn.

Fig. 6.4

the optical density is proportional to the concentration for a fixed path length) holds valid over the concentration range 0.1 to 2.4 parts per million of zinc. Aluminium was known to be one of the elements that can also form a complex with Zincon, and it was wondered if the aluminium signal plate might cause contamination and effect the result. Tests were carried out, but it was found to have no effect. The accuracy with which the measurements could be made depended mainly on the stability of the intensity of the light source, and on the red sensitivity of the photocathode of the cell. By this method the mass of zinc could be determined to within 0.005 mg. It was found that for a quick and fairly accurate mass determination, that this could be done by colour matching the layer solution to one of the calibration solutions.

6.5 Total Layer Thickness Determination

The thickness of the total low density deposit was measured by the method finally adopted by Rosenbloom[79] after a series of experiments on thickness determination. The layer was punctured so that a flake from the layer could be observed in cross section in a microscope, which had a calibrated eyepiece. The method was used successfully,

but measurement was made difficult by the fact that the layer was very flimsy and had a tendency to curl up on itself. Results could be more easily obtained from glass monitoring plates that were placed in the evaporating system, and had a coating of aluminium the same as the targets before the low density deposit. A micrograph of the cross-section of a 15 μm layer of low density ZnS on a glass plate is shown in Fig. 6.5. A depth of focus measurement also gave a quick and accurate result in this case. The low density deposit was scratched to expose the aluminium layer, and ~~then~~ the microscope was focused, firstly, on the specks in this layer, and then on the specks in the surface of the low density deposit. In each case the focus was adjusted to produce the smallest diffraction pattern of the specks. The target thickness was easily measured from the micrometer adjustment for the vertical movement of the objective. This could be read to within 0.5 μm.

6.6 Estimation of the Density of the KCl and ZnS Deposits

For single layers of either KCl or ZnS, the thicknesses could be measured as above and the masses deposited, determined either by section 6.3 or 6.4. By a simple diameter measurement of the layer to obtain the area covered,

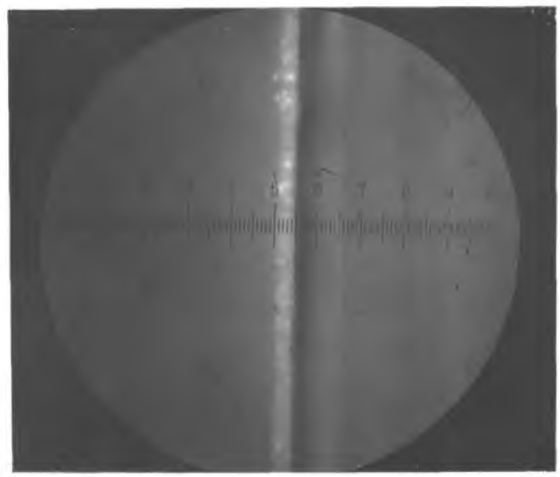

Fig. 6.5. ZnS thickness cross-section ~ 15μm.
(The white line is the ZnS deposit; scale, 1 small division = 3μm.)

Fig. 6.6. Electron micrograph of a ZnS deposit on a copper mesh
(from the same evaporation as used in Fig. 6.5.)
Black areas ZnS Scale 1μm.
White areas vacuum

the volume of the deposit could easily be calculated by using the value for the thickness obtained. Hence the density of the deposit could be found using the known value for the mass. These densities were best expressed as a percentage of the bulk density of the material. The range of values obtained for both KCl and ZnS was ≈ 2-6% of their bulk densities. In Fig. 6.6 an electron micrograph of a low density zinc sulphide deposit is shown. It is interesting to compare this result with the one already reported by Filby et al [80] for potassium chloride Both were evaporated in a similar argon atmosphere onto copper meshes, and their structure looks very similar.

6.7 Calculation of the Thicknesses of the Two Low Density Layers in a composite Target

Using the techniques described in the previous sections it is possible to determine for a given composite layer, the mass of KCl present m_1, the mass of ZnS present m_2, and the total thickness of the low density deposits t. If t_1 is the thickness of the KCl deposit and t_2 the thickness of the ZnS deposit, it is possible to write down an expression for the ratio of these two thicknesses,

$$\frac{t_1}{t_2} = \frac{m_1}{m_2} \frac{\rho_{2b}}{\rho_{1b}} \frac{S_2}{S_1} \qquad (6.1)$$

where

ρ_{1b} is the bulk density of KCl = 1.98 gms/cc

ρ_{2b} is the bulk density of ZnS = 4.2 gms/cc

S_1 is the percentage of the bulk density for the KCl deposit

S_2 is the percentage of the bulk density for the ZnS deposit

It has already been stated in section 6.6 that the layer density for the two materials is approximately the same ratio of the density of their corresponding solids, (3% is a nominal ratio obtained for each material). Hence S_2/S_1 in equation (6.1) has a value of the order of unity. Thus the measurement of the two masses gives a fairly accurate measurement for the ratio of the two layer thicknesses.

Also,

$$t_1 + t_2 = t \qquad (6.2)$$

and since t has been accurately measured (± 10%), the absolute values of t_1 and t_2 can be calculated by solving the two simultaneous equations (6.1) and (6.2) for their

corresponding values. For example a composite target whose thickness was 16.5 μm had deposits of 0.98 mg of KCl and 0.3 mg of ZnS, it can easily be shown that t_1 = 14.5 μm and t_2 = 2 μm.

CHAPTER 7

PROPERTIES OF THE COMPOSITE TARGET

7.1 The T.S.E. Gain (Measured under Video Signal Generating Conditions)

The T.S.E. gain was measured for a composite target under conventional scanning conditions, by means of a pulsed light experiment that has already been described by Filby[81] in earlier work on KCl targets. Briefly the arrangement is to use a line selector circuit to trigger a pulse generator that produces a pulse of short duration (≈ 10μS< line period), which turns on a cathode ray tube with a short persistence phosphor for a similar time once per frame. This light patch is imaged onto the photocathode of the camera tube, the output of which is displayed on an oscilloscope that is triggered by the line selector. The positioning of the selected line and the delaying of the pulse are adjusted so that the signals due to the charging current and the scanning beam read-out current do not overlap.

The charging current, which is due to the T.S.E. electrons leaving the reading side of the target during the duration of the light pulse gives rise to a blacker than

black signal level in the video waveform. The normal scanning beam read-out of the stored charge from the light patch will have the opposite polarity to the charging signal.

For a given signal plate potential V_{sp} the height of the charging signal was measured for different primary energies. At primary energies less than 3 KeV the polarity of the charging signal was reversed, and produced a constant amplitude at all energies. This was taken as a measure of the primary current, and so the T.S.E. gain could be obtained from the two pulse height measurements.

The T.S.E. gain of a composite target that had a very small coating of ZnS (0.045 mg) is shown in Fig. 7.1. If this is compared with the results obtained by Filby[82] for the normal KCl target it will be seen that the form is very similar. The presence of the ZnS has caused a slight reduction of the T.S.E. gain, but not enough to cause a dramatic decrease in the value of the equilibrium potential VE ≈ 80v. The first cross-over potential V_1 has been increased to be ≈ 45v which is intermediate between the values obtained for pure KCl and ZnS layers.

The T.S.E. gain as a function of primary energy of another composite target is shown in Fig. 7.2, for a signal

Fig.7.1

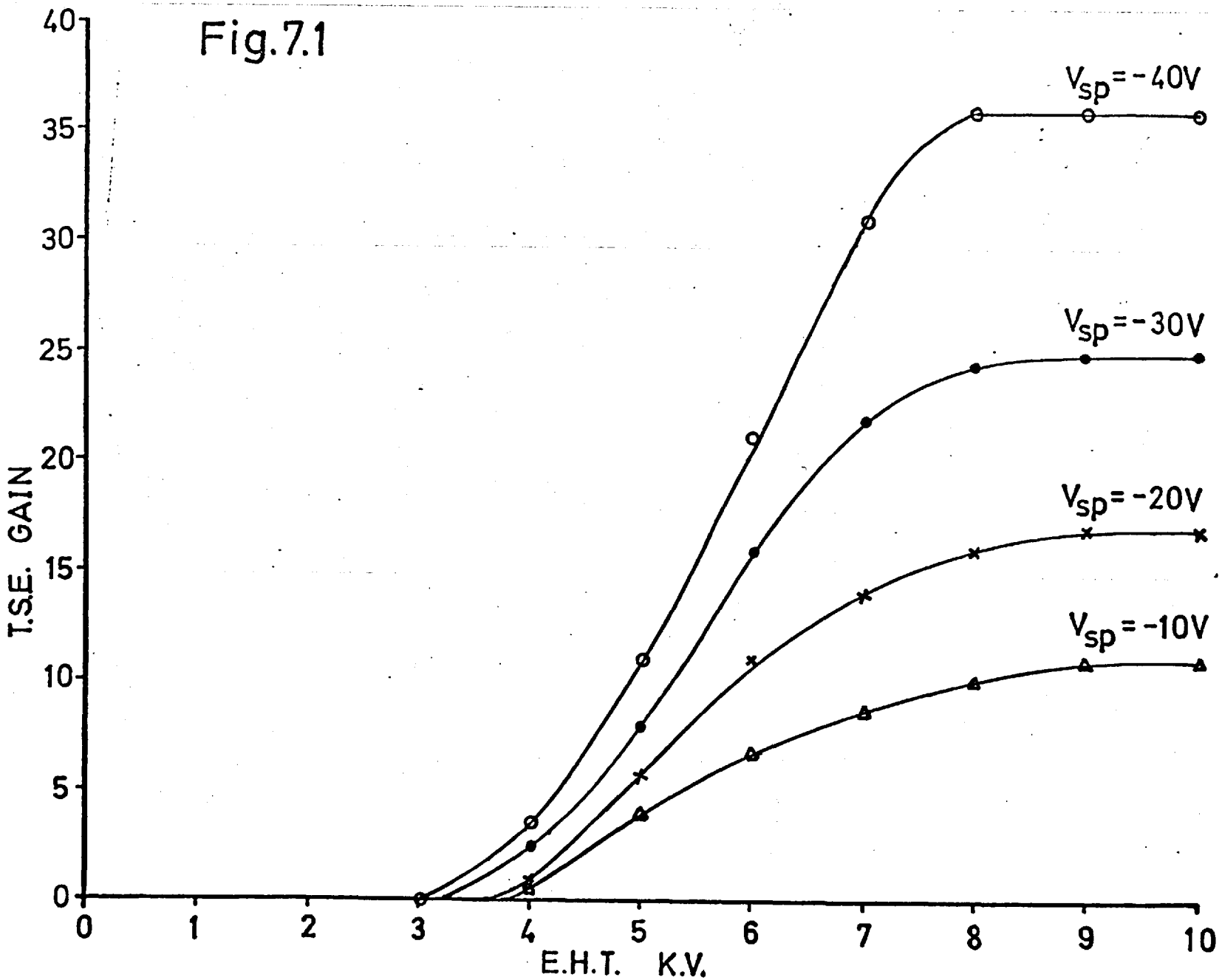
T.S.E. GAIN
E.H.T. K.V.
V_{sp} = -40V
V_{sp} = -30V
V_{sp} = -20V
V_{sp} = -10V
0
5
10
15
20
25
30
35
40
0
1
2
3
4
5
6
7
8
9
10

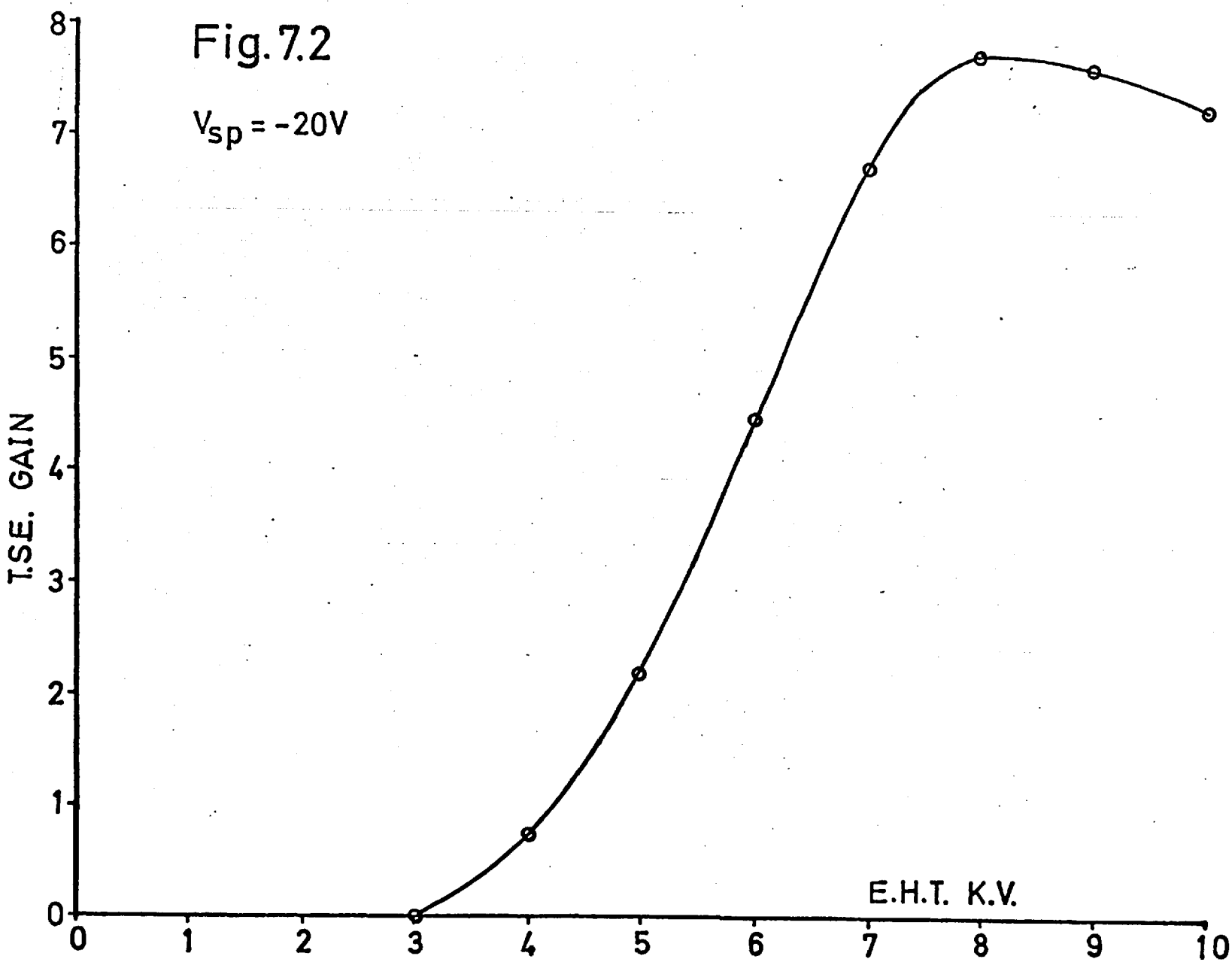
Fig. 7.2
V_{sp} = -20V
T.S.E. GAIN
E.H.T. K.V.
0
1
2
3
4
5
6
7
8
9
10

plate potential of -20v. The gain is about half that of the previous case for the same signal plate potential, and is the result of the ZnS coating being much thicker, ≈ 1.5μm (i.e. 0.22 mg deposited). Unlike the results for the uncoated KCl target, and the thinly coated target of Fig. 7.1, there is a maximum value of the gain ($G'_{T.S.E.} \approx 8$) occurring at approximately 8 KeV. This is probably caused by the fact that the more energetic the primary electrons, the deeper into the target they will penetrate before creating most of their secondaries, which will be able to leave the exit surface as T.S.E. electron. Beyond a certain incident energy the primaries will begin to lose their energy in the ZnS layer, which being a poorer secondary emitter will produce fewer secondaries, thus the gain will decrease. With this particular thickness of ZnS, the lowering of the T.S.E. gain produced a low value for the equilibrium potential ($V_E \approx 25v$), and the first cross-over potential approached that of a completely ZnS layer ($V_1 \approx 90v$).

7.2 The S.E.C. Gain

This was measured in the simultaneous writing and reading mode. The primary current was first measured on an electrometer, then the mean current from the signal plate was measured on the electrometer using a sufficiently long time constant so that the effects of the charging current and reading current for the T.S.E. component cancelled. This mean current was the sum of the S.E.C. current supplied to the target by the scanning beam, and the primary writing current. Hence the S.E.C. gain could be calculated.

The S.E.C. gain measured as a function of the primary energy is shown in Fig. 7.3 for a composite target (ZnS mass 0.11 mg, thickness 1 μm), at constant signal plate potential of 40v. It can be seen that there is a maximum value for the gain at an energy 8 KeV. This is not significantly different from the value obtained for normal KCl targets. From measurements on plain ZnS layers a maximum S.E.C. gain was obtained for a primary energy of 12 KeV. These results show that the ZnS layer in the composite target has not drastically altered the S.E.C. characteristics from those of the normal KCl target.

The dependence of the S.E.C. gain on the signal plate

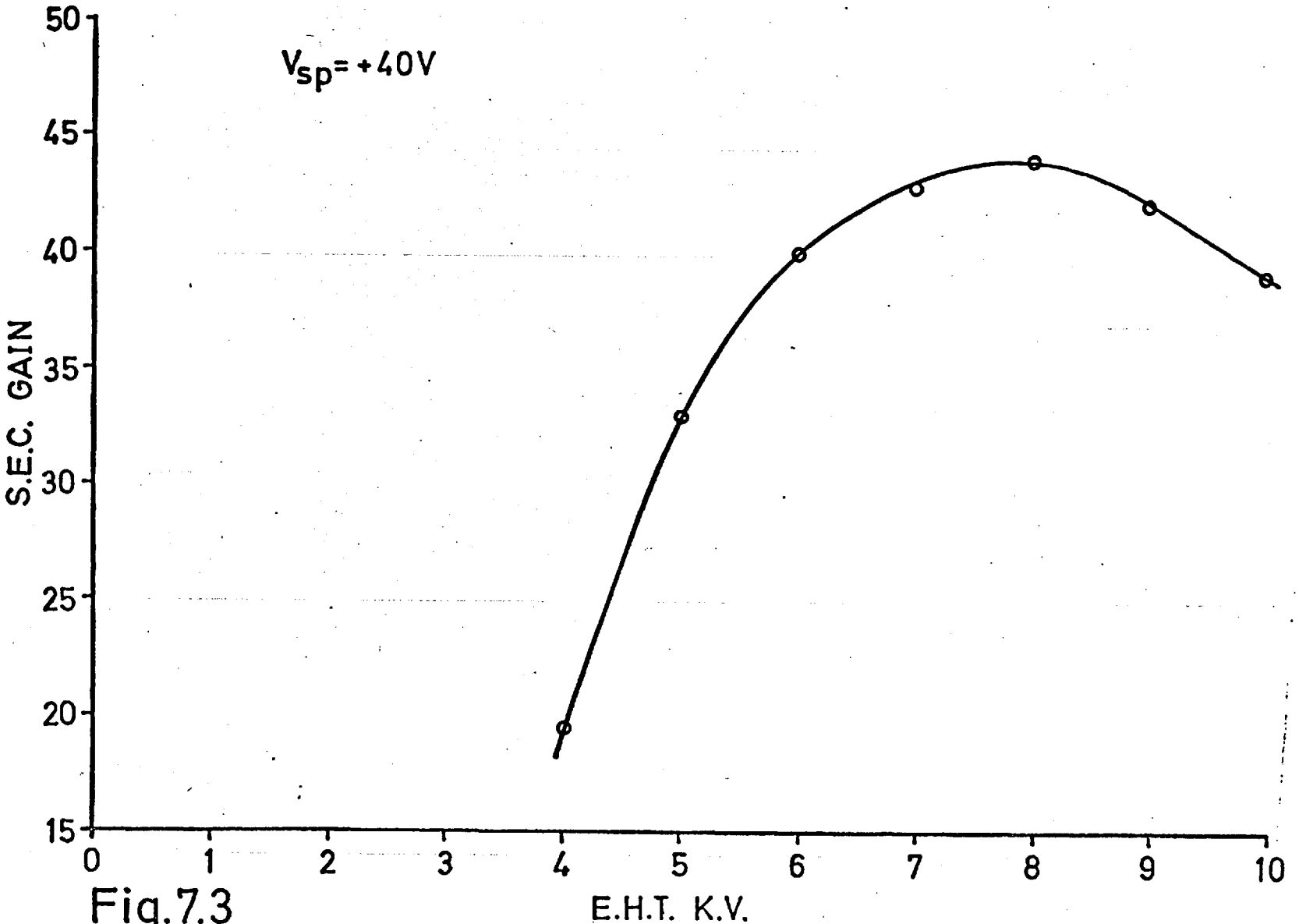

Fig.7.3

potential for the same composite target can be seen in Fig. 7.4. This is also very similar to the results obtained for normal KCl targets. The magnitude of the gain at negative signal plate potentials for the reversed condition is however less in proportion to that for the KCl targets

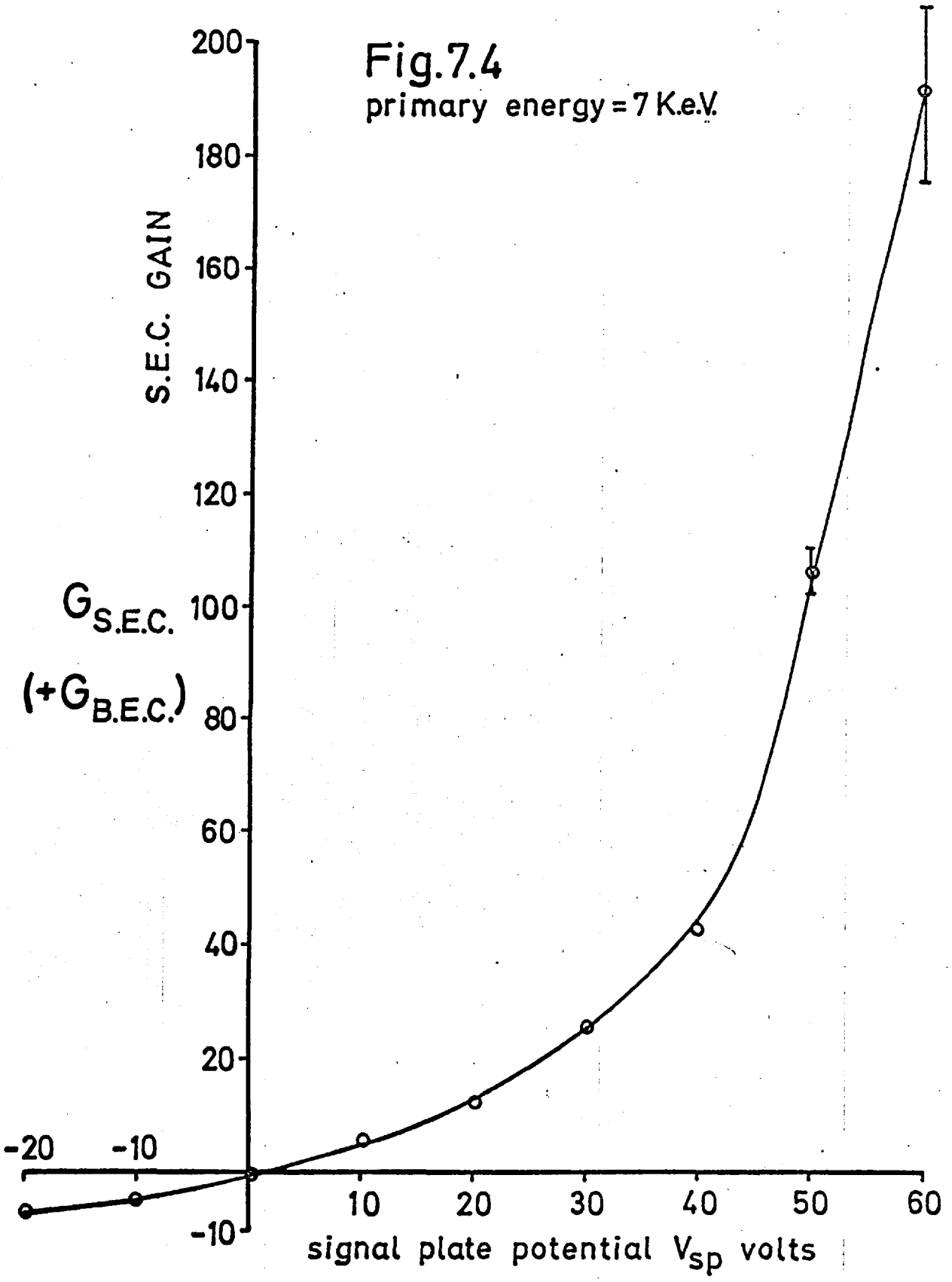
Fig.7.4
primary energy = 7 K.e.V.
S.E.C. GAIN
$G_{S.E.C.}$
$(+G_{B.E.C.})$
200
180
160
140
120
100
80
60
40
20
-10
-20
-10
10
20
30
40
50
60
signal plate potential V_{sp} volts

7.3 The Inference of B.E.C. Gain

It was concluded by Filby[83] et al,[83] that because the magnitude of the S.E.C. gain was less for negative potentials of the signal plate than for the corresponding positive values, then there must be another component to the gain at positive signal plate potentials. This was termed a B.E.C. (Beam Electron Conduction) gain, and this was attributed to the fact that for the positively charged areas on the target surface where the reading beam could land, there could be some electrons from the beam, which were not needed to neutralise the charge, which could penetrate into the pores, though the layer to the signal plate to add to the signal current. Such a process is analogous to the operation of a triode valve, the beam current flowing to the signal plate for a particular area of the target surface being controlled by the potential excursion for that area.

Although it is possible to postulate the existence of a B.E.C. gain, it is difficult experimentally to separate this contribution from that of S.E.C., since both only give rise to a current from the signal plate on reading, unlike the T.S.E. component which produces a charging current during writing. It is also not meaningful to take as a measure

of the B.E.C. gain the difference of the magnitudes of the S.E.C. gains for the same magnitude of signal plate potential but of opposite polarities. This is because the penetrating primary will cause an asymetrical production of secondaries through the layer as more will be produced towards the end of the range of the primary than at the beginning. The gain being the product of the number of secondaries produced and the collection efficiency, is unlikely to be the same for a reversal of electric field since the secondaries will have to travel further through the layer to be collected in one direction than for the other. Also when the signal plate is at a negative potential so the S.E.C. and T.S.E. gain components are opposing each other, the magnitude of the S.E.C. gain will be limited by that of the T.S.E. gain, thus preventing the measurement of high values of the S.E.C. gain if the T.S.E. gain is low.

In addition to what has already been said there are five more facts that ought to be considered when trying to substantiate the existence of a B.E.C. gain component.

1. The target capacitance (see section 7.6) appeared to increase at high positive signal plate potentials. For example, a target which gave a constant value

of 60 pf/cm^2 at lower signal plate potentials produced a value of ≈ 130 pf/cm^2 when the signal plate potential was increased to +40v. This could readily be explained by the fact that additional charge to that stored during the writing process could be supplied to the signal plate during the reading process by the action of B.E.C. A graph showing the dependence of target capacitance on signal plate potential, for two different target thicknesses has been given by Boerio et al[84]. The thin target showed a steep increase in capacitance with signal plate potential, whist the thicker target showed only a slight increase. This is just the result one would expect if B.E.C. is the process involved, although this was not the explanation offered by the authors.

2. For a target of average thickness (∿ 10 μ m), if the signal plate potential was increased above ∿ + 55v a spurious "white" signal occurred. This was obviously due to the reading beam penetrating through the layer to the signal plate and although at such high potentials the beam penetration

was not image dependent, it did illustrate that the reading beam could pass through the layer to provide a signal.

3. It was found for thin targets (thickness < 5μm), that although the S.E.C. gain was lower than that of an average thickness target at low positive signal plate potentials, it appeared to surpass it at higher potentials. (i.e. the gradient of the gain against signal plate potential was very steep at only $\sim$ + 10 v). Also beam penetration occurred at a much lower potential, ($V_{sp} \simeq$ + 20 V). Higher secondary emission is unlikely to occur in the thinner target because the primary energy loss would be less for the same incident energy. B.E.C. appears to be the major component to the gain for thin targets at positive signal plate potentials.

4. The time response (lag, see section 7.7) for S.E.C. targets is usually very good at most signal plate potentials. For a normal target capacitance the signal current is reduced to negligible proportions

after the first scan (for 25 frames/sec system), provided the signal plate potential is less than ∿+ 30v. Above this value, lag becomes noticeable and at +40 V the lag is quite objectional. This change in the time response is obviously an indication of a different signal generating process occurring in addition to those of S.E.C. and T.S.E., it has all the characteristics of B.E.C. and is further discussed in section 7.7.

5. Some claims are being made for measured S.E.C. gains of the order of 500-1000, for the normal KCl target. The author has measured similar high gains for some KCl targets at high signal plate potentials (∿+40 V), but does not believe the gain is largely of S.E.C. orgin. An estimate can be made of the highest attainable total charge gain, from the consideration of energy conservation. A typical value for the primary energy of the imaging electrons to obtain an optimum gain for a KCl target is 7 KeV. Also reasonably reliable values of the band gap [85] energy and the electron

affinity[86] for KCl are 9.4 eV and 0,5 eV respectively. Thus the minimum energy required to liberate a free secondary electron is ~10 eV, providing the KCl is sufficiently pure that the band structure has not been drastically modified. These figures yield a maximum value for the total gain of 700, but this is still making two rather unrealistic assumptions. Firstly, that the collection efficiency for the secondary electrons is 100%, and secondly, that the secondaries are emitted with zero energy. In practice the secondaries will be emitted with various energies, the most probable energy of emission for the distribution is possibly ~ 3 eV. This increases the energy required per secondary to 13 eV, and the maximum possible attainable gain to 540. Since it is unlikely that all the primary energy would be used in the production of secondaries, and experimental results have yielded values even greater than these theoretical limits, it appears that some other process such as B.E.C. must be occurring.

7.4 Transfer Characteristics

A curve is shown in Fig. 7.5 for a composite target that was measured in the demountable system, although similar results were obtained for sealed off tubes. The primary current density J_p, was obtained, by measuring the current (on an electrometer) which flowed to a stencil in front of the target. The stencil contained a 1 cm^2 rectangular aperture, the current through which could be calculated by knowing the window ratio of the stencil. The signal current was obtained by measuring the height of the video pulse from the aperture on an oscilloscope and calculating the signal current from the known value of input impedance for the head amplifier.

It can be seen that the gamma is constant over three orders of magnitude of the current density, and can be represented by

$$i_{sig} = KJ_p^{\gamma} \qquad (7.1)$$

The value of γ is almost unity (0.92) over the constant part of the curve, but decreases rapidly to zero for $J_p \sim 10^{-8}$ A/cm^2 when the signal current saturates at $\sim$0.3 μA, being

Fig. 7.5

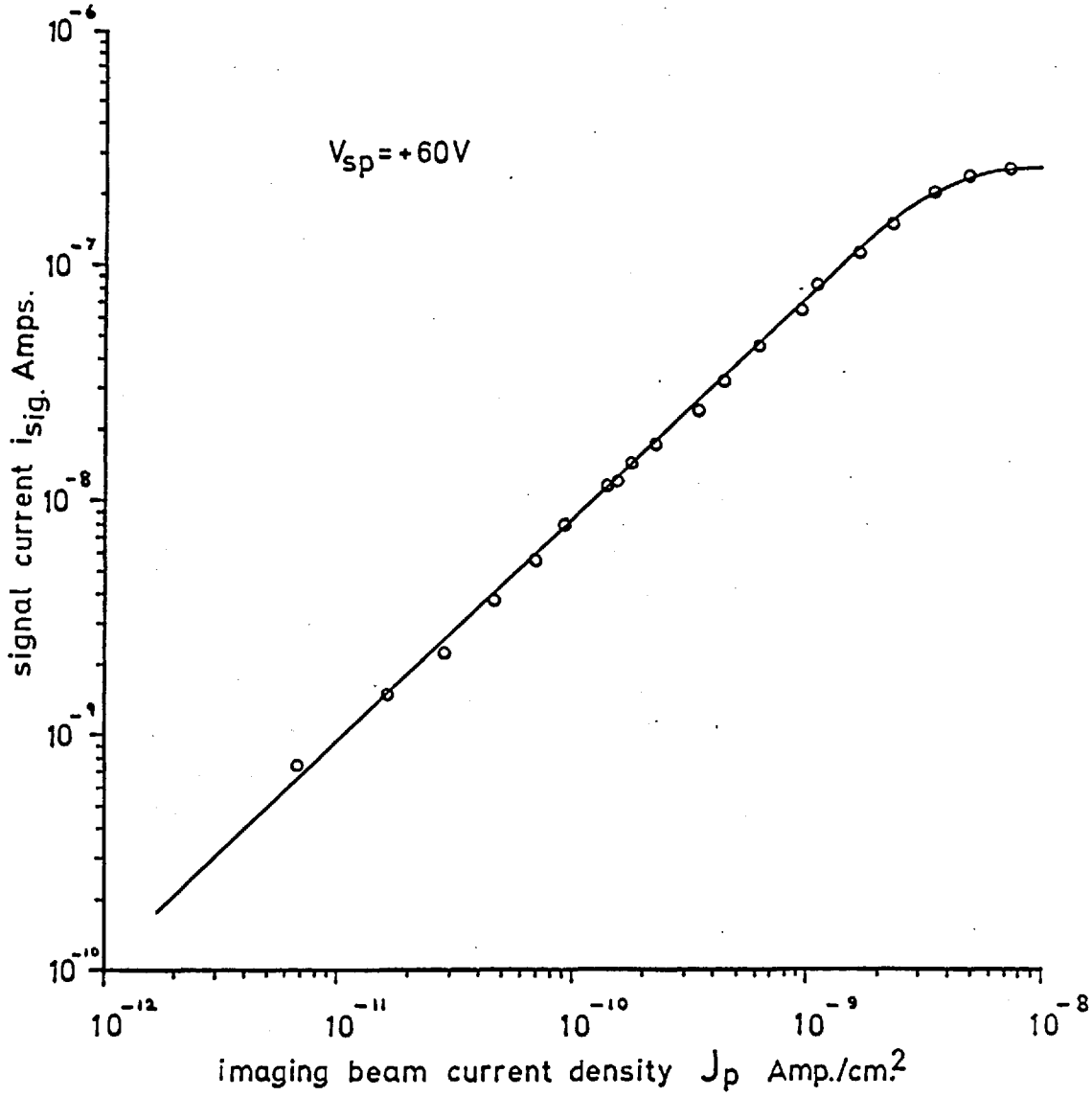
V_{sp} = +60V
signal current i_{sig} Amps.
10^{-6}
10^{-7}
10^{-8}
10^{-9}
10^{-10}
10^{-12}
10^{-11}
10^{-10}
10^{-9}
10^{-8}
imaging beam current density J_p Amp./cm.^{2}

limited by that of the beam current. These results were obtained for a reasonably thick composite target (thickness KCl = 14.5μm, ZnS = 2μm) which could be operated at high positive signal plate potentials before the effects of beam penetration occurred. As the signal plate potential (V_{sp} = +60v) was large in comparison to the target surface potential excursion, the internal electric field of the target did not vary much with signal strength, nor therefore did the gain. This enabled the gamma to approach unity over much of its range. At lower signal plate potentials however, the potential excursion could be a large percentage of this potential, and the internal electron field decreased at only a modest signal strength causing a decrease in the gamma of the characteristic at this level.

7.5 Modulation Transfer Function (M.T.F.)

The square wave response was measured for tubes by using a set of metallic bar patterns of various spatial frequencies. These were etched into .001" copper foil, using photoresist techniques, and made to a format which fitted a Baum projector, so that an image could be formed on the photocathode of the tube with a demagnification of five times. This enabled higher spatial frequencies than

could be etched into the foil to be displayed.

Fig. 7.6 shows the square wave response $r(f_s)$ for a tube which contained a composite target 9μm thick. This was measured under repetitive scanning conditions (405 line 50 field system), the amplitude of the video signal being measured on an oscilloscope at each spatial frequency. Although such a measurement is easy to perform, it is not the easiest to handle mathematically, since the signal profile changes with amplitude. The sine wave response is much more useful since the profile remains constant in this case, only the modulation depth varying with the spatial frequency of the signal. Accurate sinusoidal test patterns of high contrast are however difficult to make, but the sine wave response $R(f_s)$ can be computed from the square wave response by using the power series expansion,

$$R(f_s) = \frac{\pi}{4}\left(r(f_s) + \frac{r(3f_s)}{3} - \frac{r(5f_s)}{5} + \frac{r(7f_s)}{7} + \frac{r(11f_s)}{11} - r\frac{(13f_s)}{13} - r\frac{(15f_s)}{15} + r\frac{(19f_s)}{19} - \frac{r(17f_s)}{17} + B_k r\frac{(kf_s)}{k} \ldots\ldots\right)$$

$$\text{where } B_k = (-1)^m(-1)^{\frac{k-1}{2}} \text{ if } r = m \qquad (7.2)$$

$$B_k = 0 \quad \text{if } r<m$$

k is odd

Fig.7.6

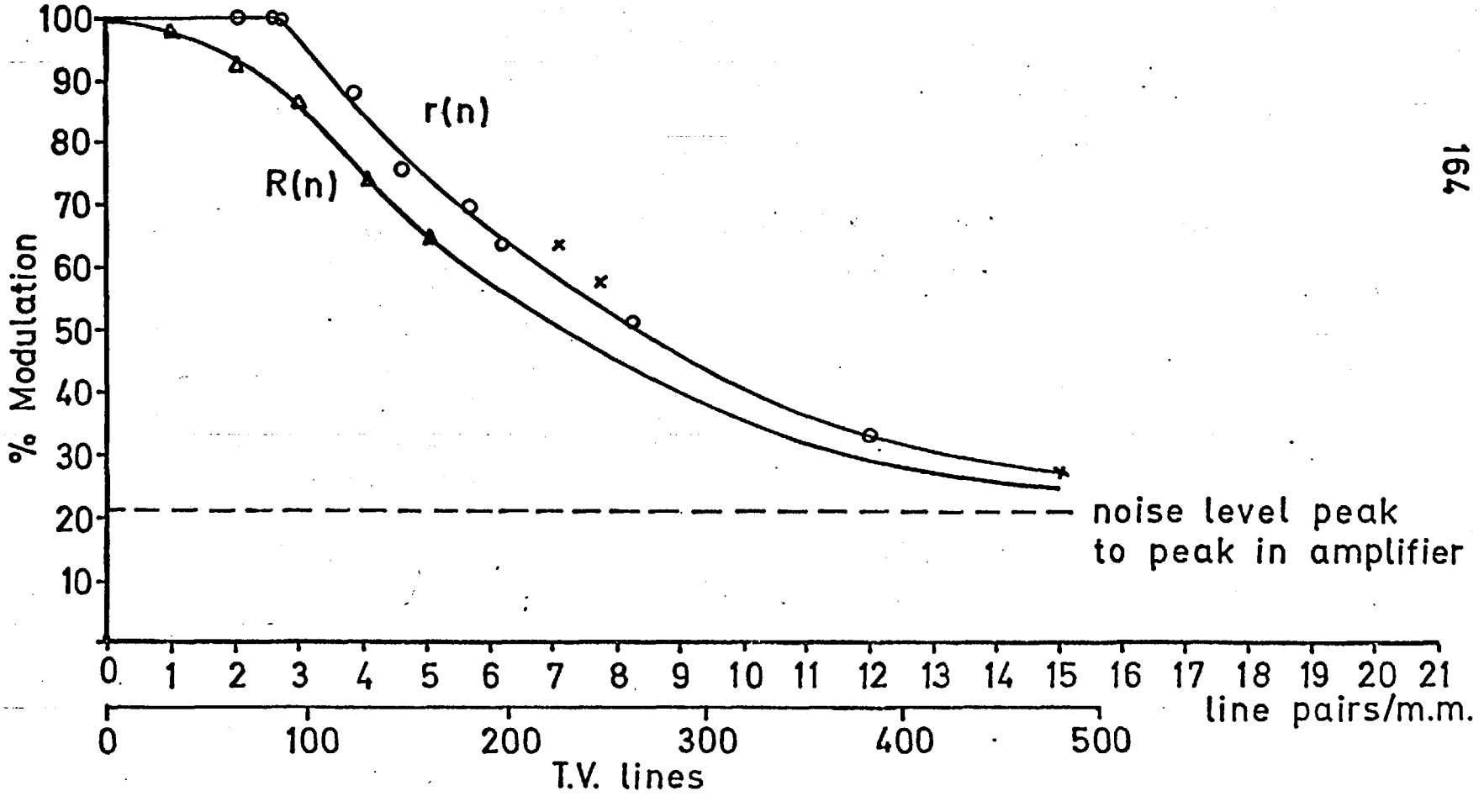
r(n) = measured square wave response
R(n) = computed sine wave response
100
90
80
70
60
50
40
30
20
10
% Modulation
r(n)
R(n)
noise level peak
to peak in amplifier
0 1 2 3 4 5 6 7 8 9 10 11 12 13 14 15 16 17 18 19 20 21
line pairs/m.m.
0 100 200 300 400 500
T.V. lines

m is the total No. of primes into which k can be factored and r is the No. of different prime factors in k.

This computed response is also shown in Fig. 7.6, and from what has been said in section 1.5 it is largely the product of the responses of the target and the aperture of the scanning beam. Unfortunately it is difficult to separate these two components. Firstly the beam profile is not well defined since as the low velocity beam is scanning an insulator there will be a beam sharpening effect, and also the change in potential of the target surface during discharge will cause the focus to alter. Secondly the target response cannot be considered purely by Krittman's analysis[35] since repetitive scanning was used, and a certain amount of scattering of the imaging electrons does exist.

7.6 Target Capacity

The capacitance per unit area of a target was determined by imaging a uniform 1 cm^2 rectangular patch onto the target, and measuring both the charge stored, and the potential excursion of the storage surface after a given exposure. The charge could easily be obtained by measuring the signal

current on read-out, from the video waveform, for the rectangular patch, and calculating the time spent during read-out actually scanning the patch. The potential excursion of the storage surface was measured by setting the gun cathode to a more positive potential just before read-out, so that on read-out the patch was barely visible. The minimum cathode potential increase which produced no signal on read-out, from similar exposures was taken as a measure of the potential excursion.

A typical value of capacitance measured for a 9 μm thick target at low signal plate potentials ($V_{sp} \sim +10v$) is $\sim 160 pf$ cm^2, this compares favourably with the calculated value for a 9 μm thick layer of 97 pf/cm^2 by assuming the permitivity of the layer is unity. This assumption is justified because of the low density nature of the deposit. This indicates that the majority of the charge is stored near the surface of the layer. The higher values of capacitance measured at higher signal plate potentials ($V_{sp} > + 30v$) are unlikely to be due to stored charge residing at some "effective" depth inside the layer, but is more likely to be due to B.E.C. as already discussed in section 7.3.

7.7 Lag

The target capacity for usual target thicknesses (10-20μm) is such that discharge lag is not a problem at normal scanning speeds. Also charge regeneration (or target lag) is known not to occur over a range of low signal plate potentials. Thus under normal conditions the response is fast, and suitable for dynamic imaging.

It has been reported that for the normal KCl target, the gain suddenly increases for signal plate potentials above 35 v, (Boerio et al[84]). This increase in gain was accompanied by a certain amount of target lag. Both observations were interpreted by them as being the onset of an electron bombardment induced conductivity (E.B.I.C.) process. From what has been said about B.E.C. this could equally well account for the increase in gain at high signal plate potentials, so it was of some interest to investigate the target lag, and to try and establish if it were of E.B.I.C. origin.

The method employed was to measure whether the charge regeneration was time-dependent. The decay of E.B.I.C. is by no means instantaneous after the bombarding beam has been turned off, but persists for a comparatively long time (in the range from several milliseconds to many seconds).

A block diagram of the experimental arrangement is shown in Fig. 7.7. A staircase-waveform generator was used as a divide-by-five circuit to pulse-on for 10 μsec every fifth frame, a cathode ray tube having a short persistence P.16 phosphor. The resulting pulsed light spot which was stationary and defocused, was imaged by a transfer lens onto the photocathode of a camera tube containing a composite target. The tube was scanned on a 405 line 50 fields/sec system, but the line scanning density was so arranged that each field completely discharged the target. This meant that the picture element sampling rate was every 20 ms, effectively using a ∿ 200 line system. By means of the delayed pulse generator the time between the light pulse and the first scan of the selected line could be varied in the range 0-20 m sec.

The oscilloscope waveforms of the selected line on five alternate scans can be seen in Fig. 7.8 for four different signal-plate potentials. The first scan occurred 25 μsec after the light pulse. At low signal plate potentials, the timing of the light pulse could be observed by the negative pulse produced by the charging current due to the transmitted secondary emission (T.S.E.) electrons. The T.S.E. gain measurements of section 7.1 were made from

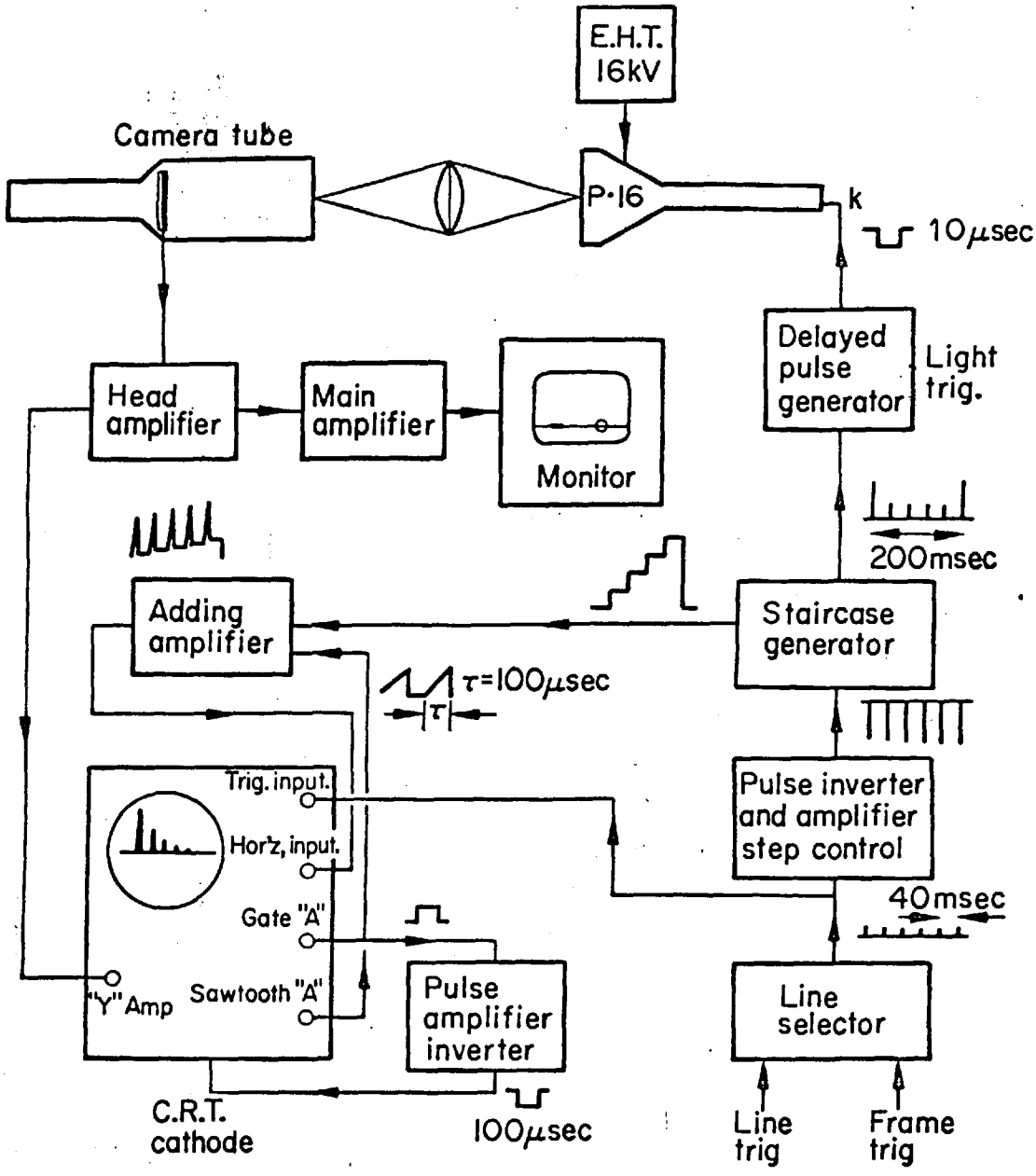

Fig. 7.7 Block diagram of lag-measuring equipment.

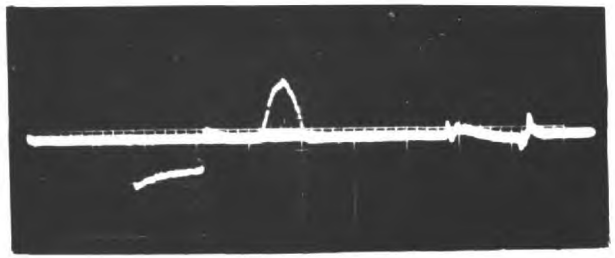

V_{sp}=5V

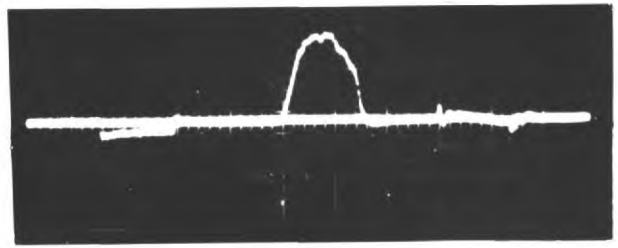

V_{sp}=10V

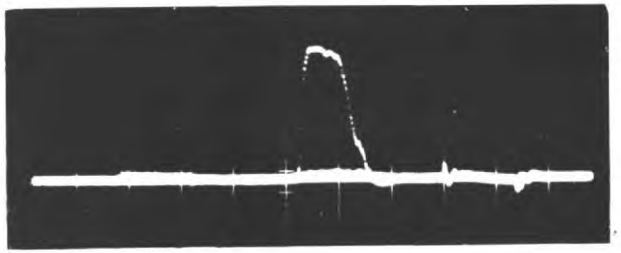

V_{sp}=20V

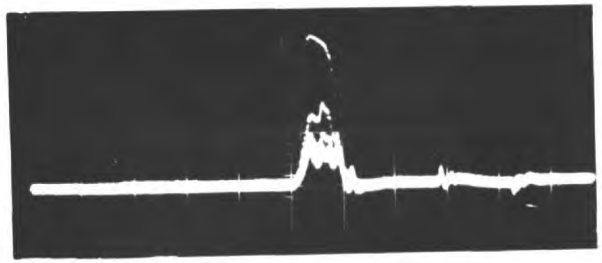

V_{sp}=40V

Fig.7.8 Selected line waveforms showing target lag
5 scans superimposed

similar pulse observations. The pulse is clearly visible for signal plate potentials of 5v and 10v, but the higher the potential the smaller is the pulse height, and the lower is the T.S.E. gain. As can be seen in Fig. 7.8, at the three lower signal plate potentials there is no evidence of charge regeneration. However, at 30v and 40v there are residual charges which are read-out in each of the five displayed scans (alternate field scans not displayed). The profile of the lag was displayed more graphically by displacing the succeeding scans using a signal from the staircase generator to drive the X-deflexion amplifier of the oscilloscope (see Fig. 7.9).

When the time delay between the light pulse and the first scan is increased, the amplitude of the subsequent scans relative to the first could be expected to decrease if there were E.B.I.C. effects. In fact no such time-dependence was found when the delay was increased to 20 ms; in a separate test the delay was increased to 10 sec and even then only a slight change was observed. It was concluded that E.B.I.C. effects occur only to a small extent in the S.E.C. target.

The signal plate potential at which lag becomes evident is also close to the potential at which the gain

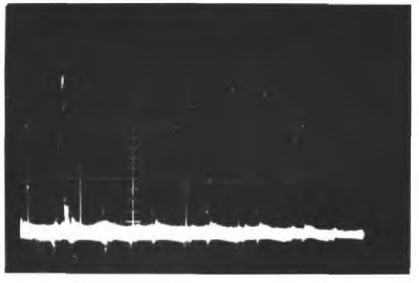

V_{sp} = 10V

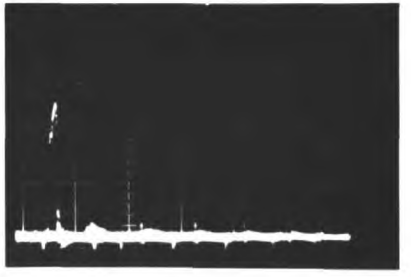

V_{sp} = 20V

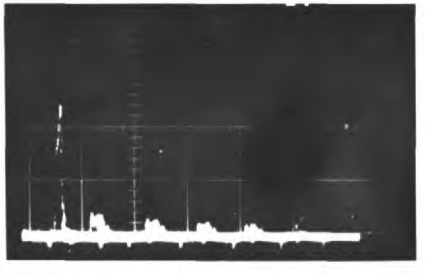

V_{sp} = 30V

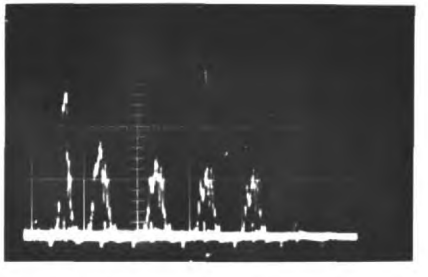

V_{sp} = 40V

Fig. 7.9 Selected line waveforms showing target lag 5 scans displaced to show lag profile

starts to rise steeply (see Fig. 7.4). This indicates the two effects are linked to the same physical process; already B.E.C. has been offered as an alternative explanation for the increase in gain at high signal plate potentials, but the lag is not so easy to explain by this process. The experiment has shown that the residual signal obtained in a given scan depends on the number of scans rather than the storage time, and this indicates that the scanning beam is associated with the lag mechanism. A possible explanation is that the penetrating beam electrons produce positive charges within the target by secondary emission. The neutralization of these charges would be a slow process since the penetrating beam electrons on nearing the signal plate will have acquired energies near that of the first secondary emission cross-over energy of KCl ($\sim$ 15 eV). At higher signal plate potentials it might not be possible to neutralise the charges; such a condition may also exist when permanent beam penetration is observed.

7.8 Cross-Over V_1

The first cross-over potential V_1 of the scanned surface of a target was measured by increasing the signal plate potential by a known amount whilst the scanning beam

was turned off. The surface which had previously been stabilised at gun cathode potential was now positive with respect to the gun, so that when the scanning beam was turned on it would land. The generated video signal was observed for a blacker than black component which would indicate that anode potential stabilisation would be developing, and that the signal plate had been advanced by a potential greater than V_1. By repeated measurements with different signal plate advances, V_1 could easily be found; care had to be taken to make sure that the potential of the collector mesh was always at least a few volts more positive than the highest signal plate potential ~~setting~~ advance.

As has already been stated in Chapter 5 the measured value of V_1 for the normal KCl target was quite low, ≈ 15v, whilst that for the composite target was higher ≈ 50-100v depending upon the ZnS covering.

7.9 Equilibrium Potential V_E

This was attained by flooding the target with a primary electron beam for a sufficiently long time whilst the reading beam was turned off, and the mesh nearest the target was at a high enough potential so as notto limit the potential excursion of the storage surface.

The equilibrium potential was measured by sampling

the storage surface with the reading beam. The signal plate potential was lowered by an amount considered to be greater than V_E, and then it was increased in small increments back towards its original value, for each increment the reading beam was momentarily pulsed on for one frame scan to see if any video signal was developed. The change in potential of the signal plate at which the signal was first observed gave a value for V_E.

A check on this value was obtained by setting the signal plate negative with respect to the reading gun cathode by an amount equal to the equilibrium potential. An image was then presented to the target at a sufficiently high level of illumination that a video signal should be easily observable (allowing for the much reduced target gain). No signal was observed, but on increasing the signal plate potential by a small increment a video signal could be seen. Similar values were obtained by both methods, typical values for a composite target were $\sim$ 25v whilst those for normal KCl targets were $\sim$ 80v.

7.10 Integration and Charge Storage

Although ZnS falls into the semiconductor class of solids it does not appear to have made any dramatic change in the value of the storage time. This is still

exceedingly long (∿ several days) and integration times are limited by the background of the particular tube. Single exposures of $4\frac{1}{2}$ hours have been made which show an acceptable background level over the majority of the target area.

The good storage properties are probably due to the fact that lateral and trans-layer charge leakage is difficult because of the porous nature of the target material, and also because KCl is a very good insulator.

CHAPTER 8

GAIN ENHANCEMENT FROM LOW DENSITY LAYERS

8.1 Method of creating an enhanced gain

As has been already stated, S.E.C. targets are particularly suitable for the integration of low-light level images. Such images can be integrated for periods of several hours before being read out in a single frame.

The author has found that it is possible to operate in this mode, temporarily at a higher target gain for a given signal plate potential by using the following preparatory procedure. The target is flooded with a uniform beam of electrons from the photocathode, while the reading beam is switched off, and the potential of the target surface is allowed to rise, so that it is more positive than the signal-plate (i.e. the electric field in the target is reversed). The surface potential will be limited by either the potential of the nearest mesh (which is set +20V more positive than the signal-plate) or for the case of a composite target, by its equilibrium potential. When the surface has reached its limiting positive potential, the flood beam is switched off, and the surface is reduced to gun cathode potential by turning on the reading beam. With the conventional KCl target it is necessary to lower the signal plate potential

before switching on the reading beam to prevent it hitting the target surface while it is above the first cross over potential. As the target discharges, and its surface potential stabilises, the signal plate can be gradually returned to its operating potential. However, with a composite target the cross over potential is so high that this precaution is unnecessary.

The gain of a target after the above preparation can be more than doubled. It was observed that the amount of enhancement was dependent on the signal plate potential V_{sp}. For example, with a typical composite KCl - ZnS target at V_{sp} = +4V the increase in gain was about four times, at V_{sp} = +10V, it was doubled, but at V_{sp} = +30V, there was no enhancement. Although the gain of this target at the above signal plate potentials was low (4 to 25), the effect has also been observed with KCl targets where the gain is relatively high at low signal plate potentials. Unfortunately, this effect does not appear to give a gain higher than can be realised merely by increasing the signal plate potential (e.g. the enhanced gain at V_{sp} = +4V is equivalent to a normal working gain at V_{sp} = +12V, similarly the enhanced gain at V_{sp} = +10V is equivalent to a normal working gain at V_{sp} = +18V). The phenomenon is, however, of some interest as it does help in understanding the physics of the gain process, and it may have some practical application, since

as is described in Section 8.3 negative images can be formed. These could be used in the correlation of optical images, or for simple logic operations.

8.2 A qualitative explanation of the enhancement process

The enhanced gain obtained after this preparatory procedure is believed to be due to positive charges being stored inside the target. The potential distribution V(z) which is thought to exist through the target is shown in Fig. 8.1 for two different signal levels. In each case the signal plate potential is +20V, and z_t is the target thickness measured from the signal plate to the target surface. Fig. 8.1(a) shows the imaging beam producing a potential excursion ΔV of 5V on the target surface. This is considered to be a strong signal since it is near the maximum that can be used before beam-bending effects become objectionable. In this case there are two main reasons why the positive charge is being stored near the target surface. Firstly, the greater proportion of the secondaries are produced in this region by the imaging electrons which have lost most of their initial energy. Some of these secondaries leave the surface (T.S.E. electrons), but the majority are collected by the signal plate after travelling through the target (S.E.C. electrons). Both these electron-collecting processes leave positive charge stored near the surface. Secondly, any positive charges produced inside the

Fig. 8.1

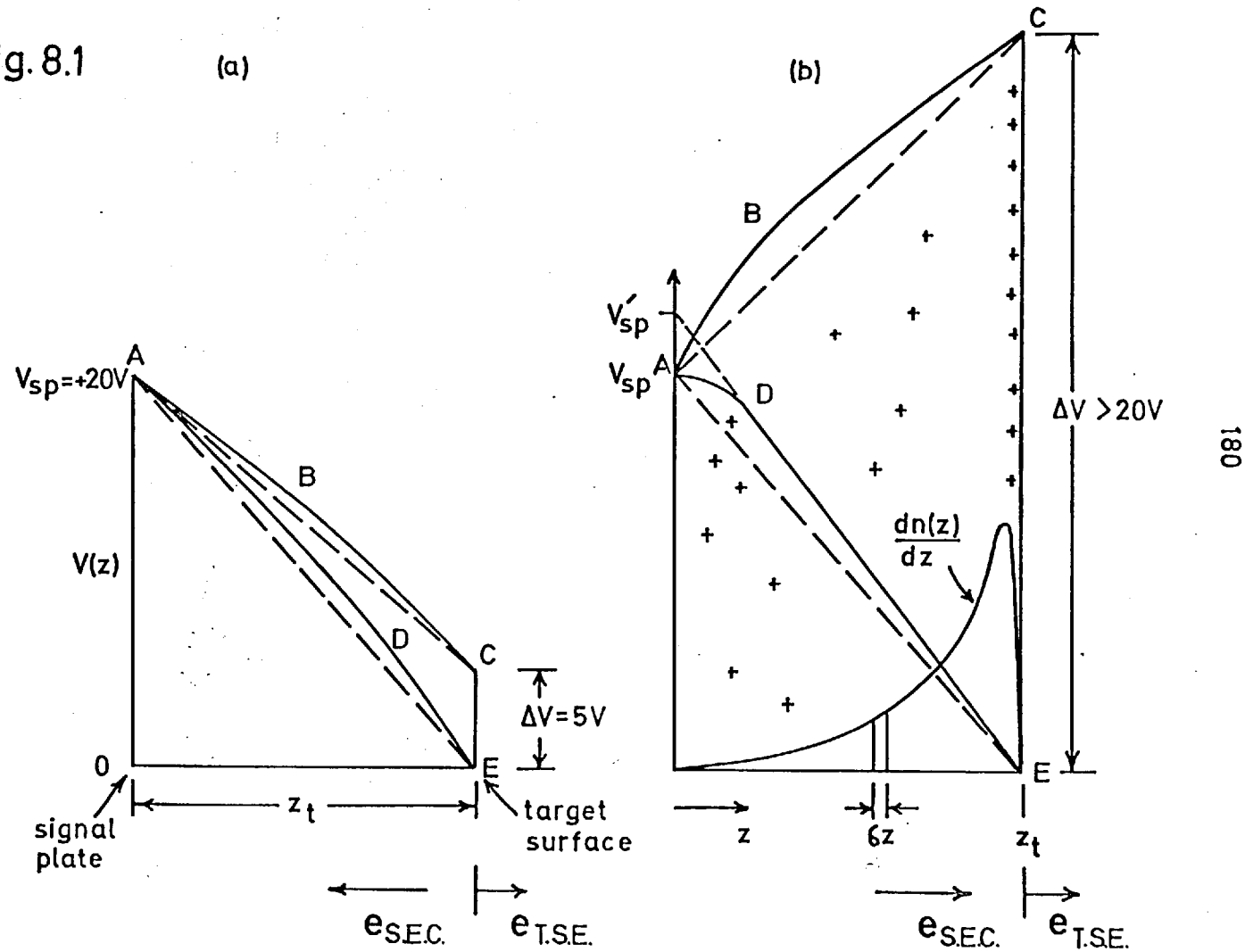
(a)
V_{sp}=+20V
A
B
V(z)
D
C
ΔV=5V
0
E
z_t
signal plate
target surface
$e_{S.E.C.}$
$e_{T.S.E.}$
(b)
C
B
V'_{sp}
V_{sp}
A
D
ΔV >20V
$\frac{dn(z)}{dz}$
E
z
δz
z_t
$e_{S.E.C.}$
$e_{T.S.E.}$

target will tend to be neutralised by the S.E.C. electrons which originated near the target surface, and were travelling towards the signal plate under the influence of the internal field. Fig. 8.1(a) shows the potential distribution after integrating the signal (A B C), and also after reading (A D E).

The potential distribution (A B C) shown in Fig 8.1(b) is typical of an overload state, and shows what happens during the enhancement procedure. The surface potential has become higher than that of the signal plate, causing the electric field to reverse so that the S.E.C. electrons now travel towards the surface. Positive charge is stored on the surface, but there will also be positive charges within the target. Since the rate of production of secondaries $\frac{dn(z)}{dz}$ increases as the imaging electrons pass through the target (in consequence of their energy loss), the number of positive charges produced in an elemental layer δz will increase with z. In this case, however, the number of S.E.C. electrons entering an elemental layer will be less than the number of positive charges created therein, and hence a net positive charge will build up. (This is in contrast to Fig. 8.1(a), where the surface was more negative than the signal plate, with the S.E.C. electrons travelling in the opposite direction and exceeding in number the positive charges produced in the layer δz, so that no internal charge resulted). This will be especially the case near the signal plate, where the rate

of production of secondaries will be very low. Equilibrium will be established when the field due to these changes causes electrons to leave the signal plate. The curve ABC shows the potential distribution during charging, and ADE that after cathode potential stabilisation.

After cathode potential stabilising it can be seen that the internal field gradient is greater for Fig 8.1(b) than for Fig 8.1(a), (except near the signal plate). Since the gain of the target is dependent on the electric field in the region where the secondaries are being produced (recombination is less likely to occur when the field is high), the gain of the target for the state shown in Fig 8.1(b) will be higher initially than that of Fig.8.1(a). For a given signal plate potential V_{sp}, it is possible to define an "effective signal plate potential" V'_{sp} for the prepared state which would produce the same higher internal field near the target surface, if there were no internal positive charges present, (e.g. for V_{sp} = +20V, then V'_{sp} was found to be +23V by similar methods to those mentioned in section 8.1).

During the integration of an image on a target in this prepared state, the S.E.C. electrons travelling towards the signal plate will combine with, and neutralise, the internal positive charges, causing the internal field, and hence the gain, to fall. Most of this internal charge will eventually

be removed after many charging and read-out cycles, and then the potential distribution will revert to that of 8.1(a) This was demonstrated by preparing the target, and then observing the amplitude of the video waveform when an optical image of constant luminous intensity was focused onto the photocathode, while the target was scanned at 25 frames/sec. A plot is shown in Fig. 8.2 for a target whose signal plate potential V_{sp} was +10V; it can be seen that the gain decays to one half of its initial value with a time constant ~5 secs (i.e. 125 frames).

It should be stressed that although these enhancement effects are noticeable under special preparation, for a tube in normal use with repetitive scanning little internal charge builds up to alter its performance. A high intensity light input (such as a flash bulb in the field of view) might cause a certain amount of internal charge build up, but this will be small unless the duration of this overload is long. In practice no difficulty with persistent images (either positive or negative, see section 8.3) has been encountered.

The fact that the amount of enhancement is dependent on the signal plate potential is thought to be a consequence of the neutralisation of positive charges within the layer by the scanning beam. It is known that the beam can penetrate right through the layer to the signal plate when its

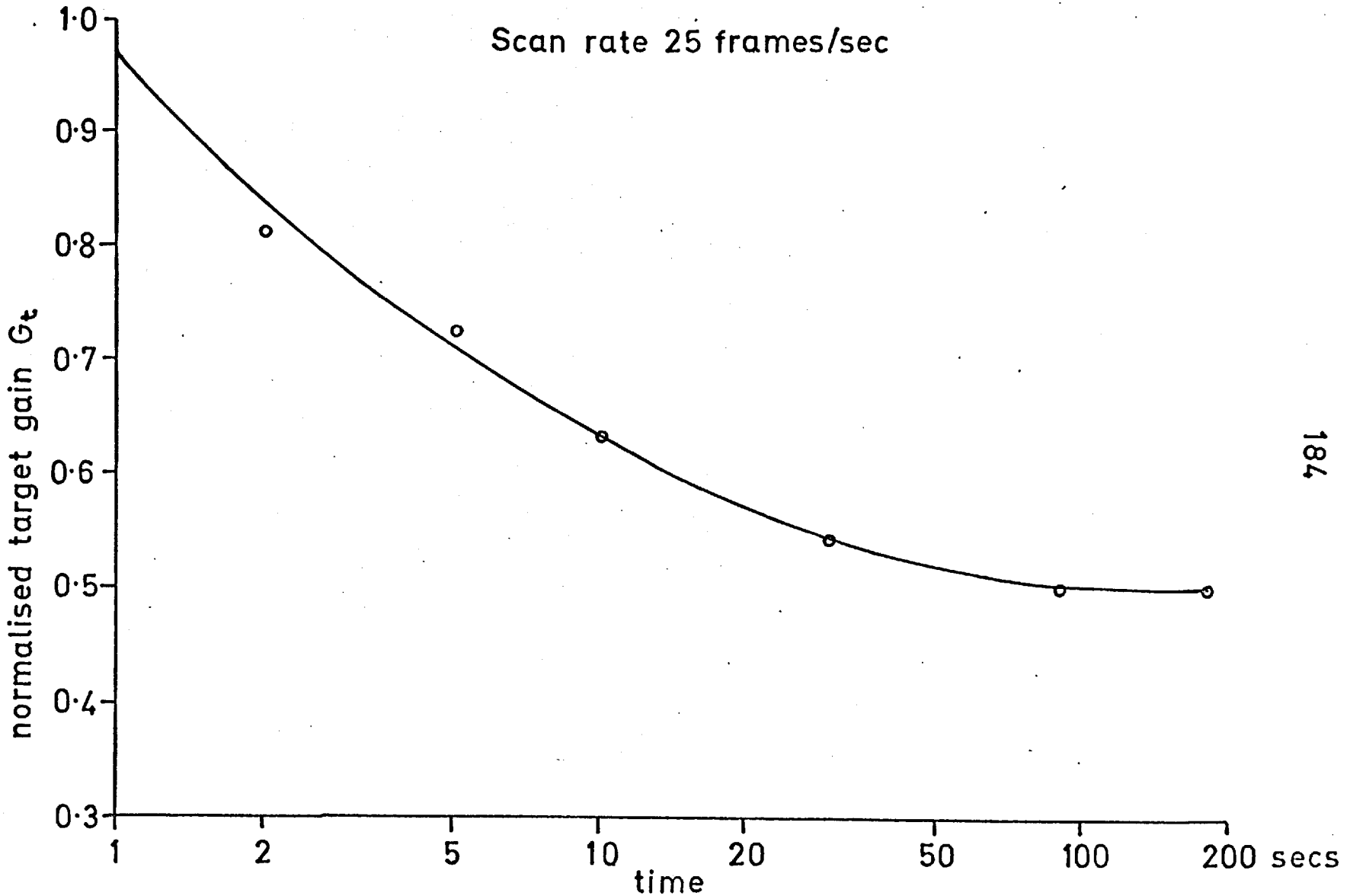

Fig. 8.2 Decay of target gain with time after initial charging

potential is high. It therefore seems plausible that for this condition, any positive charges produced during the flooding process will be neutralised when the scanning beam is used to cathode potential stabilise the surface, and thus there will be no enhancement of the gain.

8.3 Negative images

It is possible to make use of the phenomenon of gain enhancement to produce negative images. Consider Fig 8.3(a), this shows a potential plot for one line of a target with internal charge and with the surface cathode potential stabilised. (This corresponds to ADE of Fig 8.1(b), but with the line direction x on the target surface included). Now consider a vertical white bar image to be displayed for a few seconds while scanning at 25 frames/sec, the internal charge in the illuminated area will be neutralised to a certain extent. Fig 8.3(b) shows the potential distribution after many scans, with the light image on just before a line is scanned, and Fig 8.3(c) shows that after the light has been switched off, so that the whole surface has been brought to gun cathode potential by the action of the scanning beam. The internal charge in the illuminated area has, to some extent, been neutralised, therefore the gain in this area will now be less. If the target is now flooded with a uniform beam of electrons, the surface potential for the previously

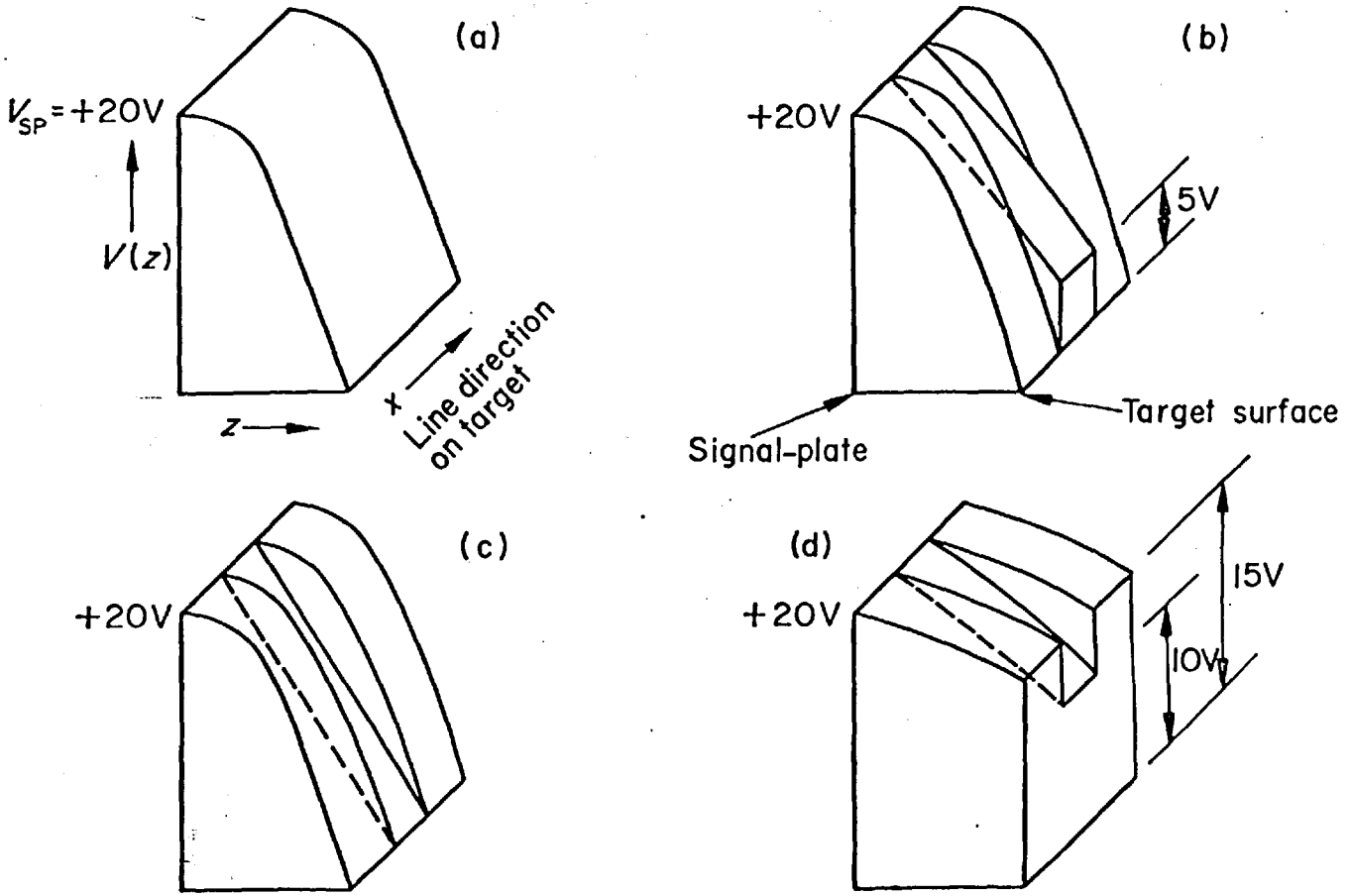

Fig. 8.3 Potential distribution diagrams illustrating formation of negative images: (a) target prepared before writing image, (b) writing and reading white vertical bar image, (c) cathode-potential stabilization after writing, and (d) after uniform flooding.

unilluminated areas will rise higher than those that were illuminated. This is shown in Fig 8.3(d) and it can be seen that a negative image has formed. In order to obtain a 5V signal amplitude the surface potential was allowed to rise by 10-15V (see Fig 8.3(d)). Before reading out the charge pattern the signal plate potential must be lowered by 10V so that the surface potential is reduced to the range 0-5V, to prevent severe beam bending occurring, and to improve the image contrast. Fig 8.4 shows photographs of a test pattern that was used in similar experiments. Fig 8.4(a) is a photograph of the image generated from the video signal during the display part of the cycle (as shown in Fig 8.3(b)), the signal plate potential was +20V. Fig 8.4(b) is the negative image obtained on read-out after the uniform flooding (as shown in Fig 8.3(d)). This image appears slightly blurred; this is because several negative images,each slightly out of registration, have been produced in several separate exposure cycles, without preparing the target at the beginning of each cycle to replenish the neutralised internal charge.

8.4 Correlation of optical images

It is possible to carry out simple logic operations by successively storing negative and then positive images. This is best explained with reference to Fig 8.5 After

Fig. 8.4.

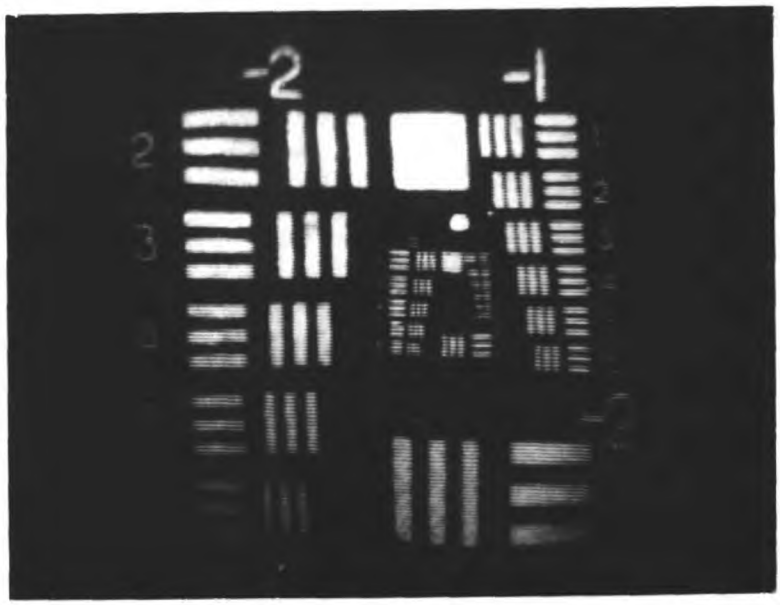

(a) positive image displayed, Vsp = +20V.

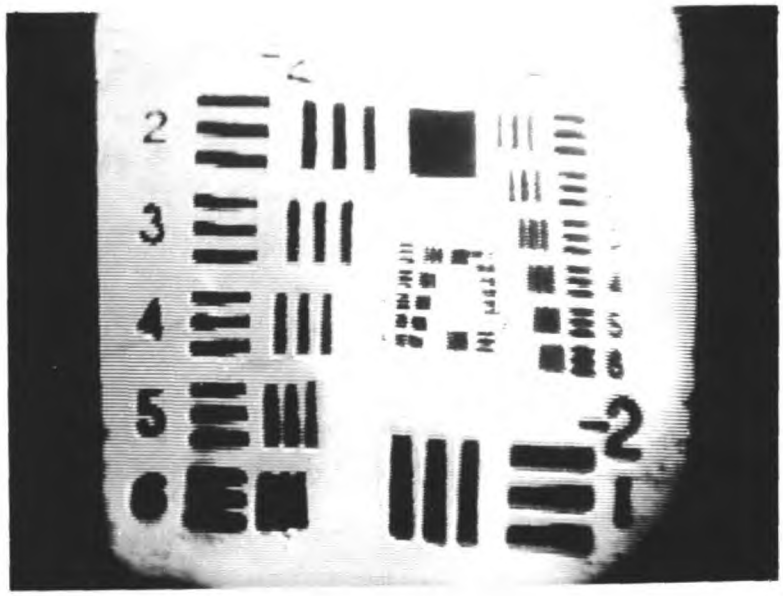

(b) negative image read-out at Vsp = +10V. after flooding.

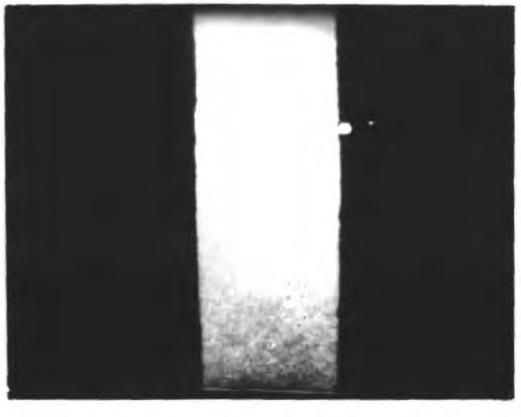

(a)

image displayed and stored
as a latent negative image.

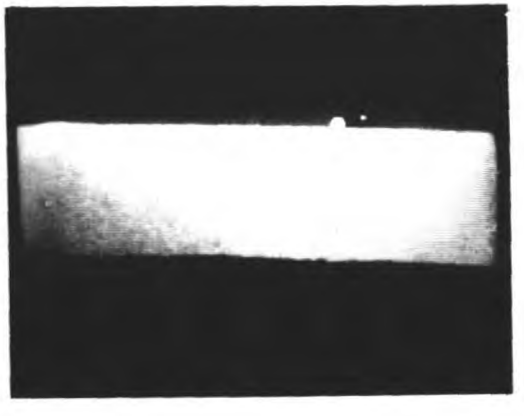

(b)

image written
as positive image

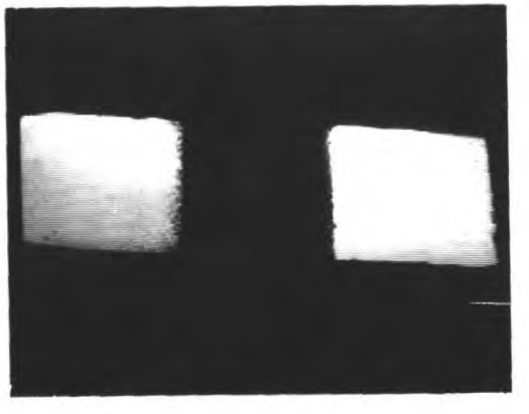

(c)

resultant
read-out

Fig. 8.5.

preparing the target, a white vertical bar image was displayed (see Fig 8.3(b)), as shown in the monitor photograph of Fig 8.5(a). This was internally stored after cathodèc potential stabilising the target surface (see Fig 8.3(c)) as a latent negative image. Then instead of uniformly flooding to obtain a negative image as in Fig 8.3(d), a second image was exposed. In this case it was a white horizontal bar, as is shown in Fig 8.5(b). The signal plate potential was lowered by a similar amount before read-out as in Fig 8.3(d). The result is shown in Fig 8.5(c), where it can be seen that the area common to Figs 8.5(a) and (b) has been removed from the image of (b) in Fig 8.5(c). This common area need not be completely removed but can be displayed as a half-tone, the intensity of which will depend upon the exposure for Fig 8.1(a), and the amount of lowering of the signal plate potential before read-out.

This simple example illustrates the possibility of performing auto-correlations and cross-correlations of optical images in such a form that the output is a video signal.

CHAPTER 9

TUBES AND ANCILLARY EQUIPMENT

9.1 Various Types of Tube

In parallel with the target investigations that were made with the demountable system, sealed off tubes were also constructed. These were made to demonstrate the feasibility of low light level image detection, with the various photocathode-target combinations available. Altogether four different tube types were contructed:

1. Normal KCl target with no stabiliser mesh
2. Normal KCl target with close spaced stabiliser mesh
3. Composite KCl-ZnS target with wide spaced mesh
4. Tube as in 3. but with intensifier section.

(a) The construction of the standard S.E.C. tube

By taking advantage of the information gained from the problems encountered in the early prototype tubes investigated by Filby et al[87], tubes of the type 1. to 3. have been made that are not so prone to leaks, have better background and geometry, and are less prone to corona discharge from the image section E.H.T. The main features of the tube design were decided upon early in the author's

research period and will not be described in detail since a full account has already been given by Filby[88].

Fig. 9.1 shows diagramatically this basic design. The whole tube was designed around the C.P.S. Emitron scanning section, and so the electromagnetic image section was arranged to form a single loop focus in the same solenoid. The photocathode 1. was processed in a separate compartment 2. so that the image section was not contaminated with alkali vapours which could produce low work function surfaces, and possibly attack the target. Both S.9, S.11 and S.20 photocathodes were used in various tubes. The S.20 photocathodes had white light sensitivities of 80-160 μA/lumen. This was considerably higher than the S.9 photocathodes, which had sensitivities ≈ 30-60 μA/lumen. For some applications however, the S.9 was preferred since its sensitivity was found to be more stable than that of the S.20 which had a tendency to decrease with age. The axial field was produced in the image section 3. by applying a potential across a series of annular electrodes which were internally connected by a resistor chain. The charge image was formed on the target 4. which was mounted on an assembly along with the meshes 5. and 6. For KCl targets the stabiliser mesh 5. was either absent or mounted $\sim$ 0.5 mm from the target. This spacing was increased $\sim$ 2 mm for the KCl - ZnS targets. The field mesh 6. was mounted $\sim$ 1 cm from the target. These spacings,

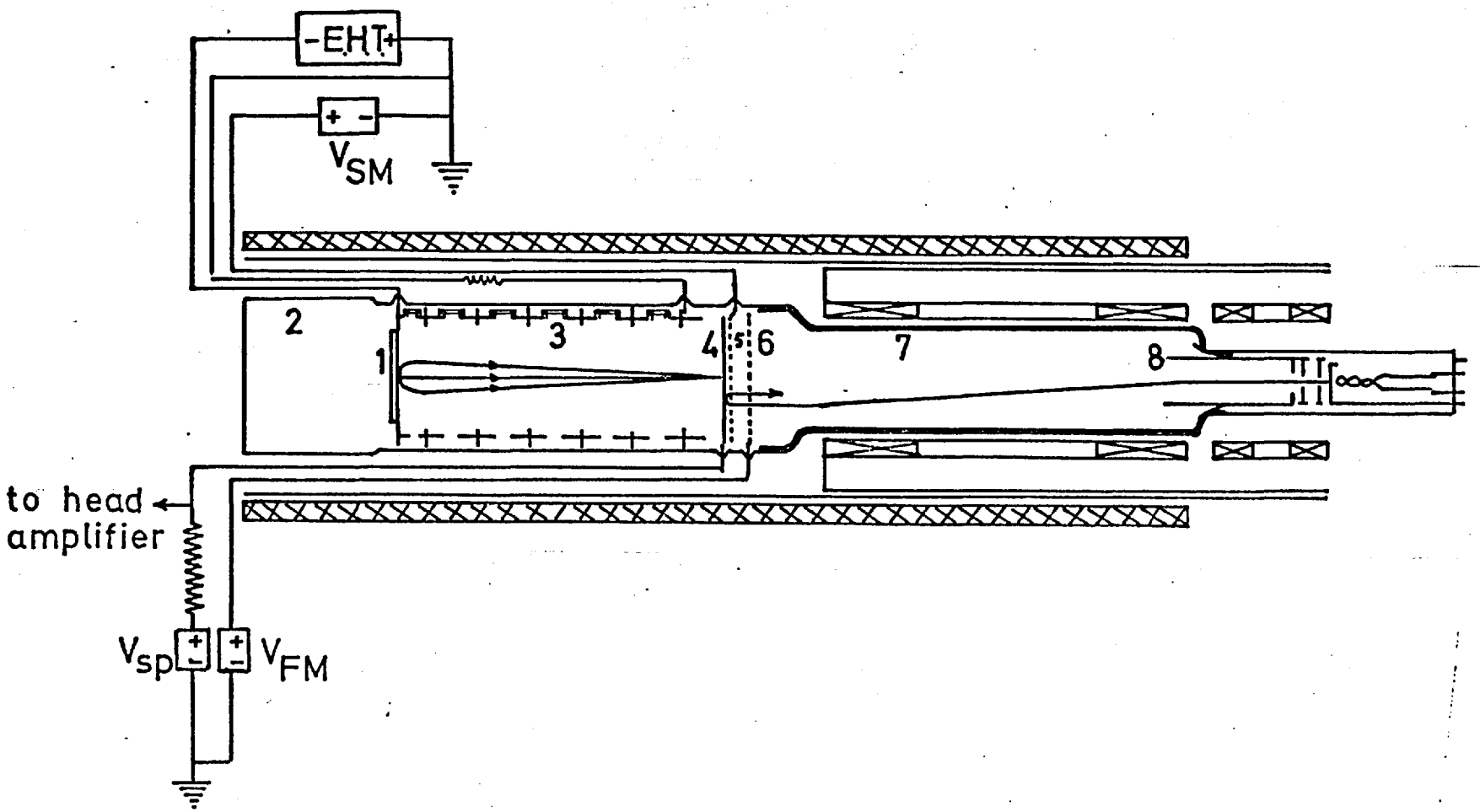

Fig.9.1 S.E.C. camera tube

together with the normal working potentials of the meshes, produced electric fields on either side of the mesh 5. that were approximately equal, and hence the power of the lenslets created by the mesh apertures of 5. was zero, preventing any degradation on read-out by this effect. The wall-anode 7., was deposited on the inside of the glass wall of the tube either by painting on bright platinum or gold paint, which had to be fired in at $\sim 600^{\circ}C$, or by evaporating a thin aluminium layer. The electron gun 8., was a complete vidicon assembly, the cathode of which was ~~found~~ formed just prior to the photocathode processing.

A few photographs are shown in Figs. 9.2 to 9.5 of images that were generated by some of these tubes using the normal 405 line, 50 fields/sec standard.

(b) The Contruction of the Intensifier S.E.C. Tubes

This highly sensitive tube, incorporates a cascade intensifier stage in the writing section of the single vacuum envelope. A diagram is shown in Fig. 9.6; the reading section is very similar to that described for the tubes in section (a) and uses the same C.P.S. Emitron scanning yoke. The target 1, and the meshes 2. and 3. are similarly mounted on three ceramic rods and clipped to the appropriate tungsten pins. The main differences are in the writing

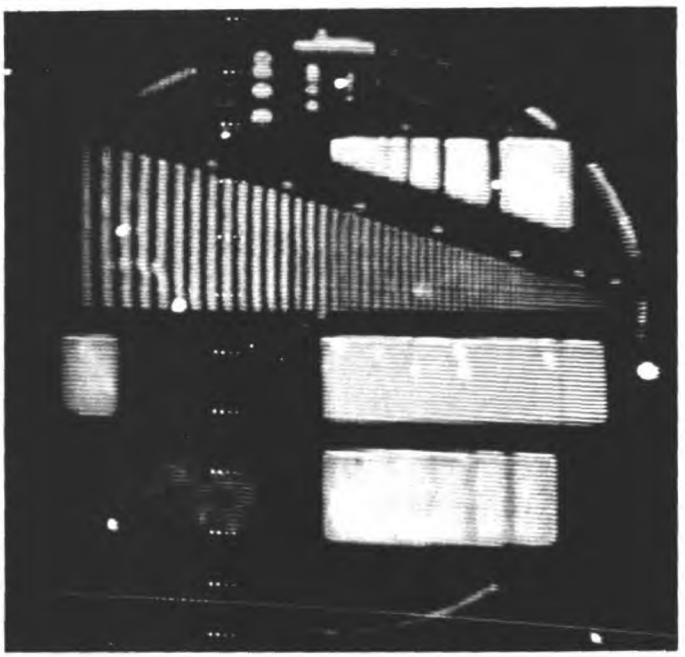

Fig. 9.2. Normal KCl tube with stabiliser mesh spaced at 0.5mm. from the target. Baum pattern image 8mm. diameter on the target Vsp = +20V G_t = 130, white light sensitivity of photocathode = 150μA/lumen, 10min. charge integration, photocathode illumination ~ 10^{-7}ft. cds.

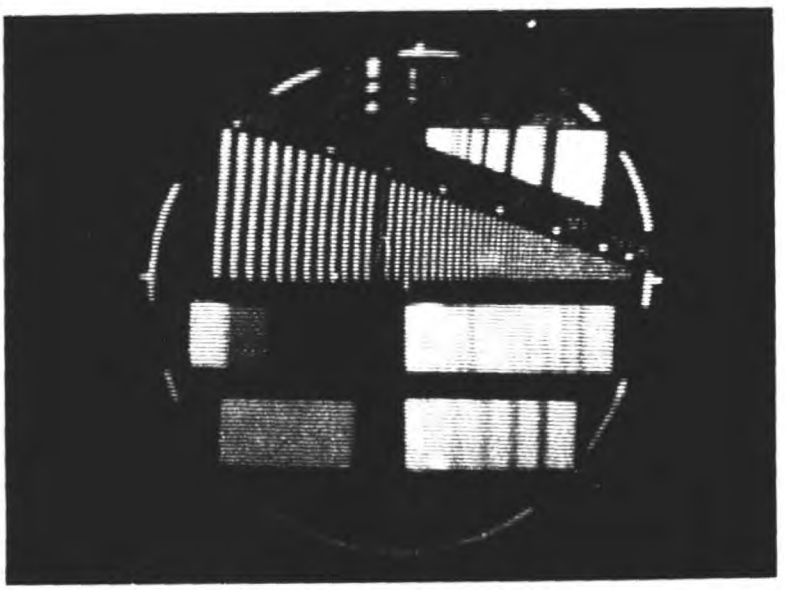

Fig. 9.3. KCl-ZnS tube, with nearest mesh spaced at 2mm. from the target. Baum pattern image 8mm. diameter on the target. Vsp = +22V $G_{S.E.C.}$ = 12.

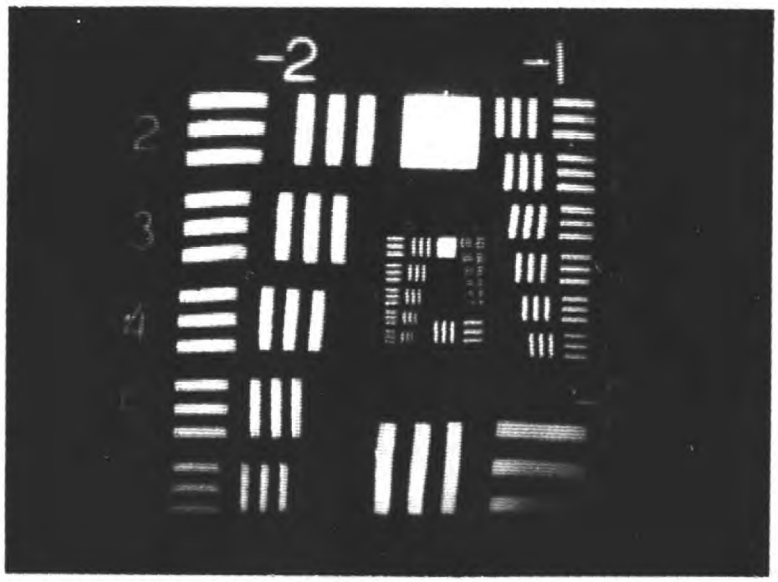

Fig. 9.4. KCl-ZnS tube (same as in Fig. 9.3.)
Image is of a U.S.A.F. pattern (raster size on target: 24mm. x 18mm.) Vsp = 11.5V. $G_{S.E.C.} = 6.$

Fig. 9.5. A similar KCl-ZnS tube. Photograph shows a half-tone image of a deer being fed (no gamma correction) Vsp = 30V. $G_t = 60.$

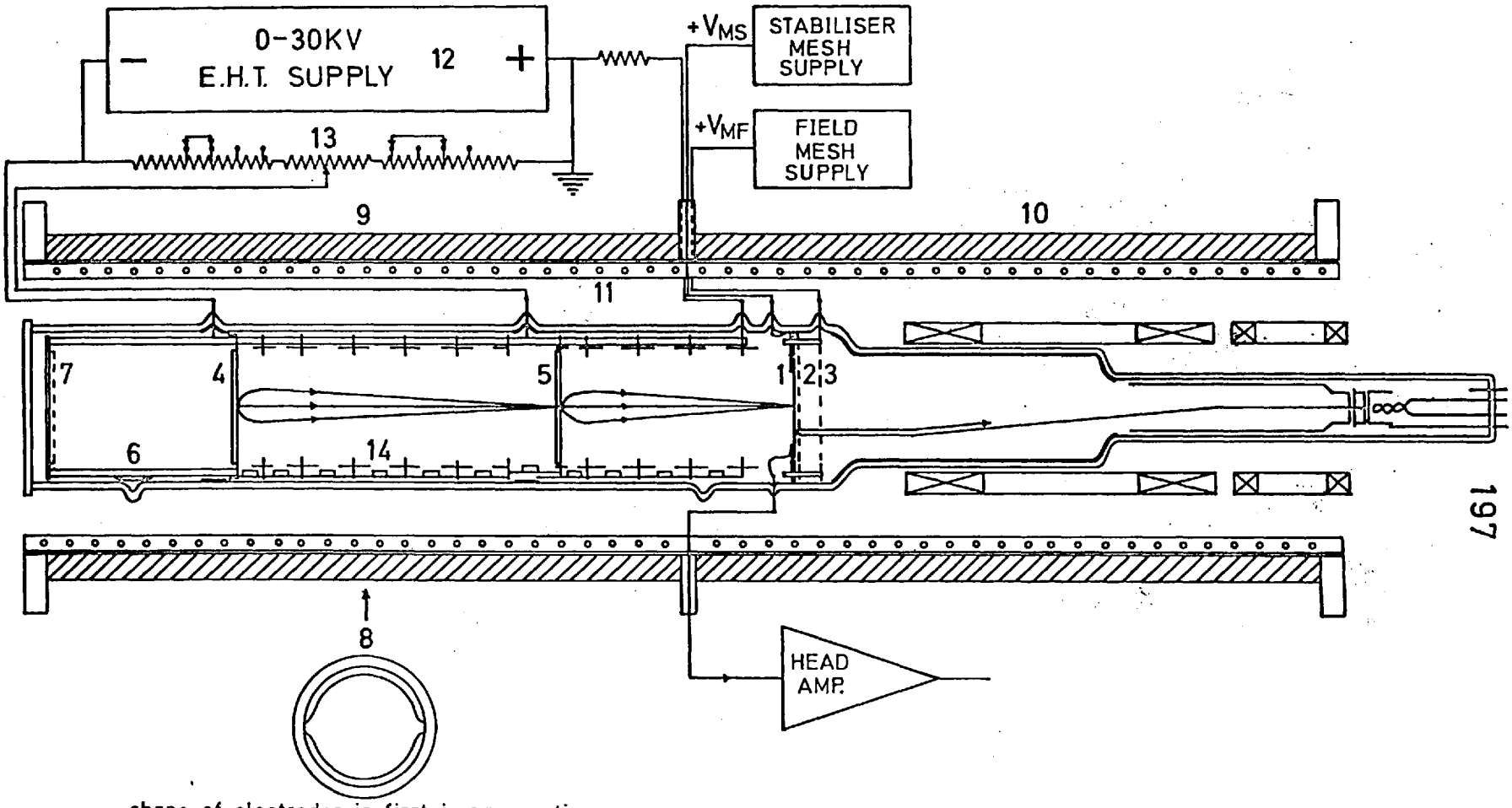

Fig. 9.6. Intensifier S.E.C. camera tube

section, because of the extra image section this has to be slightly longer than in the standard tube, but this is not so long as it might have been, because the final focussing distance to the target has been reduced to 9 cms instead of the standard 13 cms. This was possible because of the extra scanning power that was available for when the solenoid focussing current had to be increased. The target image section required about 7-8 KV for maximum target gain, and the cascade image section required about 15 KV for maximum light output from the phosphor, hence the photocathode 4. to cascade screen 5. distance had to be $\sim$ 12.5 cms. Both image sections were jigged up onto three long ceramic rods spaced at 120° intervals round the circumference of the annuli. This enabled the two image sections, and springs and catches for the photocathode processing compartment 6, all to be installed in the tube as one unit, quickly and easily soon after the target assembly was mounted. This was desirable to reduce the possibility of water vapor contamination of the target to a minimum.

During photocathode processing the photocathode plate was clipped in the position 7. and the cascade screen was situated in the normal photocathode position 4. with its

phosphor side facing the target. The tight fitting stainless steel skirt attached to the photocathode mount at 4. prevented alkali vapours from the photocathode processing compartment passing into the image sections, where they could form low work function surfaces, and attack the phosphor and the target storage material. The two photocathodes were processed by first sliding an antimony evaporator into the middle of the compartment so that the surfaces at 7. and 4. could be coated. The thickness of the deposit was monitored by measuring a 35% drop in optical transmission of the plate at 7. The alkali vapours were then introduced from channels in a side ampule, and after activation, the side arms were sealed off. Once the tube had been removed from the pump the cascade screen and the photocathode plate were positioned and locked into their normal working positions. The electrodes in the first image section had to be suitably shaped as in 8 (similar to those in a cascade tube[89]) so that the screen could pass through the first image section. The screen then had to be rotated so that its photocathode surface was facing the target before finally clipping it into the position 5. The photocathode plate was simply moved from 7. to 4. in a straight forward displacement.

After experiencing some difficulty in producing good S.20 photocathodes in this tube, it was decided to make antimony-cesium photocathodes of either S.9 or S.11 response instead. The S.11, besides being easier to make has the added advantage that its spectral response peaks in the blue part of the spectrum, which is a good colour match to the light emission from the P.11 phosphor on the screen.

From the total of the six I.S.E.C. tubes which were constructed, the tube which gave the most promising results was a tube which was processed with a simple antimony-cesium photocathode, having an S.9 response. This tube had a white light sensitivity $\sim$ 60 μA/lumen, and no detectable change was found in the sensitivity even after a month. A certain amount of background appeared in the tube when the overall E.H.T. was greater than 12 KV, & for this reason it was not desirable to try and run the tube at maximum sensitivity with 22 KV overall.

Images of good geometry and resolution ($\sim$15 l.p./mm) could however be obtained with as little as 3 KV across the target image section (i.e. with $\sim$ 6 KV for the intensifier stage amounting to $\sim$ 9 KV overall), at a light level which would have produced no useful signal for 3 KV across an ordinary S.E.C. tube. The electron gain G_p of the

cascade screen with ∿ 6 KV on the intensifier stage was ≃ 24, and for ∿ 8 KV, G_p ≃ 45. No measurement of the target gain G_t was made, because unfortunately the target ruptured before this was done. It can be seen, however, from the above figures for the intensifier electron gain, that even a target gain G_t ≃ 10 would yield a low light level performance which would be better than the best, ordinary, S.E.C. tubes. This must not be considered as the limit for such tubes, because being a recent development only a few tubes have been made, and one can expect the techniques to improve with experience.

A photograph is shown of this tube alongside a standard tube in Fig. 9.7.

9.2 Camera Equipment

The camera that was used for the standard tubes was an old C.P.S. Emitron camera. The solenoid was extended by adding on a few extra coils to accommodate the image section. The camera had its advantages, being a well engineered piece of equipment with rack and pinion focus controls, etc. It was easy to use, but for this particular tube, bringing the target and mesh connections out of the photocathode end of the solenoid, (see Fig. 9.1), it had its disadvantages. Firstly it meant bringing the

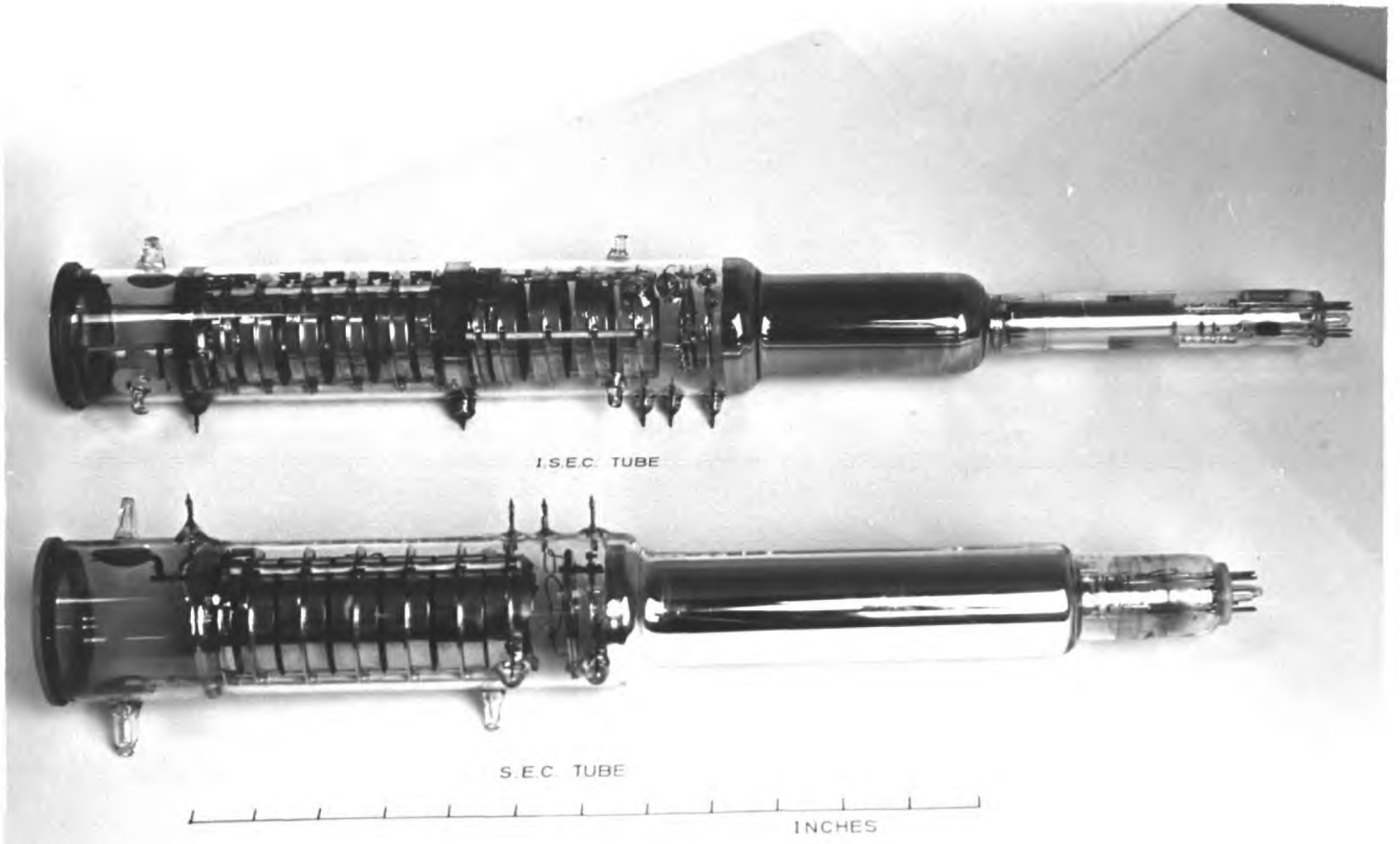

Fig. 9.7.

signal plate lead out passed the E.H.T. supply lead for the image section. This made the video prone to pick-up from slight corona discharge around the image section. Secondly, because of the long image section the signal-plate lead had to be long, and since this also had to be screened the stray capacitance was unnecessarily high producing unwanted shunting of the high frequency signals.

For the intensifier tube an even longer solenoid was required, so it was decided to design a completely new camera tube test bed. The salient features of the design can be seen in Fig. 9.6. The long focussing solenoid has been made in two halves 9. and 10., and was so arranged that the split occurred in the region of the signal plate pin. They formers for the two halves had circular brass cheeks at their ends, between which the two coils were wound in a continuous multilayer fashion from 18 guage enamelled copper wire. This wire was of heavier guage than was used in the multicoil solenoid of the C.P.S. Emitron camera, and enabled a low voltage, high current stabilised transistor power supply to be used. The two halves were aligned and allowed to move longitudinally between rails on a duralumin base plate. When assembledas one long solenoid the two middle cheeks were

butted against one another and the signal plate and mesh leads were brought out at this point through channels cut half in each cheek face. Each half of the solenoid could be liquid cooled by means of a copper tubing helix which was set into the outerwall of an inner lining perspex cylinder.

The focus of the two image sections was controlled by a variable 0-30 KV E.H.T. supply 12. The ratio of the two image section voltages being set by the potential divider resistance box 13., which was an order of magnitude lower in resistance than the internally mounted resistor chain 14, that connected the annular electrodes in the tube to establish the axial electric field. The whole writing section of the tube was encapsulated in a tight fitting perspex cylinder to prevent electrical breakdowns (not shown), which also served the purpose of locating the tube in the centre of the solenoid. In the writing section the Araldite potted C.P.S. Emitron scanning yoke was located.

A photograph is shown in Fig. 9.8 where the split solenoid halves 1. and 2., E.H.T. focussing box 4., stabilised current supply 5., and a slow scan F.E.T. head amplifier 3. can all be clearly seen. The lens barrel of a Baum projector can also be seen in front of the camera at 6.

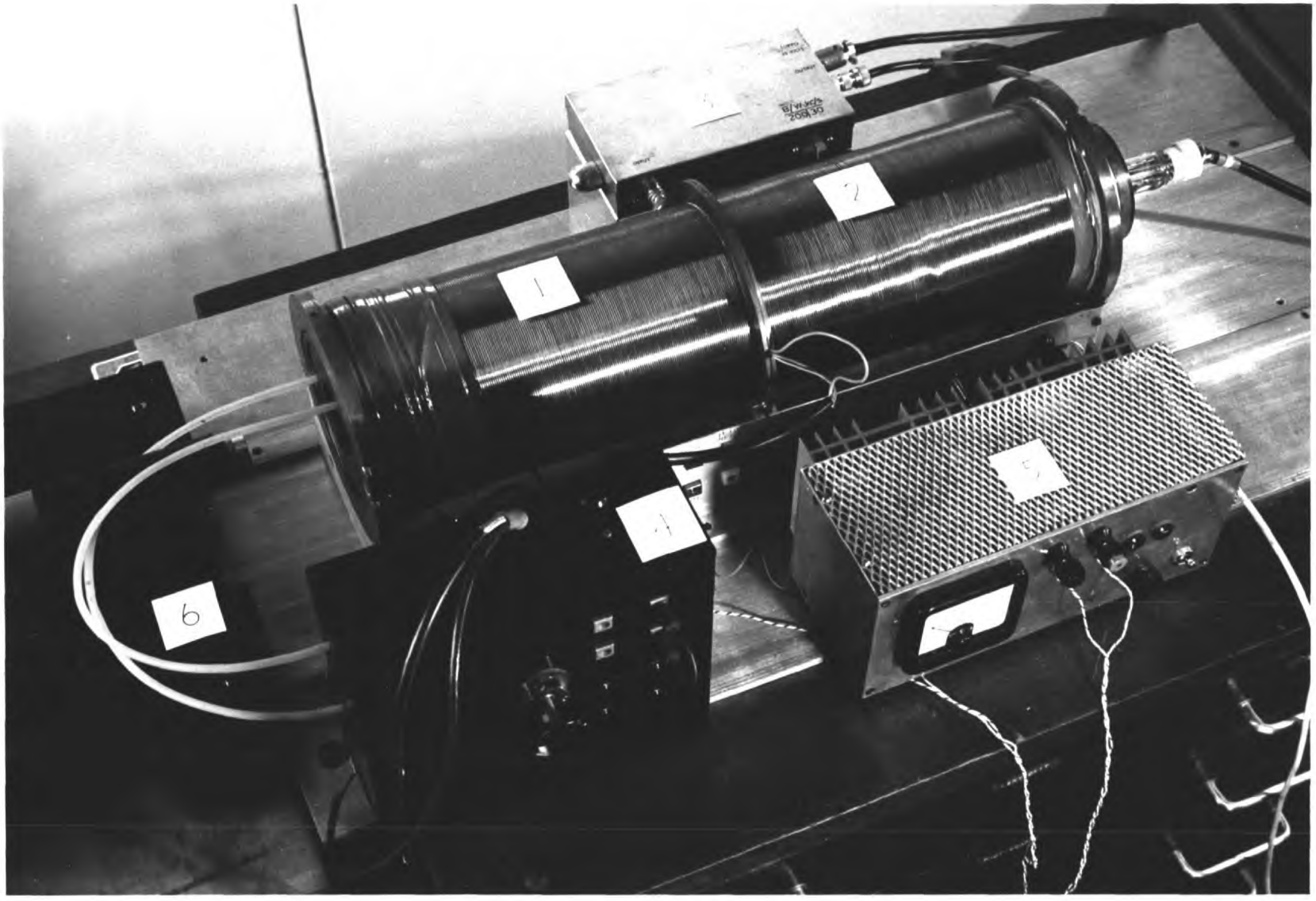

Fig. 9.8.

9.3 Television Camera Channel

(a) The Conventional 405 line 50 fields per sec. System

A large proportion of the measurements that have been made on targets in the demountable system, or in sealed off tubes, have been carried out using a closed circuit, conventional television channel similar to the E.M.I. type 10270-C. This is a 405 line system in which the lines are interlaced, one frame being made up of two fields of 202½ lines; the framing rate being 25 per second (i.e. 50 fields/sec.). This was a useful piece of equipment for observing the behaviour of these targets under conventional scanning conditions, and in particular to see if lag was objectionable.

However, for certain scientific applications this channel was not all that was to be desired. It has already been shown in Chapter 3 that there is an optimum bandwidth for a given tube-head amplifier combination for which the signal to noise ratio is a maximum. This imposes a requirement on the scanning such that once the required vertical resolution in terms of T.V. lines has been decided upon (for the given application), then the frame read-out time is fixed. These optimum conditions cannot be met when one is tied to a conventional television standard, but for an application

where the camera is used for a long integration of several hours of a single frame image, then there is no hardship in having to wait a few seconds to read-out the frame, so that the optimum signal to noise ratio can be obtained. Also as the final result is to be a single frame, stationary image that will be recorded, then there is no virtue in including interlace in the scanning, which can be troublesome particularly if photometric measurements from the video waveform are required.

(b) The Variable Scan Rate Equipment

An early attempt at improving the signal to noise ratio, by scanning at non-conventional rates was made by using a slow scan system that was originally built by Mende for a similar purpose. Apart from a transistorised frame scan amplifier being added, the whole system used valves, the video circuits were virtually copies of the conventional scan equipment except for the fact that time constants had been adjusted for the duration of the longer pulses, and for the frequency response of the narrower bandwidth (15 KHz). Although some useful work was done with this system, it was thought that perhaps a better, and more versatile system could now be made by making use of recent semidonductor technology. A study of the noise characteristics of some

F.E.T. transistors (see Chapter 3) has indicated that such a device should give an improvement for the first amplifying stage in the head amplifier, over that of the E80F (low noise pentrode) in Mende's system. It was also thought that in order to optimise the signal to noise ratio as far as possible for various tube-head amplifier combinations, it would be useful to have a range of different standards.

This was done by building a completely new system that was fully transistorised and had a variable scan rate. The design is rather unconventional for a television system, and has been designed mainly with the scientific user in view. A block diagram of the complete system is given in Fig. 9.9.

The line standards were obtained by using the binary division of the chain of bistables 1. to 10. This was used since it is a very stable form of division and very immune to noise pulse triggering. This was driven by one of three oscillator frequencies which constituted the three different line frequencies. These were chosen as 50 Hz, 400 Hz and 12.8 KHz. The 50 Hz frequency was derived from a low voltage winding on a transformer and was squared by the Schmitt trigger 12. so as to provide accurate timing for the binary

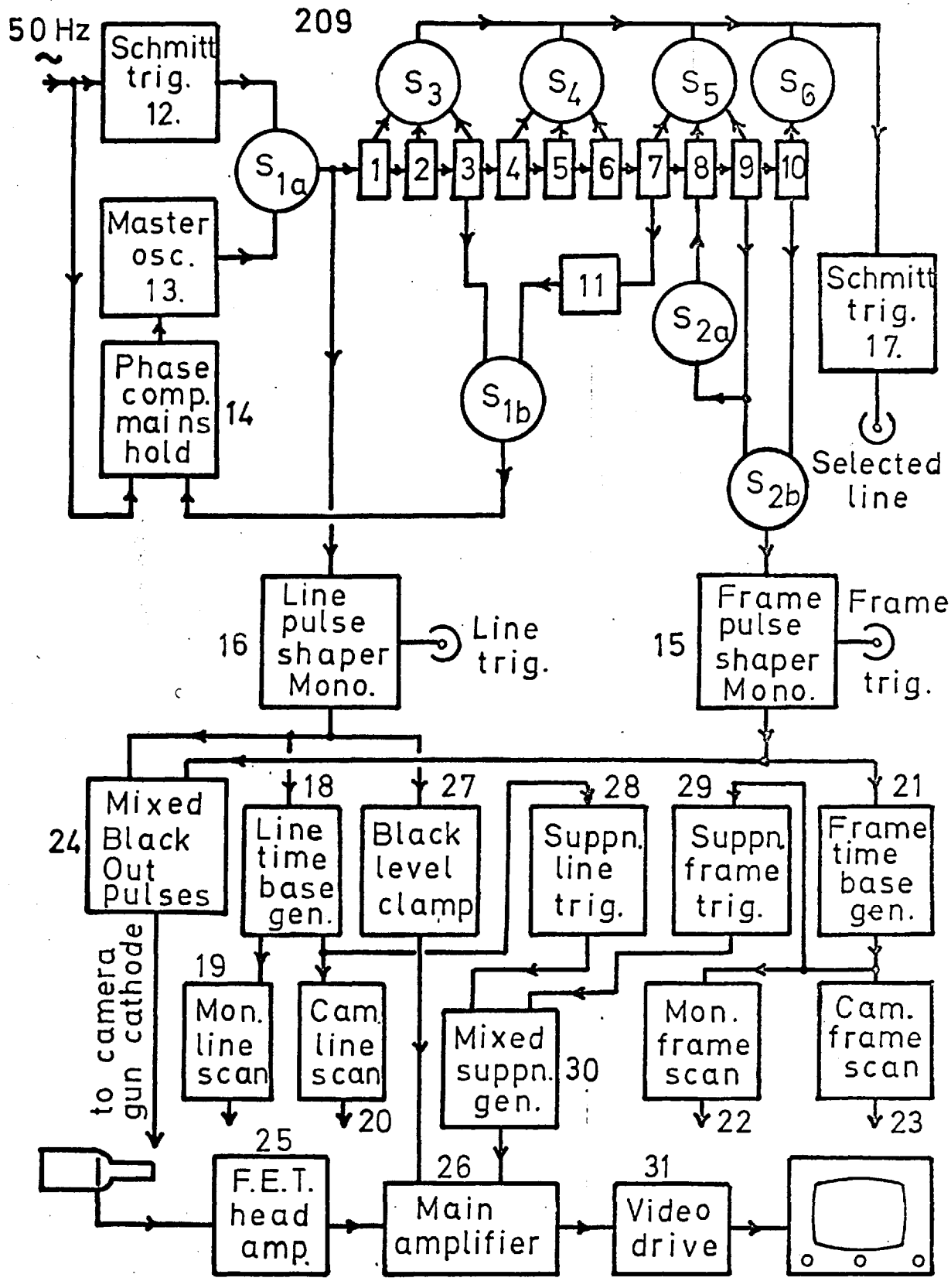

S_1 line frequency switch :- 50Hz, 400Hz, 12·8KHz.
S_2 line standard switch :- 384, 512, 768, 1024.

Fig. 9.9.

chain trigger. The 400 Hz and 12.8 KHz were both generated by the master oscillator 13; this was a simple blocking oscillator in which a capacitor could be switched to obtain either frequency. To prevent any effects of 50 Hz hum bar drift, both of these line frequencies were locked to the mains. This was done by extracting a 50 Hz pulse at a suitable point in the binary chain, and comparing the phase with the 50 Hz mains in 14. which provided a correction voltage for the master oscillator that was proportional to the phase difference, and which would correct the frequency accordingly. The switch S1 is the line frequency switch; S1a selects either the 50 Hz mains pulses or the 400 Hz and 12.8 KHz master oscillator pulses; S1b selects the 50 Hz comparison pulse, which for the 400 Hz line frequency is obtained from the bistable 3, and for the 12.8 KHz a 50 Hz pulse cannot always be obtained from the bistable 8. because of the switching in this part of the circuit, so a 100 Hz pulse is obtained from bistable 7. and divided by two by bistable 11.

The line standard depends upon the stage at which a frame trigger pulse is extracted from the division chain. This is arranged by the switch S2; using the complete ten bistables each to provide a division by two, the overall

division is 1024, and so such a line standard is achieved by providing a suitably shaped frame trigger pulse from the monostable 15 when driven by 10 via S2b. For a 512 line standard S2b obtains the frame trigger from 9. Two other standards are provided when using either the ten or only nine bistables by feeding back a pulse from 9. to 8. via switch S2a so that 8. and 9. act as a combined ÷ 3 circuit. This then reduces the line standard to 768 when all ten bistables are used, and to 384 when only the nine are used. Thus the combination of three line frequencies and four line standards gives a large selection of possible bandwidths required. Suitably shaped line trigger pulses are obtained from the monostable 16. which is fed with the same pulses that drives the binary chain. The frame trigger pulses are obtained from a similar monostable 15. which is fed from the output of the chain. Apart from these two trigger pulses which are also provided at external sockets for external triggering facilities such as for oscilloscopes, there is a third trigger pulse outlet, the selected line pulse. This is a pulse which occurs once per frame and can be set to occur at the beginning of any particular line in the frame, and can be used on any of the four possible line standards. This is particularly useful for triggering

an oscilloscope so that one particular line of video can be displayed. The selected line pulse was obtained by identifying the line number in the binary chain corresponding to the required line. This was done by having rotary switches S_3, S_4, S_5 and S_6, which could connect either output of each bistable to the Schmitt trigger 17 via an AND gate. The Schmitt trigger would then only produce a pulse if there were simultaneously positive signals present at all of the selected outputs of each bistable. This will only occur once per frame for any selected line number. The selection switches are wired in octaves so that the first switch S_3 enables the selected line to be adjusted in unity steps one to eight, the second switch S_4 in steps of eight, the third switch S_5 in steps of sixty four, and the last switch S_6 in steps of five hundred and twelve. Although it is difficult to work in octaves to obtain the line number this is not really necessary, since a line is usually selected, not by its number but by the particular part of the image where it happens to pass through. What is more important than the line number is to be able to select lines in a region of interest in the frame in either fine or coarse steps.

It is from the line and frame trigger pulses that the

rest of the control waveforms are generated. The line scan is generated by a constant current F.E.T. generator 18. which is reset with each pulse from 16. This provides a very linear sawtooth waveform which is used to drive two D.C. coupled amplifiers 19. and 20., the former to supply the line scanning coils of the monitor and the latter those of the camera. Line shift in both cases is provided by altering the standing currents in the amplifiers. A similar arrangement is used for the frame scan, 21 being the time base generator with 22. and 23. the monitor and camera scan D.C. coupled amplifiers. Mixed black out pulses are provided by the pulse amplifer 24. to the gun cathode of the camera tube so as to prevent the scanning beam discharging the target during either the line or the frame flyback. The amplifier has two inputs to two transistors (one for the line and the other for the frame trigger pulses) serving a common load, so as to behave as a NOR gate and mix the line and frame pulses. This output feeds a high voltage transistor inverting amplifier, the pulse height of which can be varied. This pulse height adjustment can be used to estimate the voltage excursion on the target surface, since if the pulse height is less than the voltage excursion on the target the flyback lines will be visible,

but if the pulse height is greater than this excursion no flyback lines will be seen. Thus, for the point at which the flyback lines just cease to be visible the voltage excursion on the target will be given by the pulse height setting.

The video is directly coupled from the signal plate of the tube into the F.E.T. head amplifier 25., This is possible because the potential of the gun cathode and all of the other gun electrons can be varied with respect to the signal plate so as to adjust the polarisation across the target. The head amplifier has an F.E.T. cascode stage at the input which consists of two 2N3819 J.F.E.T. transistors; these were not sold especially as low noise F.E.T.'s but were cheap and readily obtainable, and have remarkably good noise characteristics for their price. It was planned to adjust the operating parameters of the amplifier using these general purpose F.E.T.'s and when the conditions were favourable to substitute the more expensive F.E.T.'s, such as the 2N3684 for which the theoretical performance is given in Fig. 3.4 of Chapter 3, or perhaps to include the more recent low noise F.E.T. BFW56. This was not done, because of the shortage of time available, and the long dispatch times quoted for these devices.

The 2N3819 F.E.T. has a similar noise voltage per root cycle to these special low noise devices, ($\sim$ 4nV/$\sqrt{\sim}$) for frequencies greater than $\sim$ 100 KHz. At lower frequencies the low noise devices become progressively better (e.g. at 10 Hz for the 2N3819 e_n = 200 nV/$\sqrt{\sim}$, but for the BFW56, e_n = 20 nV/$\sqrt{\sim}$). The input impedance of the head amplifier was 10^8 ohms; this is a factor of 10 less than the value assumed for the calculations of Chapter 3 (which are displayed graphically in Fig. 3.4) but this had to be used as a compromise because of the effects of stray capacitance. This will not have much effect on the signal to noise ratio, except when using very small bandwidths, and then the effect can be observed by appropriately displacing the $(N_R/S)^2$ component line to the right in Fig. 3.4. The output impedance of the amplifier was $\sim$ 50 ohms provided by an emitter follower so that it could be matched to the input impedance of the main amplifier 26. The head amplifier had a unity voltage gain (but a very large power gain) and a flat frequency response over its entire pass band. The bandwidth was curtailed at the high frequency end by providing two $\frac{1}{2}$ L, C, T-type filters which produced sharp roll-offs for bandwidths of 30 KHz and 200 KHz. These two bandwidths were suitable for most line standards

at the two line frequencies of 50 Hz and 400 Hz. The 12.8 KHz line frequency standard has not yet been used, as a suitable line scan power amplifier for this frequency has yet to be designed and built. This was not considered a priority item as the E.M.I. channel could be used for results in this region with line frequencies $\sim$ 10 KHz and 16 KHz.

In spite of some of the shortcomings in this design over the theoretical results of chapter 3, the amplifier has produced some improvements over the theoretical best possible performance of the R5559 valve head amplifier, even if it were operated at its optimum bandwidth of 200 KHz For a tube of the type M (shunt capacitance $\sim$ 10 pf) connected to the input to the F.E.T. amplifier, the measured equivalent input noise current i_n was 3.3pA and 18.3pA at bandwidths of 30 KHz and 200 KHz respectively. Since the read-out is for a storage tube it is more meaningful to quote a quantity Nn, the equivalent number of noise electrons stored per picture point such that,

$$Nn = \frac{i_n \Delta T}{e} = \frac{i_n}{2ef_b} \qquad (9.1)$$

From the above noise currents, equation 9.1 gives values for Nn of 312 and 286 electrons at bandwidths of 30 KHz and 200 KHz respectively. It can be seen that the number of noise electrons per picture point is almost constant for the variation in bandwidth considered. This is also seen to be the case in Fig. 3.4 where the theoretical signal to noise ratio as a function of bandwidth for the tube type M can be seen. This shows an optimum S.N.R. at a bandwidth of 25 KHz. The fact that the number of noise electrons per picture point is slightly more for the 30 KHz bandwidth than for the 200 KHz bandwidth is the consequence of using the 2N3819 transistor in place of the 2N3684. Since, although the noise voltage generator values are similar at high frequencies, at a frequency of 10 Hz, e_n for the 2N3819 is ten times that of the 2N3684. There is also the fact that the input impedance used was a factor of ten less than assumed in Fig. 3.4 and this would make the effects of the noise worse at small bandwidths.

Comparing these results with those obtainable from valve amplifiers, Mende[90] has quoted the number of equivalent noise electrons stored per picture point to be 480 for

a high slope triode operating at optimum scanning bandwidth. A figure of 360 electrons per picture point is the theoretical value obtained for the tube type M at the optimum bandwidth in Fig. 3.1

The curves in Figs. 3.1 and 3.4 are given in terms of signal to noise ratios, this can be done for the experimental F.E.T. amplifier by assuming a maximum stored target charge of 10^5 electrons per picture point. The values then obtained are 50 dB for the 30 KHz bandwidth and 51 dB for the 200 KHz bandwidth. These values are not much worse than the theoretical optimum value of 53 dB given in Fig. 3.4 for the type M case.

The signal level that is presented to the main amplifier 26. is such that any noise contributions from these additional stages will be negligible. Apart from providing a certain amount of voltage gain, which is frequency independent inside the required passband, the amplifier has to process various pieces of pulse information. The main requirements are to black level clamp, and to suppress the video output for a period when the scan is flying back. The main amplifier 26. consists of four stages, the first two are A.C. coupled common emitter mode amplifers, followed by two D.C. coupled emitter follower stages. The first emitter

follower receives its bias from the black level clamp circuit 27. The second acts as a gated amplifier being switched by the suppression pulses via an isolation diode. These two stages are D.C. coupled by a normally forward biased diode which acts as a peak white limiter. The black level clamp circuit is pulsed at line frequency from 16., and consists of a pair of complementary transistors with two diodes which when pulsed always present a low impedance path between the reference potential and the base of the first emitter follower stage. The mixed line and frame suppression pulses which gate the output of the amplifier are unique in as much as both line and frame suppression pulse widths are independently variable, so that a variable width black boarder can be inserted around the raster. This was introduced as a means of preventing the metal target ring being displayed as a bright overload signal because of the continual beam acceptance at a conductor. The target area could not be deliberately under scanned to eliminate the ring in the non-suppressor mesh type tubes, because of the fear of charging of the unscanned areas which would lead to dielectric breakdown.

These particular pulses are generated in a rather novel way by means of the circuits 28, 29 and 30. The circuit

28. consists of two Schmitt triggers, which are both supplied with the waveform from the line time base generator 18. By means of variable resistors the levels can be set at which each Schmitt trigger will turn over. These are so arranged that one trigger occurs near the beginning of the linear ramp and the other near the end. It is these two controls which set the width of the black border down the left and right hand sides of the monitor screen. An identical circuit 29., which is supplied with the frame time base waveform supplies trigger pulses that control the width of the back boarder at the top and bottom of the monitor screen. All four trigger pulses, which have been suitably differentiated and clipped to spikes, are fed to the mixed suppression pulse generator 30. This consists of a pair of bistables, the two frame suppression trigger pulses alternatively change the state of the first bistable so that a frame suppression pulse is generated of suitable width and phase in relation to the frame scan. This output is used to gate the output of the second bistable which is similarly fed with the two line suppression trigger pulses. The mixed suppression output is then fed to a long tailed pair amplifier which is a D.C. coupled to the output stage of the main amplifier 26. The high

voltage video drive 31., required at the gun cathode of the monitor was provided by a single high voltage transistor connected as a common emitter D.C. coupled amplifier.

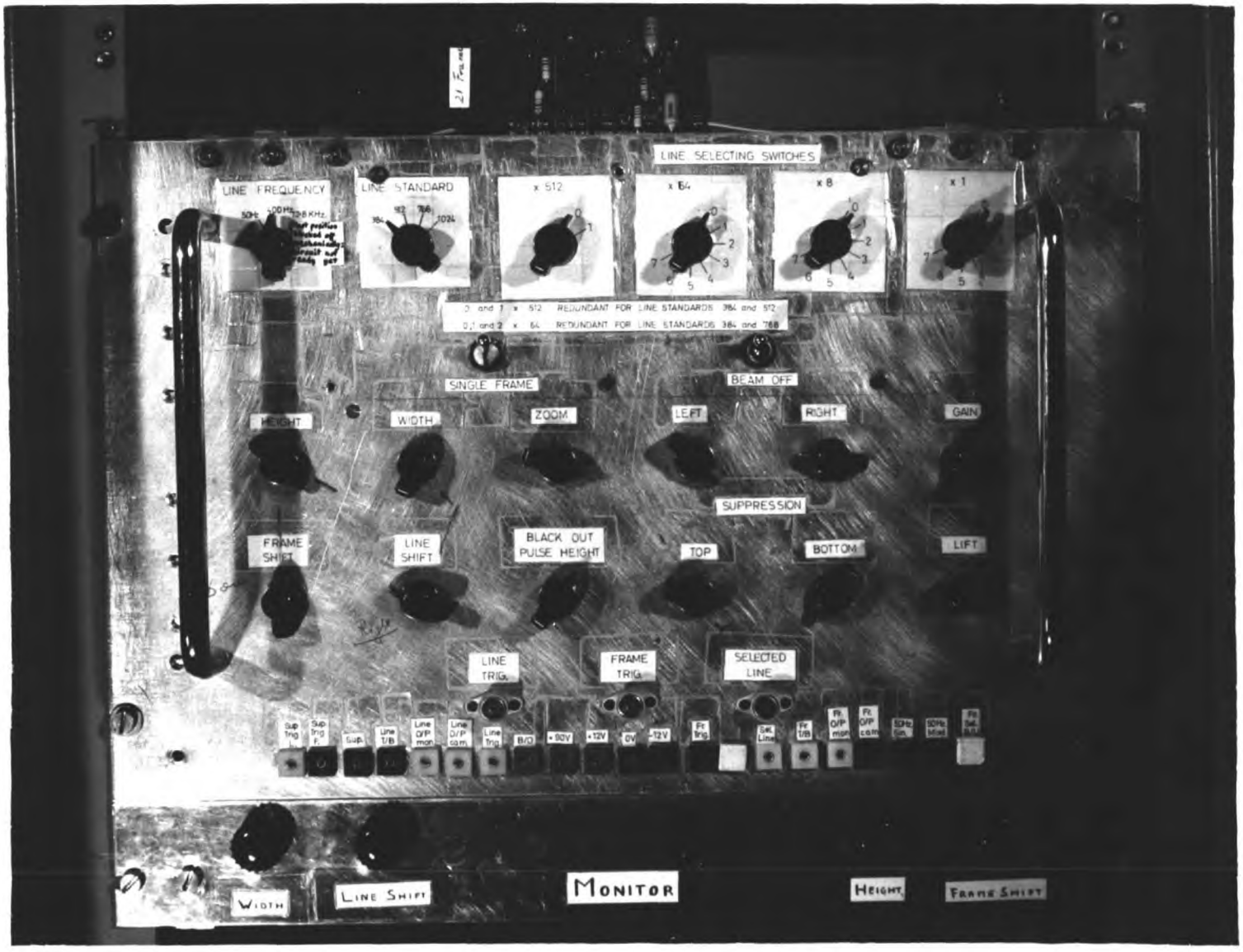

Fig.9.10 Control Panel of Variable Scan System

CHAPTER 10

CONCLUSIONS

The S.E.C. camera tube has held the promise of a better camera tube to come for some years now. Its initial claim to a high target gain coupled with good storage properties, and a low lag made it an attractive looking device. This thesis has attempted to look more deeply into the properties of the S.E.C. target, to try and understand the physical processes involved, and to try and improve the design from such understanding.

As was shown in Chapter 5, the stability could be improved by coating the surface of a KCl target with a thin layer of a poorer secondary emitting material. ZnS was found by the author to be suitable; the thickness of the coating however was a compromise between the stability and gain required of the target. To a certain extent it was found that one could trade a higher first cross-over potential for a lower target gain. A solution to this problem has been described in Chapter 9; the I.S.E.C. tube. Here the reduced target gain, (which is the result of the high degree of stability being built into the target) has been more than offset by the pre-target gain of an intensifier screen.

However, there is no point in having the gain higher than necessary because of the limited storage capacitance of the target. For most scientific applications it is considered necessary to have the photoelectron shot noise higher than the amplifier noise; with improvements in head amplifier design along the lines indicated in Chapter 3 a lower target gain will be acceptable.

The main properties of the target were dealt with in Chapter 7. The main finding there which cannot be too strongly expressed is that the gain at high signal plate potentials is not due to S.E.C. processes, although it is indistinguishable from the S.E.C. gain from experimental gain measurements. Very high gains $\sim$ 500 - 1000 cannot be explained on a secondary emission theory basis, but the accompanying lag seems to indicate that B.E.C. (Beam Electron Conduction) is responsible.

Observations by the author have also found that these targets do not have a unique value for the gain at a given signal-plate potential. It has been found that this depends upon the amount of internal charge stored in the layer. It has been found possible to produce enhanced gains by suitably charging the layer, and to create negative images by an application of this technique. It is possible

that these properties could be a disadvantage in certain applications, but there is also the possibility that these properties could be used to advantage (e.g. for image correlations).

S.E.C. camera tubes with potassium chloride targets, protected by stabiliser meshes are currently being made available by the Westinghouse Corporation, both in electrostatic and magnetic focused forms, some with fibre optic end-plates. Typical performance figures obtained for these tubes indicate that the resolving power for static imaging is slightly worse that that of an image orthicon, but considerably worse than an isocon at the same face plate illumination. For dynamic imaging, however, the isocon is less desirable because of the effects of lag. The S.E.C. tube does not suffer as badly under these conditions, and for such a tube with return beam orthicon mode read-out, the resolving power at a given illumination is marginally better than an isocon.

To try and arrive at some criterion, to say whether these camera tubes are better than any of the others presently available, is a rather meaningless task, since the merits of individual properties depend so much on the application for a particular tube. The three most favourable

properties of the S.E.C. target are:

1. good charge storage
2. a high target gain
3. low lag (providing the signal plate potential is below $\sim$ + 30v)

These properties, especially 1. and 2., lend themselves well to the detection of faint low contrast images by prolonged charge integration and so one would expect to find applications for this device wherever such images are to be found (e.g. astronomy, spectroscopy, microscopy, etc.). Unfortunately these properties alone are not the only requirements for most applications. If accurate photometric work is to be done in any of these fields then the Transfer Characteristic of the device has to be known or at least to be predictable under all circumstances, and if the spatial frequencies present in the image are to be preserved the resolving power must be adequate.

Another application, could be to meet the needs of the every day requirements of broadcasting. In this case the properties 2. and 3. would be most favourable, and could mean the design of a compact highly sensitive, low lag, camera. It would be necessary however to improve the

resolution in terms of the number of T.V. lines per picture height. There is a limit to the resolution in terms of line pairs per mm, set by the target thickness, (see Chapter 1.) and if one attempts to make the target thinner, then one is up against the problems of increased discharge lag caused by the increase in target capacity, and a reduced true S.E.C. gain (although B.E.C. gain can be high, but this will be accompanied by high lag). The resolving power will also be impaired by the presence of fixed pattern noise, which gets appreciably worse as the target thickness becomes thinner. This is due to the fact that the storage layer is made up of agglomorates of the low density material, and is a fundamental property of the nature of the material.

To overcome these two main drawbacks it would be necessary to fabricate large area targets to achieve the required number of T.V. lines. The handling and production of such large area targets would however be no mean task. It would also mean that the prevention of target blemishes would have to be well controlled. Even if all these requirements could be met there is still a high probability that objectionable positive, or possibly negative, images having considerable lag could occur, by gain enhancement processes, if the target were subjected to an overload condition

such as accidently being exposed to a bright source.

The question now arising is, how can S.E.C. targets be further improved ? It is important when trying to answer this question to differentiate between the practical and the fundamental limitations. The gain and the resolution (in line pairs/mm) are fundamental properties for a target of given material and thickness. The area of a target and the number of blemishes it contains are practical limitations, and can possibly be improved with refined production techniques.

At the present time blemishes are a serious limitation to the efficient production of S.E.C. tubes. The number of blemishes could possibly be decreased by careful design of the evaporation boat to eliminate imperfections in the evaporated deposit, but it will not decrease the probability of the deposit becoming dusted onto the nearest mesh which can then behave as a storage mesh, and introduce blemishes in the read-out. A composite target with a wider spaced mesh does help to prevent the second effect being a nuisance.

The probability of finding a material with a much higher gain than potassium chloride does seem very small. There are possibly several materials which might give marginal

improvements. The problem of retaining a similar gain for a composite target to that of a normal KCl target is a difficult one. In this case one must expect some reduction in gain, since one is using a poorer secondary emitting material near the surface, which is where an appreciable number of the secondaries are formed. A better secondary emitter than KCl would possibly be the solution, but such a material is unlikely to exist.

In the opinion of the author the applications to which the S.E.C. camera tube will be put in the future are small. It is unlikely to be adopted for widespread broadcasting applications even if the problem of the target blemishes is overcome, because of the rather limited resolution, and the possibility of objectionable "after" images of either a positive or negative nature, following an overload condition. For astronomical observations, the fact that the target has good storage properties, and a high gain, seems to indicate that it should be useful for the detection of faint low contrast images, by charge integration, over long periods. However, to carry out any serious phâtometric measurements on such images, (which is a basic measurement in most astronomical observations), the Transfer Characteristic has to be an accurately defined

function. This is not an accurately reproducible quantity for an S.E.C. tube, since its form depends upon the nature of the image, and on how much internal charge may be stored in the layer (the enhanced gain effect). This variation in gain, preventing a unique Transfer Characteristic to be quoted will probably prevent the tube from being widely used by ground-based astronomers. Some preliminary work has been done on ground-based telescopes with S.E.C. tubes by Green and Hansen[91] but they made no critical comparison with any of the electronographic tubes, with which they will have to compete. Since no information was given about the photometric accuracy obtained, or of the effects of fixed pattern noise from the target, it is difficult to draw any definite conclusions at this stage. A field where the S.E.C. tube may continue to do some useful work is in the field of satellite-borne astronomy. Here the easy access of information via a telemetric link, is more important than the photometric accuracy. There have already been several examples of such uses[92,93,94] including the Apollo 11 mission. The latter example included a rather novel demonstration of how the low lag and high sensistivity of an S.E.C. tube could be utilized to produce a compact colour camera, using a single tube and rotating

colour filters to provide a field sequential colour signal.

Nozawa[94] using an ultra-violet sensitive S.E.C. camera tube (Uvicon) is engaged in doing accurate photometric work in the ultra-violet region, as a part of the Orbiting Astronomical Observatory (O.A.O.) programme. Here the photometric accuracy is relying upon being able to accurately measure target parameters such as the Transfer Characteristic, point by point over the target surface, recording any spatial dependence. This information is programmed into a computer which processes the video data. As ultra-violet photometry is something which cannot be done at a ground-base observatory the S.E.C. tube should be capable of considerable success in this field, because it is necessary to store the images and transmit them back to Earth by a television link.

An application where the S.E.C. tube should at present play a high role, is in military night surveillance systems. Here very high definition is not usually required, nor is photometric accuracy and tubes can be made small and simple. Most of the applications are for dynamic imaging, using either helicopters or aircraft, and the S.E.C. tube is known to behave well under such conditions since the target lag is low. Also fixed pattern target noise and blemishes

are less objectionable under dynamic imaging conditions. It might, however, be necessary to pulse off the E.H.T. of the image section whenever an unexpected high light level occurred (such as a bomb bursting) to protect the target from internal charging, and preventing spurious signals.

APPENDICES

A.1 Derivation of amplifier term in equation (2.25) for F

If the amplifier was the only component of noise in the system, then the equivalent quantum efficiency, using equation (2.26) would be,

$$\xi^{-1} = \frac{\bar{n}_{slpp}}{\left(\frac{S}{N}\right)^2_{App}} = \frac{\bar{n}_{sl}}{\left(\frac{s}{n}\right)^2_{A}} \qquad (A.1.1)$$

where $\bar{n}_{slpp}$ is the number of photons per picture point

Therefore $\bar{n}_{sl}\left(\frac{n}{s}\right)^2_{A} = \bar{n}_{slpp}\left(\frac{N}{S}\right)^2_{App}$ (A.1.2)

Now in Appendix A.3, it can be seen that for the case of the valve head amplifier

$$\left(\frac{N}{S}\right)^2_{App} = \frac{1}{n^{-2}_{s5pp}}\left[(\alpha+\beta)\frac{1}{f_b} + \eta f_b\right] \qquad (A.1.3)$$

where, α is the Johnson noise coefficient

β is the grid shot noise coefficient

and η is the anode shot noise coefficient

Now if f_A is the equivalent spatial cut-off frequency of the head amplifier in l.p./mm then,

$$\bar{n}_{slpp} = \frac{\bar{n}_{sl}}{4f_A^2} \qquad (A.1.4)$$

$4f_A^2$ being the number of picture points per unit area.

Substituting equations (A.1.3) and (A.1.4) in equation (A.1.2) we get,

$$\bar{n}_{sl}\left(\frac{n}{s}\right)_A^2 = \frac{\bar{n}_{sl}}{4f_A^2} \cdot \frac{\left[(\alpha + \beta)\frac{1}{f_b} + \eta f_b\right]}{\frac{\bar{n}_{sl}^2}{16f_A^4} \cdot \sigma_l^2 \bar{G}_p^2 \bar{G}_t^2}$$

$$= \frac{4f_A^2}{\sigma_l^2 \bar{G}_p^2 \bar{G}_t^2 \bar{n}_{sl}} \left[(\alpha+\beta)\frac{1}{f_b} + \eta f_b\right] \qquad (A.1.5)$$

A.2.

The threshold exposures required for detectors to obtain a given resolving power

The absolute photon limited resolving power is given by equation (2.7) which for a 100% contrast image is,

$$f_s = \bar{E}_o^{\frac{1}{2}} \times 5.5 \times 10^4 \text{ line pairs/m.m.} \qquad (A.2.1)$$

An image of low contrast m_o increases the threshold exposure for a given resolving power from E_o to E_1 such that

$$\bar{E}_1 = \frac{\bar{E}_o}{m_o^2} \qquad (A.2.2)$$

Additional noise introduced into the system giving a noise factor F, increases the exposure again from $\bar{E}_1$ to $\bar{E}_2$

$$\text{i.e. } \bar{E}_2 = \bar{E}_1 F = \frac{\bar{E}_o F}{m_o^2} \qquad (A.2.3)$$

For real detectors the M.T.F. will increase the threshold exposure again from $\bar{E}_2$ to $\bar{E}_3$ for the same resolving power,

$$\text{i.e. } \bar{E}_3 = \frac{\bar{E}_2}{r_{syst}^2} = \frac{\bar{E}_1 F}{r_{syst}^2} = \frac{\bar{E}_o F}{m_o^2 r_{syst}^2} \qquad (A.2.4)$$

where r_{syst} is the square wave response of the system and F is a constant throughout the exposure range. However, for a constant noise source F is proportional to $\bar{E}^{-1}$, and hence the resolving power is proportional to the exposure, and under these conditions

$$\bar{E}'_1 = \frac{\bar{E}'_o}{m_o} \qquad (A.2.5)$$

$$\bar{E}'_2 = \bar{E}'_1 F = \frac{\bar{E}'_o F}{m_o} \qquad (A.2.6)$$

and $$\bar{E}'_3 = \frac{\bar{E}'_2}{r_{syst}} = \frac{\bar{E}'_1 F}{r_{syst}} = \frac{E'_o F}{m_o r_{syst}} \qquad (A.2.7)$$

A.3.

The Signal to Noise ratio obtainable from a valve head amplifier

Consider the signal plate of a tube connected to a signal resistor R of a valve amplifier, which is shunted by a stray capacitance C.

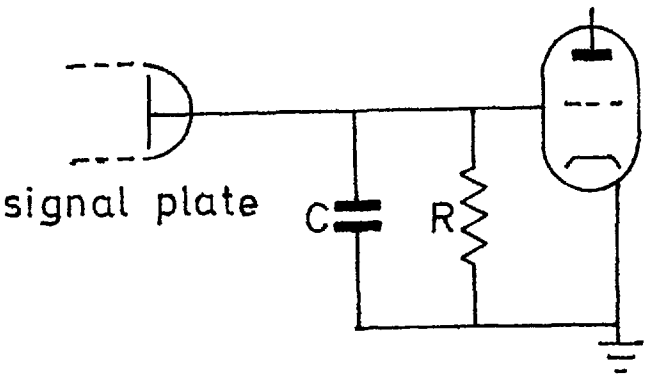

Letting Z be the impedance of the RC combination then,

$$Z = \frac{R}{1 + j\omega CR} = \frac{R(1 - jwCR)}{1 + \omega^2C^2R^2} \qquad (A.3.1)$$

where ω is the angular frequency of the signal.

The effective noise resistance of the input circuit due to the resistor R is equal to the real part of the impedance Z,

i.e. $$\mathcal{R}Z = \frac{R}{1 + \omega^2C^2R^2} \qquad (A.3.2)$$

The frequency characteristic of the input circuit however, is given by the modulus of the complex impedance,

i.e. $$|Z| = \sqrt{ZZ^*} = \frac{R}{\sqrt{1 + \omega^2C^2R^2}} \qquad (A.3.3)$$

It can be seen that at high frequencies, $|Z|$ and hence the input signal will be small, thus to obtain

a flat overall frequency/amplitude characteristic, the gain A of the amplifier has to have a form which is the inverse of the input characteristic of equation(A.3.3)

$$\text{i.e.} \quad A = A_o\sqrt{(1 + \omega^2C^2R^2)} \qquad (A.3.4)$$

where A_o = zero-frequency gain

Now if R_n is the noise equivalent resistance of the input valve, then the total noise voltage squared at the input grid, in a small frequency band df is equal to,

$$V_{ni}^2 = 4kT\,(R_n + \mathfrak{R}Z)df \qquad (A.3.5)$$

where T = Absolute temperature of the circuit

k = Boltzman's constant

The noise output voltage squared is given by,

$$V_{no}^2 = \int_o^{f_b} V_{ni}^2 A^2 df$$

$$= \int_o^{f_b} 4kT(R_n + \mathfrak{R}Z)A^2 df$$

i.e. substituting equation (A.3.5)

Now substituting equations (A.3.2) and (A.3.4) into the above expression gives,

$$V_{no}^2 = 4kTA_o^2 . \int_o^{f_b} \left[R_n(1 + \omega^2C^2R^2) + R\right] df \qquad (A.3.6)$$

where f_b is the upper frequency limit of the pass band. the integrandof equation (A.3.6) is termed the noise spectrum, as it shows the variation of the output noise with frequency.

In order to have a direct comparison between the signal current at the input with a noise current, it is useful to convert equation (A.3.6) to an effective input

noise current I_{ni}. Then,

$$I_{ni}^2 = \frac{V_{no}^2}{A_o^2 R^2} = 4kT \int_o^{f_b} \left[\frac{R_n}{R^2}(1 + \omega^2 C^2 R^2) + \frac{1}{R} \right] df \qquad (A.3.7)$$

There is also another source of noise which cannot be neglected due to the fluctuations in the grid current.

The mean square grid current fluctuation = $2e i_g \int_o^{f_b} df$ (A.3.8)

Thus from equations (A.3.7) and (A.3.8),

$$I_{ni}^2 = 4kT \left[\left(\frac{R_n + R}{R^2} \right) f_b + \frac{4}{3}\Pi^2 f_b^3 C^2 R_n + \frac{e i_g}{2kT} f_b \right] \qquad (A.3.9)$$

To compare this noise current with the signal current i_s, obtainable from the tube we can write,

$$i_s = \frac{e \bar{n}_{s5pp}}{\Delta T} \qquad (A.3.10)$$

where $\bar{n}_{s5pp}$ = mean number of electrons stored per picture point

ΔT = dwell time of the scanning beam on a picture element

The minimum bandwidth required of the amplifier is given by,

$$f_b = \frac{1}{2\Delta T} \qquad (A.3.11)$$

Therefore, from equations (A.3.10) and (A.3.11) it can be seen that,

$$i_s = 2e\bar{n}_{s5pp} f_b \qquad (A.3.12)$$

Now from equations (A.3.9) and (A.3.12) and assuming $R_n \ll R$ as will invariably be the case then,

$$\frac{I_{ni}^2}{i_s^2} = \left(\frac{N^2}{S}\right)_{App} = \frac{kT}{e^2 \bar{n}_{s5pp}^2} \left[\frac{1}{Rf_b} + \frac{4}{3}\Pi^2 C^2 R_n f_b + \frac{e i_g}{2kTf_b} \right] \qquad (A.3.13)$$

which can be written as,

$$\left(\frac{N^2}{S}\right)_{App} = \frac{1}{\bar{n}^2_{s5pp}} \left[(\alpha+\beta)\frac{1}{f_b} + \eta f_b\right] \qquad (A.3.14)$$

where $\alpha = \frac{kT}{e^2 R}$ is the Johnson noise coefficient for the signal resistor (A.3.15)

$\beta = \frac{i_g}{2e^2}$ is the grid shot noise coefficient (A.3.16)

and $\eta = \frac{4\pi^2}{3}\frac{kT}{e^2}C^2 R_n$ is the anode shot noise coefficient (A.3.17)

A.4. The Signal to Noise ratio obtainable from an F.E.T. head amplifier

The equivalent input noise current squared I^2_{nil} for the Johnson noise of the signal resistor R and the noise voltage generator e_n of the FET 2N3684 is given by equation (A.3.7) by substituting for R_n from equation (3.8). Then,

$$I^2_{nil} = \frac{V^2_{no}}{A^2_o R^2} = 4kT \int_o^{f_b}\left[\frac{10^6 f^{-0.75} + 4\pi^2 10^6 C^2 f^{1.25}}{R^2} + \frac{1}{R}\right]df \qquad (A.4.1)$$

$$= 4kT\left[\frac{10^6 f_b^{0.25}}{0.25R^2} + \frac{4\pi^2 10^6 C^2 f^{2.25}}{2.25} + \frac{1}{R} f_b\right]$$

As R is large ($\approx 10^9\Omega$) the first term will be negligible for all practicable bandwidths.

An expression can now be written for the noise to signal power ratio for these two components using equations (A.4.1) and (A.3.12).

$$\text{i.e. } \left(\frac{N}{S}\right)^2_{Appl} = \frac{kT}{e^2 \bar{n}_{s5pp}} \left[\frac{1}{Rf_b} + \frac{4\pi^2 10^6 C^2}{2.25} f_b^{0.25}\right]$$

$$= \left(\frac{N_R}{S}\right)^2 + \left(\frac{N_{Cl}}{S}\right)^2 \qquad \text{(A.4.2)}$$

The first term can be related to the Johnson noise of the signal resistor, and the second term to the channel current shot noise.

The total noise current squared I^2_{ni2} at the input due to the noise current generator i_n, is given by integrating the empirical expression given by equation (3.9) for the noise current per root cycle as shown in Fig.3.2 over the required bandwidth.

$$\text{i.e. } I^2_{ni2} = \int_o^{f_b} i_n^2 \, df \qquad \text{(A.4.3)}$$

$$= \int_o^{f_b} (1.7 \times 10^{-15} + 3.8 \times 10^{-17} f^{0.55})^2 df \quad \text{amp}^2$$

$$= \int_o^{f_b} (2.9 \times 10^{-30} + 1.3 \times 10^{-31} f^{0.55} + 1.4 \times 10^{-33} f^{1.1}) df \quad \text{amp}^2$$

$$= 2.9 \times 10^{-30} f_b + 8.3 \times 10^{-32} f_b^{1.55} + 6.9 \times 10^{-34} f_b^{2.1} \quad \text{amp}^2$$

This expression can also be expressed along with equation (A.3.12) as a noise to signal power ratio,

$$\text{i.e. } \left(\frac{N}{S}\right)^2_{App\,2} = 2.8 \times 10^{-3} \frac{1}{f_b} + 8.1 \times 10^{-5} f_b^{-0.45} + 6.7 \times 10^{-7} f_b^{0.1}$$

$$= \left(\frac{N_{G1}}{S}\right)^2 + \left(\frac{N_{G2}}{S_5}\right)^2 + \left(\frac{N_{G3}}{S}\right)^2 \qquad \text{(A.4.4)}$$

this is assuming a value of 10^5 electrons/picture point for $\bar{n}_{s5pp}$.

This shows that the gate noise current component can be represented by three components with different bandwidth dependences.

Thus the total noise to signal power ratio is,

$$\left(\frac{N}{S}\right)^2_{App} = \left(\frac{N}{S}\right)^2_{App1} + \left(\frac{N}{S}\right)^2_{App2} \qquad (A.4.5)$$

$$= \left(\frac{N_R}{S}\right)^2 + \left(\frac{N_{C1}}{S}\right)^2 + \left(\frac{N_{G1}}{S}\right)^2 + \left(\frac{N_{G2}}{S}\right)^2 + \left(\frac{N_{G3}}{S}\right)^2$$

A.5 Relationships between scanning frequencies, bandwidth, and equivalent spatial frequency cut-off

If n is the number of T.V. lines, then for a 4 x 3 aspect ratio there will be $\frac{4}{3}n^2$ picture elements (neglecting the blanking period) and therefore,

$$\frac{4}{3}n^2 \Delta T = T_f \qquad (A.5.1)$$

where ΔT is the picture element dwell time

and T_f is the frame scan time

which can be written using equation (A.3.11) and the fact that the frame frequency $f_f = \frac{1}{T_f}$,

Therefore,

$$\frac{2}{3}n^2 f_f = f_b \qquad (A.5.2)$$

As the maximum number of cycles per line is $\frac{2n}{3}$ then the line frequency f_L can be written,

$$f_L = \frac{f_b}{\frac{2}{3}n} \qquad (A.5.3)$$

Now from equations (A.5.2) and (A.5.3) the bandwidth can be expressed as a function of the line and frame frequency.

i.e. $$f_b = \frac{\frac{2}{3}f_L^2}{f_f} \qquad (A.5.4)$$

If the picture height on the target is h, then the equivalent spatial frequency cut off f_A is,

$$f_A = \frac{n}{2h} = \frac{3f_b}{4f_L h} \qquad (A.5.5)$$

i.e. substituting in equation (A.5.3.)

A note on the limitations of the value of the signal resistor R (see page 84)

One would prefer R to be greater than 10MΩ so that the grid current shot noise coefficient β, predominates at small bandwidths. However there is obviously no point in using much larger values of R than 10MΩ to improve further the Johnson noise coefficient ∝ once the grid current shot noise coefficient is the limiting factor.

REFERENCES

1. ZWORYKIN, V. K., RAMBERG, E. G., Photoelectricity p. 204, (Wiley N.Y. 1961)

2. FARNSWORTH, P. T., J. Franklin Inst., 218, 411-444 (1934)

3. HACHENBERG, O., BRAUER, W., Advances in Electronics and Electron Physics, 11, 413-498, (Academic Press, London and N.Y. 1959)

4. TEDHAM, W. F., McGEE, J. D., British Patent. No. 406353 August 1932

5. ZWORYKIN, V. K., Jour, I. E. E., 73, 437 (1933)

6. McGEE, J. D., Proc. I.E.E. paper No. 931R, 97 Part III, 377 (1950)

7. ROSE, A., IAMES, H., R.C.A. Rev., 4, 186-199 (1939)

8. WEIMER, P. K., FORGUE, S. V., GOODRICH, R. R., Electronics, 70-73, May (1950)

9. De HAAN, E. F., International Television Conference, I.E.E., Conference Report Series, No. 5, 65-67 (1962)

10. McGEE, J. D., LUBSZYNSKI, H. G., Jour. I.E.E., 84. 468-482, (1939)

11. IAMS, H., MORTON, G. A., ZWORYKIN, V. K., Proc. I.R.E. 27, 541-547 (1939)

12. KHAN, M. A. A., Ph.D. Thesis, Univ. of London (1961)

13 MENDE, I. B., Ph.D. Thesis, Univ. of London (1965)

14. BEURLE, R. L., SLARK, N. A., Advances in Electronics and Electron Physics, 12, 247-261 (1960)

14(i) MacKay, K.G., Phys.Rev., 74 , 1606-1621 (1948)

14(ii) MacKay, K.G., Bell Lab.Record, , (1948)

15. SLARK, N. A., Ph.D. Thesis, Univ. of London (1961)

16. ROSE, A., WEIMER, P. K., LAW, H. B., Proc. I.R.E. 34, 424-432 (1946)

17. ANSBACHER, F., EHRENBERG, W., Proc. Phys. Soc., 64 362-369 (1951)

18. SCHNEEBERGER, R. J., SKORINKO, G., DOUGHTY, D. D., FEIBELMAN, W. A., Advances in Electronics and Electron Physics, 16, 235-245, (1962)

19. FILBY, R. S., MENDE, S. B., TWIDDY, N. D., Advances in Electronics and Electron Physics, 22A, 273-290 (1966)

20. GOETZE, G. W., Advances in Electronics and Electron Physics, 22A, 219-227 (1966)

21. GOETZE, G. W., BOERIO, A. H., Proc. I.E.E.E. 52, No. 9, 1007-1012, Sept. (1964)

22. FILBY, R. S., MENDE, S. B., ROSENBLOOM, M. E., TWIDDY, N. D., Nature 201, 801 (1964)

23. FILBY, R. S., MENDE, S. B., TWIDDY, N. D., Internat. J. Electronics 19, 387 (1965)

24. KNOLL, M., KAZAN, B., Storage Tubes P.18, (Wiley N.Y., Chapman and Hall, London 1952)

25. THEILE, R., TOWNSEND, F. H., Proc. Instn. Radio Engrs 40, 146, (1952)

26. HEIMANN, W., Advances in Electronics and Electron Physics, 12, 240-244 (1960)

27 LUBSZYNSKI, H. G., WARDLEY, J., Television Engineering report of the International Television Conference, I.E.E., No. 5. 59-63 (1962)

28. McGEE, J. D., LUBSZYNSKI, H. G., Jour I.E.E. 84, 468-482 (1939)

28a. BLUMLEIN, A.D., McGEE, J.D., British Patent No. 446661, 1934

28b. LUBSZYNSKI, H.G., British Patent No. 468965 Jan. 1936

29. WEIMER, P. K., R.C.A. Rev., 10, 366 (1949)

30. COPE, A. D., BRUCE, W., R.C.A. Rev., 26, 242-261 (1965)

31. MOUSER, D. P., RUGGLES, P. C., SLARK, N. A., J. Television Society, 11, 261-265, Autumn (1967)

32. FILBY, R. S., Ph.D. Thesis, Univ. of London, p.278 Appendix A.1. (1967)

33. FRYSZMAN, A., Bulletin De L'Academie Polonaise des Sciences, 15, No. 9 (1967)

34. BUTKERVICH, B. G., BUTSLOV, M. M., Radiotekhnika i Electronika, No. 3, 355-370 (1968)

35. KRITTMAN, I. M., I.E.E.E., Trans. Electron Devices ED-10, No. 6, 404 (1963)

36. BEYER, R. R., GOETZE, G. W., Advances in Electronics and Electron Physics, 22A, 241 (1966)

37. SCHADE, O. H., R.C.A. Rev., 28, 460-536 (1967)

38. MELTZER, B., J. Electronics and Control 3, 355 (1957)

39. WARDLEY, J., Advances in Electronics and Electron Physics, 22A, 211 (1966)

40. LUBSZYNSKI, H. G., TAYLOR, S., WARDLEY, J., J. Brit. I.R.E., 20, 332 (1960)

41. ROSE, A., J.S.M.P.T.E., 47, No. 4, 273 (1946)

42. ROSE, A., Jour. Opt. Soc. Amer., 38, No. 2, 196 (1948)

43. ROSE, A., Advances in Electronics and Electron Physics, 1, 131 (Academic Press, 1948)

44. SCHADE, O., R.C.A. Rev., 28, 460-536 (1967)

45. BAUM, W., Advances in Electronics and Electron Physics, 16, 393-398 (1962)

46. McGEE, J. D., AIREY, R. W., ASLAM, M., POWELL, J. R., CATCHPOLE, C. E., Advances in Electronics and Electron Physics, 22A, 114 (1966)

47. FELLGETT, P., Vistas in Astronomy (Ed. A. Beer) Vol. 1. (Pergamon Press 1955)

48. CLARK JONES, R., Photographic Science and Engineering, 2, No. 2, (1958)

49. CLARK JONES, R., Advances in Electronics and Electron Physics, 11, 87-183 (1959)

50. CHARMAN, W., HEWITT, A., Advances in Electronics and Electron Physics, 22A, 106 (1966)

51. FILBY, R. S., et al (see ref. 19)

52. GOETZE, G. W., BOERIO, A. H., Advances in Electronics and Electron Physics, 28A, 159-171; (1969)

53. BEURLE, R. L., Proc. I.E.E., 110, 1350-1364 (1963)

54. MENDE, S. B., KHAN, A. A., TWIGGY, N. D., Internat J. Electronics, 19, No. 4, 361 (1965)

55. WHITE, E. L. C., HARKER, M. G., Proc. I.E.E., 97 408 (1950)

56. JAMES, I. J. P., Proc. I.E.E., 99, 802, (1952)

57. THEILE, R., Advances in Electronics and Electron Physics, 12, 288, (1960)

58. R.C.A. NUVISTORS, Industrial & Military Booklet

59. Van der ZIEL, Private Report p.158-163

60, BLALOCK, T.V., I.E.E.E., Trans. Nuclear Sci., 457-467 (1966)

61. SMITH, K. F., CLINE, J. E., I.E.E.E., Trans. Nuclear Sci., 468-476 (1966)

62. FILBY et al (see ref. 19)

63. FILBY, R. S., Ph.D. Thesis, Univ. of London (1967)

64. FILBY et al (see Ref. 23)

65. McGEE, J. D., Archiv der Elektrischen Ubertragung, 9, 355 (1955)

66. McMULLAN, D., private communication

67. HACHENBERG, O., BRAUER, W., (see ref. 3)

68. GOETZE, G. W., BOERIO, A. H., (see ref. 21)

69. GOETZE, G. W., BOERIO, A. H., Advances in Electronics and Electron Physics, 28A, 159-171, (Academic Press 1969)

70. HACKENBERG, O., BRAUER, W., Advances in Electronics, 11, 463, (1959)

71. EDGECUMBE, J., GARWIN, E. L., J. Applied Physics, 3321, July (1966)

72. HARRIS, L. J., Opt. Soc. Amer., 45, 27 (1955)

73. EMBERSON, D. L. Ph.D. Thesis, Univ. of London, 28-30 (1961)

74. FILBY, R. S., Ph.D. Thesis, Univ. of London, 186 (1967)

75. ROSENBLOOM, M. E. Ph.D. Thesis, Univ. of London (1965)

76. HOLLAND, L., Vacuum Deposition of Thin Films, 294, (Chapman and Hall 1961)

77. SNELL, F. D., Colorimetric Analysis Vol. IIA, 316, Van Nostrand

78. RUSH, R. M., YOE, J. H., Anal. Chem., 26, 1345-7 (1954)

79. ROSENBLOOM, M. E., Ph.D. Thesis, Univ of London (1965)

80. FILBY et al (see ref 19, p.280, Fig. 6)

81. FILBY, R. S., Ph.D. Thesis, Univ of London, 237, (1967)

82. IBID, Fig. 10.5, p.214

83. FILBY et al (see ref. 19)

84. BOERIO, A. H. BEYER, R. R., GOETZE, G. W., Advances in Electronics and Electron Physics, 22A, 229-239 (1966)

85. KITTEL, C., Introduction to Solid State Physics (Wiley, N.Y. 1956)

86. DEKKER, A. J., Solid State Physics (Macmillan 1958)

87. FILBY et al (see refs 22 and 23)

88. FILBY, R. S., Ph.D. Thesis, Univ. of London, 151-210 (1967)

89. McGEE, J. D. et al (see ref. 46) p.117, Fig. 3

90. MENDE et al (see ref. 54)

91. GREEN, M., HANSEN, J. R., Advances in Electronics and Electron Physics, 28B, 807 (1969)

92. MENDE, S. B., Proc. I.E.E.E., 57, No. 3 p.281-291 March (1969)

93. LOWRANCE, J. L., ZUCCHINO, P. M., Advances in Electronics and Electron Physics, 28B, 851 (1969)

94. NOZAWA, Y., DAVIS, R. J., Advances in Electronics and Electron Physics, 28B, 891, (1969)

LIST OF SYMBOLS

A amplifier gain

A_o amplifier gain at zero frequency

$\bar{a}$ mean sampling area

a_e reading beam cross sectional area

a_m area of a microphotometer aperture

C total input shunting capacitance of an amplifier

C_o optical image contrast

C_1 capacitance of unit area of a target (1 m m^2)

C_A effective input capacitance of an amplifier

C_L input capacitance from lead

C_{pp} capacitance of a picture point area of a target

C_s tube stray capacitance (from target to all other electrodes)

C_t total target capacitance

$d\bar{n}_b/dt$ mean background electron count/mm^2/sec

$dn(z)/dz$ rate of production of secondary electrons

$\bar{E}$ mean exposure level

e electronic charge

$\bar{E}_o$ absolute mean threshold exposure

$\bar{E}_1$ mean threshold exposure for image contrast $m_o(C_o)$

$\bar{E}_2$ mean threshold exposure for a noise factor F

$\bar{E}_3$ mean threshold exposure for a noise factor F and including the M.T.F. of the system

$\bar{E}_i'$ refers to the above cases $\bar{E}_i$ but for a constant noise factor

$\bar{E}_{Mi}$ maximum exposure for a tube i

$\bar{E}_{Meq}$ equivalent maximum exposure (maximum exposure that could have been made in the absence of dark current

F noise factor

F_1 noise factor for unity carrier modulation factors

f_A equivalent spatial frequency cut-off of an amplifier

f_b bandwidth of amplifier

f_{bo} optimum bandwidth of amplifier

f_f frame frequency

f_L line frequency

f_s spatial frequency

G_p electron gain of phosphor/photocathode sandwich

$G_{S.E.C.}$ Secondary electron conduction gain of a target

G_t total target gain

$G_{T.S.E.}$ Transmission Secondary Emission gain of a target

g_m mutual conductance

h picture height on target

I light intensity

I_b saturated beam current

$i_b(x)$ line spread function of beam

i_g grid current of valve

I_{ni} noise current at the input of an amplifier

i_o current constant

i_s signal current

j $\sqrt{(-1)}$

K	difference signal to noise ratio
K_c	coefficient of certainty
k	Boltzmann's constant
m_o	optical image modulation depth
m_1	mass of KCl on a target
m_2	mass of ZnS on a target
m_b	modulation depth of the scanning beam current
m_{ci}	carrier modulation factors of stages i
m_{c1}	carrier modulation factor of imaging lens
m_{c2}	carrier modulation factor of the primary photocathode and the image section
m_{c3}	carrier modulation factor of the phosphor
m_{c4}	carrier modulation factor of the second photocathode and the image section
m_{c5}	carrier modulation factor of the storage surface
N	Total number of T.V. lines
n	number of T.V. lines per unit length
n_{si}	i = 1,2,3..... denotes a particle density at a stage i considered as a signal, (a"b" denotes a background signal only)
n_i	i = 1,2,3..... denotes a particle density at a stage i including all sources of background and noise particles along with the signal
$\bar{n}_{s1}$	mean number of photons per m.m.^{2} incident on the photocathode
$\bar{n}_{s2}$	mean number of photoelectrons per m.m.^{2} leaving the photocathode
$\bar{n}_{b2}$	mean number of background electrons per mm^2 in the first image section

$\bar{n}_2$ mean number of electrons per m.m.^{2} from all sources incident on the phosphor

$\bar{n}_3$ mean number of photons per m.m.^{2} leaving the phosphor

$\bar{n}_4$ mean number of photoelectrons per m.m.^{2} leaving the photocathode of the phosphor-photocathode sandwich

$\bar{n}_{b4}$ mean number of background electrons per m.m.^{2} in the second image section

$\bar{n}_5$ mean number of stored electronic charges per m.m.^{2} on the target

$\bar{n}_{s1pp}$ mean number of photons incident during the exposure time on a picture point

$\bar{n}_{s5pp}$ mean number of electronic charges stored per picture point

N_n number of equivalent noise electrons stored per picture point

$(\frac{N_A}{S})^2$ noise to signal power ratio for anode shot noise component

$(\frac{N_G}{S})^2$ noise to signal power ratio for grid shot noise component

$(\frac{N_R}{S})^2$ noise to signal power ratio for the Johnson noise component

$(\frac{N_S}{S})^2$ noise to signal power ratio for the stored charge

$\bar{P}$ mean number of photons emitted from a source in a given time

R head amplifier signal resistor

R_L sine wave response of the lens

R_{I1} sine wave response of the first image section

R_S sine wave response of the phosphor photocathode sandwich

$R_{I.2.}$ sine wave response of the second image section

R_T sine wave response of the target

R_b sine wave response of the scanning beam

R_A sine wave response of the video amplifier

$r_L \ldots r_A$ ditto square wave responses

$R(f_s)_{syst}$ sine wave response of entire system

$r(f_s)_{syst}$ square wave response of entire system

R_B effective beam resistance

R_n equivalent noise resistance of valve

S_1 percentage of the bulk density of a KCl deposit

S_2 percentage of the bulk density of a ZnS deposit

$(\frac{s}{n})$ signal to noise ratio for unit area (1 m.m.^{2})

$(\frac{S}{N})$ signal to noise ratio for other cases

$(\frac{S}{N})_P$ signal to noise ratio for phosphor when sampled in areas of a_m

$(\frac{S}{N})_T$ signal to noise ratio for the fixed pattern noise component of the target as measured by scanning with an electron beam of cross sectional area a_e

$(\frac{s}{n})_{syst}$ signal to noise ratio of the complete system

T temperature

t total target thickness

t_1 thickness of KCl

t_2 thickness of ZnS

T_e exposure time

T_f frame time

V_1 first cross over potential

V_E equilibrium potential

V_{MF} potential of field mesh

V_{MS} potential of stabiliser mesh

V_{sp} signal plate potential

V'_{sp} effective signal plate potential

x line direction on the target

y frame direction on the target

z cross sectional direction on target

z_t target thickness

α Johnson noise coefficient of the signal resistor

β grid shot noise coefficient

γ_A the gamma correction of the amplifier

γ_p the slope of the transfer characteristic from the phosphor to the output

γ_T slope of the transfer characteristic from the target to the output

δ effective beam diameter

ΔT picture point dwell time

Δv voltage escursion on target surface

ΔV_{max} maximum allowable voltage excursion on the target surface (set by beam bending effects)

ϵ mean number of photons per electron from phosphor

η anode shot noise coefficient

θ deflection angle

λ wavelength of light

υ frequency of light

ξ equivalent quantum efficiency

ρ_{1b} bulk density of KCl

ρ_{2b} bulk density of ZnS

σ_1 quantum efficiency of primary photocathode

σ_2 quantum efficiency of photocathode in phosphor photocathode sandwich

ω angular frequency

ACKNOWLEDGEMENTS

The author would like to express his gratitude to Professor J. D.McGee for his interest in the work, and for providing the facilities in his department which enabled this work to be carried out. He would also like to express his appreciation to Dr. D. McMullan, for his guidance, and his invaluable advice on circuit design, and under whose supervision the work was done.

The author is also grateful to Dr. R. S. Filby for introducing him to the problems encountered in S.E.C. devices, and for his helpful assistance in the early part of the work. He would also like to thank Mr J. Westlake for his skill in tube assembly and processing, Mr W. T. Simpson for his workshop and laboratory assistance, and Mr S. P. Rejman for the wiring and building of the electronic equipment.

The author would like to pay a special tribute to his wife, Jackie, who had to spend so much time alone in the evenings during the last twelve months.

The author was supported during the period of this research by a grant from the English Electric Valve Company, Chelmsford and by a Research Assistantship awarded by the College.

Financial assistance for the research came from the Science Research Council.

Reprinted from *Electronics Letters*, Vol. 4, No. 17, 23rd August 1968

STABLE S.E.C. TARGET FOR TELEVISION CAMERA TUBES

Various aspects of the overload signal stability of s.e.c. targets, formed from good and poor secondary-emitting materials, are considered. It is shown that a target consisting of two layers can be made to be inherently stable to signal overload, while still having a high gain.

Layers of potassium chloride (10–20 μm thick), deposited in a low-density porous form, have been used for some years as charge-storage targets for television camera tubes.[1–3] Such targets have very high resistivity, permitting charge images to be stored for long periods, and have high gain, since each imaging electron can produce many secondary electrons inside the layer. The secondary electrons are collected by a conducting electrode (signal plate) on which the low-density layer is deposited and which is held at a positive potential relative to the surface of the layer. This surface is stabilised at the cathode potential of the reading electron gun. The signal plate is usually a thin layer of aluminium on aluminium oxide and is thin enough to transmit the imaging electrons (7 keV) which enter the target from the surface opposite the scanned surface. The secondary electrons leave positive charges within the layer, a process which has been termed 'secondary-electron conduction'[1] (s.e.c.), and the neutralisation of these charges by the reading beam produces a video signal current in the signal-plate circuit.

A potassium-choride target, while having a high gain (up to about 200), has the disadvantage that, if the intensity of the imaging beam is too high, the potential of the target surface can rise above the first secondary-emission crossover potential. The reading beam will then charge the target to anode potential instead of discharging it, and the resulting high voltage across the layer will destroy it.[4] This effect can be prevented by mounting a stabilising mesh, at a potential less than the first crossover potential, in front of the target. Because the crossover potential of potassium chloride is only 15 V, the mesh must be mounted very close to the target surface if the focus of the reading beam is not to be impaired by the lowering of the electric field at the target surface. On the other hand, if the spacing is small, the layer may be damaged by touching the mesh, the mesh may be in focus, and the increased capacitance can give rise to microphony and shunting of the signal current. In practice, a spacing of about 0·3 mm is not an entirely satisfactory compromise.

The use of materials with a higher first crossover potential than that of KCl would permit a higher mesh potential, and hence a larger spacing. Unfortunately, the secondary-emission coefficients of such materials are inevitably lower than those of KCl, and the target gains are much less. For example, a low-density layer (20 μm thick) of ZnS has a crossover potential of 100 V, but a gain of only 10, which is rather low, and it is therefore not a very attractive target material.

We have found that it is possible to prepare a high-gain target, which also has a high crossover potential, by covering a low-density layer of KCl with a very much thinner layer of low-density ZnS (see Fig. 1). Both the layers are deposited by the well known method of evaporation in an inert gas at a pressure of a few torrs.[3] Depending on the thickness of the ZnS, the gain of the target is reduced, but the crossover potential is raised; the reduction in overall gain is quite small for a thickness of ZnS, giving a crossover potential of 50 V (mean thickness of the order of few tenths of a micron). This increase in crossover potential permits the suppressor mesh to be at a higher positive potential, and hence to be mounted farther away from the target.

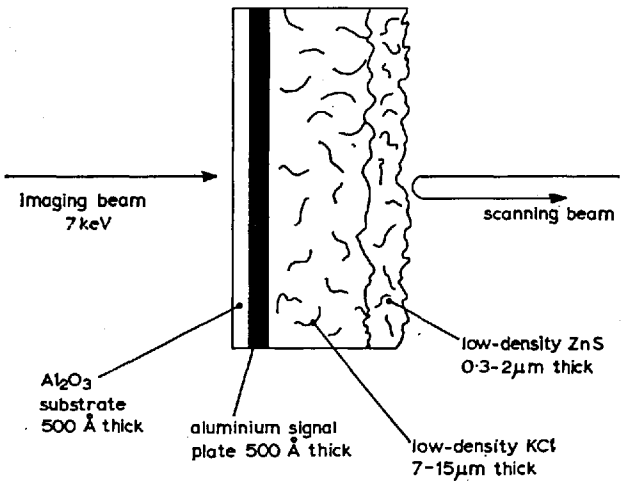

Fig. 1 *Cross-section of a composite target*

With a slightly greater thickness of ZnS, a target can be made that is completely stable, i.e. the surface potential cannot be raised by the imaging electrons above the first crossover potential, and a suppressor mesh is therefore no longer required. This condition is discussed in the remainder of this letter.

The gain G of the target, i.e. the ratio of the charge in the target to total charge in the imaging beam during the period between reading scans, has two components: the s.e.c. gain G_{sec} due to the collection of secondary electrons by the signal plate, and the transmitted secondary emission of t.s.e. gain G_{tse}, due to those secondary electrons which leave the surface of the target on the reading-beam side and are collected by the nearest positive electrode:

$$G = G_{sec} + G_{tse} \quad . \quad . \quad . \quad . \quad . \quad . \quad . \quad . \quad . \quad (1)$$

When the signal plate is at a positive potential V_{SP} with respect to the reading gun, for normal small-signal conditions, G_{tse} is negligible compared with G_{sec} because the comparatively high electric field within the layer causes all the secondaries, except those produced very close to the surface, to flow to the signal plate. Under overload conditions, i.e. if the imaging beam is very large, the surface potential will rise to a high positive value, and the internal field will diminish and then reverse. This is assuming that the potential rise is not limited by a low-potential suppressor mesh close to the target surface. As the internal field falls, G_{sec} will fall and will also reverse, whereas G_{tse} increases because more of the secondary electrons can leave the surface. When the potential across the layer reaches the equilibrium potential[1] V_E, G_{sec} is equal and opposite to G_{tse}, and G is zero. The maximum value of the potential excursion ΔV of the surface from its stabilised value (gun-cathode potential) is

$$\Delta V_{max} = V_E + V_{SP} \quad . \quad . \quad . \quad . \quad . \quad . \quad . \quad . \quad (2)$$

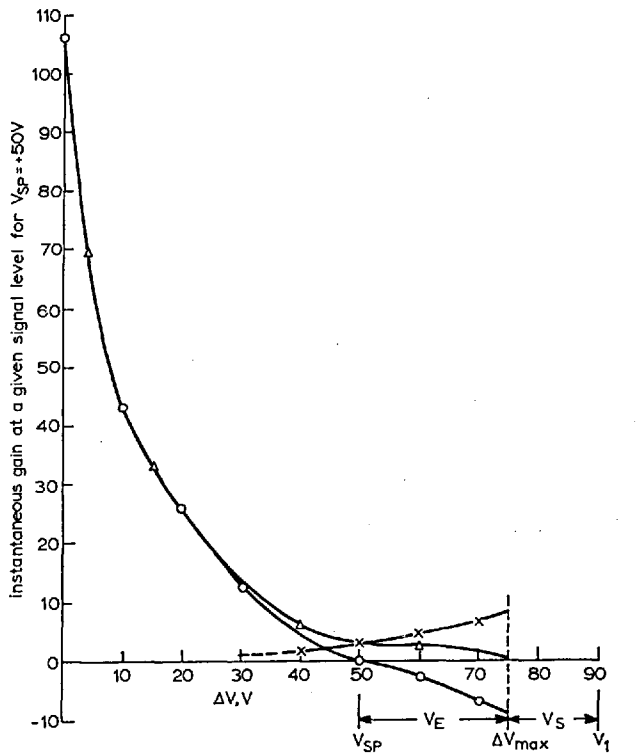

Fig. 2 *Instantaneous gain of KCl–ZnS target as a function of voltage excursion on target surface*

V_{SP} = + 50 V
O s.e.c. gain
× t.s.e. gain
Δ total gain
KCl thickness = 7·5 μm
ZnS thickness = 1·5 μm

If $\Delta V_{max} > V_1$, the first crossover potential, the reading beam will charge the surface even more positively, unless a suppressor mesh at a potential less than V_1 is fitted.

If

$$\Delta V_{max} < V_1 \quad . \quad . \quad . \quad . \quad . \quad . \quad . \quad . \quad . \quad . \quad . \quad (3)$$

the reading beam will always be able to discharge the target following an overload.

For a 7·5μm KCl target, $V_1 \simeq 15$V and $V_E \simeq 80$V, with normal mesh spacings and potentials, so that eqn. 3 cannot be satisfied with any positive signal plate potential (which is necessary for normal high-gain operation). With the KCl covered by a 1·5μm layer of ZnS, not only is V_1 increased to 90V, but V_E is only 25V, because G_{tse}, which depends on the secondary electrons produced near the surface, is also reduced. G_{sec} is also less with this thickness of ZnS, but V_{SP} can be increased to offset this. With the above values of V_1 and V_E, for the target to be stable, V_{SP} must be less than 65V; in practice, with the above layer thickness, 50V has been found to be a suitable value, since, at 55V, the reading beam starts to penetrate right through the layer to the signal plate, giving rise to spurious white signals. The gain of a typical composite target with $V_{SP} = 50$V is about 100. Fig. 2 shows G_{sec}, G_{tse} and G plotted as functions of ΔV for $V_{SP} = 50$V, with ΔV_{max} marked at the potential where $-G_{sec} = G_{tse}$. The stability margin V_S is 15V, which is ample to take account of the transient condition when the tube is switched on, and potentials may rise above the normal values because of inter-electrode charging currents. It is also sufficient to ensure good acceptance of the reading beam, and hence a rapid discharge of the target, if ΔV_{max} is reached.

D. MCMULLAN
G. O. TOWLER

Applied Physics Department
Imperial College
Prince Consort Road, London SW7, England

22nd July 1968

References

1 GOETZE, G. W., and BOERIO, A. H.: 'Secondary electron conduction (s.e.c.) for signal amplification and storage in camera tubes', *Proc. Inst. Elect Electronics Engrs.*, 1964, **52**, pp. 1007–1012
2 FILBY, R. S., MENDE, S. B., ROSENBLOOM, M. E., and TWIDDY, N. D.: 'A new television camera intended for scientific applications having a very high sensitivity and good storage properties', *Nature*, 1964, **201**, pp. 801–802
3 FILBY, R. S., MENDE, S. B., and TWIDDY, N. D.: 'The detection of faint optical images by charge integration. II: A new television camera, intended for scientific application, having a very high sensitivity and good storage properties', *Internat. J. Electronics*, 1965, **14**, pp. 387–403
4 FILBY, R. S., MENDE, S. B., and TWIDDY, N. D.: *ibid.*, p. 33

Reprinted from *Electronics Letters*, Vol. 4, No. 24, 29th November 1968

ENHANCEMENT OF S.E.C. TARGET GAIN IN TELEVISION-CAMERA TUBES

A temporary increase in the gain of an s.e.c. target has been found after the target has been flooded with imaging electrons while the reading beam is switched off. A qualitative theory to account for this enhancement is put forward. The production of negative images using this phenomenon is also described.

Television-camera tubes with secondary-electron-conduction (s.e.c.) targets are particularly suitable for the integration of low-light-level images.[1-3] Such images can be integrated for periods of several hours (the time is limited by dark current in the image section) and then read out as a single frame.

When used in this mode, it has been found that, for a given signal-plate potential, the gain of the target can be temporarily increased by using the following sequence of operations. The target is flooded with a uniform beam of electrons from the photocathode, while the reading beam is switched off, and the potential of the target surface is allowed to rise so that it is more positive than the signal plate; i.e. the electric field in the target is reversed. The surface potential is limited either by the potential of the nearest mesh (which is set 20V more positive than the signal plate) or, for a two-layer target, by its equilibrium potential.[4] When the surface has reached its limiting positive potential, the flood beam is switched off, and the surface is reduced to gun-cathode potential by turning on the reading beam. With a conventional KCl target, the signal-plate potential will also have to be varied during this stabilisation in order to prevent the reading beam hitting the target surface while it is above the first crossover potential. However, with a two-layer target, the crossover potential is so high that this precaution is unnecessary.[4]

After such a preparatory procedure, the gain of a target can be more than doubled, the degree of enhancement depending on the signal-plate potential V_{sp}. With the two-layer target previously reported,[4] at $V_{sp} = +4V$, the increase in gain is about four times, at $V_{sp} = +10V$, it is doubled, but at $V_{sp} = +30V$, there is no enhancement. The gain of this target at the above signal-plate potentials is low (4 to 25), but the effect has also been demonstrated with KCl targets with considerably higher gains at low signal-plate potentials. Unfortunately the effect does not appear to give a gain higher than can be realised merely by increasing the signal-plate potential. It does, however, help in the understanding of the multiplication process, and it may also have a practical application, since, as is described later, negative images can be formed; these could be used in the correlation of optical images.

The reason for the gain enhancement after the preparatory procedure is believed to be due to positive charges stored within the body of the target. Fig. 1 shows the potential distribution $V(z)$ which is believed to exist through the target for two different signal levels, z_t being the target thickness (signal-plate–target-surface). In each case the signal-plate potential is +20V. In Fig. 1(i), the imaging beam is producing a voltage excursion $\Delta V = 5V$ on the target surface. (This is considered to be a strong signal and is near the maximum that can be used before beam-bending effects become troublesome.) Most of the positive charge is being stored near the target surface for two reasons. First, a large proportion of the secondary electrons are produced in this region by the imaging electrons which will have lost most of their initial energy. Some of these secondaries leave the surface, but the majority are collected by the signal plate after travelling through the target (s.e.c. electrons). Both components leave a positive charge near the surface. Any positive charges produced inside the target will tend to be neutralised by s.e.c. electrons which originated nearer the target surface and were travelling towards the signal plate under the influence of the internal field. In Fig. 1(i),*abc* is the potential distribution after integrating the signal, and *ade* is that after reading.

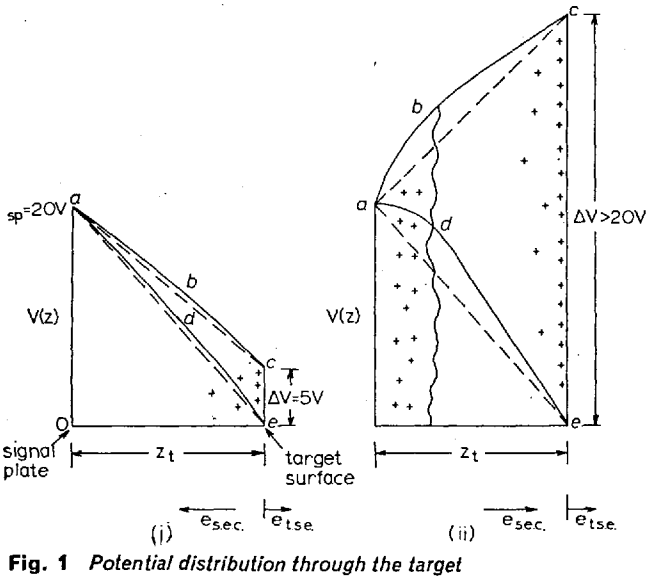

Fig. 1 *Potential distribution through the target*
Target surface potentials (i) 5V and (ii)~40V before and after cathode-potential stabilisation

Fig. 1(ii) shows the potential plot for what would normally be considered to be an overload condition, but which also occurs during the enhancement procedure. The surface potential is higher than that of the signal plate, and the s.e.c. electrons travel towards the surface, since the electric field is reversed. Positive charge is stored on the surface, but there will also be positive charges within the target. Since the rate of production of secondaries increases as the imaging electrons pass through the target (in consequence of their energy loss), the number of positive charges produced in a layer δz_t will increase with z_t. However, the number of s.e.c. electrons entering the layer will be less than the rate at which positive charges are produced, and hence a net positive charge will build up. (When the surface is more negative than the signal plate, the s.e.c. electrons travel in the opposite direction and exceed in number the positive charges produced in the layer δz_t, and hence no internal charge results.) This will be especially the case near the signal plate, where the rate of production of secondaries will be very low. Equilibrium will be established when the field due to these charges causes electrons to leave the signal plate. The potential distribution is shown as the curve *abc*, and, after cathode-potential stabilisation, by *ade*.

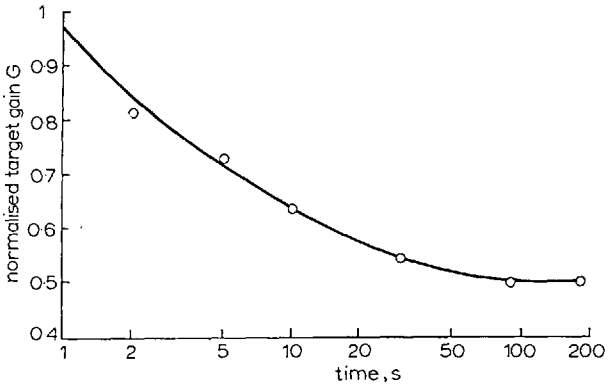

Fig. 2 *Decay of target gain with time after initial preparation*
Scan rate, 25 frames/s

It can be seen that, after cathode-potential stabilisation, there is a difference in the internal field gradient for the two cases shown in Figs. 1(i) and (ii), that for the latter being the greater (except near the signal plate). Since the gain of the target is dependent on the electric field in the region where the secondaries are being produced (recombination is less likely to occur when the field is high), the gain of the target in the condition shown in Fig. 1(ii) will be the higher initially. However, during the integration of an image, the s.e.c. electrons travelling towards the signal plate will combine with, and neutralise, the internal positive charges, and the internal field, and hence the gain, will fall. Eventually, after many charging and read-out cycles, most of the internal positive charges will be neutralised, and the potential distribution will be as shown in Fig. 1(i). This can be demonstrated by preparing the target and then observing the

amplitude of the video waveform when a constant optical image is focused on the photocathode and the target is scanned at 25frames/s. Fig. 2 shows that the gain decays to one half its initial value with a time constant of about 5s (125 frames).

In normal use with repetitive scanning, little internal charge builds up unless there is a gross light-input overload (e.g. by a flash bulb in the field of view). Unless the overload is of long duration, the build up of internal charge will be small, and no difficulty with persistent images (positive or negative, see below) is experienced.

As mentioned earlier, the degree of enhancement is dependent on the signal-plate potential. This is thought to be a consequence of the neutralisation of positive charges within the layer by the scanning beam which can penetrate right through the layer to the signal plate when the signal-plate potential is high. Under this condition, the internal positive charges produced during the flooding process will be neutralised when the scanning beam is used to return the surface–cathode potential, and there will be thus no gain enhancement.

The phenomenon of gain enchancement can be used to produce negative images. Fig. 3(i) shows the potential along one line of a target with internal charge and with the surface cathode potential stabilised. This corresponds to *ade* of Fig. 1(ii), but with the line direction x on the target surface included. If a vertical white-bar image is now scanned for a few seconds at 25 frames/s, the internal charge in the illuminated area will be neutralised to some extent. Fig. 3(ii) shows the potential distribution after several scans, with the light image on (just before the line is scanned), and Fig. 3(iii) shows that after the light is switched off, so that the whole surface is at cathode potential. The internal charge in the illuminated area has, to some extent, been neutralised, and the gain in this area will therefore be less. If the target is now flooded with a uniform beam of electrons, the potential of the previously unilluminated areas will rise higher than those that were illuminated, as shown in Fig. 3(iv); i.e. a negative image will be formed. In Fig. 3(iv) the potential of the surface has been allowed to rise 10–15V in order to give a 5V signal amplitude. To read out the charge pattern, the surface potential must first be reduced to the range 0–5V by lowering the signal-plate potential by 10V; otherwise severe beam bending would occur and the contrast would be low.

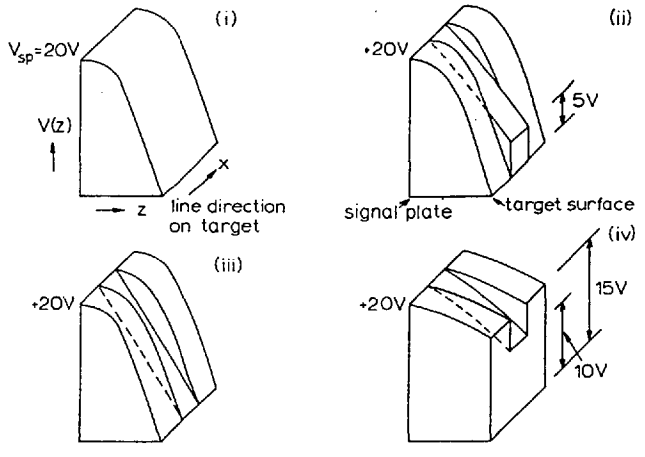

Fig. 3 *Potential-distribution diagrams illustrating formation of negative images*

(i) Target prepared before writing image
(ii) Writing and reading white vertical bar image
(iii) Cathode-potential stabilisation after writing
(iv) After uniform flooding

D. McMULLAN
G. O. TOWLER

Applied Physics Department
Imperial College
Prince Consort Road, London SW7, England

4th November 1968

References

1 GOETZE, G. W., and BOERIO, A. H.: 'Secondary electron conduction (s.e.c.) for signal amplification and storage in camera tubes', *Proc. Inst. Elect. Electronics Engrs.*, 1964, **52**, pp. 1007–1012
2 FILBY, R. S., MENDE, S. B., ROSENBLOOM, M. E., and TWIDDY, N. D.: 'A new television camera intended for scientific applications having a very high sensitivity and good storage properties', *Nature*, 1964, **201**, pp. 801–802
3 FILBY, R. S., MENDE, S. B., and TWIDDY, N. D.: 'The detection of faint optical images by charge integration. II: A new television camera, intended for scientific application, having a very high sensitivity and good storage properties', *Internat. J. Electron.*, 1965, **14**, pp. 387–403
4 McMULLAN, D., and TOWLER, G. O.: 'Stable s.e.c. target for television camera tubes', *Electron. Lett.*, 1968, **4**, pp. 360–362

Reprinted from ADVANCES IN ELECTRONICS AND ELECTRON PHYSICS
VOLUME 28 Published by Academic Press, London and New York

Some Properties of SEC Targets

D. McMULLAN† and G. O. TOWLER

Applied Physics Department, Imperial College, London, England

Introduction

It is now several years since low-density insulating layers were first used as targets in television camera tubes.[1,2] Since then camera tubes with SEC targets have become commercially available,[3] but comparatively little has been published on the mode of operation of the target.[4,5] Neither have there been any reports of targets having better characteristics than those of the original potassium chloride target.

In this paper we discuss the question of target stability, and a target having a much improved performance in this respect is described. Some experiments are reported on charge integration with single-frame read-out. These help in understanding the mode of operation of the target and in particular the internal distribution of charge. In the course of these experiments a method was found for producing negative images; it is thought that this may have an application in the correlation of optical images. Some measurements on target lag are reported and finally target resolution is discussed and attention drawn to a theoretical limitation.

Target Stability

All SEC camera-tubes which have so far been reported in the literature have used a low-density layer of potassium chloride as the target material. Such targets have a high gain (up to several hundred) but suffer from the disadvantage that, if the intensity of the imaging beam is too high, the potential of the target surface can rise above the first secondary-emission cross-over potential. The reading beam will then charge the target to anode potential instead of discharging it, and the resulting high voltage across the layer will destroy it.[5] This effect can be prevented by mounting a stabilizing mesh, at a potential less than the first cross-over potential, in front of the target. Because the cross-over potential of potassium chloride is only 15 V, the mesh must be

† Now at the Royal Greenwich Observatory, Herstmonceux, Sussex, England.

mounted very close to the target surface if the focus of the reading beam is not to be impaired by the lowering of the electric field at the target surface. On the other hand, if the spacing is small, the layer may be damaged by touching the mesh, the mesh may be in focus, and the increased capacitance can give rise to microphony and shunting of the signal current. In practice, a spacing of about 0·3 mm is a not entirely satisfactory compromise.

The use of materials with a higher first cross-over potential than that of KCl would permit a higher mesh potential, and hence a larger spacing. Unfortunately, the secondary-emission coefficients of such materials are inevitably lower than those of KCl, and the target gains are much less. For example, a low-density layer (20 μm thick) of ZnS

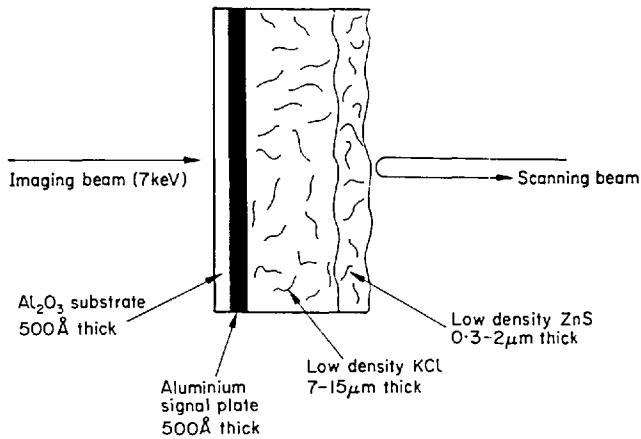

FIG. 1. Cross-section of a two-layer target.

has a cross-over potential of 100 V, but a maximum gain of only 10, which is rather low; it is therefore not a very attractive target material.

We have found that it is possible to prepare a high-gain target, which also has a high cross-over potential, by covering a low-density layer of KCl with a very much thinner layer of low-density ZnS (see Fig. 1).[6] Both the layers are deposited by the well known method of evaporation in an inert gas at a pressure of a few torr.[4,5] Depending on the thickness of the ZnS, the gain of the target is reduced, but the cross-over potential is raised; the reduction in overall gain is quite small for a thickness of ZnS giving a cross-over potential of 50 V (mean thickness of the order of few tenths of a micron). This increase in cross-over potential permits the suppressor mesh to be at a higher positive potential, and hence to be mounted farther away from the target.

With a slightly greater thickness of ZnS, a target can be made that is completely stable, i.e. the surface potential cannot be raised by the imaging electrons above the first cross-over potential, and a suppressor mesh is therefore no longer required.

Inherently Stable Target

The condition for a target to be inherently stable will now be discussed.

The gain G of the target, i.e. the ratio of the charge in the target to total charge in the imaging beam during the period between reading scans, has two components: the SEC gain G_{SEC} due to the collection of secondary electrons by the signal-plate, and the transmitted secondary emission or TSE gain G_{TSE}, due to those secondary electrons which leave the surface of the target on the reading-beam side and are collected by the nearest positive electrode. Hence:

$$G = G_{\mathrm{SEC}} + G_{\mathrm{TSE}}. \tag{1}$$

When the signal-plate is at a positive potential V_{SP} with respect to the reading gun cathode, G_{TSE} is negligible compared with G_{SEC} because the comparatively high electric field within the layer causes all the secondaries, except those produced very close to the surface, to flow to the signal-plate. Under overload conditions, that is if the imaging beam is very intense, the surface potential will rise to a high positive value, and the internal field will diminish and then reverse. This is assuming that the potential rise is not limited by a low-potential stabilizing mesh close to the target surface. As the internal field falls, G_{SEC} will fall and will also reverse, whereas G_{TSE} increases because more of the secondary electrons can leave the surface. When the potential across the layer reaches the equilibrium potential V_{E}, G_{SEC} is equal and opposite to G_{TSE}, and G is zero.[1] The maximum value of the potential excursion ΔV of the surface from its stabilized value (gun-cathode potential) is

$$\Delta V_{\mathrm{max}} = V_E + V_{\mathrm{SP}}. \tag{2}$$

If $\Delta V_{\mathrm{max}} > V_1$, the first cross-over potential, the reading beam will charge the surface even more positively, unless there is a stabilizing mesh at a potential less than V_1. However, if

$$\Delta V_{\mathrm{max}} < V_1, \tag{3}$$

the reading beam will always be able to discharge the target following an overload.

For a 7·5-μm KCl target, $V_1 \simeq 15$ V and $V_{\mathrm{E}} \simeq 80$ V with normal mesh spacings and potentials, so that relation (3) cannot be satisfied with any positive signal-plate potential (which is necessary for normal

high-gain operation). With the KCl covered by a 1·5-μm layer of ZnS, not only is V_1 increased to 90 V, but V_E is only 25 V because G_{TSE}, which depends on the secondary electrons produced near the surface, is also reduced. G_{SEC} is also less with this thickness of ZnS, but V_{SP} can be increased to offset this. With the above values of V_1 and V_E,

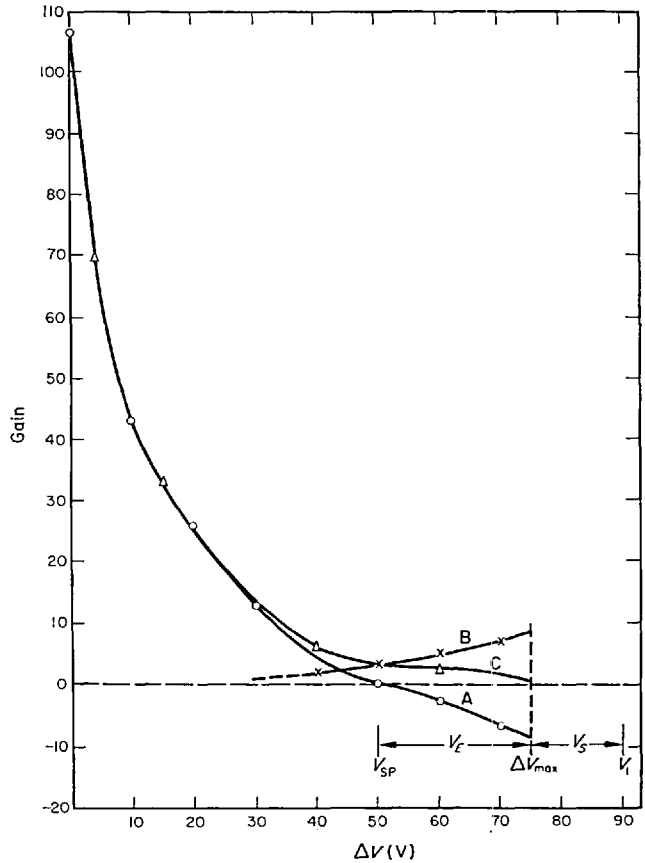

FIG. 2. Static gains of KCl–ZnS target as a function of voltage excursion on target surface; signal-plate potential $V_{SP} = +50$ V. A, SEC gain; B, TSE gain; C, total gain.

for the target to be stable V_{SP} must be less than 65 V; in practice, with the above layer thickness, 50 V has been found to be the maximum acceptable value, since at 55 V the reading beam starts to penetrate right through the layer to the signal-plate, giving rise to spurious white signals. At $V_{SP} = 50$ V there is a substantial amount of lag (see later in this paper); for negligible lag V_{SP} must not exceed 30 V. The gain of a typical composite target with $V_{SP} = 50$ V is about 100, and at

30 V it is 25. Figure 2 shows G_{SEC}, G_{TSE} and G plotted as functions of ΔV for $V_{SP} = 50$ V, with ΔV_{max} marked at the potential where $-G_{SEC} = G_{TSE}$. The stability margin V_S is 15 V, which is ample to take account of the transient condition when the tube is switched on, and potentials may rise above the normal values because of inter-electrode charging currents. It is also sufficient to ensure good acceptance of the reading beam, and hence a rapid discharge of the target, if ΔV_{max} is reached.

Charge Integration

The very high resistivity of SEC targets makes them particularly suitable for television cameras which are to be used for integrating low light-level images. The integration time is not limited by the SEC target since it can hold charge patterns for several days with no loss in information content. Rather, it is the dark current in the image section that is the limiting factor.

The usual mode of operation is to integrate the image while the scanning beam section is turned off and then to read out the charge pattern as a single frame. Before integration is commenced the surface of the target will have been brought to gun-cathode potential by the scanning beam. This normally will mean that all the charges deposited during the preceding integration will have been erased. However, we have found that under certain circumstances a residual charge is left which can increase the gain of the target. How this can occur is best described by considering the case in which the previous integration is of a uniform flood beam.

The target is flooded with a uniform beam of electrons from the photocathode while the reading beam is switched off, and the potential of the target surface is allowed to rise so that it is more positive than the signal-plate, i.e. the electric field in the target is reversed. The surface potential is limited either by the potential of the nearest mesh (which is set more positive than the signal-plate) or, in the case of a two-layer target, by its equilibrium potential. When the surface has reached its limiting positive potential the flood beam is switched off and the surface is reduced to gun-cathode potential by turning on the reading beam. With a conventional KCl target the signal-plate potential may also have to be varied during this stabilization in order to prevent the reading beam striking the target surface while it is above the first cross-over potential. However, with a two-layer target the cross-over potential is so high that this precaution is unnecessary. If the target is now used in the normal way to integrate a charge image, the target gain will be found to have increased by an amount which depends on the signal-plate potential V_{SP}. With the two-layer target described in

the previous section, at $V_{SP} = +4$ V the increase in gain is about four times, at $V_{SP} = +10$ V it is doubled, but at $V_{SP} = +30$ V there is no enhancement. The gain of this target at the above signal-plate potentials is low (4 to 25) but the effect has also been demonstrated with KCl targets with considerably higher gains at low signal-plate potentials. Unfortunately the effect does not appear to give a gain higher than can be realized merely by increasing the signal-plate potential. It does however help in the understanding of the multiplication process and it may also have a practical application since, as is described later, negative images can be formed.

The reason for the gain enhancement after the preparatory procedure is believed to be due to positive charges stored within the body of the target. Figure 3 shows the potential distribution $V(z)$ which is believed to exist through the target for two different signal levels, z_t being the target thickness (signal-plate to target surface). In each case the signal-plate potential is +20 V. In Fig. 3(a) the imaging beam is producing a voltage excursion $\Delta V = 5$ V on the target surface. (This is considered a strong signal and is near the maximum that can be used before beam-bending effects become troublesome.) Most of the positive charge is being stored near the target surface for two reasons. First, a major proportion of the secondary electrons are produced in this region by imaging electrons which have lost most of their initial energy. Some of these secondaries leave the surface, but the majority are collected by the signal-plate after travelling through the target (SEC electrons). Both components leave a positive charge near the surface. Second, any positive charges produced inside the target will tend to be neutralized by SEC electrons which originated nearer the target surface and were travelling towards the signal-plate under the influence of the internal field. In Fig. 3(a), A–B–C is the potential distribution after integrating the signal, and A–D–E is that after reading.

Figure 3(b) shows the potential plot for what would normally be considered an overload condition, but which also occurs during the enhancement procedure. The surface potential is higher than that of the signal-plate, and the SEC electrons travel towards the surface since the electric field is reversed. Positive charge is stored on the surface, but there will also be positive charges within the target. Since the rate of production of secondaries increases as the imaging electrons pass through the target (in consequence of their energy loss) the number of positive charges produced in a layer δz will increase with z. However, the number of SEC electrons entering the layer will be less than the rate at which positive charges are produced and hence a net positive charge will build up. (When the surface is more negative than the signal-plate the SEC electrons travel in the opposite direction and

exceed in number the positive charges produced in the layer δz, and hence no internal charge results.) This will be especially the case near the signal-plate where the rate of production of secondaries will be very low. Equilibrium will be established when the field due to these charges causes electrons to leave the signal-plate. The potential distribution is shown as the curve A–B–C, and after cathode potential stabilization by A–D–E.

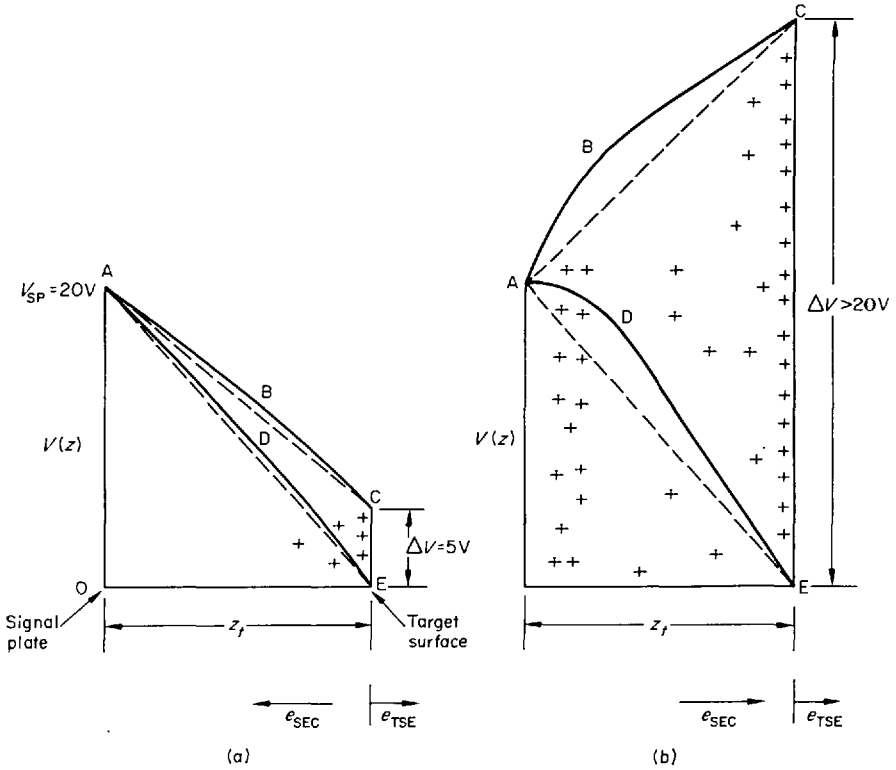

FIG. 3. Potential distribution through the target for target surface potentials: (a) 5 V, and (b) ~ 40 V before and after cathode potential stabilization.

It can be seen that after cathode-potential stabilization there is a difference in the internal field gradient for the two cases shown in Fig. 3(a) and (b), that for the latter being the greater (except near the signal-plate). Since the gain of the target is dependent on the electric field in the region where the secondaries are being produced (recombination is less likely to occur when the field is high) the gain of the target in the condition shown in Fig. 3(b) will be the higher initially. However, during the integration of an image, the SEC electrons

travelling towards the signal-plate will combine with and neutralize the internal positive charges; thus the internal field, and hence the gain, will fall. Eventually, after many charging and read-out cycles, most of the internal positive charges will be neutralized and the potential distribution will be shown in Fig. 3(a). This can be demonstrated by internally charging the target and then observing the amplitude of the video waveform when a constant optical image is focused on the photocathode and the target is scanned at 25 frames/sec.

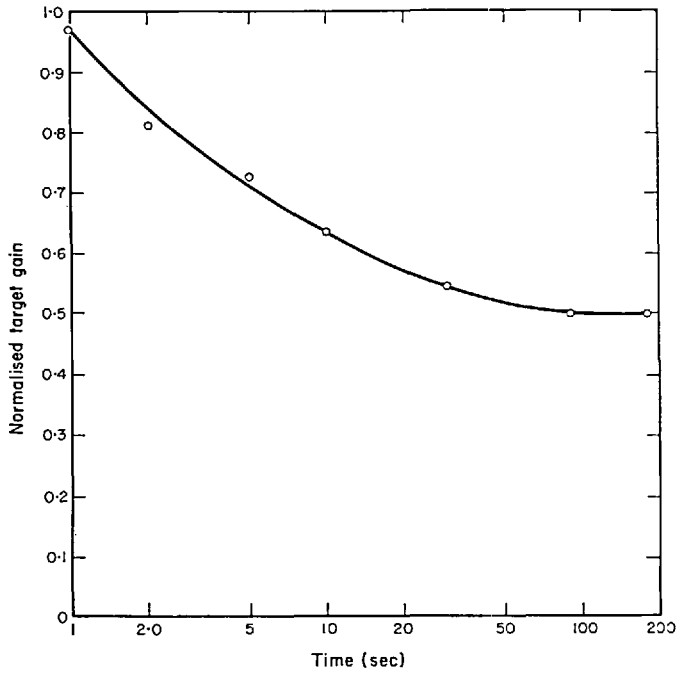

FIG. 4. Decay of target gain with time after internal charging. Scan rate 25 frames per sec.

Figure 4 shows that the gain decays to one-half its initial value with a time constant of about 5 sec (125 frames).

In normal use with repetitive scanning, little internal charge builds up unless there is a gross light-input overload (e.g. by a flash bulb in the field of view) and unless the overload is of long duration, the build-up of internal charge will be small and no difficulty with persistent images (positive or negative) is experienced.

As mentioned earlier, the degree of enhancement is dependent on the signal-plate potential. This is thought to be a consequence of the neutralization of positive charges within the layer by the scanning

beam which can penetrate right through the layer to the signal-plate when the signal-plate potential is high. Under this condition the internal positive charges produced during the flooding process will be neutralized when the scanning beam is used to return the surface to cathode potential and there will be thus no gain enhancement.

Negative Images

If a target is internally charged with a uniform beam, as described above, and the internal charge is then partially neutralized by an electron image (with the scanning beam on) a negative image can be produced during subsequent read-out after the target has again been flooded uniformly. This will now be described in detail.

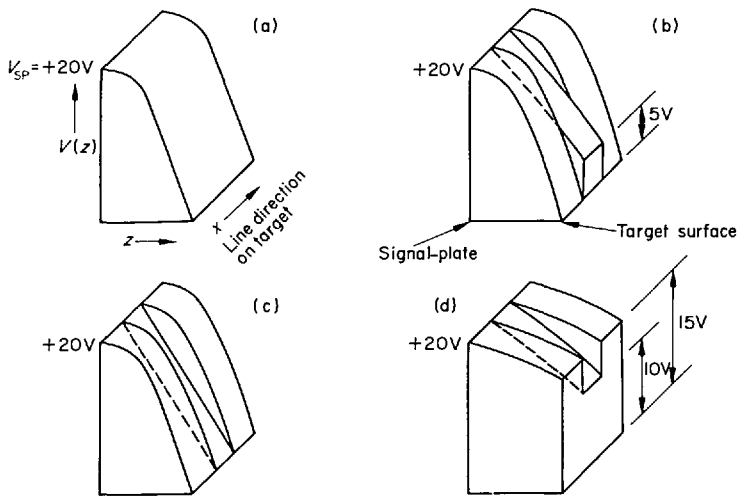

FIG. 5. Potential distribution diagrams illustrating formation of negative images: (a) target prepared before writing image, (b) writing and reading white vertical bar image, (c) cathode-potential stabilization after writing, and (d) after uniform flooding.

Figure 5(a) shows the potential along one line of a target with internal charge and with the surface cathode-potential stabilized. This corresponds with A–D–E of Fig. 3(b) but with the line direction x on the target surface included. If a vertical white bar image is now scanned for a few seconds at 25 frames/sec, the internal charge in the illuminated area will be neutralized to some extent. Figure 5(b) shows the potential distribution after several scans, with the light image on (just before the line is scanned), and Fig. 5(c) that after the light is switched off so that the whole surface is at cathode potential. The internal charge in the illuminated area has to some extent been neutralized and the gain in

this area will therefore be less; an example of this decrease in gain during continuous scanning is shown in Fig. 4. If the target is now flooded with a uniform beam of electrons, the potential of the previously unilluminated areas will rise higher than those that were illuminated, as shown in Fig. 5(d), i.e. a negative image will be formed. In Fig. 5(d) the potential of the surface has been allowed to rise 10–15 V in order to give a 5-V signal amplitude. To read out the charge pattern the surface potential must first be reduced to the range 0–5 V by lowering the signal-plate potential by 10 V. Otherwise severe beam-bending would occur and the contrast would be low.

Two optical images could be correlated by using one of them to discharge selectively an internally charged target, and the other in place of the uniform flood-beam in the final operation described above. The final read-out will then give a video signal which depends on the difference in luminance between corresponding points in the two images.

Target Lag

When a television camera is used for dynamic imaging it is desirable that the reading beam should completely discharge each picture point, and that there should be no charge regeneration after read-out. Incomplete discharge (or "discharge lag") occurs when the current in the reading beam is insufficient; normally it is only significant with high-capacity targets. SEC targets of the usual thickness (10–20 μm) have a comparatively low capacitance and discharge lag does not occur at normal scanning speeds.

Charge regeneration (or "target lag") is a major problem in camera tubes with electron bombardment induced conductivity (EBIC) targets because of the comparatively long decay time of the EBIC effect. Again, SEC targets do not exhibit charge regeneration when operated at the signal-plate potentials ($<\sim$30 V) normally used. However, if an attempt is made to increase the gain by raising the signal-plate potential, lag effects become evident. It has been suggested[4] that both the high gain and the lag are produced by EBIC processes in the target. Since another effect, beam electron conduction (BEC), has been proposed[7] as the reason for the high gains measured under these conditions, we decided to investigate whether there was any evidence of EBIC effects.

The method employed was to measure whether the charge regeneration was time-dependent. As noted above, the decay of EBIC is by no means instantaneous after the bombarding electron beam is turned off, but persists for a comparatively long time (in the range from several milliseconds to many seconds). A block diagram of the experimental arrangement is shown in Fig. 6. A staircase-waveform generator is used as a frequency divider to pulse on, for 20 μsec every tenth

frame, a cathode-ray tube having a short-persistence P·16 phosphor. The resulting pulsed light spot, which is stationary and also defocused, is imaged by a transfer lens on to the photocathode of an SEC camera tube having a two-layer target of the type described earlier in this paper. This is scanned at 200 lines, 50 frames/sec, and in odd frames one line is selected and displayed on an oscilloscope. By means of the delayed pulse generator the time between the light pulse and the first scan of the selected line can be varied in the range 0 to 20 msec.

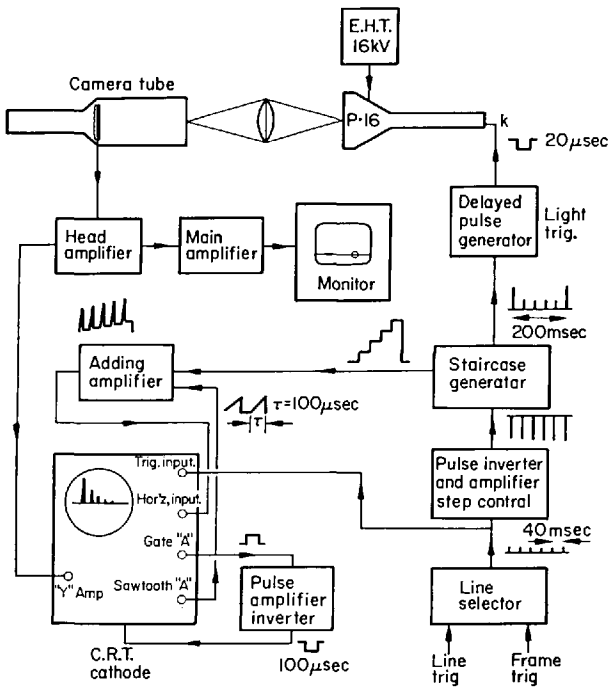

FIG. 6. Block diagram of lag-measuring equipment.

Figure 7 shows the oscilloscope waveforms for four different signal-plate potentials and with the light pulse timed to occur 25 μsec before the first read-out. When the signal-plate potential is 5 V or 10 V a negative pre-pulse can be seen; this is caused by the charging current due to transmitted secondary emission (TSE) electrons. This effect has been described by Filby *et al.*[7] At the higher signal-plate potentials the TSE gain is lower and the pre-pulse is very much smaller. As can be seen in Fig. 7, at the three lower signal-plate potentials there is no evidence of charge regeneration. However, at 40 V (and 30 V) there are residual charges which are read out on the second (not displayed), third

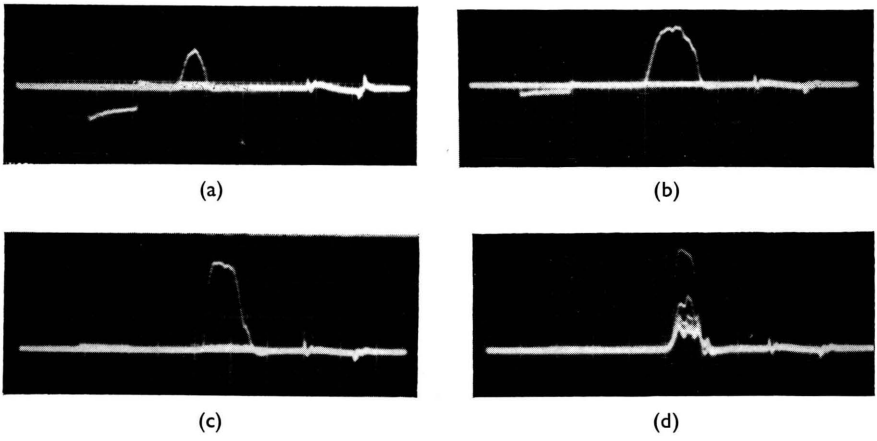

FIG. 7. Oscilloscope waveforms showing target lag; scans superimposed. Signal-plate potential: (a) 5 V, (b) 10 V, (c) 20 V, and (d) 40 V. A negative charging pulse can be seen in (a) and (b).

and subsequent scans. The profile of the lag can be displayed more clearly if the succeeding scans are displaced by a signal from the staircase generator to the X-deflexion amplifier of the oscilloscope (see Fig. 8).

When the time delay between the light pulse and the first scan is increased, the amplitude of the subsequent scans relative to the first could be expected to decrease if there were EBIC effects. In fact, no

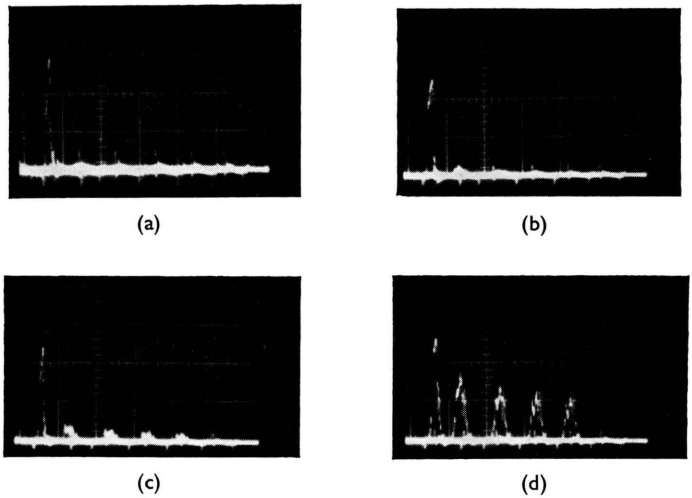

FIG. 8. Oscilloscope waveforms showing target lag; scans displaced to show lag profile. Signal-plate potential: (a) 10 V, (b) 20 V, (c) 30 V and (d) 40 V.

such time-dependence has been found when the delay is increased to 20 msec; in a separate test the delay was increased to 10 sec and even then there was only a very slight change. It therefore seems likely that EBIC occurs to only a very small extent in the SEC target.

The signal-plate potential at which lag becomes evident is close to that at which the gain curve starts to rise steeply (see Fig. 2). As was mentioned above it has been suggested that the cause of the latter is beam electron conduction (BEC). This is the penetration of the scanning beam right through the target to the signal-plate when the electric field within the target is high. The charge pattern on the surface of the target modulates the BEC electrons. At still higher signal-plate potentials there is penetration even in the absence of a surface charge pattern.

As a qualitative explanation of the large increase in the slope of the gain curve, BEC would seem to be plausible. On the other hand it is not so obvious how it can be evoked to account for the increase in lag. Even if part of the scanning beam penetrates to the signal-plate there would appear to be no reason why it should be any less effective in neutralizing the surface charges. A possible explanation is that the penetrating electrons produce positive charges within the target by secondary emission. The neutralization of such charges would be a slow process because the penetrating electrons would have energies in the region of the first secondary emission cross-over energy of the KCl ($\sim$ 15 eV). With rather higher signal-plate potentials it might be impossible to neutralize the charges, and this could be occurring when there is permanent penetration by the scanning beam.

Resolution

The resolution of a camera tube is often limited by the read-out section rather than by the target. It is interesting to consider how far the resolution could be increased if the read-out section were improved, or in other words, what is the resolution limit of the target.

At first sight the resolution of an SEC target would appear to be limited only by the scattering of the imaging electrons in penetrating the target. However, this scattering has been shown to be more directive than a Lambertian distribution,[8] and it is of minor importance. Also, because of the very high resistivity of the target there can be no loss of resolution through redistribution of charge by conduction. The actual limitation, which is a fundamental one that is common to all electrostatic devices, arises because the read-out electron beam senses the potential distribution rather than the charge distribution on the target surface. Krittman[9] has shown that the transformation of a charge pattern into a potential pattern can in itself be considered as an

imaging process, and the theoretical aperture response derived. By the use of Fourier transforms he has shown that for a target of thickness z_t, on a conducting signal-plate, the sine-wave response with electron-beam read-out is given by

$$R(f_s) = \frac{1 - \exp(-4\pi f_s z_t)}{4\pi f_s z_t}, \tag{4}$$

where f_s is the number of cycles/unit length. The electron beam is assumed to have a very small cross-section and its aperture response is not taken into account.

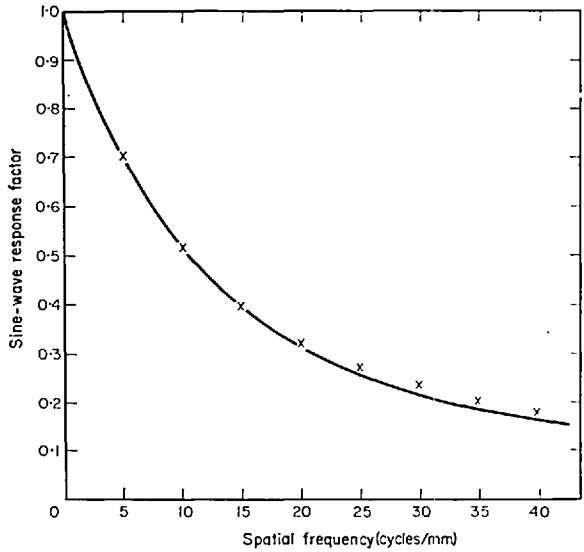

FIG. 9. Sine-wave response calculated using Eq. (4) for target thickness $z_t = 12\ \mu$m. Crosses indicate response reported by Beyer and Goetze[10] for an optically scanned tube.

An optically scanned SEC camera tube designed for high resolution has been reported by Beyer and Goetze.[10] The read-out beam was of very small diameter and beam-pulling effects were reduced by using a strong magnetic field for focusing. They estimated the sine-wave response of the target from the measured response of the complete system by making allowance for the responses of the optical lens, the imaging section, the read-out beam, and of the amplifier. The points plotted in Fig. 9 have been taken from their estimated response curve. The expression for $R(f_s)$, Eq. (4), is also plotted in Fig. 9 with $z_t = 12\ \mu$m, the value which gives the best fit to the experimental points at low frequencies where it can be expected to be most accurate.

As can be seen, the fit is extremely good; unfortunately the thickness of the target is not stated, but 12 μm would seem to be a reasonable value. The fall-off at low spatial frequencies was remarked on by Beyer and Goetze who, however, did not advance an explanation.

Krittman also reported measurements on image orthicons. He found that although there was good agreement with the theoretical curve for the first scan of a fixed pattern, the response was better for subsequent scans, particularly at low spatial frequencies. He attributed this to charge redistribution on the surface of the target, the time constant of this equilibrium being determined by the electrical characteristics of the target. If this is the case then one would not expect to observe the improvement with SEC targets because of their high resistivity. In Beyer and Goetze's tube the target was completely discharged by a flood beam between successive scans, so that their measurement was always for the first scan.

An alternative hypothesis to explain the improvement in repetitive scanning is that not all the electrons deposited by the first scan of the read-out beam combine with the positive charges of the charge pattern. These electrons could form areas of negative charge between the positive charges, and could so modify the potential field at the target surface that on subsequent scans the read-out beam electrons land only on the positive charges of the charge pattern. If this were so, then the resolution of SEC targets would also improve after the first scan.

ACKNOWLEDGMENTS

We should like to express our gratitude for the interest and advice of Professor J. D. McGee in whose department the work was carried out. We also thank Mr. J. Westlake and Mr. W. Simpson of the Applied Physics Department for their technical assistance.

We wish to acknowledge with thanks financial assistance from the Science Research Council. One of us (G.O.T.) has been supported by a grant from the English Electric Valve Co. Ltd., Chelmsford.

REFERENCES

1. Goetze, G. W. and Boerio, A. H., *Proc. Inst. Elect. Electronics Engrs* **52,** 1007 (1964).
2. Filby, R. S., Mende, S. B., Rosenbloom, M. E. and Twiddy, N. D., *Nature* **201,** 801 (1964).
3. Goetze, G. W., *In* "Advances in Electronics and Electron Physics", ed. by J. D. McGee, D. McMullan and E. Kahan, Vol. 22A, p. 219. Academic Press, London (1966).
4. Boerio, A. H., Beyer, R. R. and Goetze, G. W., *In* "Advances in Electronics and Electron Physics", ed. by J. D. McGee, D. McMullan and E. Kahan, Vol. 22A, p. 229. Academic Press, London (1966).
5. Filby, R. S., Mende, S. B. and Twiddy, N. D., *Int. J. Electronics* **14,** 387 (1965).
6. McMullan, D. and Towler, G. O., *Electronics Letters* **4,** 360 (1968).

7. Filby, R. S., Mende, S. B. and Twiddy, N. D., *In* "Advances in Electronics and Electron Physics", ed. by J. D. McGee, D. McMullan and E. Kahan, Vol. 22A, p. 273. Academic Press, London (1966).
8. Butkevich, B. G. and Butslov, M. M., *Radiotekhnika i Elektronika* **3**, 355 (1958).
9. Krittman, I. M., *I.E.E.E. Trans. Electron Devices* **ED–10**, No. 6, 404 (1963).
10. Beyer, R. R. and Goetze, G. W., *In* "Advances in Electronics and Electron Physics", ed. by J. D. McGee, D. McMullan and E. Kahan, Vol. 22A, p. 241. Academic Press, London (1966).